Electronic transport in nanoelectromechanical systems: Noise, back-action, and quantum measurement

Genehmigt von der Philosophisch-Naturwissenschaftlichen Fakultät auf Antrag von

Prof. Dr. Christoph Bruder

Prof. Dr. Alexander Shnirman

Prof. Dr. Björn Trauzettel

Basel, den 9. Dezember 2008   Prof. Dr. Eberhard Parlow
                                                                    Dekan

Summary

The important progress made in nanolitography processes in the last decades has had a profound impact in our daily lives, by making possible the miniaturization of consumer electronics. Unbeknownst to most consumers, it is nowadays possible to fabricate free-standing nanoscale devices, that will naturally vibrate under thermal or external excitation. Over the last decade, a new subfield of physics devoted to studying these objects emerged: nanomechanics.

In this thesis, we study electronic transport in such nanostructures where mechanical degrees of freedom play an important role. More precisely, we calculate the full transport properties (e.g. average current, frequency-dependent current noise) of different mesoscopic detectors in the presence of coupling to a nanomechanical oscillator. The objective of our study is twofold. First, there is a strong interest in understanding the effect that the coupling to electronic degrees of freedom has on the state of the mechanical system. We will show that under many conditions the interaction with the detector can be understood in terms of an effective thermal bath, but also discuss the limitations of this effective environment model. A second main aspect of the work presented here is the calculation of the signature of the mechanical object in the transport properties of the detector. As one of the primary goal in the field of nanoelectromechanical systems is to use the output of such electrical detectors to achieve position measurements at the quantum limit, this question obviously is of great relevance to the field.

This thesis is organized in 3 main parts, each associated with a different electronic detector. After a short introduction to nanoelectromechanical systems, we focus in Part II on a system composed a single-electron transistor coupled capacitively to a classical mechanical oscillator. We present a complete study of the transport properties of the coupled system, going beyond the usual weak-coupling approximation. In Part III, we discuss the properties of a system where a tunnel junction is coupled to the mechanical object. Looking at this system from the point of view of quantum measurement, we analyze the transport properties of a system composed of two independent tunnel junctions coupled to the same oscillator and demonstrate how, by using the cross correlated output of the two detectors, one can improve the sensitivity of position measurements beyond the usual quantum limit. In this part, we also

demonstrate that the current noise of a system composed of two tunnel junctions (one with fixed transmission amplitude, the other with position-dependent transmission amplitude) can contain information about the momentum of the mechanical oscillator. Lastly, in Part IV we study a system composed of a mechanical oscillator coupled to a superconducting single-electron transistor. The coupled dynamics of the oscillator and mesoscopic detector are in this case very complex, and we demonstrate how a numerical approach based on a solution of the Liouville equation can be used to validate results obtained from approximate analytical approaches. We also demonstrate, by looking at the frequency-dependence of the charge fluctuations on the superconducting single-electron transistor, limitations to the model where the effect of the detector back-action on the oscillator is modeled as an effective environment.

Acknowledgments

The work presented in this thesis could not have been achieved without the continued support of people around me.

First, I need to express my gratitude to my advisor, Christoph Bruder, for giving me the chance to be part of his group. I really enjoyed working under his supervision, as I felt that he always trusted me and believed in me. Moreover, he was always available for discussions, in which he gave me invaluable help and advice. I also would like to thank Björn Trauzettel, for his energy, his ability to motivate me and his contagious enthusiasm for research, as well as Wolfgang Belzig, for his support during the first few months after I joined the group. Of course, I also need to thank all the members of the theory group in Basel: my office-mates Audrey Cottet, Joël Peguiron and Dan Bohr, but also every other member of the group: Audrius Alkauskas, Massoud Borhani, Bernd Braunecker, Denis Bulaev, Stefano Chesi, Luca Chirolli, Bill Coish, Mathias Duckheim, Carlos Egues, Siggi Erlingsson, Jan Fischer, Vitaly Golovach, Daniel Klauser, Verena Koerting, Minchul Lee, Jörg Lehmann, Yong Li, Daniel Loss, Andriy Lyakhov, Roman Riwar, Beat Röthlisberger, Manuel Schmidt, Thomas Schmidt, Pascal Simon, Oleg Shalaev, Dimitrije Stepanenko, Mircea Trif, Oleksandr Tsyplyatyev, Mihajlo Vanevic, Kevin van Hoogdalem, Andreas Wagner, Ying-Dan Wang, Robert Zak and Oded Zilberberg. The time I spent in Basel would never have been as extraordinary without them.

Throughout my doctoral studies, I also benefited a lot from the discussions with other members of the NEMS community. Specifically, I would like to thank Nathan Flowers-Jacobs, Aash Clerk and the other participants and lecturers at the "NEMSSS summer school" that took place in the Summer of 2007, both for enlightening technical discussions and for the nice moments shared. Also, I sincerely thank Andrew Armour for inviting me to visit his group during my first year as a doctoral student, as well as Alexander Shnirman for accepting the role of external examiner at my thesis defense.

Naturally, my family as well as my good friends in Canada played a central role in making this thesis possible, providing constant encouragement and unconditional support. No words can adequately express my gratitude to them.

Contents

III Nanomechanics with tunnel junctions   47

V Conclusion and outlook   161

12 Conclusions and outlook   163

VI Backmatter   167

A The MacDonald formula   169

B The Caldeira-Leggett master equation   171

C Derivation of the condition on quantum-limited detection   177

Bibliography   179

Curriculum Vitae   197

List of Publications   198

Part I

Nanomechanical systems: an introduction

Nanoelectromechanical systems: Applications and fundamental interests

> **mechanics,** *n.* The branch of applied mathematics that deals with the motion and equilibrium of bodies and the action of forces, and includes kinematics, dynamics, and statics. Now often distinguished as classical mechanics (as opposed to *quantum mechanics*).
>
> Oxford English Dictionary

The definition of the word "mechanics" as found in the Oxford English dictionary (reprinted above) nicely expresses the prevailing preconception of the overall physics community that mechanical systems are described by the laws of classical mechanics. As people are mostly accustomed to mechanical systems that are *huge* on the microscopic scale (e.g. a pendulum clock), their opinion is actually quite justified: classical mechanics governs the macroscopic world, and quantum mechanics the behavior of objects at the atomic scale. In this regard, mechanical systems with typical dimensions of a few hundreds of nanometers (nanomechanical systems) are of a particular fundamental interest: at these scales the distinction between *micro* and *macro* or, by extension, between *classical* and *quantum* becomes blurry.

Besides being relevant in the study of fundamental issues like the quantum-to-classical transition, nanoelectromechanical systems (NEMS) have a huge technological potential, mainly as highly sensitive sensors. The purpose of this chapter is to give the reader a broad overview of the field of "nanomechanics", covering both technological applications of nanometer-scale mechanical systems as well as explaining their relevance in fundamental research. The chapter is organized as follows: in Sec. 1.1 we define precisely what the term 'nanoelectromechanical system' refers to. Then, in

Sec. 1.2 we discuss the technological applications of such devices before (Sec. 1.3) explaining how nanomechanical systems can be used to probe questions of fundamental interest in quantum physics.

1.1 Nanoelectromechanical systems

In a recent review[Blencowe05a], M. P. Blencowe defined nanoelectromechical systems as "nano-to-micrometer scale mechanical resonators coupled to electronic devices of similar dimensions". While this definition is not very precise, it efficiently summarizes the two defining characteristics of NEMS: these are very small objects with active mechanical degrees of freedom whose mechanical response is either controlled or monitored via an electronic device placed nearby.

Typically, the mechanical element of the NEMS is a cantilever: a long, thin, freestanding rod that is clamped at either one or two ends to a substrate. In the limit of low amplitude oscillations, the cantilever effectively acts as a harmonic oscillator whose properties are a function of both the geometry of the device as well as the material used in the fabrication. In this thesis, we will mostly concentrate on systems where the mechanical element is a doubly-clamped cantilever of length l, width w and thickness t. For this geometry, the fundamental flexural mode of a rod corresponds to the fundamental mode of a harmonic oscillator[Cleland04] of with effective mass (M), spring constant (k) and frequency Ω given by

$$M_{\text{eff}} = 0.735 ltwr \tag{1.1a}$$

$$k_{\text{eff}} = \frac{32Et^3w}{l^3} \tag{1.1b}$$

$$\Omega_{\text{eff}} = 2\pi(1.05)\sqrt{\frac{E}{r}}\frac{t}{l^2} \tag{1.1c}$$

with r is the density of the material used and E its Young's modulus. This strong dependence of the device characteristics on its geometry combined with the wide range of materials that can be used to create the cantilever[1] make it possible to create mechanical devices that operate in very different regimes. As mentioned in [Schwab02], nanometer-sized resonators of frequency ranging from hundreds of kHz to 1 GHz and of mass between 10^{-15} and 10^{-21} kg have been demonstrated. An important characteristic of mechanical resonators is that they exhibit extremely high quality factors – much higher than LC oscillator – with typical Q ranging from 10^3 to 10^5 [Ekinci05a]. This makes mechanical oscillator perfect candidates for low power applications and

---

[1]For example, nanomechanical oscillators have been fabricated from, for example, Si single-crystals[Cleland96], GaAs / AlGaAs [Blick98], SiC [Yang01], AlN [Cleland01], metals [Flowers-Jacobs07] and even carbon nanotubes [Jensen06].

for fundamental research, as a high Q translates to a weak coupling to the environment.

As stressed in the first sentence of this section, the mechanical element is only one part of the nanoelectromechanical system. To be able to effectively monitor the mechanical oscillations, one needs a transduction stage that converts a mechanical input into an electrical signal. In principle, one could also use an optical transducer, i.e. convert mechanical motion to an *optical* signal. Such systems, referred to as "optomechanical systems", will not however, be discussed in this thesis. Over the years, a multitude of different transduction methods have been demonstrated (see e.g. [Ekinci05a] for a description of many transduction mechanisms), but no kind of electrical transducers shows more promise for high-sensitivity position measurement at the nanoscale than mesoscopic electronic systems like the (superconducting) single-electron transistor and the tunnel junction. Importantly, these transducers can be very precisely described theoretically, a property that will prove invaluable when it comes to evaluate the efficiency of these detectors (Sec. 4.2). This is the kind of detectors on which we will focus in this thesis.

1.2 Applications

Mechanical systems have been used for a long time as high-precision force sensors. Already in 1785, Coulomb used a *mechanical* torsion balance to establish the $1/r^2$ dependence of the electrostatic force between two charges. With the progress in technology, many applications have been found for mechanical systems that can be controlled or monitored electrically. As of today, the typical size of the mechanical systems used in commercial application ranges between 1mm and 1μm: these are called microelectromechanical systems (MEMS). Typical applications of MEMS range from inkjet printer heads, pressure sensors, to accelerometers controlling the deployment of airbags in cars. The usage of MEMS in commercial devices is forecasted to increase dramatically over the next few years: according to a french think tank, the total market from MEMS-based system should reach USD 103B by 2012, from USD 40B in 2006[yol08].

What about NEMS? More precisely, for which type of application is it useful to put efforts into scaling down MEMS into NEMS? To answer this question, we can look at the attribute scaling of mechanical systems with system size. Defining for a moment a typical lengthscale ℓ of the system, i.e. $l = \tilde{l}\ell$, $w = \tilde{w}\ell$ and $t = \tilde{t}\ell$, and looking at the

scaling the effective parameters defined in Eq. (1.1), we find

$$M_{\text{eff}} = \left[0.735 \tilde{l} \tilde{t} \tilde{w} r \right] \ell^3 , \tag{1.2a}$$

$$\Omega_{\text{eff}} = \left[2\pi (1.05) \sqrt{\frac{E}{r} \frac{\tilde{t}}{\tilde{l}^2}} \right] \frac{1}{\ell} , \tag{1.2b}$$

$$k_{\text{eff}} = \left[\frac{32 E \tilde{t}^3 \tilde{w}}{\tilde{l}^3} \right] \ell . \tag{1.2c}$$

Going from the microscale to the nanoscale (decreasing ℓ) therefore leads to a decreased mass, an increased typical resonance frequency as well as a decreased stiffness k_{eff} of the resonator. A direct consequence of this scaling of the resonator's attributes with size is that, from a technological point of view, NEMS offer an advantage over MEMS in the realm of mass-sensing, high frequency applications, and ultrasmall-force detection.

The case where it is easier to understand the intrinsic advantage of NEMS over MEMS is mass-sensing. In a resonant mechanical mass sensor, one measures the shift in resonant frequency of the oscillator as the particles that have to be weighted deposit on the cantilever. To a good approximation, the shift Δf is given by[Ekinci05a]

$$\Delta f = -\frac{\Delta M}{2M} f . \tag{1.3}$$

As the sensitivity δM of the device is related directly to Δf, one expects the sensitivity of such devices to scale like ℓ^{-4}: by going to the nanoscale regime, one both decreases the mass (increasing the relative mass difference ΔM that is to be measured) as well as increases the frequency of the oscillator, leading to a larger (in absolute magnitude) frequency shift. Recently, a NEMS-based mass-sensor with a sensitivity of 1.3×10^{-25} kg Hz$^{1/2}$ has been demonstrated[Jensen08]. This sensitivity allows to monitor the deposition of *single* Au atoms on the resonator, an important step towards the development of fully mechanical mass-spectrometers[Knobel08].

For force-sensing applications, it is the reduced stiffness of the resonator with reduced ℓ makes NEMS-based systems attractive. Intuitively, the response of a very stiff (high k) resonator to a small force is much smaller than the response of a very compliant (low k) resonator to the same force. NEMS-based detection system have demonstrated zeptonewton-scale force sensitivities at cryogenic temperatures[Mamin01]. This exquisite force sensitivity opens the door to exciting applications like magnetic resonance force microcopy at the single spin level[Sidles91; Rugar04].

1.3 Nanomechanical systems in basic science

Besides a great potential for technological applications, the miniaturization of MEMS into NEMS also opens new research avenues in fundamental science. As shown in

Eq. (1.2b), the mechanical resonance frequency Ω typically increases for smaller resonators and devices with $\Omega = 2\pi \times 1\text{GHz}$ have been demonstrated. Since nowadays experimentalists worldwide are able to easily cool solid-state devices to temperatures of only a few dozens mK, cooling down nanomechanical resonators to temperatures of the order of $T \sim \hbar\Omega/k_B$ seems within experimental reach (recall that $10\text{mK} \sim 200\text{MHz}$). At this point, it is expected that the quantum-mechanical behavior of the harmonic mode could be observed, a remarkable feat when one remembers that the resonator, while "small" by daily-life standards, is composed of about millions of atoms and is therefore quite large by quantum standards. Such a mechanical oscillator in the quantum mechanical regime could in principle be prepared in a superposition of states that are macroscopically different (for example, a superposition of two wave packets positioned at a finite distance from each other), or even to entangle a resonator with a two-level system[Armour02]. The study of macroscopic quantum systems as well as their interplay with the environment (causing decoherence) is perhaps the most stunning example of the possibilities offered by NEMS in basic research[2].

As of today, the quantum-mechanical behavior of a mechanical system has still not been demonstrated experimentally. Nevertheless, a great deal of basic science has been achieved using nanoscale mechanical systems, for example in condensed matter physics. In 2000 such systems have been used to demonstrate that heat transport in ballistic phonon systems is quantized[Schwab00], thereby confirming the existence of a phononic equivalent of the Landauer formula for charge transport[Pendry83]. They also have been used to probe spin-torque effects at interfaces between ferromagnetic and normal (non-ferromagnetic) materials[Mal'shukov05; Zolfagharkhani08]. More generally, mechanical systems found an application as experimental playgrounds in many fields of physics, including non-linear dynamics (chaos, synchronization) [Shim07; Lifshitz08], stochastic processes (for example, via a demonstration of mechanical stochastic resonance [Badzey05]), the Casimir force [Buks01], etc.

On the experimental level, a great deal of efforts has been put towards achieving quantum-limited position measurement. Indeed, a prerequisite to any study of quantum behavior in a mechanical system is to be able to monitor the position of the mechanical system extremely accurately. While the basics of quantum measurement will be explained in detail in Chap. 4, let us just mention at this point that quantum mechanics enforces a limit to the sensitivity of a position measurement of any harmonic oscillator. This limit holds whatever the state of the oscillator, i.e. it is possible to make a quantum-limited measurement of a harmonic oscillator in a thermal state characterized by a "high temperature" $T \gg \hbar\Omega/k_B$. There are many conditions that must be fulfilled in order for a position measurement to reach the quantum limit

---

[2]For a more detailed commentary regarding the role of NEMS in the study of the quantum-classical transition, see [Ball08] or the older [Schwab05].

(Sec. 6.1.2); importantly, not all detectors (i.e. the electronic part of the NEMS) satisfy these conditions and a thorough theoretical analysis of the different possible position detectors must be carried out in order to identify those that could in principle lead to quantum-limited position measurement.

More generally, important efforts have been made by many theoretical groups to study the behavior of quantum systems (qubits, mesoscopic detectors, spins) coupled to mechanical resonators. Importantly, the frequency range in which mechanical resonators operate sets them apart from other 'harmonic-oscillator like' systems like optical cavities[Raimond01] and superconducting striplines[Wallraff04]; they are therefore characterized by different physics. The work presented in this thesis fits nicely this broad description.

As will be shown in the next parts, we investigated three "quantum systems" (detectors) coupled to a mechanical oscillator: the single-electron transistor (Part II), the tunnel junction (Part III) and the superconducting single-electron transistor (Part IV). Even if the specific question investigated in each part differs, throughout this thesis we used an appropriate description of *both* the mechanical degree of freedom and the detector in an effort to describe (i) the effect of the detector on the oscillator as well as (ii) the signature of the coupling to the oscillator in the detector's output. Read on to learn how we used the concepts of noise and measurement back-action to gain new insights about nanoelectromechanical systems.

1.4   Detailed outline of the thesis

Before continuing, we take a brief moment to discuss the structure and content of the thesis. The main part of the text is comprised of 3 parts (II - IV).

In Part II, we study a system composed of a single-electron transistor (SET) coupled to a mechanical oscillator. In Chap. 2, we will introduce the system in detail, commenting on the basic theoretical description of the SET as well as describing the experimental realization of the system considered. In Chap. 3, we present a numerical study of this system in the strong coupling regime. This chapter is mainly derived from [Doiron06], but also contains a previously unpublished section regarding the system properties away from the charge degeneracy point (Sec. 3.4).

In Part III of the thesis, we study tunnel junction displacement detectors. As one of the main issues discussed in this section is quantum measurement, we start in Chap. 4 with a short review of continuous measurements in quantum mechanics. In Chap. 5, we explain the basics of quantum measurement with tunnel junctions, reviewing both theoretical and experimental work on the topic. In Chap. 6, we introduce the 'effective environment' model often used in the context of NEMS to describe the effect of detector back-action on the mechanical oscillator and derive the quantum limit on the

sensitivity of a position measurement. In this chapter, we also give an example of how to use the effective environment approach by describing the back-action of a tunnel junction position detector on a resonator. In Chap. 7, we discuss the equation-of-motion approach that will be used in the following chapters. Interestingly, in Sec. 7.2 we rederive the effective environment model introduced in Chap 6 by using a Born-Markov master equation approach. In the last section of 7, we detail how the master-equation approach can be used to derive the results that will be presented in Chaps. 8 and 9. Chapter 8 presents the work originally published as[Doiron07]. In this chapter, we demonstrate how, by using detector cross correlations, the quantum-mechanical bound on the sensitivity of a position measurement (derived for a single detector) can be overcome. In Chap. 9, we demonstrate that, by using two tunnel junctions (with only one of them coupled to a mechanical oscillator), the total current noise can be used to measure the *momentum* of the oscillator. The content of this chapter was originally published as[Doiron08].

Part IV of this thesis is devoted to the study of a mechanical oscillator coupled to a superconducting single-electron transistor. In Chap. 10, we describe the system and its experimental realizations, using the linear-response approach to understand the different regimes in which the detector can drive the oscillator. Part of the discussion presented in this chapter is adapted from [Koerting08]. The author of this thesis was mainly involved with the numerical aspects of the study presented in [Koerting08], and Chap. 11 presents a detailed summary of a numerical approach based on the solution of the Liouville equation that was used in this context.

Concluding remarks are presented in Part V. Appendices, one on the MacDonald formula, one on the Caldeira-Leggett model of quantum dissipation and one that contains a derivation of the condition on quantum limited detection [Eq. (4.17)], can be found after the conclusion.

Part II

Nanomechanics with single-electron transistors

Nanomechanical oscillators coupled to single-electron transistors

In this first part of the thesis, we will focus on the interaction of a nanomechanical oscillator with a single-electron transistor (SET). Historically the SET was first recognized as an amazingly sensitive electrometer. However, already in 1993 it was proposed that the SET charge sensitivity could be leveraged to measure displacement[White93]. As we will show in this chapter, this is a consequence of the equivalence between (i) varying the charge on a gate capacitively coupled to the SET island while keeping the gate capacitance constant like in an electrometer or (ii) varying the capacitive coupling between the gate and the island while keeping the charge on the gate fixed, like in a displacement meter.

This chapter is organized as follows. Before discussing the interaction of single-electron transistors with mechanical systems, we take a moment to introduce, in Sec. 2.1, the operating principle of the SET. Since many high-quality reviews are available on the topic[Devoret92; Kastner92; Devoret00], we will keep this discussion short. Afterwards, in Sec. 2.2, we review recent experimental and theoretical advances regarding displacement measurement using single-electron transistors.

2.1   The single-electron transistor

A single-electron transistor is formed by putting two tunnel junctions in series, forming an 'island' as depicted in Fig. 2.1. This island is coupled capacitively to an electrostatic gate, via the gate capacitance C_G. Taking into account the finite capacitance of each tunnel junction (C_L, C_R), the total capacitance of the island is $C_\Sigma = C_G + C_L + C_R$. By making the central island sufficiently small, the energy cost to add a charge e (the charging energy $E_c = e^2/2C_\Sigma$) can be made much larger than the thermal energy $k_B T$. In this limit (and for junction resistances $R > h/e^2$), the electron number on the island

n is a well-defined integer.

In the 'orthodox theory' of the SET, transport in this system is the consequence of a sequence of independent tunneling events. In this sequential tunneling regime, the tunneling rates are governed directly by the electrostatic energy difference between states with different number of charges on the island. The orthodox theory of the SET will be detailed in the next section so here we will just try to explain qualitatively the operating principle of this detector. The main idea behind the SET is that its transport properties heavily depend on the voltage applied at the capacitively-coupled gate. Indeed, in presence of this gate, the electrostatic energy of a charge Q on the island is given by $E_{el} = -QV_G + Q^2/2C_\sigma$, which can be rewritten (up to some constant) as [Kastner92]

$$E = E_c \left(n - n_0\right)^2 \qquad (2.1)$$

where

$$n_0 = \frac{C_G V_G}{e} , \qquad (2.2)$$

is an 'equilibrium charge' that minimizes the energy of the system induced by the capacitive coupling to the gate on the island. This charge can be varied continuously (i.e. it does not only take integer values) by tuning the gate voltage. When $n_0 = n$ is an integer, the charge fluctuations on the island are heavily suppressed (we take the bias voltage as smaller than the charging energy). Since transport is impossible without charge fluctuations, the charge current in this case vanishes: this is the Coulomb blockade regime. On the other hand, when $n_0 - \lfloor n_0 \rfloor \sim 1/2$, the energy difference between the states with n and $n + 1$ charges on the island becomes minute, allowing charge fluctuations and therefore transport. The important dependence of transport properties in n_0 is what makes the SET an excellent electrometer, which demonstrated charge sensitivity of the order of $10^{-5} e \, \mathrm{Hz}^{-1/2}$ [Schoelkopf98].

To conclude this short introduction to the SET, we note that the current through the island never vanishes completely, even in the Coulomb blocade region. Indeed, in this regime higher-order processes (cotunneling), involving the simultaneous tunneling of 2 or more electrons leads to a small 'leakage current'.

2.2 The SET as a displacement detector

Practical implementations of oscillator-coupled SET transistors can be realized by combining nanofabricated resonators with metallic SETs, as depicted in Fig. 2.1. In this case, one uses the resonator *itself* as a second gate, applying a voltage V_N between metallized the beam and the island. In the experimentally relevant limit where the displacement of the oscillator is very small with respect to the distance between

the resonator's equilibrium position and the island, the capacitive coupling C_N between the resonator and the island can be written as $C_N(x) = C_N^0 + (dC_N/dx)x$. In this case, a displacement Δx of the oscillator corresponds to a change

$$\Delta n_0 = \left[V_N \frac{dC_G}{edx} \right] \Delta x \tag{2.3}$$

of the equilibrium charge n_0 on the island. This change in n_0 is reflected in the transport properties of the SET, such that by monitoring the current fluctuations through the SET on can infer the position fluctuations of the mechanical oscillator. As seen from Eq. (2.3), the coupling between the SET and the resonator is a function of (i) a geometric coefficient $\frac{dC_N}{dx}$ that is typically fixed for a given sample and (ii) the voltage V_N applied on the resonator. In practice, the coupling between the SET and the resonator can therefore be tuned by adjusting this voltage. Following a detailed semi-classical
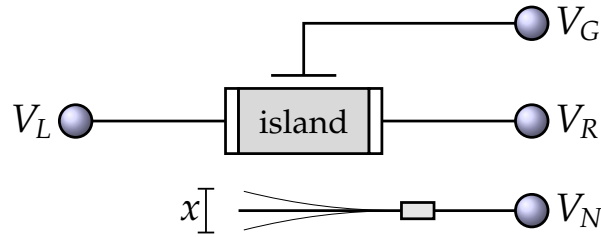
Figure 2.1: Schematic representation of a SET-based displacement detector. The resonator (depicted as a cantilever clamped at one end) is coupled capacitively to the island and acts as a second, x-dependent, gate.

analysis [Blencowe00; Zhang02] of this experimental setup, the first experimental realization of the device depicted in Fig. 2.1 was demonstrated by Knobel and Cleland in 2003[Knobel03]. In this experiment, a 3μ long, 250 nm wide, and 200nm thick doubly-clamped cantilever located 250 nm away from the SET island was patterned in a GaAs single crystal. The frequency of the fundamental in-plane mode of the beam was measured to be 116MHz, with a quality factor around 1700. Using this device, the authors demonstrated a measurement sensitivity[1] of 2.0×10^{-15}m Hz$^{-1/2}$ at 30mK. In this case, an improvement of about two orders of magnitude in the sensitivity would had been necessary to be able to monitor the purely thermal displacement fluctuations of the oscillator; only driven oscillations could be detected. This being said, in this experiment the authors compared the sensitivity of the SET-based displacement detector

---

[1]The measurement sensitivity is a measure of the output noise due to the detector, referred back to the oscillator. It will be formally defined, along with the quantum limit on measurement sensitivity, in Sec. 6.1.2

with the more common magnetomotive detection scheme [Cleland96] and found the SET-based method to provide substantially improved sensitivity.

From a theoretical point of view, much work has also been done regarding this system. For example, the transport properties of the SET coupled to a classical oscillator were shown to be greatly influenced by the state of the oscillator [Chtchelkatchev04]. Strong feedback effects in the weak-coupling regime were investigated in [Blanter04; Blanter05] and demonstrated to be possible only in the presence of energy-dependent tunneling rates [Usmani07]. Perhaps the most complete analysis of the dynamics of the coupled system in the weak-coupling limit was presented in [Armour04b; Armour04a], and reviewed concisely in [Blencowe05a]. In these two articles, it was demonstrated that the effect of the SET on the oscillator could be modeled as an effective thermal environment: in this regime, the interaction with the SET damps the oscillator's motion, bringing it to a gaussian (thermal) state. The description of the system used in these articles will be described in detail in Sec. 3.1.

2.3 Mechanical degrees of freedom in SET-like systems,

Before concluding this chapter, we note that the configuration presented before, with a cantilever capacitively coupled to a SET, is not the only relevant experimental realization of a system where both charging energy and 'mechanical' degrees of freedom play a role. These two elements are central to discussions regarding electronic transport through molecular systems, as they can be characterized by a large charging energy and an important electron-phonon coupling (see e.g. [Park00; Koch05; Hubener07; Pistolesi08]). Another related system is the "electronic shuttle", where instead of using the SET as a way to measure the displacement of a nearby oscillator, the central island of a SET is *itself* allowed to mechanically oscillate between the two leads, such that electrons can tunnel on the island if the island has approached one lead and leave it again once it has mechanically moved to the other lead. These shuttles have been investigated in great detail [Gorelik98; Weiss99; Erbe01; Gorelik01; Pistolesi04; Isacsson04; Novotny04; Pistolesi06].

Electrical transport through a single-electron transistor strongly coupled to an oscillator

In this chapter, we will consider a SET transistor coupled to a classical harmonic oscillator. This system has already been studied extensively [Armour04a; Armour04b]. However, previous studies investigated the regime where the coupling between the oscillator and the SET is weak and the question what happens when the coupling is increased is still of great theoretical interest,[Blencowe05a] even if this regime might not be readily accessible in the current generation of experiments. In this chapter, we will use a combination of a master-equation approach and a numerical Monte Carlo procedure to calculate the electrical current, its second and third cumulants, and study how they are modified by coupling to the oscillator, in the regime where the coupling is strong. We will also study the frequency dependence of the transport noise.

The chapter is organized as follows: in Sec. 3.1, we present in more detail the system under study, reviewing the model and the master-equation approach used in [Armour04b] to study this system in its weak-coupling limit. This section also introduces the important dimensionless coupling parameter κ that is the ratio of the typical mechanical energy scale and the source-drain voltage. Next, in Sec. 3.2, we present a calculation of the third cumulant of the current in the weak-coupling limit. The remainder of the chapter presents our numerical results. First, we present results in the 'symmetric' case where the average charge state of the island is $\langle N \rangle = 0.5$: in Sec. 3.3.1, we calculate the probability distributions of the position of the oscillator if the SET is in state N or $N + 1$ using a numerical Monte Carlo procedure and find that the Gaussian form predicted by the weak-coupling approach is modified dramatically in the strong-coupling regime. In Sec. 3.3.2, we calculate the average current
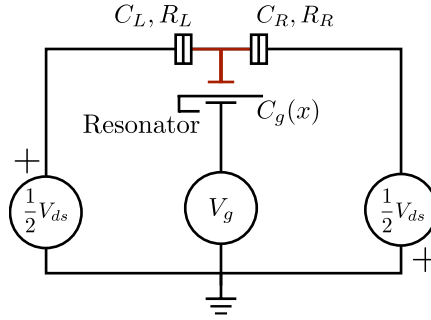
Figure 3.1: Circuit diagram of the system studied. The gate capacitance of the SET depends on the displacement of a mechanical oscillator, leading to a coupling of the electrical transport through the device and the mechanical motion of the oscillator.

through the device, then, in Secs. 3.3.3, 3.3.4 we complete our studies of the system at the charge-degeneracy point by looking at current noise and the third cumulant of the current. The last part of the chapter presents numerical results away from the degeneracy point.

3.1 Coupled SET-oscillator system description

To describe the coupled SET-nanomechanical oscillator system, we use the formalism introduced in [Armour04b]. The system we consider is shown in Fig. 3.1 in a schematic way. It consists of two symmetric tunnel junctions, each with resistance R and capacitance C, connected in series. Transport through the SET is described using the orthodox model, where only two charge states are considered and where the current arises only from sequential tunneling.[Averin91; Beenakker91] In this case, transport is governed by four tunneling rates Γ_i^σ where $i = R, L$ is the lead index and $\sigma = +, -$ indicates the direction of the tunneling. In this work, we adopt the convention that the forward $(+)$ direction, given by the polarity of the bias voltage, is from the right to the left lead. The tunneling rates can be calculated using Fermi's golden rule and are a function of the difference in free energy ΔE of the system before and after a tunneling event

$$\Gamma_i^\sigma = \frac{1}{Re^2} \Delta E_i^\sigma f(\Delta E_i^\sigma) , \tag{3.1}$$

where $f(x) = (1 - e^{-x/k_B T_e})^{-1}$, with T the electronic temperature. The energy differences ΔE_i^σ are given by

$$
\begin{aligned}
\Delta E_L^+ &= -\Delta E_L^- = eV_{ds}\left(\frac{1}{2} + (2N - 2N_g + 1)\frac{E_c}{eV_{ds}}\right) \\
\Delta E_R^+ &= -\Delta E_R^- = eV_{ds}\left(\frac{1}{2} - (2N - 2N_g + 1)\frac{E_c}{eV_{ds}}\right) ,
\end{aligned}
\tag{3.2}
$$

where V_{ds} is the applied drain-source voltage, $E_c = e^2/(2C + C_g)$ is the charging energy of the island and $N_g = C_g V_g/e$ is the optimal number of charges on the island. Knowing the different rates, the average current I flowing through the SET can be calculated using

$$
I/e = P_{N+1}\Gamma_L^+ - P_N\Gamma_L^- = P_N\Gamma_R^+ - P_{N+1}\Gamma_R^- ,
\tag{3.3}
$$

where $P_{N(N+1)}$ is the probability to find the island in charge state $N(N+1)$ in the stationary limit.

Our model of the SET remains valid as long as its charging energy E_c is large compared to the electronic thermal energy $k_B T_e$ and the source-drain bias eV_{ds}. We will neglect higher-order tunneling processes (cotunneling).

In this work, the nanomechanical oscillator is modeled as a single, classical, harmonic oscillator of mass M and frequency Ω. Introducing a time scale

$$
\tau_t = Re/V_{ds}
\tag{3.4}
$$

which has the physical meaning of an average time between tunneling events, we can use the dimensionless parameter

$$
\epsilon = \Omega\tau_t = \Omega\frac{Re}{V_{ds}}
\tag{3.5}
$$

to compare the typical electrical and mechanical timescales.

A particular state of the oscillator is represented by a position x and velocity u. We choose $x = 0$ to be the equilibrium point of the oscillator when N charges are on the SET. When the charge state of the island is changed, for example, from N to $N + 1$, the change in the electrostatic forces between the oscillator (kept at constant potential V_g) and the SET effectively shifts the equilibrium position of the resonator. The distance between the equilibrium positions when N and $N + 1$ charges are on the island defines a natural lengthscale x_0 of the problem,

$$
x_0 = \frac{-2E_c N_g}{M\Omega^2 d} .
\tag{3.6}
$$

Here, d is the distance separating the oscillator's equilibrium position and the SET island, such that the gate capacitance depends on x like $C_g(x) \sim (d + x)^{-1} \sim 1 - x/d$.

From now on, we will also use dimensionless rates, i.e., all the rates will be given in units of τ_t^{-1}.

Coupling a SET and a nanomechanical oscillator system is readily done by using the oscillator itself as the SET's gate (Sec. 2.2). In this configuration, the capacitive coupling between the oscillator and the SET depends on the distance between them and, by extension, on the oscillator's position, effectively allowing one to monitor the dynamics of the oscillator via the SET. As long as the amplitude of the oscillations around its equilibrium position is small compared to the distance d separating the oscillator and the SET island, the gate capacitance $C_g(x)$ can be treated as linear in x. As a consequence, we obtain position-dependent dimensionless tunneling rates of the form

$$\Gamma_L^{+(-)}(x) = (-)\left[\Delta_L - \kappa\frac{x}{x_0}\right]f\left((-)\left[\Delta_L - \kappa\frac{x}{x_0}\right]eV_{ds}\right)$$
$$\Gamma_R^{+(-)}(x) = (-)\left[\Delta_R + \kappa\frac{x}{x_0}\right]f\left((-)\left[\Delta_R + \kappa\frac{x}{x_0}\right]eV_{ds}\right),$$

(3.7)

where the coefficients[1]

$$\Delta_L = \frac{1}{2} + (2N - 2N_g + 1)\frac{E_c}{eV_{ds}} - \kappa N$$
$$\Delta_R = \frac{1}{2} - (2N - 2N_g + 1)\frac{E_c}{eV_{ds}} + \kappa N$$

(3.8)

are the position-independent part of the full dimensionless rate $\Gamma_i^\sigma(x)$ that fulfill $\Delta_L + \Delta_R = 1$. Here

$$\kappa = M\Omega^2 x_0^2/(eV_{ds})$$

(3.9)

is a dimensionless coupling parameter that will play an important role in the following. Note that Δ_L, Δ_R can become negative in the strong-coupling limit. The average dimensionless current in the presence of position-dependent rates can be calculated as an average of the different rates weighted by the probability to find the oscillator at a position x:

$$I = \int_{-\infty}^{\infty} dx \left(P_{N+1}(x)\Gamma_L^+(x) - P_N(x)\Gamma_L^-(x)\right)$$
$$= \int_{-\infty}^{\infty} dx \left(P_N(x)\Gamma_R^+(x) - P_{N+1}(x)\Gamma_R^-(x)\right),$$

(3.10)

with $P_{N(N+1)}(x)$ the probability to find the oscillator at position x while the island charge state is $N(N+1)$.

---

[1]These coefficients were called Γ_L, Γ_R in Ref. [Armour04b]. Since they are *not* rates (e.g., they can become negative in the strong-coupling limit), we have chosen a different notation

In the zero-temperature limit, the Fermi functions in Eqs. (3.7) are in fact Heaviside step functions that determine the possible transport direction as a function of the position of the oscillator. Indeed, at zero temperature, $x^L = \Delta_L x_0/\kappa$ and $x^R = -\Delta_R x_0/\kappa$ define points where the current direction at lead L and R changes sign. For $x^R < x$, the current in the right junction can only be directed towards the island while in the opposite case only charge transfer from the island to the right lead is possible. Equivalently, transfer through the left junction is allowed from the island to the lead if $x < x^L$ and from the lead to the island otherwise. It is interesting to note that transport can be blocked altogether via this mechanism, leading to so-called 'distortion blockade' [Pistolesi07]. For example, if $N+1$ electrons are on the island and the oscillator is in position $x > x^L$, transport of the extra charge from the island to any lead is effectively forbidden, our choice of bias direction imposing $x^R < x^L$. This possibility is discussed in more detail in Sec. 3.3.

The canonical way of dealing with an SET in the sequential tunneling regime is to introduce a master equation for the different charge states of the island. If the oscillator is coupled to a nanomechanical oscillator, such a simple master equation cannot be written, since the tunneling rates depend on the stochastic evolution of the oscillator. Following Ref. [Armour04b] we can introduce the probability distributions $P_N(x, u; t)$ and $P_{N+1}(x, u; t)$ to find at a time t, the oscillator at position x, u in phase space and the SET in charge state N and $N+1$ respectively and, derive a master equation for these new objects:

$$\frac{\partial}{\partial t} P_N(x, u; t) = \Omega^2 x \frac{\partial}{\partial u} P_N(x, u; t) - u \frac{\partial}{\partial x} P_N(x, u; t) \tag{3.11a}$$
$$+ \left[\Gamma_L^+(x) + \Gamma_R^-(x)\right] P_{N+1}(x, u; t) - \left[\Gamma_R^+(x) + \Gamma_L^-(x)\right] P_N(x, u; t) \, ,$$

$$\frac{\partial}{\partial t} P_{N+1}(x, u; t) = \Omega^2 (x - x_0) \frac{\partial}{\partial u} P_{N+1}(x, u; t) - u \frac{\partial}{\partial x} P_{N+1}(x, u; t) \tag{3.11b}$$
$$- \left[\Gamma_L^+(x) + \Gamma_R^-(x)\right] P_{N+1}(x, u; t) + \left[\Gamma_R^+(x) + \Gamma_L^-(x)\right] P_N(x, u; t) \, .$$

As pointed out in Ref. [Armour04b], when the coupling between the oscillator and the SET is weak ($\kappa \ll 1$) and when the gate voltage V_g is such that the system is tuned far from the Coulomb-blockade region, one can make the approximation that $x^L \to \infty$ and $x^R \to -\infty$ and then write the tunneling rates as

$$\Gamma_L^+(x) = \Delta_L - \kappa \frac{x}{x_0} \, , \qquad \Gamma_L^-(x) = 0 \, ,$$
$$\Gamma_R^+(x) = \Delta_R + \kappa \frac{x}{x_0} \, , \qquad \Gamma_R^-(x) = 0 \, . \tag{3.12}$$

This weak-coupling form of Eq. (3.7) effectively corresponds to neglecting any back-currents and the possibility of position-induced current blockade. However, the master equation is then simple enough to allow analytical solutions.

3.2 Weak-coupling case : Analytic approach to the calculation of transport properties

Originally, the interest in SETs was motivated by the suppression of the current in the Coulomb-blockade regime and the high sensitivity of the current to small variations of the gate voltage. However, it is clear that a complete description of the transport processes in these devices requires not only knowledge of the current, but also of current-current correlations like e.g., the current noise [Hershfield93; Korotkov94]. Recently, higher-order correlations have also been studied both theoretically and experimentally in nanoscale devices, in the framework of full counting statistics (FCS) (see [Nazarov03] for a collection of articles on this topic, and Refs. [Bagrets03; Belzig05] for a description of FCS in the context of transport through SETs). The FCS approach consists in studying the probability distribution $\mathcal{P}_n(t_0)$ that n electrons are transferred through one lead of the SET within a time period t_0, in the limit where t_0 is by far the longest time scale in the problem. The full information about the transport properties is contained in the cumulants of this distribution function, the first three of which are given by the average $\mu_1 = \langle n \rangle$, the variance $\mu_2 = \langle n^2 \rangle - \langle n \rangle^2$, and the skewness $\mu_3 = \langle (n - \langle n \rangle)^3 \rangle$ that measures the asymmetry of the distribution. For example, the current $I = e\langle n \rangle / t_0$ is proportional to the mean of this distribution, while the zero-frequency shot noise power $S(0) = e^2 \mu_2 / t_0$ is determined by its second cumulant.

It is instructive to start by considering the weak-coupling case $\kappa \ll 1$, since in this regime we can calculate the noise and higher cumulants without resorting to Monte Carlo simulations by solving directly for $\langle n^i(t_0) \rangle$ in the long-time limit ($t_0 \gamma \gg 1$). In this section, we generalize the work that was done in [Armour04a] where a method to calculate the current-noise using the moments of the steady-state probability distribution $P_{N(N+1)}(x, u)$ of the oscillator in phase space was described. In this approach, the current-noise is calculated from the solution of the equation of motion of $\langle n^2(t) \rangle$, the average square of the number of charges that went through a lead in a time t. Here, we extend this method for the calculation of higher cumulants by deriving the equation of motion for the general quantity $\langle n^m(t) \rangle$ from which the m−th cumulant can be extracted.

To proceed, we write a master equation for the probability $P^n_{N(N+1)}(x, u; t)$ to find, at time t, the oscillator at position x with velocity u, the island being in charge state $N(N+1)$, and n charges having passed through a lead of the SET in the interval $[0; t]$. We will again make the assumptions leading to Eq. (3.12). Considering for definitiveness the left lead, at zero temperature and neglecting any extrinsic damping, one finds [Armour04a]

$$\frac{\partial}{\partial t}P_N^n(x,u;t) = \Omega^2 x\frac{\partial}{\partial u}P_N^n(x,u;t) - u\frac{\partial}{\partial x}P_N^n(x,u;t)$$
$$+ \Gamma_L^+(x)P_{N+1}^{n-1}(x,u;t) - \Gamma_R^+(x)P_N^n(x,u;t) \ , \tag{3.13a}$$

$$\frac{\partial}{\partial t}P_{N+1}^n(x,u;t) = \Omega^2(x-x_0)\frac{\partial}{\partial u}P_{N+1}^n(x,u;t) - u\frac{\partial}{\partial x}P_{N+1}^n(x,u;t)$$
$$- \Gamma_L^+(x)P_{N+1}^n(x,u;t) + \Gamma_R^+(x)P_N^n(x,u;t) \ . \tag{3.13b}$$

where the rates are taken from Eq. (3.12). Defining the coupled moments $\langle x^j u^k n^m \rangle$ and $\langle x^j u^k n^m \rangle_{N+1}$ as

$$\langle n^m x^j u^k \rangle = \sum_n n^m \int du \int dx\, x^j u^k \left[P_N^n(x,u;\tau) + P_{N+1}^n(x,u;\tau) \right] \ , \tag{3.14a}$$

$$\langle n^m x^j u^k \rangle_{N+1} = \sum_n n^m \int du \int dx\, x^j u^k P_{N+1}^n(x,u;\tau) \ , \tag{3.14b}$$

one can calculate the equation of motion for these quantities using Eq. (3.13). With x in units of x_0 and u in units of u_0, one finds

$$\frac{d}{d\tau}\langle x^j u^k n^m \rangle_{N+1} = -k\epsilon^2 \left[\langle x^{j+1} u^{k-1} n^m \rangle_{N+1} - \langle x^j u^{k-1} n^m \rangle_{N+1} \right] + j\langle x^{j-1} u^{k+1} n^m \rangle_{N+1}$$
$$- \langle x^j u^k n^m \rangle_{N+1} + \Delta_R \langle x^j u^k n^m \rangle + \kappa \langle x^{j+1} u^k n^m \rangle \ , \tag{3.15a}$$

$$\frac{d}{d\tau}\langle x^j u^k n^m \rangle = -k\epsilon^2 \left[\langle x^{j+1} u^{k-1} n^m \rangle - \langle x^j u^{k-1} n^m \rangle_{N+1} \right]$$
$$+ j\langle x^{j-1} u^{k+1} n^m \rangle + \sum_{i=0}^{m-1} \binom{m}{i} \left[\Delta_L \langle x^j u^k n^i \rangle_{N+1} - \kappa \langle x^{j+1} u^k n^i \rangle_{N+1} \right] \ . \tag{3.15b}$$

Here, averages that are independent of n (averages of the form $\langle x^j u^k n^0 \rangle$) are time-independent and can be evaluated in the stationary limit, i.e., Eqs. (3.15a-3.15b) can be used to generate a closed linear system of equations.[2] The terms $\langle x^j u^k \rangle$ of order $j + k = c$ are connected to the terms $\langle x^j u^k \rangle_{N+1}$ of order $j + k = c - 1$. This means that to solve for a moment $\langle x^j u^k \rangle$, we must use the $c + 1$ equations of the type of Eq. (3.15b) where $j + k = c$ and the c equations of the type of Eq. (3.15a) where $j + k = c - 1$. This method can be used to calculate any moment of the form $\langle x^j u^k \rangle$ and $\langle x^j u^k \rangle_{N+1}$. Knowledge of $\langle x^j u^k \rangle$ enables one to calculate the long-time behavior of the coupled moments of the charge and oscillator's position in phase space $\langle x^{j'} u^{k'} n^i \rangle$, and thus the i-th moment $\langle n^i \rangle$ of $\mathcal{P}_n$.

---

[2]These equations agree with the system of equations shown in the Appendix of [Armour04b]; the factor k^2 displayed there is a typo and should read k.

The ratio of the zero-frequency shot noise power and the average current (times e), or equivalently, the ratio of the second and first cumulants of $\mathcal{P}_n$ is called Fano factor and is readily calculated using this approach. Since it shows a complex dependence on the coefficients Δ_L, Δ_R, and on the parameters κ and ϵ, it is convenient to expand the result in powers of κ. Introducing a parameter α defined via $\alpha = \Delta_L - (1+\kappa)/2$ (or, equivalently, $\alpha = -\Delta_R + (1-\kappa)/2$) that measures the difference between Δ_L and its value at the degeneracy point, one can write down the Fano factor in a way that underlines its symmetry with respect to this point:

$$\frac{\overline{S}(0)}{eI} = \frac{1}{2} + 2\alpha^2 + 4\alpha^2\kappa + 6\alpha^2\kappa^2 + \left(\frac{1}{2} - 2\alpha^2\right)\frac{\kappa}{\epsilon^2} - \left(\frac{1}{2} + 2\alpha^2\right)\frac{\kappa^2}{\epsilon^2} + \mathcal{O}(\kappa^3) . \quad (3.16)$$

For $\epsilon \ll 1$, the Fano factor is dominated by the term $\sim \kappa/\epsilon^2$, like in the case where one considers a system of two SETs coupled by an oscillator.[Rodrigues05] Finally, we note that current conservation implies that the Fano factor is identical in both leads.[Blanter00]

Equation (3.15) is one of the main result of this chapter, as it allows for the calculation of higher cumulants of the current by integrating the equation of motion for the moments of the form $\langle x^j u^k n^m(t)\rangle$ with $m > 0$. For example, we calculated the normalized third cumulant $\mu_3/\langle n\rangle$ of $\mathcal{P}_n(t_0)$. The results are presented in Fig. 3.2. We stress that these results have been obtained by integrating the equation motion for $\langle n^3(t)\rangle$ valid in the weak-coupling regime and not via a Monte Carlo simulation. Starting from the value $1/4$ at $\kappa = 0$,[Bagrets03] the normalized third cumulant decreases rapidly when κ is increased. On further increase of κ, it reaches a minimum at an ϵ-dependent value of κ. The inset of Fig. 3.2 shows that the leading contribution to the normalized third cumulant in the weak-coupling regime is of the form ϵ^{-4}. As a consequence, we note that the asymmetry of the probability distribution $\mathcal{P}_n$ that is determined by μ_3, can effectively be tuned by changing the frequency of the oscillator or τ_t. The scaled quantity $\epsilon^4\mu_3/\langle n\rangle$ shows contributions of higher-order corrections in ϵ to the normalized third cumulant.

3.3 Numerical study of the strong coupling regime at the degeneracy point

We now present our numerical investigation of the system beyond the weak-coupling approximation. We note that, in this section, we will not study the effect of extrinsic damping (i.e., a finite quality factor of the oscillator) and of finite temperatures, since they were discussed extensively in [Armour04a; Armour04b].
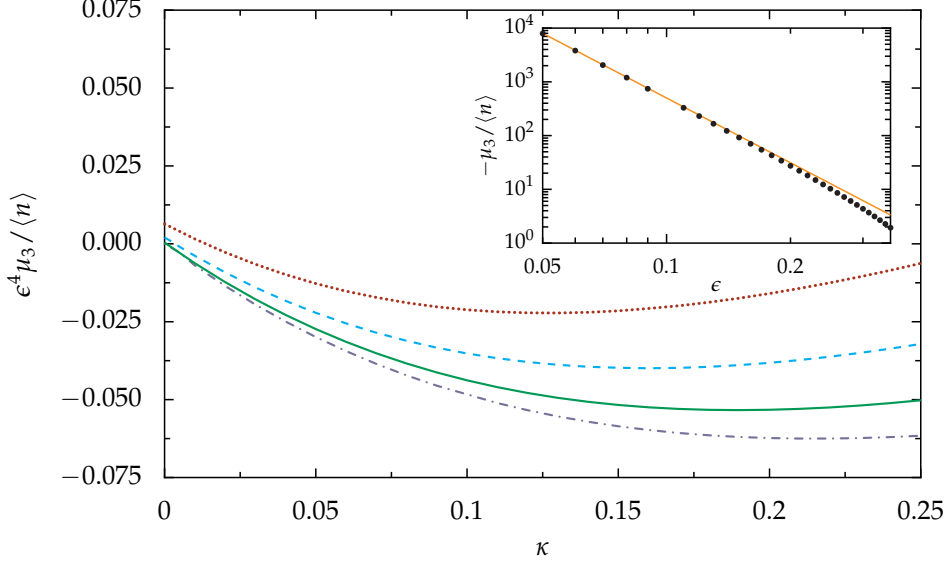
Figure 3.2: Normalized third cumulant as a function of κ for different values of ϵ, as calculated within the weak-coupling approximation and scaled by ϵ^4. Dotted line: $\epsilon = 0.4$, dashed line: $\epsilon = 0.3$, solid line: $\epsilon = 0.2$, dash-dotted line: $\epsilon = 0.1$. The inset shows the ϵ-dependence of the normalized third cumulant at $\kappa = 0.1$ (symbols), as calculated within the weak-coupling approximation. The solid line is a fit to a power law $\sim \epsilon^{-4}$. These results were obtained by integrating the equation of motion for $\langle n^3(t) \rangle$ following from Eq. (3.15).

3.3.1 Dynamics of the oscillator in the strong-coupling regime

In the weak-coupling limit $\kappa \ll 1$, it was found[Armour04b] that the interaction between the SET and the oscillator introduces an intrinsic damping mechanism. The damping, characterized by a decay rate $\gamma = \kappa\epsilon^2$ (in units of τ_t^{-1}) leads to a steady-state solution for the probability distributions $P_{N(N+1)}(x, u)$. In particular, the probability distributions $P_{N(N+1)}(x) = \int du\, P_{N(N+1)}(x, u)$, from which one can calculate the average current, have been shown to be well approximated by Gaussians centered at $x = 0$ and $x = x_0$ for P_N and P_{N+1}, respectively. From this thermal-like stationary state, it was proposed that the back-action of the detector on the resonator could me modeled as an effective thermal bath[Blencowe05a], with associated damping rate $\gamma = \kappa\epsilon^2$ and effective temperature $T_{\text{eff}} = eV_{ds}\langle P \rangle_N \langle P \rangle_{N+1}$. This idea of modeling the back-action of the detector as an effective thermal bath will be a recurring theme throughout this thesis: it will be introduced formally in Sec. 6.1.

One of the main goals of the work presented in this chapter is to study deviations from the weak-coupling behavior. Without the simplifications possible for $\kappa \ll 1$

leading to Eq. (3.12), the stationary probability distributions $P_{N(N+1)}(x, u)$ can no longer be investigated analytically and numerical methods must be used. In this work, we used a Monte Carlo approach to simulate the stochastic nature of the SET-nanomechanical oscillator system in the parameter regime where the typical mechanical energy $M\Omega^2 x_0^2$ is comparable to the bias energy eV_{ds}. Details of our implementation of the Monte Carlo method are given in Sec. 3.6.

We study the probability distribution of the oscillator in the charge-degenerate case, where $\langle P_N \rangle = \langle P_{N+1} \rangle$, with $\langle P_N \rangle = \int dx P_N(x)$. At this point, the current flowing through the SET is maximal. In the presence of the oscillator, charge degeneracy is reached when $\Delta_L = 1/2 + \kappa/2$. This relation, exact in the weak-coupling limit, has been empirically verified over the whole range of κ studied. In the weak-coupling limit, this relation can be shown using $\langle P_{N+1} \rangle = \Delta_R$. In our case, at the degeneracy point symmetry considerations impose $\langle x \rangle = x_0/2$ and the position dependence of the rate $\Gamma_R^+(x)$ must be taken into account, such that $\langle P_{N+1} \rangle = \frac{1}{2} = \Delta_R + \kappa \langle x/x_0 \rangle$. This effectively corresponds to $\langle P_{N+1} \rangle = \Delta_L - \kappa/2$.

As can be seen from Fig. 3.3, as κ is increased, the stationary position probability distribution evolves continuously from the weak-coupling Gaussian form to a distribution showing two sharp peaks at $x = 0$ and $x = x_0$ in the limit where $\kappa = 1$. This evolution is the result of a sharpening of each of the two subdistributions $P_{N(N+1)}(x)$ around their equilibrium position when κ is increased, allowing one to resolve the two subdistributions individually. This should not only be seen as natural consequence of the fact that the typical distance x_0 scales like $\sqrt{\kappa}$. In fact, the main cause of the appearance of the two sharp peaks is that small amplitude oscillations about each of the two equilibrium points become very stable when κ is increased.

We also note that the qualitative shape of each subdistribution evolve when κ is increased. While at low coupling the subdistribution $P_N(x)$ (resp. $P_{N+1}(x)$) is symmetric about $x = 0$ (resp. $x = x_0$), this is not the case for $\kappa \gtrsim 0.4$. This asymmetry arises only at higher coupling since for low κ, the probability to find the oscillator at $x < x^R$ or $x > x^L$ is negligible. When $\kappa \gtrsim 0.4$, the probability of the oscillator being in a region transport is forbidden becomes important. Symmetry breaking arises since these regions are located only on one side of each equilibrium point.

Finally, we note that the important changes in $P_{N(N+1)}(x)$ that accompany a variation in κ are also seen in the stationary velocity subdistributions $P_{N(N+1)}(u) = \int du P_{N(N+1)}(x, u)$. These are approximatively given by $P_N(u/\epsilon u_0) \simeq P_N(x/x_0)$ and $P_{N+1}(u/\epsilon u_0) \simeq P_{N+1}((x - x_0)/x_0)$, where $u_0 = x_0/\tau_t$ is the typical velocity scale in the problem.

For $\kappa > 1$, our numerical investigations show that the current is strongly suppressed, rendering the intrinsic damping mechanism discussed at the beginning of this section ineffective. In this case, the system cannot be characterized by a steady-
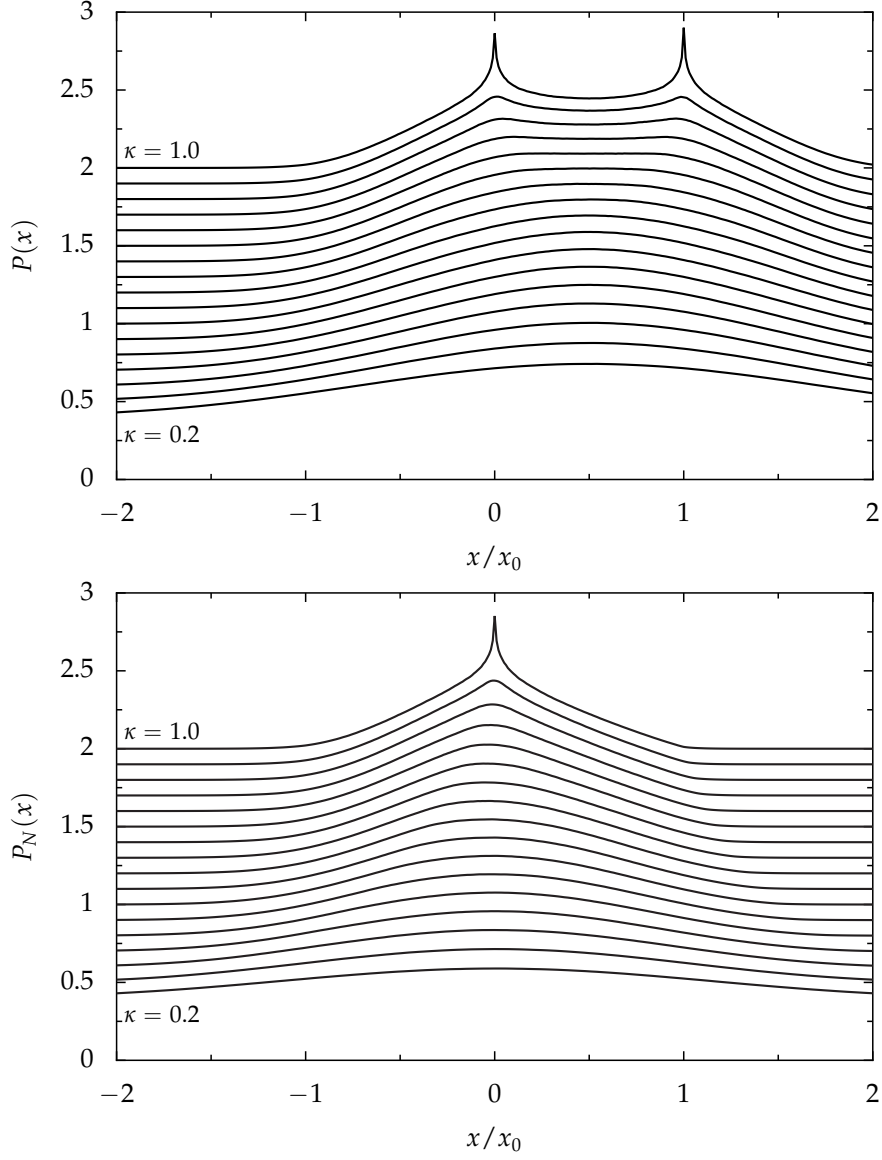
Figure 3.3: Upper panel: Total probability distribution $P(x) = P_N(x) + P_{N+1}(x)$ of the oscillator's position for different values of the coupling constant κ [Eq. (3.9)]. Lower panel: Probability distribution $P_N(x)$ to find the oscillator at position x if the SET is in charge state N. $P_{N+1}(x)$ can be obtained by the symmetry relation $P_{N+1}(x) = P_N(1/2 - x)$. In both panels, lines are shifted for clarity by 2κ, and the difference between neighboring curves is $\Delta\kappa = 0.05$. All calculations were done at $\epsilon = 0.3$ and at the charge-degeneracy point. For the definition of ϵ, see Eq. (3.5).
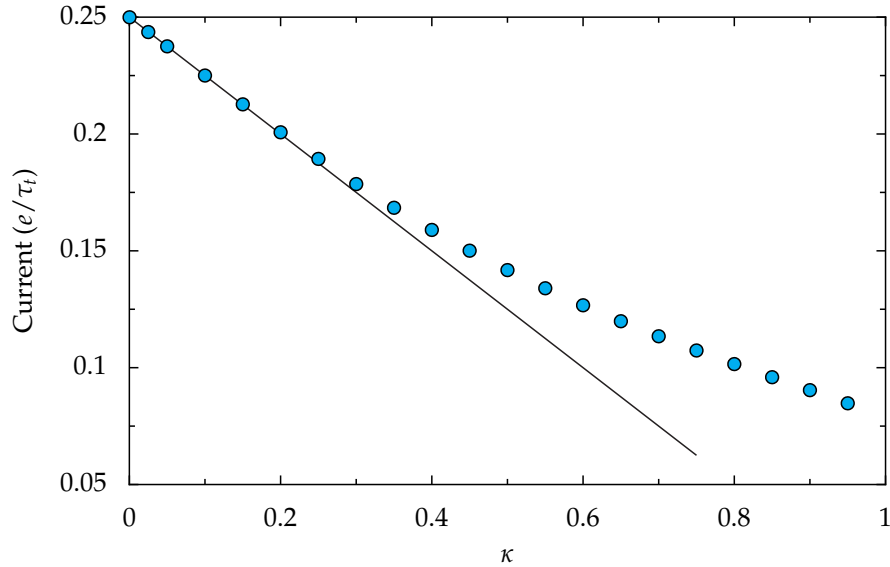
Figure 3.4: Current (in units of e/τ_t) as a function of κ at the degeneracy point $\langle P_N \rangle = \langle P_{N+1} \rangle$, for $\epsilon = 0.3$. The dots are the results of the Monte Carlo calculation and the solid line is the analytic form found within the weak-coupling approximation.

state probability distribution, and our model is not appropriate. Therefore, we only studied the parameter range $\kappa \leq 1$. A similar reasoning applies to Coulomb-blockade region, where the damping of the oscillator's motion is severely suppressed.

3.3.2 Average current

The average current flowing through the SET is closely tied to the oscillator's position distributions via the position-dependent tunneling rates. Consequently, one expects that the deviations from the weak-coupling behavior observed in $P(x) = P_N(x) + P_{N+1}(x)$ would affect the current characteristics when κ is increased.

Just like in the previous section, we focus on the degeneracy point where the average charge state of the island is $N + 1/2$. At this point, the weak-coupling theory predicts[Armour04b] that the current decreases linearly with increasing κ: $I = \frac{1-\kappa}{4}(e/\tau_t)$. This decrease in the current can be explained in a qualitative way by the reduction of the overlap of the distributions $P_N(x)$ and $P_{N+1}(x)$ as the coupling is increased, each distribution becoming more localized around its equilibrium point, see Fig. 3.3.

Figure 3.4 shows the average current as a function of κ. Like in the weak-coupling limit, the localization of the different probability distributions around its equilib-

rium points leads to an overall decrease in the current when the coupling grows stronger. For $\kappa \gtrsim 0.3$, however, we see that the numerical results deviate from the weak-coupling behavior: for stronger coupling the current is higher than the weak-coupling result. This can be explained using the rates given by Eq. (3.12). When either $\int_{x^L}^{\infty} dx\, P_{N+1}$ or $\int_{-\infty}^{x^R} dx\, P_N$ is not negligible, these rates allow unphysical backward currents that are not present in the full master equation. For example, a point located at $x > x^L$ in the steady-state probability distribution $P_{N+1}(x, u)$ would contribute negatively to the average current when using the rates calculated within the weak-coupling approximation while it would not contribute to the current when taking into account the full expression for the rates given in Eq. (3.8).

Over the range of frequencies that we studied numerically ($0.1 \leqslant \epsilon \leqslant 0.4$), the current was found to be practically independent of ϵ for all but the strongest couplings ($\kappa \gtrsim 0.8$). For instance, at $\kappa = 0.9$, the difference between the calculated currents at $\epsilon = 0.1$ and $\epsilon = 0.4$ is on the order of a few percent.

3.3.3 Zero-frequency noise and higher cumulants

In this section, we study in detail the second and third cumulants of the probability distribution function $\mathcal{P}_n(t_0)$ in the case of a coupled SET-nanomechanical system.

It is unfortunately not straightforward to generalize the method described in Sec. 3.2 for calculating the cumulants of $\mathcal{P}_n$ outside the weak-coupling regime. The presence of x-dependent Fermi functions in the tunneling rates as well as the possibility of charge flow against the direction set by the bias voltage due to the position of the oscillator gives rise to a system of equations that is not closed and cannot be solved analytically. Even if we neglect transport against the dominant direction of the current $\Gamma_j^-(x) \simeq 0$, but keep the position dependence of the Fermi distributions in $\Gamma_j^+(x)$, it is still not possible to derive a system of equations coupling only objects of the form $\langle x^j u^k n^m \rangle$. Therefore, we will use a numerical approach to evaluate the cumulants of $\mathcal{P}_n$.

Indeed, the Monte Carlo method described in Sec. 3.6 can be used to measure the FCS of electron transport, analogously to the experimental approach used in [Gustavsson06]. A very long Monte Carlo run is divided into intervals of duration $t_0 \gg \gamma^{-1}$, here, $\gamma = \kappa \epsilon^2$ is the damping constant defined at the beginning of Sec. 3.3.1; γ^{-1} is the longest intrinsic time scale of the problem. By counting the number of charges going through one lead during each interval, one can reconstruct the probability distribution $\mathcal{P}_n(t_0)$, and from it calculate the cumulants.

We study current correlations at the charge degeneracy point, where the average charge state of the island is $N + 1/2$. The top panel of Fig. 3.5 compares the weak-coupling Fano factor to the numerical Monte Carlo results for different values of the

coupling parameter κ. Naturally, for $\kappa \lesssim 0.2$, the agreement between the numerical results and those obtained analytically is very good. Beyond this point, the numerically calculated Fano factor shows an interesting non-monotonic behavior, with a maximum at $\kappa \sim 0.35$ and a minimum at $\kappa \sim 0.85$. The lower panel of Fig. 3.5 also shows the evolution of the normalized third cumulant of $\mathcal{P}_n$, giving the asymmetry of this probability distribution about its mean $\langle n \rangle$. Starting from the $\kappa = 0$ value of $1/4$ derived for a simple SET device, our results show that this quantity is, in the weak-coupling limit, very sensitive to variations of κ. Indeed, the normalized third cumulant changes sign twice in the region $\kappa \lesssim 0.35$, reaching a maximum value approximatively in the middle of this region. This contrasts with the strong-coupling behavior: $\mu_3 / \langle n \rangle$ stays practically constant for $0.5 \lesssim \kappa \lesssim 0.9$.

We will now address the question of the dependence of the previous results on the frequency of the oscillator. Figure 3.6 shows the dependence of the Fano factor and the normalized third cumulant as a function of κ for different values of ϵ. First, we note that the actual value of the Fano factor is increased dramatically for lower oscillator frequencies, as expected from the term $\sim \kappa / \epsilon^2$ that dominates in the low-frequency regime. In the weak-coupling region ($\kappa \lesssim 0.3$), the magnitude of the normalized third cumulant is also heavily affected by a change in frequency, in agreement with the weak-coupling leading order dependence $\sim \epsilon^{-4}$. Despite these major changes in magnitude of both the Fano factor and the normalized third cumulant, the overall qualitative effect of an increase in coupling does not seem to depend heavily on ϵ, in the frequency range we investigated. In particular, the position of the maximum in the Fano factor remains constant. Also, the normalized third cumulant always shows a change of sign, albeit at an ϵ-dependent value of κ, and goes to a positive for $\kappa \to 1$. Remarkably, the value of the normalized third cumulant is much less sensitive to ϵ in the strong-coupling regime. This might be the signature of a transport regime in the $\kappa \to 1$ region that is radically different of the one found for $\kappa \simeq 0.2$.

3.3.4 Frequency-dependent noise

In systems that exhibit internal dynamics like the one we study, it is especially interesting to look at the frequency-dependence of the current-current correlations. In Ref. [Armour04a], the frequency-dependent noise $S(\omega)$ of a SET weakly coupled to a nanomechanical oscillator was thoroughly studied. It was found that, the noise spectrum shows only two peaks at finite frequency at Ω' and $2\Omega'$, where $\Omega' = \Omega\sqrt{1 - \kappa}$ is the effective frequency of the damped harmonic oscillator. In this section, we extend the work of Ref. [Armour04a] by studying the frequency-dependent noise power $S(\omega)$ in the strong-coupling regime ($0.2 \lesssim \kappa < 1$).
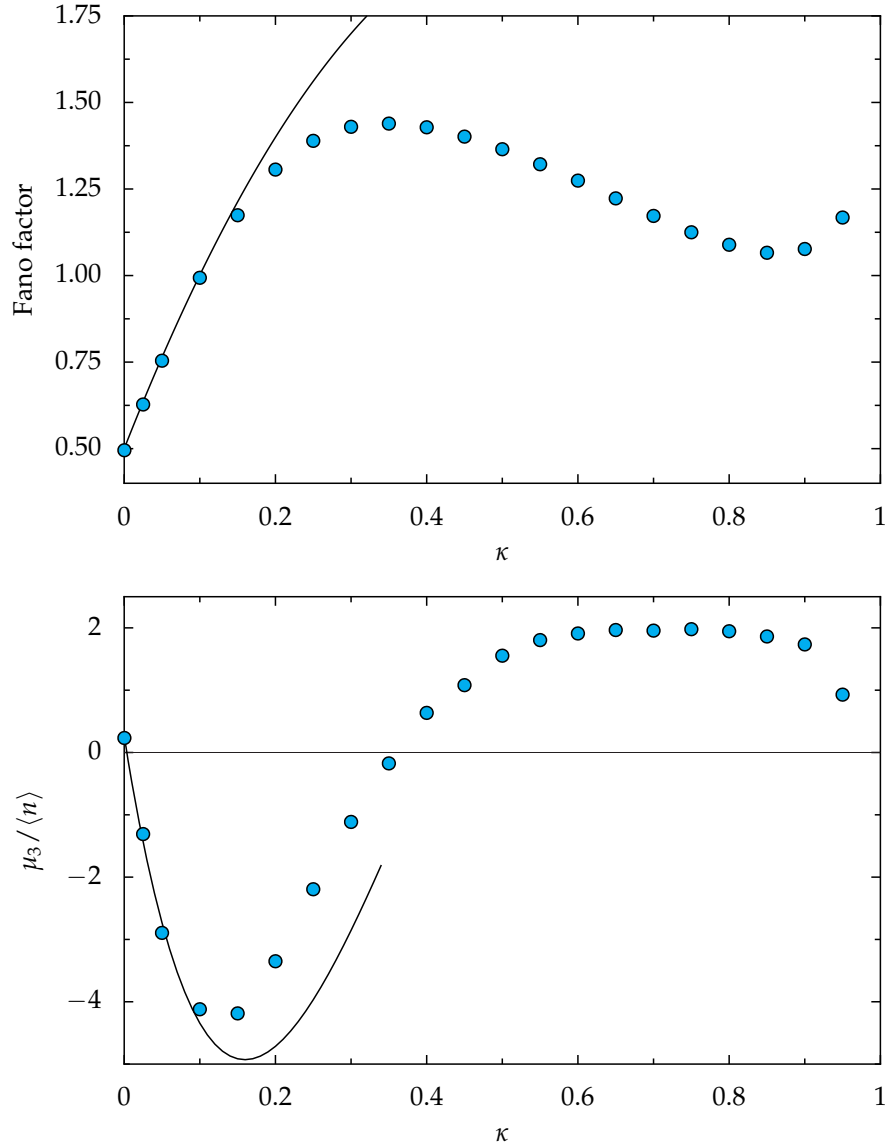
Figure 3.5: Upper panel: Fano factor as a function of κ at the degeneracy point $\langle P_N \rangle = \langle P_{N+1} \rangle$. The dots are the results of the numerical calculation and the solid line is the analytic form found within the weak-coupling approximation. Lower panel: Normalized third cumulant μ_3 of the probability distribution $\mathcal{P}_n$. For both panels, $\epsilon = 0.3$.
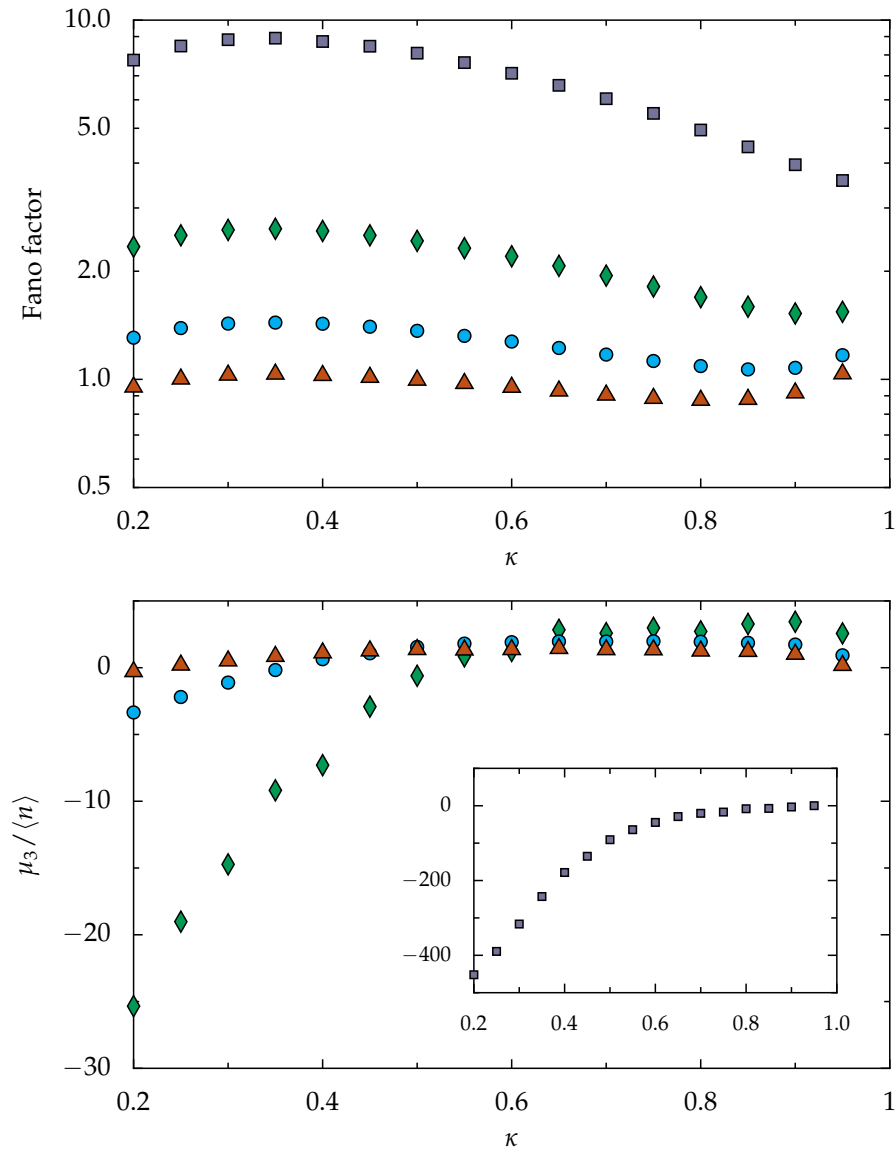
Figure 3.6: Fano factor (upper panel) and normalized third cumulant (lower panel and inset) as a function of κ for different values of ϵ: $\epsilon = 0.1$ (squares in the upper panel and in the inset), $\epsilon = 0.2$ (diamonds), $\epsilon = 0.3$ (circles), and $\epsilon = 0.4$ (triangles). Note the logarithmic y-axis in the upper panel.

In order to calculate the frequency-dependent noise using our Monte Carlo method, we follow the approach developed by MacDonald [Appendix A] that was used recently to study the noise properties of mesoscopic systems, including coupled SET-nanomechanical systems in the weak-coupling regime. In general, the symmetrized-in-frequency current noise power at junction i is defined as (see Chap. 4)

$$\overline{S}_{i,i}(\omega) = \frac{1}{2} \int_{-\infty}^{\infty} d\tau \, e^{i\omega\tau} \langle \{\delta I_i(\tau), \delta I_i(0)\} \rangle \, , \qquad (3.17)$$

To proceed with the MacDonald approach, $\delta I_i = I_i - \langle I_i \rangle$, must be assumed to be a statistically fluctuating variable, such that the autocorrelation function $\langle \delta I_i(\tau), \delta I_i(0) \rangle$ is independent of t. In this case, the MacDonald formula relates the fluctuation δn about the average of the number of charges n that went through a junction in time τ,

$$\delta n_i(\tau) = n_i(\tau) - \langle I_i \rangle \tau = \int_t^{t+\tau} dt' \left(I_i(t') - \langle I_i \rangle \right) \, , \qquad (3.18)$$

to the current-noise power via

$$\overline{S}_{i,i}(\omega) = \omega \int_0^{\infty} d\tau \, \sin(\omega\tau) \frac{\partial}{\partial\tau} \langle (\delta n_i(\tau))^2 \rangle \, , \qquad (3.19)$$

where $\langle (\delta n_i(\tau))^2 \rangle = \langle n_i^2(\tau) \rangle - \langle I_i \rangle^2 \tau^2$. Since $\langle n^2(\tau) \rangle$ and $\langle I_i \rangle$ are easily accessible through the Monte Carlo simulation, $S(\omega)$ can be calculated by taking a numerical time-derivative of $\langle (\delta n_i(\tau))^2 \rangle$ and then evaluating the Fourier sine-transform. Note that we consider only the particle current fluctuations here. The electrical current noise at finite frequencies includes a contribution from displacement currents, which depend on the capacitive couplings between the island and the leads[Blanter00]. Since we assume that our frequencies of interest are much smaller than the relevant RC-frequencies, we can neglect the displacement currents here, see e.g. the discussion in Refs. [Cottet04b; Cottet04a].

The results of the Monte Carlo simulation are shown in Fig. 3.7. Like in the weak-coupling case, $\overline{S}(\omega)$ shows two main finite-frequency features. Surprisingly, even for strong coupling, we do not find any features for frequencies higher than 2Ω. We find a low-frequency peak that defines the frequency Ω' (which will be different from the weak-coupling prediction $\Omega\sqrt{1-\kappa}$ in the general case). The second feature evolves from the peak located at $2\Omega'$ predicted by the weak-coupling theory. While both peaks are considerably broadened by an increase in the coupling strength, their respective shapes evolve in a qualitatively different way. Whereas the first peak is shifted in absolute frequency, the second peak broadens in a very asymmetric way, with much of the weight shifting to lower frequencies. The slope of its left shoulder decreases with increasing κ until it forms a plateau at around $\kappa \sim 0.7$. On increasing κ even
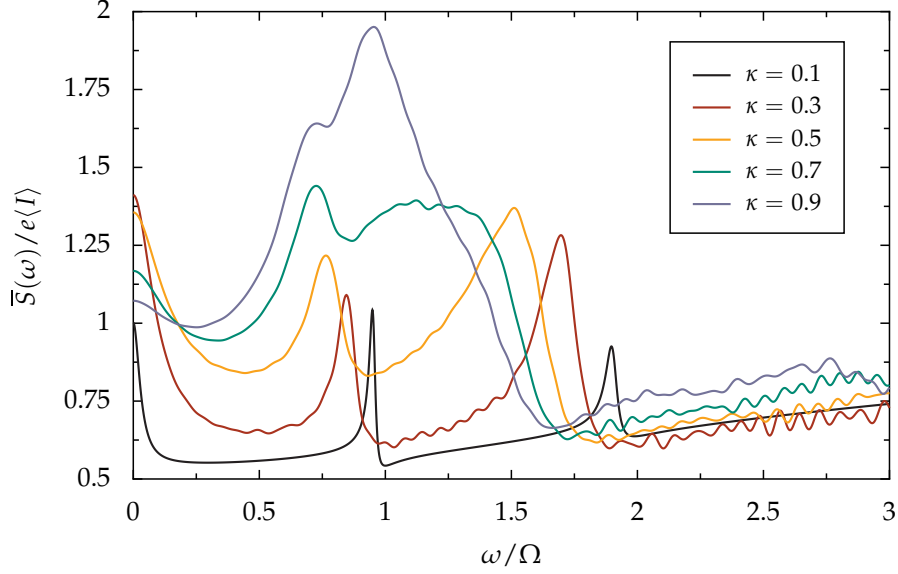
Figure 3.7: Frequency-dependent noise power in the strong-coupling regime. In each curve, the SET is tuned to the charge-degeneracy point and $\epsilon = 0.3$.

further, the two peaks merge, leading to super-Poissonian frequency-dependent noise throughout the frequency range $\omega < 1.5\Omega$.

Figure 3.8 shows the position of the maxima of the first peak in the frequency-dependent noise power as a function of κ. By comparing the position of the first peak extracted from the curves shown in Fig. 3.7 (data points in Fig. 3.8) to the weak-coupling prediction $\Omega' = \Omega\sqrt{1-\kappa}$ (solid line in Fig. 3.8), we find quantitative agreement only for $\kappa \lesssim 0.2$. Beyond this point, the ratio Ω'/Ω still decreases, albeit slowly, when κ is increased. It reaches a saturation value $\Omega' \sim 0.7\Omega$ for $\kappa \gtrsim 0.7$.

This behavior can be understood by interpreting the frequency shift in terms of an effective damping mechanism caused by electron tunneling. Since there is no damping without current, the natural modification of the weak-coupling damping constant $\gamma = \kappa\epsilon^2$ in the strong-coupling regime is to renormalize the weak-coupling result by the probability P^* to find the oscillator in a position where in principle current is allowed, i.e., for $x^R < x$ and charge state N, or $x < x^L$ and charge state $N+1$. Defining a renormalized damping constant $\gamma^{sc} = P^*\kappa\epsilon^2$, it is possible to estimate the position of the first peak as a function of κ using values of P^* extracted from curves presented in Fig. 3.3. The result is shown as the dashed curve in Fig. 3.8 and agrees with the data points obtained by the Monte Carlo method in a quantitative way.
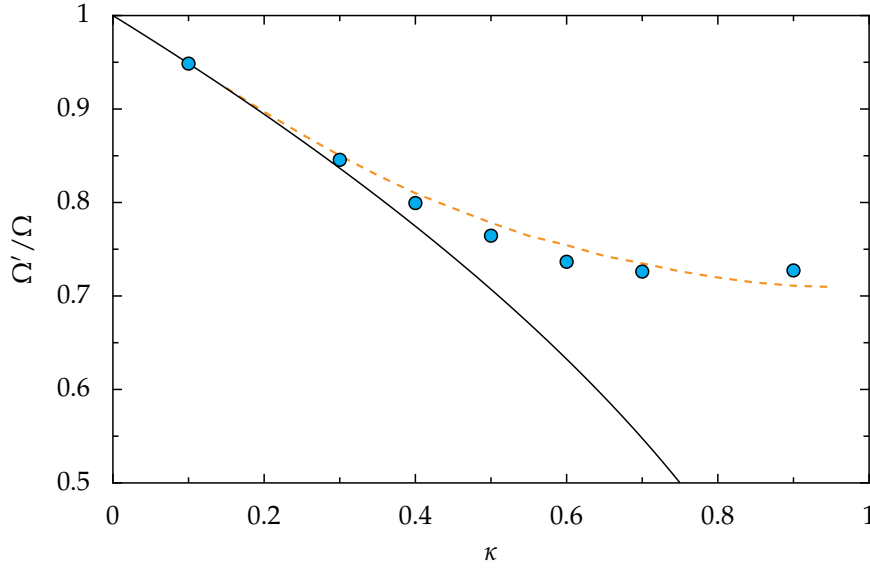
Figure 3.8: Position Ω' of the first peak in the frequency-dependent noise power as a function of κ. The solid line gives the weak-coupling prediction $\Omega\sqrt{1-\kappa}$, the data points are the numerical Monte Carlo results, and the dashed line was obtained using an effective damping constant, see text.

3.4 Numerical study of the transport properties away from the degeneracy point

The numerical results presented thus far explained how the strong oscilllator-SET coupling affects the electronic transport when the SET is gated at the degeneracy point $\langle N \rangle = 1/2$, where current is maximal. This is the point where one can expect the weak-coupling approximation to be the most accurate, since away from this point the approximation used to get from Eq. (3.7) to Eq. (3.12) is less likely to be valid. In this section, we present a numerical investigation how of the oscillator affects the transport properties of the SET when $\langle N \rangle \neq 1/2$.

Like in Eq. (3.16), we will consider a change in the gate voltage via the asymmetry parameter $\alpha = \Delta_L - (1+\kappa)/2$. Figure 3.9 shows the calculated average current as a function of α for different coupling strengths. Strikingly, $I(\alpha)$ shows a pronounced discontinuity at $\alpha = \pm(1-\kappa)/2$. Beyond this point, the current vanishes completely for all values of κ. This blockade of purely mechanical origin, and was coined 'distortion-blockade' by some authors [Pistolesi07].[3] It can be seen as a classical analogue of the Franck-Condon blockade, responsible for current suppression in sys-

---

[3]The original title of Ref. [Pistolesi07] was *Distortion blockade in a classical nano-electromechanical resonator*.
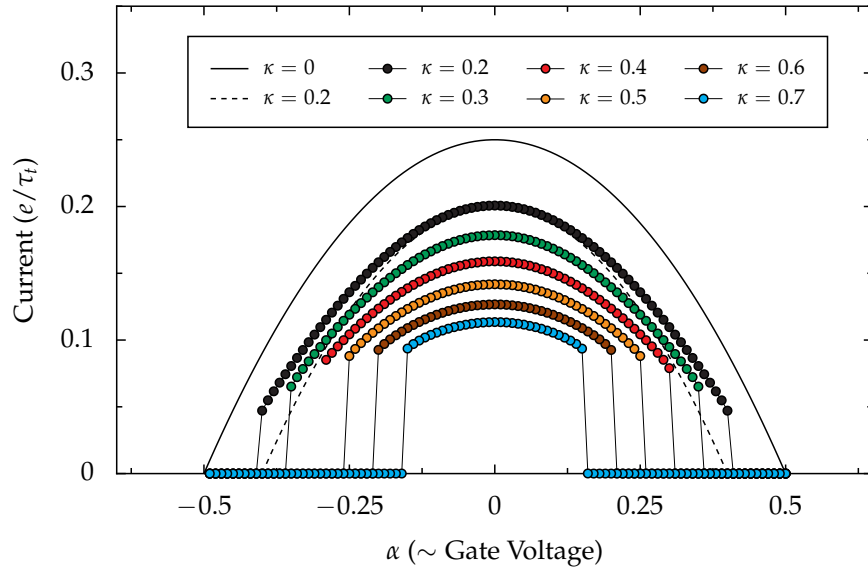
Figure 3.9: Average current as a function of the asymmetry parameter ($\sim$ gate voltage), for different coupling strengths. The solid line is the analytical result for $\kappa = 0$, and the dashed line the average current for $\kappa = 0.2$ within the weak-coupling approximation. All the numerical curves show a pronounced discontinuity: when the asymmetry parameter reaches a (κ-dependent) threshold value, the current is heavily suppressed.

tems with strong electron-phonon interaction like, for example, some single-molecule devices[Braig03; Weig04; Koch05; Koch06; Mozyrsky06]. These results should be compared with the analytic form for the current in the weak coupling regime that can be calculated from Eq. (3.10),

$$\langle I \rangle = \frac{(\frac{1-\kappa}{2})^2 - \alpha^2}{1 - \kappa} . \tag{3.20}$$

In Fig. 3.9, we plotted the weak-coupling result for $\kappa = 0.2$, as the dashed-dotted line. As discussed earlier, the agreement with the numerical results soon gets worse as the system is tuned away from the degeneracy point. As discussed in Sec. 3.3.2, this disagreement is again due to unphysical counter-currents that do are not included in the original master equation but that are introduced in the weak-coupling approximation when Eq. (3.12) becomes violated. Also, the weak-coupling approximation does not capture the discontinuity in the average current that occurs when the asymmetry in increased.

The relative simplicity of our classical system allows for a simple interpretation of the current suppression. For transport to happen, the system must be allowed to
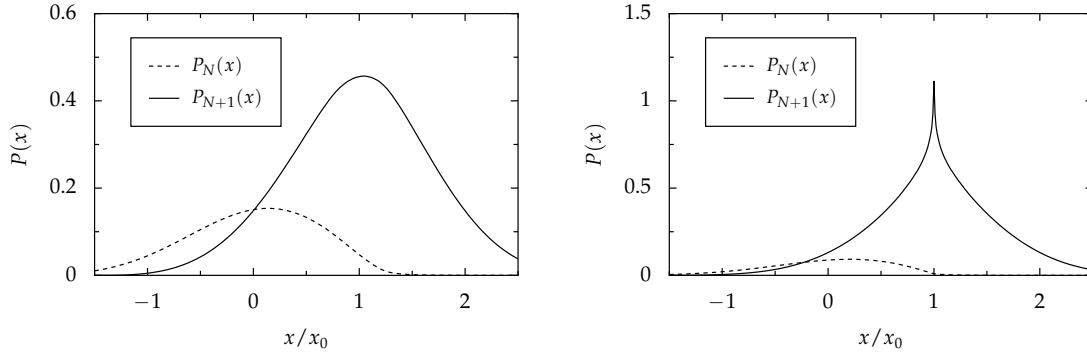
Figure 3.10: Left panel: $P_{N(N+1)}(x)$ for for $\kappa = 0.4$ and $\alpha = -0.2$, relatively close to the discontinuity. Right panel: $P_{N(N+1)}(x)$ for for $\kappa = 0.4$ and $\alpha = -0.3$, at the discontinuity.

fluctuate between the N and $N+1$ charge states. Just before the discontinuity, the system is on average strongly localized close to the equilibrium position of the oscillator associated with one of the two charge states, depending on the sign of α. This can be seen from Fig. 3.10, where $P_N(x)$ and $P_{N+1}(x)$ is plotted both close to the discontinuity and at the last point before the current suppression. For charge transport to happen, the charge state of the island must oscillate between N and $N+1$. However, a change of charge state in our model is associated with a change of the equilibrium position of the oscillator. On top of the usual electrical energy cost associated with charge transfer, there is therefore a mechanical energy barrier that must be overcome for transport to happen (the $\propto \kappa$ term in Eq. (3.7)). To illustrate this, let us look more closely at the situation depicted in the right panel of Fig. 3.10, in the case where there are $N+1$ charges on the island and the oscillator is almost localized at $x = x_0$. In this case, $\Gamma_L^+ = \Delta_L - \kappa x/x_0 = \alpha + (\kappa + 1)/2 - \kappa x/x_0$, such that for $x \sim x_0$, $\Gamma_L^+ \sim 0$. The situation is similar for Γ_L^-, such that overall in this case the transport is heavily suppressed. In this case, the configuration with $N+1$ charges on the island and $x \sim x_0$ is therefore quite stable[4]. Once the $N+1 \rightarrow N$ transition occurs, a finite current can flow through the island for a considerable time, until the $N \rightarrow N+1$ transition happens at the same time as $x \sim x_0$. Close to the threshold value for α, the system therefore exhibits bistability, switching between current-carrying and current-blocking states.

---

[4]By *quite stable*, we mean *not completely stable*, as, in a numerical experiment, x never is identically x_0.

3.4.1 Analysis of the bistability regime

We can analyze this bistable behavior more quantitatively. In the bistable regime, transport properties can be written in terms of the switching rates between the two states and the average current in each state. Noting "1" the current-carrying state and "0" the state where current is suppressed, the total average current through the system is given by the current in state 1 weighted by the probability to be in state 1,[Jordan04]

$$\langle I \rangle = \frac{\Gamma_{0,1}}{\Gamma_{0,1} + \Gamma_{1,0}} I_1 \tag{3.21}$$

where $\Gamma_{i,j}$ is the rate at which the system switches from state i to j and I_1 is the average current in state 1. In the last expression, we assumed that the current in the 'off-state' (0) is $I_0 \sim 0$. The discontinuity in the current for $|\alpha|$ greater than the threshold value needs to be interpreted as $\Gamma_{0,1}(\alpha) \propto \Theta[(1-\kappa)/2 - |\alpha|]$. Beyond a threshold value for α, the off-state is, at least at zero temperature, stable: once the system reaches it, it does not switch back to the on-state.

The signature of this bistable regime can be seen in the current noise [Jordan04; Flindt05b; Pistolesi07; Harvey08], where an added telegraph-type contribution to the noise[Machlup54] leads to a significant enhancement of the Fano factor close to the threshold[5]. Taking $I_0 = 0$, the full Fano factor can be written as a sum of two contributions[Jordan04]: (i) the noise associated with I_1 (noted F_1), weighted by the probability to find the system in this state, and (ii) the telegraph-noise associated with the switching between the two metastable states

$$F = \frac{\Gamma_{0,1}}{\Gamma_{0,1} + \Gamma_{1,0}} F_1 + \left(I_1 \frac{\tau_t}{e} \right) \frac{\Gamma_{1,0} \tau_t}{(\Gamma_{0,1} \tau_t + \Gamma_{1,0} \tau_t)^2} \ . \tag{3.22}$$

When the typical timescale between switching events is much longer than τ_t (ie., when $\Gamma_{ij}\tau_t \ll 1$), then the telegraph-noise contribution dominates. Beyond the threshold, taking $\Gamma_{0,1} = 0$, then the Fano factor becomes $\propto (\Gamma_{1,0}\tau_t)^{-1}$ and the important difference between the typical electronic transport timescale τ_t and the switching timescale $\Gamma_{1,0}^{-1}$ leads to a considerable increase in the Fano factor. As depicted in Fig. 3.11, this scenario is confirmed numerically. We can try to estimate the switching rate $\Gamma_{0,1}$, by adopting the point of view that a potential barrier separates the current-carrying (1) state from the localized state where current is blocked (0) [Pistolesi07]. Indeed, we know that the $N+1 \rightarrow N$ charge transfer can happen for all $x < x^L$, with $x^L = x_0 \Delta_L / \kappa$ as defined earlier. In other words, the $0 \rightarrow 1$ transition is allowed only when the oscillator's energy $E > E_b$, with $E_b \equiv m\omega^2(x^L - x_0)^2$. The energy E_b can be seen as a

---

[5]The Monte Carlo procedure used is not adapted to the evaluation of the Fano factor in the region where current is suppressed. In this case the calculation of the Fano factor involves the numerical evaluation of the ratio of two very small quantities. For $a \rightarrow 0, b \rightarrow 0$ expression of the kind a/b are numerically very badly behaved.
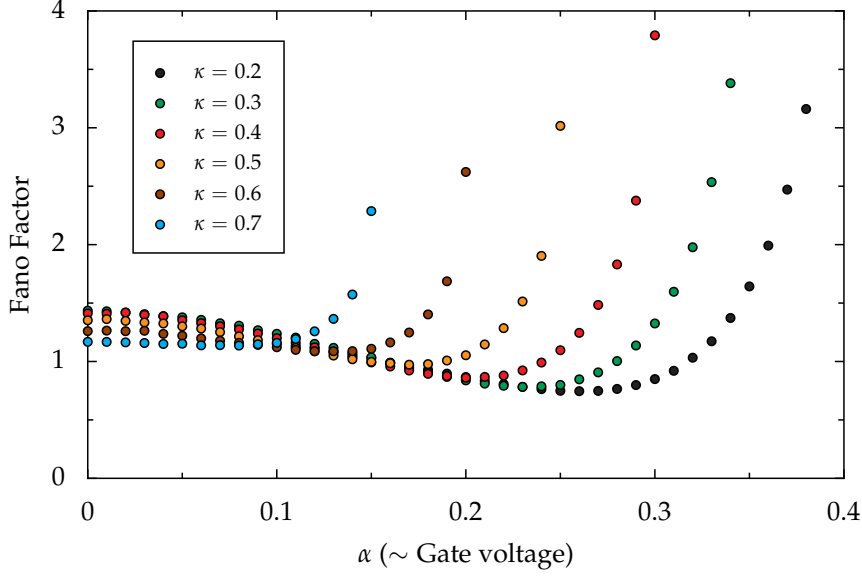
Figure 3.11: Fano factor as a function of the asymmetry parameter ($\sim$ gate voltage), for different coupling strengths. For each value of κ, the Fano factor diverges when $|\alpha|$ approaches the critical value $\alpha_c(\kappa) = (\kappa + 1)/2$. The results are symmetric with respect to $\alpha = 0$. Due to numerical limitations, the Fano factor was calculated only in the range of α where the average current is non-zero.

potential barrier that must be overcome for transport to happen. It can be rewritten in terms of the difference between α and the critical value $\alpha_c(\kappa) = (\kappa + 1)/2$ where the current displays the discontinuity at zero temperature

$$E_b(\kappa) = \frac{1}{\kappa}\theta[|\alpha| - |\alpha_c(\kappa)|]\left(|\alpha| - |\alpha_c(\kappa)|\right)^2 \tag{3.23}$$

3.4.2 Finite-temperature studies

In a classical system at zero temperature, the effective potential barrier separating the localized and current carrying states can never be overcome unless $E - \Delta_0 > 0$, making it difficult to estimate the relevance of the energy scale E_b. The zero-temperature results merely indicate the presence of such a potential barrier without allowing to probe its dependence on system parameters. However, at finite temperatures the situation is quite different, as thermal fluctuation enable the barrier to be crossed. To estimate the rate $\Gamma_{0\rightarrow 1}$ at which thermal fluctuation bring the system over the barrier, we can use Kramer's reaction rate theory [Kramers40; Hänggi90] whose main result
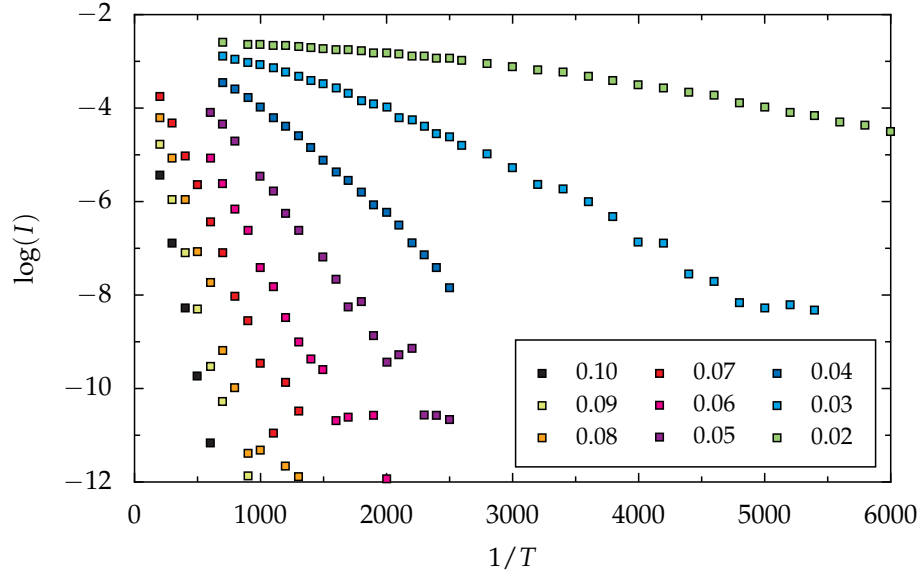
Figure 3.12: Natural logarithm of the current in units of e/τ_t as a function of the inverse of the bath temperature eV/k_BT for different values of the "distance to the current discontinuity" $|\alpha| - |\alpha_c(\kappa)|$ (number given in the legend). System parameters used for this plot: $\kappa = 0.6$, $\epsilon = 0.3$, and weak external damping $\gamma_0 = \kappa\epsilon^2/100$.

states that

$$\Gamma_{0,1} \sim A e^{-\frac{E_b}{k_BT}} , \tag{3.24}$$

with the pre-factor A typically depending on the shape of the potential configuration and details of the problem. Thermally activated escape from the potential minimum is exponentially suppressed when the temperature is much lower than the barrier's height, a result also known as Arrhenius's law. By running Monte Carlo simulations with the oscillator coupled to a thermal bath at finite temperature (see Sec. 3.6.1 for details), we could test our model for E_b, as well as test whether the features encountered earlier survive at finite temperatures.

The Arrhenius plot presented in Fig. 3.12 confirms that, at low temperatures and for all values of the asymmetry parameter α, the transport is mainly due to thermally activated switching to the current-carrying state of the SET. Indeed, for low currents, the logarithm of the current (taken in units of e/τ_t) behaves like a linear function of the inverse temperature. Due to the relatively high number of simulations needed to create this figure, each point was estimated from an average over only 50000 runs. Combined with the fact that the current is displayed on a logarithmic scale that magnifies the numerical imprecisions at low current, this explains the pretty large scatter
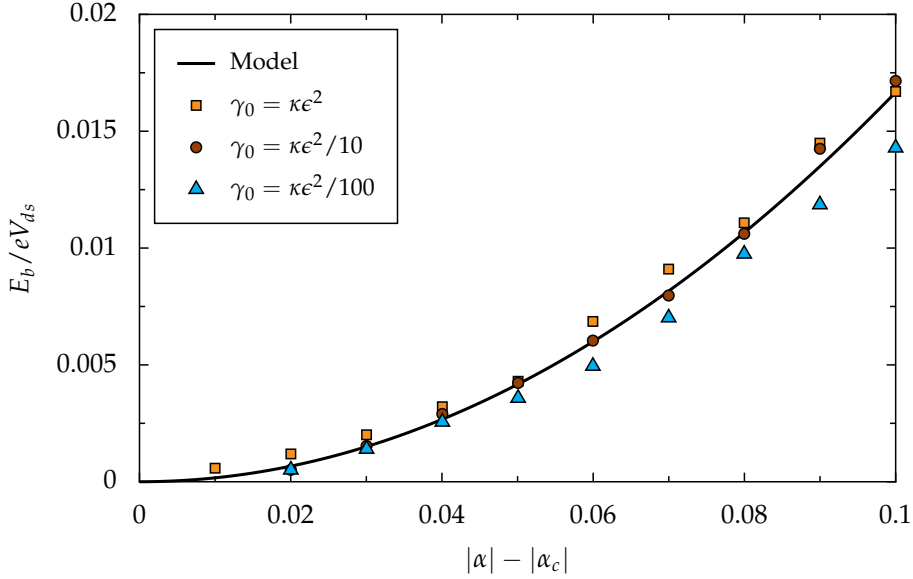
Figure 3.13: Barrier height governing the switching between the zero-current state to the current-carrying state, as a function of $|\alpha| - |\alpha_c|$, for $\kappa = 0.6, \epsilon = 0.3$, for different values of external damping γ_0. The symbols were obtained by numerically fitting $\log(I) = f(1/T)$ curves obtained numerically (see Fig. 3.12 for an example). The solid line is the prediction from the simple model of Eq. (3.23).

of the data points on this figure. However, the numerical accuracy is good enough to prove the hypothesis of thermally activated switching. We can push the analysis a step further and numerically evaluate the barrier height E_b by fitting the linear (low current) part of each curve. This was done for a specific value of the coupling ($\kappa = 0.6$). The results are presented in Fig. 3.13, for three different values of the extrinsic damping γ_0. The agreement between the values extracted numerically and the model presented at the end of Sec. 3.4.1 is very good, considering that there are no fit parameters in the model. Also, we note that the observed variation of E_b with the value of the external damping rate (not included in the model) is minimal, considering that γ_0 is varied over two orders of magnitude. The good agreement between our model and the numerically extracted barrier heights makes increases our confidence in the model we presented. It also makes it less likely that the current discontinuity could be observed experimentally. Indeed, within our model, extremely low temperatures are needed for the discontinuous behavior in the current to be observable, since for $k_B T \gtrsim E_b$ the discontinuity is rapidly washed out. Using $E_b/eV_{ds} \propto (|\alpha| - |\alpha_c|)^2$, we see that the observed zero temperature behavior is due to a barrier of vanishingly small height at the discontinuity. Numerically, for $\kappa = 0.6, \epsilon = 0.3, \gamma_0 = 0.1\kappa\epsilon^2$, we

41

can confirm that already at $k_B T = 0.001 e V_{ds}$ the current goes to zero as smoothly as in the uncoupled case.

3.5 Summary

In this chapter, we have studied the strong-coupling limit of a SET transistor coupled to a classical harmonic oscillator. We have used a combination of a master-equation approach and a numerical Monte Carlo procedure to calculate the position distribution of the oscillator, the electrical current, and the zero-frequency noise in both the weak-coupling and strong-coupling regime. With increasing coupling, we found that the position distribution of the oscillator evolves from a broad Gaussian to a a function sharply peaked around each of the charge-state dependent equilibrium positions of the oscillator. We found that the average current in the strong-coupling regime is higher than the value predicted by the weak-coupling theory and that the Fano factor varies in a non-monotonic fashion when coupling is increased. We have generalized the weak-coupling theory to allow the calculation of higher cumulants of the current, and have presented results for the third cumulant. In the weak-coupling regime, the third cumulant was found to depend strongly on the frequency of the oscillator, whereas in the strong-coupling regime it becomes practically independent of this parameter. We have also studied the frequency-dependent transport noise. Even in the strong-coupling regime, there are no peaks for frequencies higher than 2Ω, and the two peaks found in the weak-coupling limit merge on increasing the coupling strength. By introducing a generalized expression connecting the damping rate in the strong-coupling regime, we were able to understand the evolution of the oscillator's damping-renormalized frequency as a function of coupling. Analyzing the system away from the degeneracy point, we found an interesting discontinuity in the average current as a function of gate-voltage that is related to 'distortion-blockade'. This blockade was interpreted as a sign of bistability in the system.

3.6 Details of the Monte Carlo approach used

Monte Carlo methods have been used for a long time to calculate numerically the transport properties of mesoscopic systems like SETs[Amman89]. When dealing with a simple SET system, the idea of the Monte Carlo approach is to solve the master equation for the charge states of the SET by discretizing time into small intervals and allowing charge transfer to and from the dot with a probability of tunneling P_t that is proportional to the tunneling rates and the time interval $\Delta \tau_t$ between two attempts.

If the SET is coupled to a harmonic oscillator, we can proceed in a similar way, by considering charge transfer attempts at a finite frequency $(\Delta \tau_t)^{-1}$, where $\Delta \ll 1$ is a

dimensionless step size. The success probability $P_t^{i,\sigma}$ for a charge transfer is evaluated from the oscillator's position-dependent instantaneous rates $\Gamma_i^\sigma(x)$ calculated at the time of the attempt. This value is then compared to a randomly chosen double precision number $0 \leq \mathcal{N} \leq 1$. If $\mathcal{N} < P_t^{i,\sigma}$, then the charge transfer takes place. Between different attempts, the oscillator's state evolves according to the classical equation of motion, whose solution depends on the charge state of the SET, the equilibrium position of the oscillator being shifted by x_0 when the charge state is changed from $N \rightarrow N + 1$ or by $-x_0$ in the opposite case. At the beginning of each run, the state of the system is determined randomly from the stationary probability distributions $P_N(x, u)$ and $P_{N+1}(x, u)$. In practice, this can be implemented by using the final state of the $(n - 1)$-th Monte Carlo run as the initial state of the n-th run. We use the high-quality, high-performance `MRG32k3a` number generator[L'Ecuyer99] distributed with the Intel MKL library.

We consider runs of total time $t_0\tau_t$, such that each run consists of $N_s = t_0/\Delta$ steps. Both the time scales $t_0\tau_t$ and $\Delta\tau_t$ are chosen in a way such that increasing t_0 or decreasing Δ does not affect the value of the different physical quantities we extract from our calculation. In practice, this corresponds to choosing $\Delta < 0.02$ and $t_0\tau_t$ an order of magnitude greater than the typical damping time γ^{-1}.

A consequence of this last constraint is that the Monte Carlo approach is particularly useful in the strong-coupling regime, where the number of steps N_s per run can be kept relatively small, allowing for more runs to be made in the same amount of computer time. Most results obtained in the strong coupling limit are the result of Monte Carlo simulations consisting of (for each data point) 2.5×10^6 runs, with $t_0 = 3000\tau_t$ and $\Delta = 0.02$. For the calculation of the frequency-dependent current noise, we had to increase the length of the simulation considerably in order to better resolve the peaks and remove high-frequency ($\omega > 2\Omega$) noise. In this case, we took 600×10^6 runs, with $t_0 = 1000\tau_t$ and $\Delta = 0.025$.

As can be seen in Fig. 3.14, our code reproduces the analytical results of [Bagrets03] for the dependence of the Fano factor and the third cumulant on the a y coefficients $\Delta_L - \Delta_R$ in the $\kappa = 0$ limit. Also, we note that the probability distributions $P_N(x, u)$ and $P_{N+1}(x, u)$ that we calculate using the Monte Carlo approach coincide with the results one finds when solving Eq. (3.11) on a grid[Armour04b].

3.6.1 Finite temperature simulations

To study the effects of a finite temperature bath on the transport properties of the SET, we used an approach based on the stochastic differential equations for x, p for a
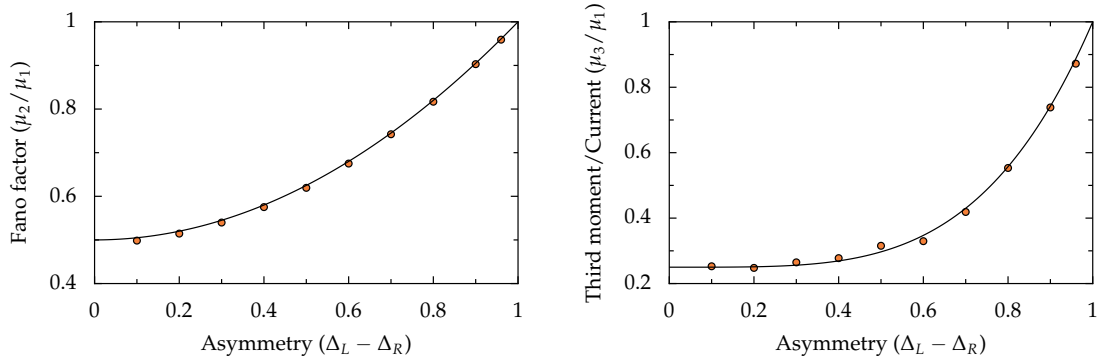
Figure 3.14: Comparison of the Monte Carlo results (dots) and the exact results found in Ref. [Bagrets03], for the Fano factor (left) and third moment (right) in the uncoupled case ($\kappa = 0$). This simulation was done with 10^6 runs, with $t_0 = 1000\tau_t$ and $\Delta = 0.025$.

classical damped harmonic oscillator[Breuer02],

$$dx(t) = \frac{1}{M}p(t)dt \, , \tag{3.25a}$$

$$dp(t) = -M\Omega^2 x(t)dt - \gamma_0 p(t)dt + \sqrt{2M\gamma_0 k_B T}dW(t) \, , \tag{3.25b}$$

with dW the increment of a Wiener process[vanKampen92], $dW(t) \equiv W(t + dt) - W(t)$ and γ_0 the intrinsic damping rate of the oscillator associated with the finite quality factor of the oscillator. In an effort to reduce the number of parameters in our in our zero-temperature study, we had set this intrinsic damping to zero for all simulations. However, since the connection to the thermal bath is done via the damping rate (cf. fluctuation-dissipation theorem) we cannot set $\gamma_0 = 0$ to study the effects of finite temperatures. Besides this point, Monte Carlo simulations at finite temperature proceed in a very similar as the zero-temperature ones, except that the stochastic differential equation (3.25) governing the evolution of the oscillator must also be integrated numerically. To proceed, we first rewrite the noise contribution in Eq. (3.25b) in a more numerically convenient form. Thinking of the Wiener process as integrated gaussian white noise, the differential element ΔW can be written as $\xi_t dt$, with ξ_t a gaussian-distributed random contribution, with mean 0 and variance dt (evidently, in the numerical simulation, dt is small but finite). A second set of random numbers must therefore be generated to simulate thermal noise. This time, the MCG31 random number generator (also distributed as part of the Intel MKL library) was used, in GAUSSIAN_BOXMULLER mode, to generate gaussian-distributed random numbers. Since a linear function of a gaussian-distributed random variable is itself a gaussian-distributed random variable (with different mean and variance), our im-

plementation used gaussian-distributed random numbers, with mean zero and unit variance[6].

Finally, we note that not all numerical methods available for the solution of ordinary differential equations can be easily adapted to solve stochastic differential equations like Eq. (3.25). We first tried a simple "Euler" algorithm to compute the evolution of the oscillator's state, but this technique did not prove accurate enough to be useful. With a time step of $0.005\tau_t$, numerical errors introduced by the Euler algorithm effectively pumped energy in the system. This of course conflicts with any attempt to calculate the temperature dependence of the transport properties. To solve this problem, we instead used a predictor-corrector (Heun) algorithm[Press96] to solve the equation of motion of the oscillator. With this technique, the energy pumped in the system when using a time step of $0.005\tau_t$ is seven order of magnitude less important than when the Euler method was used.

---

[6]To be precise, we coded the stochastic differential equations (9.13-9.14) of Ref. [Lemons02], where the noise contribution to dp is given in terms of the unit variance, mean zero, gaussian distribution.

Part III

Nanomechanics with tunnel junctions

Quantum measurement

At the undergraduate level, quantum measurements are usually abstracted to the maximum, i.e. one writes "we measure observable q" without paying any attention to *how* the measurement is done. Given a state $|\psi\rangle$, the operator $\hat{q}$ as well as its eigenstates $|q_n\rangle$, the probability to measure the (non-degenerate) eigenvalue q_n is

$$P_n = |\langle \psi | q_n \rangle|^2 \; ; \tag{4.1}$$

this is the von Neumann measurement postulate. Amusingly enough, quantum mechanics makes it easy to calculate the outcome of a measurement but difficult to describe in detail what happens *during* a measurement.

During the last few decades, there has been a growing desire to use quantum coherence in technological applications (e.g. for quantum computing). For these applications to materialize, a thorough understanding of the process of quantum measurement is necessary: one must understand how to describe the interaction of a (typically macroscopic) detector with a quantum system. In this chapter, we will review the advances made since the 1980's in the description of quantum measurement, specifically focusing on aspects related to the measurements used in the context of nanoelectromechanical systems. We therefore will not discuss 'quantum non-demolition' (QND) measurements[Braginsky80; Braginsky95], where the detector is coupled to an observable that commutes with the Hamiltonian, making the quantum measurement repeatable. Although some possible implementations QND measurements for nanoelectromechanical systems have been proposed (see e.g. [Santamore04; Ruskov05a; Martin07; Jacobs08]), they have yet to be demonstrated experimentally.

4.1 Basics of quantum measurement

If it occupies a central place in quantum mechanics, why is the question of measurement almost never discussed in the context of *classical* mechanics? In classical mechanics, the act of measuring something - say, the speed of a boat - does not affect the system: the properties of the measured object are not modified in any way by the measurement. This is not the case in quantum mechanics, where every measurement of an observable that does not commute with the Hamiltonian leads to a back-action that disturbs the state of the quantum-mechanical system. This back-action can be seen as a consequence of the Heisenberg uncertainty principle. For example, we know that because the position and momentum operators do not commute, $[\hat{x}, \hat{p}] = i\hbar$, the product of the uncertainties on position and momentum is bound from below:

$$\Delta x \Delta p \geq \frac{\hbar}{2} \ . \tag{4.2}$$

The Heisenberg uncertainty principle ensures that a very sensitive measurement of position (which would decrease Δx) is accompanied by a back-action that increases the uncertainty on the momentum of the measured object.

4.1.1 The Heisenberg microscope

The best way to illustrate the concepts of quantum-limited measurement and quantum back-action is via an example, the so-called Heisenberg microscope. Let's therefore consider the very simple example of a position measurement of a free particle of mass M in one dimension. Imagine doing a position measurement with a tunable error Δx_{meas}, i.e. the measurement outcome is

$$x = x_1 \pm \Delta x_{\text{meas}} \ . \tag{4.3}$$

The momentum perturbation caused by the measurement can be read from Eq. (4.2):

$$\Delta p_{\text{pert}} \geq \frac{\hbar}{2\Delta x_{\text{meas}}} \ . \tag{4.4}$$

Now consider a second measurement of position at a time τ after the first measurement. At this time, the uncertainty on the position measurement will be the sum of the measurement uncertainty Δx_{meas} and a contribution from the perturbation in the momentum caused by the first measurement,

$$\Delta x_{\text{add}}(\tau) = \frac{\Delta p_{\text{pert}} \tau}{M} \ . \tag{4.5}$$

The second measurement outcome can therefore be written

$$x = x_2 \pm \left(\Delta x_{\text{meas}} + \frac{\hbar \tau}{2\Delta x_{\text{meas}} M}\right) \ . \tag{4.6}$$

From these two measurements, we can infer the momentum and the position of the oscillator

$$x = \frac{x_1 + x_2}{2} \,, \qquad p = M\frac{x_1 - x_2}{\tau} \,, \tag{4.7}$$

as well as the uncertainties on the evaluation of each quantity. For the position measurement

$$\Delta x = \frac{1}{2}\left[(\Delta x_{\text{meas}})^2 + (\Delta x_{\text{meas}})^2 + \left(\frac{\hbar\tau}{2M}\frac{1}{\Delta x_{\text{meas}}}\right)^2\right]^{1/2}. \tag{4.8}$$

The error Δx contains terms that are (i) proportional and (ii) inversely proportional to the error Δx_{meas} on each measurement. As a consequence, there is an optimal value $(\Delta x_{\text{meas}})^2 = \hbar\tau/2M$ that minimizes the overall error. When Δx_{meas} is too large, the sum of the different measurement errors dominates the total measurement error. On the other hand, if Δx_{meas} is made too small, then the added back-action noise will be the main contribution to the total error. At the optimal point, the total measurement error is equal to the error introduced by the quantum-mechanical back-action Δx_{add} and

$$\Delta x = \Delta x_{\text{SQL}} = \sqrt{\frac{\hbar\tau}{2M}} \,. \tag{4.9}$$

The last equation introduced the so-called *standard quantum limit* (SQL), the uncertainty on a position measurement where Δx_{meas} is optimally chosen to minimize the total error. Different choices of Δx_{meas} lead to $\Delta x > \Delta x_{\text{SQL}}$. Proceeding in a very similar way, we can show that the error on a measurement of p obtained from Eq. (4.7) is always such that

$$\Delta p \geq \Delta p_{\text{SQL}} \equiv \sqrt{\frac{\hbar M}{2\tau}} \,. \tag{4.10}$$

The product of the two standard quantum limits $\Delta x_{\text{SQL}}\Delta p_{\text{SQL}} = \hbar/2$ is "Heisenberg-limited" in the sense where it is exactly equal to $\hbar/2$.

While simple, the example of the Heisenberg microscope introduces the main concepts of quantum measurement. Importantly, it shows that a measurement will only be quantum-limited once the measurement error and the error due to quantum-mechanical back-action are of comparable magnitude.

Finally, we note that even if we presented a derivation of the standard quantum limit using the simple example of a free particle, there is an equivalent quantity for the case of the position measurement of an harmonic oscillator of frequency Ω and mass M. In this case, one finds[Caves80; Braginsky95]

$$\Delta x_{\text{SQL}} = \sqrt{\frac{\hbar}{2M\Omega}} \,. \tag{4.11}$$

This quantity will be discussed in Sec. 6.1.2.

4.2 Continuous linear quantum measurement

The previous discussion, while instructive, did not provide a precise description of what happens during a quantum measurement. Moreover, it did not relate the measurement error to concrete properties of the detector used. In this section, following the linear-response approach pioneered by Averin[Averin03a; Averin03b] and Clerk[Clerk03b; Clerk04a], we describe how the Heisenberg uncertainty principle manifests itself in the context of a linear continuous measurement of a quantum system.

Let's first clarify the question of what we mean by linear continuous quantum measurement. The meaning of 'continuous' is pretty obvious: in a continuous measurement, one turns on the interaction between the detector and the quantum system to be measured and then continuously measures (classically) the output of the detector. This continuous monitoring can be seen as a sequence of individual measurements. In this context, Braginsky and Khalili explain that linear continuous measurements are those where the uncertainty relation for the observable monitored is independent of the state of the measured object[Braginsky95]. For example, the two-time uncertainty relation for the position measurement of a free particle reads $\Delta x(t)\Delta x(t') \geq \hbar|t - t'|/2M$; it depends only on the mass M of the particle (a constant) and not on the quantum state of the free particle. They also note that this is the most important class of quantum measurements[1].

Figure 4.1 presents a schematic view of the quantum measurement process. The total Hamiltonian of the system depicted on this figure can be written as

$$H = H_S + H_D + H_{\text{int}}. \, , \tag{4.12}$$

with H_S the Hamiltonian of the quantum system that is to be measured, H_D the detector's Hamiltonian and finally H_{int} models the interaction between the quantum system and the detector. At this point, it is easy to draw a parallel between a continuous linear quantum measurement and an open quantum system, where open quantum system refers to a quantum object ($\sim H_S$) coupled to a bath ($\sim H_D$) via an interaction term H_{int} (see for example [Breuer02]). In this context, coupling to a bath can be used, for example, to model environment-induced decoherence of a two-level system. The main difference between both problems is that often, in the context of open quantum systems, the (typically macroscopic) bath is considered to be in equilibrium and unaffected by the coupling to the (typically microscopic) quantum system. On the contrary, the output of any useful detector *is* affected by the quantum system.

---

[1]Naturally, there also exist nonlinear quantum measurements. For example, the perturbation caused to x by a measurement of the energy of a harmonic oscillator E can be evaluated from the uncertainty relation $\Delta E\Delta x \geq \hbar|\langle p\rangle|/2M$ [Braginsky95]. In this case, the right-hand side of the uncertainty relation is $\propto |\langle p\rangle|$ and therefore depends on the state of the system.
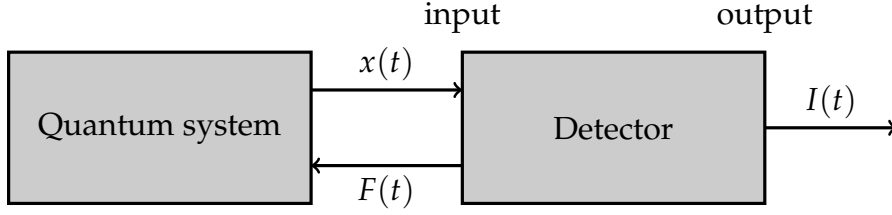
Figure 4.1: Schematic representation of a continuous linear quantum measurement.

We consider the general interaction Hamiltonian

$$H_{\text{int}} = A\hat{F}\hat{x} \,, \tag{4.13}$$

with A a dimensionless coupling constant, $\hat{x}$ an observable of the quantum system (to be measured) and $\hat{F}$ the operator characterizing the input port of the detector. The output port of detector is characterized by an observable $\hat{I}$. The strength of the linear-response approach presented here is that it allows the study of a very generic system, without the need for further description of the detector. Conclusions reached using this approach are therefore quite universal, provided the coupling between the system and detector is weak, such that the response of the detector to variations of the quantum systems remains linear.

To evaluate the response of the detector to a change in the quantum system, we expand the time-evolution operator $U(t) = \exp(-iHt/\hbar)$ with H as given in Eq. (4.12) to lowest order in H_{int}. Using the expansion, the expectation value for $I(t)$ can be written (see e.g. [Bruus04])

$$\langle I(t) \rangle = \langle I(t) \rangle_0 + A \int dt' \lambda(t - t') \langle x(t') \rangle \tag{4.14}$$

with $\lambda(t - t')$ the x-to-I gain given by

$$\lambda(t - t') = \frac{1}{i\hbar}\theta(t - t')\langle [\hat{I}(t), \hat{F}(t')] \rangle \,, \tag{4.15}$$

where the average is taken over the stationary density matrix of the detector in the uncoupled ($A = 0$) case. In general, we will be interested in the Fourier transform of the gain,

$$\lambda(\omega) = \int_{-\infty}^{\infty} d\tau e^{i\omega\tau}\lambda(\tau) \,. \tag{4.16}$$

As proven in Appendix C, quantum mechanics imposes a constraint on the gain of a detector[Clerk04a]:

$$\bar{S}_I(\omega)\bar{S}_F(\omega) \geq \frac{\hbar^2}{4}\left(\text{Re}[\lambda(\omega) - \lambda'(\omega)]\right)^2 + \left(\text{Re}[\bar{S}_{IF}(\omega)]\right)^2 \,, \tag{4.17}$$

with $\overline{S}$ the symmetrized correlation functions (we denote $\delta\hat{I} = \hat{I} - \langle I \rangle$)

$$\overline{S}_I(\omega) = \frac{1}{2} \int_{-\infty}^{\infty} dt \, e^{i\omega t} \langle \{\delta\hat{I}(t), \delta\hat{I}(0)\} \rangle \,, \tag{4.18}$$

$$\overline{S}_F(\omega) = \frac{1}{2} \int_{-\infty}^{\infty} dt \, e^{i\omega t} \langle \{\delta\hat{F}(t), \delta\hat{F}(0)\} \rangle \,, \tag{4.19}$$

$$\overline{S}_{IF}(\omega) = \frac{1}{2} \int_{-\infty}^{\infty} dt \, e^{i\omega t} \langle \{\delta\hat{I}(t), \delta\hat{F}(0)\} \rangle \,, \tag{4.20}$$

and where we introduced the "reverse gain"

$$\lambda'(\omega) = \frac{1}{i\hbar} \int_0^{\infty} dt e^{i\omega t} \langle [\hat{F}(t), \hat{I}(0)] \rangle \,. \tag{4.21}$$

This last quantity describes the gain in a situation where one couples x to I in an attempt to measure F.[2]

Equation (4.17) is one of the main results regarding quantum measurement that can be obtained using a linear response approach. Essentially, it expresses the fact that a detector with finite gain $\lambda \neq 0$ will exert a back-action force S_F on the quantum system that is inversely proportional to the bare output noise S_I of the uncoupled detector. At equal gain λ, a detector with lower S_I will perturb the quantum system more (i.e. larger S_F) than a detector with high S_I. For a detector where both sides of Eq. (4.17) are equal, a strong parallel can therefore be drawn to the simple example given in Sec. 4.1.1, where a measurement with smaller Δx_{meas} lead to an increased back-action force. In the present case however, Eq. (4.17) expresses the quantum-mechanical constraint *in terms of concrete, measurable, parameters of the detector*.

It is also important to emphasize that Eq. (4.17) is an *inequality*. Detectors for which both sides of the equation are *equal*,

$$\overline{S}_I(\omega)\overline{S}_F(\omega) = \frac{\hbar^2}{4} \left(\text{Re}[\lambda(\omega) - \lambda'(\omega)] \right)^2 + \left(\text{Re}[\overline{S}_{IF}(\omega)] \right)^2 \,, \tag{4.22}$$

are said to be "quantum-limited". In this case, it can be shown that all the information acquired by the detector about the quantum system is contained in the detector's output[Clerk03a]. In other words, no information is lost by these detectors.

Of course, not all detectors are quantum-limited and some are only in certain regimes. This can be illustrated particularly nicely by considering the case of the single-electron transistor studied in Part 1 of this thesis. As discussed in Sec. 2.1, this device can be operated in one of two regimes: sequential tunneling or cotunneling. From a classical point of view, the former regime looks extremely attractive.

---

[2]The reverse gain has been shown to vanish completely ($\lambda' = 0$) for most mesoscopic detectors (SET, tunnel junctions) [Clerk03b].

It is characterized by a large current and a large sensitivity ($\sim dI/dx$). By comparison, the cotunneling regime seems much less attractive, as one expects smaller currents and, correspondingly, a reduction in the absolute *magnitude* of the sensitivity. As shown in Refs. [Shnirman98; Averin00; Mozyrsky04], this classical point of view is totally wrong and the SET is a quantum-limited detector *only* in the cotunneling regime. When operated in the sequential tunneling regime, the increased gain of the SET can be shown to be accompanied by an even more pronounced increase of back-action (charge) noise of the detector that leads to a departure from the quantum limit. This can be understood intuitively from the information theoretical ("no information should be lost") point of view. In the sequential tunneling regime, the electron tunnels from a lead to the island, where it remains for a finite time, before tunneling again to the second lead. The finite dwell time on the island leads to phase-averaging and therefore to a loss of information, contrary what happens during a - phase coherent - cotunneling event. The lesson to be learned from this example is that the quantum-limit is defined in terms of the *interplay* between bare-output noise, back-action noise and sensitivity, and not in terms of individual parameters.

4.2.1 Continuous monitoring of a qubit and the Korotkov-Averin bound

More insight about continuous quantum measurements can be gathered by treating the example of a qubit measurement. Equation (4.17) also applies in this case, as during our derivation no assumption whatsoever was made about the system we were studying.[3] In this subsection, we will present a derivation of the 'Korotkov-Averin' bound[4] on the signal-to-noise ratio of a continuous weak measurement of a qubit. This bound appears as a direct consequence of Eq. (4.17).

To begin, we consider a two-level system (qubit) coupled to a detector measuring σ_z. The Hamiltonian of the total system is given by $H = H_0 + H_{\text{det}} + H_{\text{int}}$, with

$$H_0 = -\frac{\epsilon \hat{\sigma}_z + \Delta \hat{\sigma}_x}{2} \, , \tag{4.23}$$

$$H_{\text{int}} = -\frac{\hat{\sigma}_z}{2} \hat{F} \, , \tag{4.24}$$

with $\hat{\sigma}_i$s the Pauli matrices and where we absorbed the dimensionless coupling constant A in $\hat{F}$. Again, we will use linear-response arguments so we do not need to specify H_{det}, the Hamiltonian of the bare detector. As before, we will simply assume that it couples to the quantum system via an operator $\hat{F}$ and that we read-out the output

---

[3]We treated $\hat{x}, \hat{F}$ as general quantum-mechanical operators without ever specifying H_D or H_S.

[4]This result was first derived in [Korotkov01b; Korotkov01a; Averin03a] and is also discussed in, e.g. [Goan01; Ruskov03; Shnirman04]

variable $\hat{I}$. Assuming that the detector's response time is much faster than any intrinsic timescale of the qubit, we can consider the back-action noise to be δ-correlated

$$\langle \hat{F}(t+\tau)\hat{F}(t)\rangle_0 = S_F\delta(\tau) , \qquad (4.25)$$

$$\langle \hat{I}(t+\tau)\hat{F}(t)\rangle_0 = S_{IF}\delta(\tau - 0^+) , \qquad (4.26)$$

with the infinitesimal shift in the delta-function playing the role of a finite response-time of the detector. Since we consider δ-correlations, the gain $\lambda(\omega)$ is frequency-independent. It is given by[Eq. (4.16)]

$$\lambda = \frac{-i}{\hbar}\int_0^\infty dt e^{i\omega t}\langle[\hat{I}(t),\hat{F}(0)]\rangle = \frac{2}{\hbar}\text{Im}\int_0^\infty dt e^{i\omega t}\langle \hat{I}(t)\hat{F}(0)\rangle = \frac{2}{\hbar}\text{Im}S_{IF} . \qquad (4.27)$$

Using $I(t) = I_0(t) - \lambda\sigma_z(t)/2$, we can write the total[5] current-noise $\overline{S}_{I,\text{tot}}$ as [Jordan05]

$$\overline{S}_{I,\text{tot}}(\omega) = \overline{S}_I(\omega) + \frac{\lambda^2}{4}\overline{S}_z(\omega) , \qquad (4.28)$$

where $\overline{S}_z = \int dt \exp(i\omega t)\langle\{\sigma_z(t),\sigma_z(0)\}\rangle$ must be explicitly calculated, taking into account the coupling to the detector. This can for example be done by expanding the evolution operator for σ_z (including both the evolution due to the qubit Hamiltonian and the contribution associated with H_{int}) to second-order in $\hat{F}$ and then tracing out the detector degrees of freedom using Eq. (4.25)[Korotkov01b]. One finds that the evolution of the matrix elements σ_{ij} of $\sigma_z(t)$ follow

$$\dot{\sigma}_{11} = \Delta\text{Im}[\sigma_{12}] , \qquad (4.29a)$$

$$\dot{\sigma}_{12} = (i\epsilon - \Gamma_\phi)\sigma_{12} - i\Delta\sigma_{11} , \qquad (4.29b)$$

$$\dot{\sigma}_{22} = -\dot{\sigma}_{11} \qquad (4.29c)$$

where we introduced the dephasing rate[Makhlin01; Averin03a][see also Sec. 5.1]

$$\Gamma_\phi = \frac{\overline{S}_F}{2\hbar^2} . \qquad (4.30)$$

In the case where $\sigma_z(t)$ has the largest variations over time ($\epsilon = 0$), the σ_z fluctuation spectrum is found by solving Eq. (4.29) for $\langle\sigma_z(t)\sigma_z\rangle$:

$$\overline{S}_{I,\text{tot}}(\omega) = \overline{S}_I(\omega) + \frac{\lambda^2}{4}\frac{2\Gamma_\phi\Omega^2}{(\omega^2 - \Omega^2)^2 + \omega^2\Gamma_\phi^2} , \qquad (4.31)$$

where we denoted $\Omega = \Delta/\hbar$ the frequency of the qubit.

---

[5]We use the notation $\overline{S}_{I,\text{tot}}$ to describe the total symmetrized output current noise of the detector in presence of coupling and keep $\overline{S}_I$ to denote the bare symmetrized current-noise, in the absence of coupling.

In the fast detector limit we are considering, the bare current noise $\overline{S}_I(\omega)$ can be seen as constant background in $\overline{S}_{I,\text{tot}}$ close to Ω. The second contribution ($\propto \lambda^2$) to the total output noise can then be seen as the 'signal' part of the total detector output. This signal is maximum exactly at $\omega = \Omega$, and it is given by $\lambda^2/2\Gamma_\phi$. Recalling the expression of Γ_ϕ in terms of the spectral density of the back-action noise S_F, we can rewrite the maximal signal as $\overline{S}_{\text{max}} = \hbar^2\lambda^2/\overline{S}_F$. This allows for the ratio $\mathcal{R}$ of signal-over-noise to be written as

$$\mathcal{R} = \frac{\overline{S}_{\text{max}}}{\overline{S}_I} = \frac{\hbar^2\lambda^2}{\overline{S}_F\overline{S}_I} \ . \tag{4.32}$$

Using Eq. (4.17) (with $\lambda' = 0$), this becomes

$$\mathcal{R} = \frac{4\hbar^2\lambda^2}{\hbar^2\lambda^2 + 4(\mathrm{Re}\overline{S}_{IF})^2} \leq 4 \ , \tag{4.33}$$

where the equality is reached for (i) a quantum-limited detector that fulfills the equality in Eq. (4.33) and (ii) $\mathrm{Re}\overline{S}_{IF} = 0$. The signal-to-noise ratio in a weak-measurement of a qubit is therefore bounded: it cannot be made higher than 4. This result, known as the Korotkov-Averin bound, is universal: it does not depend on the details of the experimental measurement setup or on the physical implementation of the qubit. It is valid as long as the measurement is weak enough to be described accurately using linear-response. In Sec. 8.2, we will show that an equivalent relation arises when considering the linear measurement of the displacement of a nanomechanical oscillator.

The tunnel junction as a quantum measurement device

From the first experimental confirmation of the quantization of the conductance in mesoscopic systems[Wees88; Wharam88] to the development of the "full counting statistics" approach to transport[Levitov92; Levitov96], the study of the tunnel junction (or, more generally, of the quantum point contact) played a crucial role in the development of central concepts in mesoscopic physics. One of the reasons why the study of these devices proved so fruitful is without a doubt their intrinsic simplicity. These devices lend themselves to a relatively simple theoretical description that reproduces accurately their behavior. In this chapter, after a short introduction describing the use of the tunnel junction for qubit measurements, we will focus on explaining how tunnel junctions can be used as position detectors, reviewing both recent theoretical and experimental developments in this area.

5.1 Qubit measurement and measurement-induced dephasing

There is a strong conceptual overlap between the measurement of quantum states in two-level systems and the measurement of the position of nanomechanical oscillators, and it is therefore instructive to review the basics of qubit measurements using tunnel junctions[1]. To use a tunneling detector to measure the quantum state of a two-level system, one needs to engineer a device where the transmission amplitude of the

---

[1]In this thesis, a "tunnel junction" is considered to be a low transparency "quantum point contact", such that quantities that are of higher-than-second order in the tunneling amplitude are taken to be zero.

junction varies depending on whether the qubit is in the $|1\rangle$ or $|2\rangle$ state[2],

$$t_{\text{tot}} = t_0 + A\hat{\sigma}_z \, , \tag{5.1}$$

with t_0 the bare tunneling amplitude of the junction and A a coupling constant. Such systems have been studied at length, both theoretically [Gurvitz97; Levinson97; Aleiner97; Korotkov02; Pilgram02; Clerk03b; Averin05] and experimentally[Buks98; Hayashi03; Petta04]. While we do not want to review this system in detail, it turns out that it allows for a nice, simple, illustration of the concept of measurement-induced dephasing[Averin06], a concept that can also be applied to position measurements. In a nutshell, measurement-induced dephasing refers to the fact that measuring the system destroys coherent superposition of states, leading to an (exponential) decay of the non-diagonal elements of the density matrix.

This can be better understood by considering the following example, inspired from [Averin05]. Consider a two-level system (with $H = \epsilon\sigma_z/2$), prepared in state $|\psi\rangle = c_1|1\rangle + c_2|2\rangle$, with $|c_1|^2 + |c_2|^2 = 1$. The system is coupled to a tunnel junction detector whose transmission amplitude is given by Eq. (5.1). In our example, this state-dependent amplitude will be described by two scattering matrices[Datta95] $S_{|1\rangle}$ and $S_{|2\rangle}$, each of the form

$$S_{|i\rangle} = \begin{pmatrix} r_i & t_i^* \\ t_i & r_i^* \end{pmatrix} . \tag{5.2}$$

Consider now an electron (in state $|\text{incoming}\rangle$) coming from the left lead that scatters at the junction coupled to the qubit. Schematically, the measurement process is written

$$|\text{incoming}\rangle \otimes c_1|1\rangle + c_2|2\rangle \rightarrow c_1 \left[r_1|L\rangle + t_1|R\rangle \right] |1\rangle + c_2 \left[r_2|L\rangle + t_2|R\rangle \right] |2\rangle \, , \tag{5.3}$$

where in final state (right of the arrow) the electron is in the left lead ($|L\rangle$) provided it was reflected or in the right lead ($|R\rangle$) if it was transmitted. Tracing out the electronic state, we can look at the evolution of the element $\rho_{j,k}$ of density matrix of the qubit due to the measurement, (where $j, k = \{1, 2\}$)

$$\rho_{j,k} = c_j c_k^* \rightarrow c_j c_k^* \left[t_j t_k^* + r_j r_k^* \right] \, . \tag{5.4}$$

Since $|t_j t_k^* + r_j r_k^*| \leq 1$, one sees that an individual measurement decreases the magnitude of the off-diagonal elements of the density-matrix while keeping the diagonal elements unchanged ($|t_j|^2 + |r_j|^2 = 1$). Combining a sequence of measurements during a finite time, one finds exponentially-decaying matrix elements $|\rho_{1,2}(\tau)| = |\rho_{1,2}(0)|e^{-\Gamma_\phi \tau}$ [Averin05]. In the tunneling regime,

$$\Gamma_\phi = \frac{eV}{2h} \left[|t_1| - |t_2| \right]^2 = \frac{eV}{2h} A^2 \, , \tag{5.5}$$

---

[2]We denote $|1\rangle, |2\rangle$ the eigenstates of σ_z

provided the state-dependent transmission amplitude is given by Eq. (5.1). As will be shown in Sec. 7.2, a very similar relation can be derived for *position* measurements using scattering detectors.

5.2 Displacement measurement with tunnel junctions: Theoretical investigations

In the present section, we shortly outline recent theoretical progress regarding the tunnel junction displacement detector. Very intuitively, for a tunnel junction to be used to measure the displacement of a nanomechanical oscillator the tunneling amplitude of the junction must be a function of the position of the oscillator,

$$t_{\text{tot}} = t_0 + A f(\hat{x}) . \tag{5.6}$$

As will be shown in Sec. 5.3, many different experimental approaches can be used to reach this goal. However, they can all be described within the same general theoretical framework.

Historically, the idea to use electron tunneling was first developed in the context of gravitational-wave sensing[Bocko88]. At the time, the idea was basically to use a scanning tunneling microscopy type of experimental setup to monitor the displacement of large masses. This idea was further explored, with many different groups using semiclassical approaches to estimate the back-action (associated with momentum kicks of the oscillator due to electron tunneling) associated to displacement measurement of large classical masses[Stephenson89; Yurke90; Presilla92; Onofrio93; Schwabe95]. A general feature of these investigations is that tunneling is treated like the problem of transmission of a particle through a barrier (the vacuum) of x-dependent width.

The first fully quantum approach to the problem of a tunnel junction coupled to a harmonic oscillator was presented in[Mozyrsky02]. The Hamiltonian used in this paper can be written as a sum of three parts: the Hamiltonian of the leads (H_{leads}), the Hamiltonian of the quantum harmonic oscillator (H_{osc}) and an interaction (tunneling) Hamiltonian (H_{tun}) between the systems.

$$H_{\text{leads}} = \sum_k \varepsilon_k c_k^\dagger c_k + \sum_q \varepsilon_q c_q^\dagger c_q , \tag{5.7a}$$

$$H_{\text{osc}} = \frac{M\Omega^2 \hat{x}^2}{2} + \frac{\hat{p}^2}{2M} , \tag{5.7b}$$

$$H_{\text{tun}} = \sum_{k,q} f_{k,q}(\hat{x}) c_k^\dagger c_q + \text{H. c.} , \tag{5.7c}$$

with $k(q)$ is a wave vector in the right (left) lead. This Hamiltonian is also the starting point of the work presented in Chaps. 6-9 of this thesis and of many other investigations of this system[Smirnov03; Clerk04b; Wabnig05; Wabnig07; Pauget08].

The common link between the methods used in each of those papers it that they all adopt the second-quantized Hamiltonian [Eq. (5.7c)] to describe the interaction between the oscillator and the junction instead of solving the full problem of transmission through a barrier. Most studies were performed in the linear approximation $f_{k,q}(\hat{x}) = f_{k,q}^0 + f_{k,q}^1 \hat{x}$, but an exponential dependance of the tunneling amplitude on the position was also studied[Smirnov03].

Using the Hamiltonian given in Eq. (5.7), the effect of the tunnel junction on the oscillator as well as the average current through the junction was calculated[Mozyrsky02; Smirnov03], followed by calculations of current noise in the Markovian[Clerk04b; Wabnig05] and non-Markovian limits[Wabnig07]. We keep the details of these calculations for later (Chap. 7), and instead present the different experimental implementations of Eq. (5.7) in NEMS.

5.3 Displacement measurement with tunnel junctions: Experimental realizations

The quantum point contact detector was used in the context of displacement measurement of a radio-frequency nanomechanical oscillator for the first time in 2002 [Cleland02], where a quantum point contact embedded in the resonator was shown to be sensitive enough to measure the displacement of a *driven* oscillator. The next experimental milestone was reached in 2007, when two different groups demonstrated experimentally displacement detection with the sensitivity required to resolve the brownian motion of an (undriven) oscillator using two different implementations of a quantum point contact [Flowers-Jacobs07; Poggio08]. We will now present these experiments in more detail[3].

5.3.1 Quantum point contact mounted on the resonator

As we just mentioned, the first step towards displacement measurement using point contact was made by creating a QPC directly on the nanomechanical resonator. In [Cleland02], a GaAs-AlGaAs heterostructure was etched into an approximately 10μm long, 4μm wide and 720nm thick doubly-clamped beam. To form the quantum point contact, top gates were evaporated directly on the surface of the resonator, constraining further the 2D electron gas formed at the interface between the two semiconductors. Owing to to the intrinsic piezoelectric character of GaAs, the out-of-plane flexural vibrations of the beam generated an out-of-plane electric field that acted in a similar way as a top gate on the transmission characteristics of the point contact, adding a displacement-dependent contribution to the QPC transmission ampli-

---

[3]We note that the concept of "displacement sensitivity" will be formally defined in Sec. 6.1.2.

tude. The displacement sensitivity of the device was measured to be on the order of $3 \times 10^{-12} \mathrm{m}/\sqrt{\mathrm{Hz}}$, a better figure than what had been achieved using optical interferometry on nanoscale cantilevers. However, the device was not sensitive enough to resolve the thermal motion of the resonator (on the order of $1 \times 10^{-15} \mathrm{m}/\sqrt{\mathrm{Hz}}$ for this device at 4.2K). Moreover, the displacement sensitivity was shown to be limited by voltage-noise in the amplification circuit and not by shot-noise or back-action due to the measurement.

5.3.2 Atomic point contact

The next major experiment was carried out in the group of Konrad Lehnert at the University of Colorado at Boulder[Flowers-Jacobs07]. A schematic representation of the experimental setup used is depicted in Fig. 9.1. Their experimental device consisted of a doubly-clamped Au nano-resonator originally attached to a gate electrode via a small constriction. Using electromigration, a small ($\sim$ 1nm) gap between the gate and the resonator was created, allowing the latter to undergo brownian motion. Due to the large intrinsic energy scales of the atomic point contact (the work function of gold is $W \sim$ 5eV and the bias voltage usally is $V \sim$ mV) the device could be operated at relatively high temperatures ($T \sim$ 10K), where the thermal motion of the beam is increased. The device exhibited 5 mechanical resonances in the frequency range comprised between 18 and 58 MHz, each with a typical quality factor around 5000.

This device was sensitive enough to measure the displacement of the undriven beam, achieving a displacement imprecision $\sqrt{S_x} = 2.3\mathrm{fm}/\sqrt{\mathrm{Hz}}$. Even more interesting, it was shown that the measurement sensitivity was limited by the QPC itself, and not by the noise of the post-amplification circuit used, and this throughout the whole gain range explored in this experiment. In the low gain region, the shot noise from the QPC dominated the total output noise. By increasing the gain, the ratio of shot noise over back-action noise could be reduced, as expected [Eq. (6.19)]. Moreover, even at the highest gain the shot noise contribution to the noise remained higher than the noise due to post-amplification circuit (which scales like one over the second power of the gain). Unfortunately, experimental issues limited the maximum gain that could be applied without seriously heating the device and therefore it was not possible to reach the back-action dominated measurement regime. Moreover, while one expects the atomic point contact to be a quantum-limited detector (Sec. 6.2.3) and therefore be characterized by a product $\sqrt{\bar{S}_I \bar{S}_F}$ that fulfills Eq. (4.22), a greatly increased back-action force was observed, and $\sqrt{\bar{S}_I \bar{S}_F} = (1700 \pm 400)(\hbar|\lambda|/2)$ was measured at the optimal measurement point. The reason why the back-action noise measured was more important than predicted is still an open issue. At this optimal point, the total added displacement noise was measured to be $\sqrt{\bar{S}_{x,\mathrm{add}}} = (42 \pm 9)\sqrt{\bar{S}_{x,\mathrm{add}}^{\mathrm{min}}}$.

5.3.3   Off-board quantum point contact

A different approach to displacement measurement with a scattering detector was developed at IBM's Almaden research laboratory[Poggio08]. In this case the device used was basically a simple gate-defined QPC coupled capacitively to the nanomechanical resonator (a simply-clamped cantilever in this case) that was brought in proximity to the QPC[4]. By applying a static voltage difference between the 2DEG and the cantilever, the displacement of the resonator could be monitored by looking at the current through the QPC. Like for the SET system (Sec. 2.2), in this case the resonator acted as a second, position-dependent, gate. This approach is novel in the sense that the resonator and the QPC are more or less independent of each other. This represents an immense advantage over earlier experimental schemes since:

- Both the resonator and the QPC can be optimized independently.

- The 2DEG does not need to be chemically etched to fabricate the resonator, a step that decreases considerably the 2DEG's mobility [Cleland02].

- The resonator does not need to be built from a piezoelectric material.

- There is no need to evaporate top gates on the resonator, typically degrading its quality factor.

- A single QPC can be used to measure different cantilevers.

The authors measured the displacement spectral density around a mechanical resonance of their cantilever located at about 5kHz, using the QPC as well as laser-interferometry[Mamin01]. The measurement done with QPC showed a pronounced improvement in terms of sensitivity, achieving a displacement imprecision of 4×10^{-12}m$/\sqrt{\text{Hz}}$, a full order of magnitude better than the optical measurement. However, due to the relatively low frequency of the cantilever, the electrical measurement was limited by $1/f$ charge noise: the measurement was therefore not limited intrinsically by the QPC (shot or back-action noise). This low-frequency noise floor corresponds to a displacement imprecision of ~ 65 times the quantum limit. Besides the $1/f$ noise, another downside of this approach as presented here is that the interaction between the cantilever and the metallic gates used to define the QPC lead to a significant (up to one order of magnitude) decrease of the quality factor of the mechanical resonance when a voltage is applied to either the cantilever or the gates, due to non-contact friction caused by near-surface fluctuating electric fields interacting with static

---

[4]During the measurement, the tip of cantilever was kept at a height of $z = 70$nm, measured perpendicularly from the surface of the heterostructure. This is a relatively large distance when compared to the expected tip displacement due to thermal forces: $x_{th} \sim 0.14$nm at 4.2K for the device studied.

surface charge[Stipe01]. Luckily, the importance of this effect can be reduced by using local oxidation to define the QPC (see e.g. [Graf06]) instead of using metallic top gates.

Tunnel junction coupled to an harmonic oscillator: what can you learn from linear response?

In Chap. 4, we used the linear-response approach to derive the general condition under which a detector can be said to be quantum-limited [Eq. (4.22)]. In the present chapter, we again use a linear-response approach, this time to discuss the effect of measurement as seen from the quantum system. Also, while the discussion of Chap. 4 remained very general and applies to many physical systems, we now focus our attention to nanoelectromechanical systems and study explicitly the displacement measurement of a harmonic oscillator using a linear detector. We will first describe the effects of measurement using a generic detector on a quantum harmonic oscillator, reviewing the main results obtained by Clerk in Ref. [Clerk04a], an article that proved quite influential in the field of nanomechanics. Afterwards, in Sec. 6.2, we apply the linear-response theory to treat explicitly the pedagogical example of a tunnel junction displacement detector.

6.1 Linear response for a general detector: the *quantum noise* approach

We again consider a coupled detector – quantum-system setup like the one discussed in Sec. 4.2. This time the quantum system is a quantum damped harmonic oscillator, characterized by a damping rate γ_0. The coupling between the detector and the

oscillator takes the form[1]

$$H_{\text{int}} = A\hat{F}\,\hat{x} \;, \tag{6.1}$$

with $\hat{x}$ the position operator of the oscillator, $\hat{F}$ a typical observable of the input port of the detector and A a dimensionless coupling constant. In the weak-coupling ($A \to 0$) limit, Clerk showed[Clerk04a, Appendix A], via a perturbative calculation of the oscillator's Keldysh Green's functions[2], that the displacement of the oscillator obeys the Langevin equation

$$M\ddot{x}(t) = -M\Omega^2 x(t) + \left[-\gamma_0 M\dot{x}(t) + F_0(t) \right] + \left[AF(t) - A^2 \int dt'\gamma(t-t')M\dot{x}(t') \right]. \tag{6.2}$$

In this equation, M and Ω are respectively the oscillator's renormalized mass and frequency. The terms contained in the first set of brackets originate from the coupling of the oscillator to the thermal environment: γ_0 is the damping rate of the oscillator in the absence of the detector and $F_0(t)$ represents a thermal fluctuating force. For the equilibrium ohmic bath at temperature T_0 considered here, the symmetrized correlation function of F_0 is given by

$$\bar{S}_{F_0}(\omega) = M\gamma_0\hbar\omega \coth\left(\frac{\hbar\omega}{2k_B T_0}\right) \;. \tag{6.3}$$

The most interesting part of Eq. (6.2) is contained in the rightmost bracket. This term, that vanishes in the $A = 0$ limit, describes the influence of the detector on the oscillator. It contains both a 'fluctuation force' term (F) and a 'damping' term (γ) proportional to $\dot{x}$. Clerk showed that the spectrum of $F(t)$ can be directly related to the symmetrized-in-frequency force noise of the detector

$$\bar{S}_F(\omega) = \frac{1}{2}\int_{-\infty}^{\infty} dt e^{i\omega t}\langle\{\delta\hat{F}(t)\delta\hat{F}(0)\}\rangle = \frac{1}{2}[S_F(\omega) + S_F(-\omega)] \;, \tag{6.4}$$

where again

$$S_F(\omega) = \int_{-\infty}^{\infty} dt e^{i\omega t}\langle\delta\hat{F}(t),\delta\hat{F}(0)\rangle \;, \tag{6.5}$$

---

[1]In [Clerk04a], the interaction Hamiltonian is defined as $H_{int} = -A\hat{F}\hat{x}$ in Eq. (1), but this is inconsistent with Eqs. (2) and (11). Other results of [Clerk04a] generally are not affected by the presence of a minus sign. Finally, in the next sections we will define the interaction as $\hat{F}\,\hat{x}$, without explicitly mentioning A. It is introduced here mainly because it is useful to be able to tune the interaction strength to optimize displacement sensitivity (Sec. 6.1.2).

[2]We will not discuss in detail Clerk's derivation of Eq. (6.2), since in Sec. 7.2, we will show explicitly how this result can be recovered using an equation-of-motion approach.

is the unsymmetrized force noise spectrum, calculated in the $A \to 0$ limit. In frequency space, the damping rate $\gamma(\omega)$ can also be written in terms of $S_F(\omega)$:

$$\gamma(\omega) = \frac{1}{2M\hbar\omega} \left[S_F(\omega) - S_F(-\omega) \right] . \qquad (6.6)$$

It is proportional to the anti-symmetrized force noise of the detector.

Taken together, Eqs. (6.2), (6.5) and (6.6) allow the back-action of a totally generic detector to be understood as the coupling of the oscillator, via a damping rate $\gamma(\omega)$, to a second bath characterized by a fluctuation spectrum $S_F(\omega)$. Extraordinarily, these quantities can be expressed *solely* in terms of the unsymmetrized noise spectrum of the (uncoupled) detector. A simple calculation of $S_F(\omega)$ for a specific detector therefore allows to understand how a harmonic oscillator is affected when coupled to this detector[Clerk05]. This result is very similar to the case discussed in [Pilgram02], where the measurement-induced dephasing and relaxation rates of a qubit could be written in terms of a similar correlator. It also explains the denomination "quantum-noise" approach: the effect of the detector on the oscillator can be understood from a combination of the symmetrized and anti-symmetrized noise correlators of the detector, the anti-symmetrized part of the noise often being referred to as a 'quantum' contribution.

6.1.1 Effective temperature

Looking closely at Eq. (6.2), it is difficult not to notice the strong similarity between the form of the couplings of the oscillator to the environment and to the detector. Usually, in a Langevin equation, an equilibrium thermal bath is characterized by a dissipation term (γ_0) and a fluctuation term, both related to each other via the temperature through a fluctuation-dissipation relation [Eq. (6.3)]. Since in general detectors are out-of-equilibrium systems[3], we cannot expect the detector-induced dissipation and fluctuation terms to also be related via the physical temperature of the detector. However, in the context of nanomechanical systems, it is still useful to define an *effective* temperature $T_{\text{eff}}(\omega)$ via which $\gamma(\omega)$ and $\overline{S}_F(\omega)$ are related

$$\overline{S}_F(\omega) \equiv M\gamma(\omega)\hbar\omega \coth \left(\frac{\hbar\omega}{2k_B T_{\text{eff}}(\omega)} \right) . \qquad (6.7)$$

Using the concept of an effective temperature, we reestablished the equilibrium fluctuation-dissipation relation between $\overline{S}_F$ and γ, even for a non-equilibrium detector. The price to pay for this is that the effective temperature of the detector is now generally *frequency-dependent*. While at first the idea of such a frequency-dependent

---

[3]In fact, one can show[Clerk03b] that a quantum-limited detector cannot be in equilibrium.
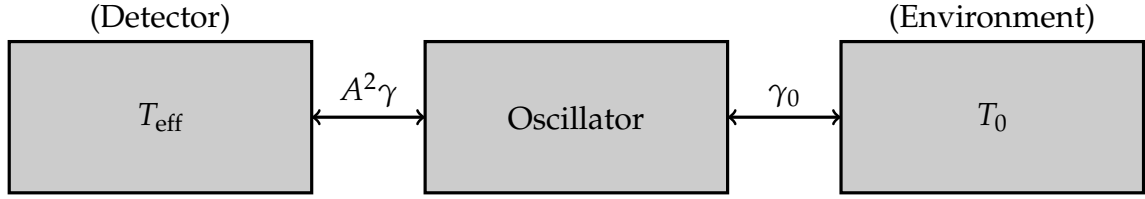
Figure 6.1: The oscillator coupled to two independent thermal baths. The first one (right) is the physical thermal environment, at temperature T_0 while the second bath (left) represents the detector acting as an effective thermal bath at temperature T_{eff}.

temperature might seem useless, it recently proved invaluable in providing a simple way to understand different schemes of "back-action cooling" of nanomechanical oscillators (see e.g. [Naik06b] or Sec. 10.3.2). Indeed, as the response-function of nanomechanical oscillators is strongly peaked around Ω, this system is sensitive mainly to $\gamma(\Omega)$ and $T_{\text{eff}}(\Omega)$.[4] We note that in general the effective temperature will be related to some internal energy scale of the detector and totally unrelated to a physical temperature. For example, in Sec. 6.2, we will show that in the case of a tunnel junction displacement detector the effective temperature is given by half the bias voltage applied between the two leads.

Since, for $x \ll 1$,

$$x \coth(x) = 1 + \mathcal{O}(x^2) \,, \tag{6.8}$$

in the high-temperature limit ($T_0, T_{\text{eff}}(\Omega) \gg \hbar\Omega/k_B$), Eqs. (6.3) and (6.7) simplify considerably, and, at the resonance, we find

$$\overline{S}_F = 2M\gamma k_B T_{\text{eff}} \,. \tag{6.9}$$

In this limit, the coupling of the oscillator to the two baths (the detector and the environment) is easily understood in terms a coupling to a single bath at temperature T_{tot} via a damping rate γ_{tot}, with

$$\gamma_{\text{tot}} = A^2\gamma + \gamma_0 \,, \tag{6.10a}$$

$$T_{\text{tot}} = \frac{A^2\gamma T_{\text{eff}} + \gamma_0 T_0}{\gamma_{\text{tot}}} \,. \tag{6.10b}$$

A consequence of Eq. (6.10) is that, as was demonstrated in [Naik06b], the physical temperature of the oscillator can be experimentally tuned from the cryostat tem-

---

[4]In general, in this text when the frequency-dependence of $\gamma(\omega)$ or $T_{\text{eff}}(\omega)$ is omitted, we implicitly consider $\omega = \Omega$.

perature T_0 to the effective detector temperature T_{eff} by going from the uncoupled ($\gamma_{\text{tot}} = \gamma_0$) regime to the strongly coupled ($A^2\gamma \gg \gamma_0$) one.

6.1.2 Total output noise and bound on the added displacement noise

Linear response does not only allow to estimate the detector's back-action on the oscillator, but also to calculate the signature of the coupling with the oscillator in the detector's output, via

$$I(t) = I_0(t) + A\lambda x(t) \,, \tag{6.11}$$

where $x(t)$ is governed by the Langevin equation [Eq. (6.2)]. Since the back-action force [$F(t)$] due to the detector and the thermal force [$F_0(t)$] are uncorrelated, we can write [Averin03a]

$$x(t) = \int_0^\infty d\tau g(\tau)[F_0(t-\tau) + F(t-\tau)] \tag{6.12}$$

with $g(\tau)$ the inverse Fourier transform of the oscillator's response function

$$g(\omega) = \frac{1}{M} \frac{1}{(\omega^2 - \Omega^2) + i\omega(\gamma_0 + A^2\gamma(\omega))} \,. \tag{6.13}$$

The total output noise spectrum is (classically) [Averin03a; Clerk04a]

$$\overline{S}_{I,\text{tot}}(\omega) = \overline{S}_{I,\text{eq}}(\omega) + \overline{S}_{I,\text{add}}(\omega) \,. \tag{6.14}$$

Here, we separated the contribution of the equilibrium fluctuations of the oscillator (written in terms of the output I, i.e. $\overline{S}_{I,\text{eq}}$) from the rest of the output. For simplicity, we work in the limit where the detector-induced damping $A^2\gamma$ is small with respect to the coupling to the environment γ_0 such that the $g(\omega)$ can be taken as independent of the detector. Explicitly, we find

$$\overline{S}_{I,\text{eq}}(\omega) = |A\lambda(\omega)|^2 |g(\omega)|^2 \overline{S}_{F_0}(\omega, T_0) \,, \tag{6.15}$$

$$\overline{S}_{I,\text{add}}(\omega) = \overline{S}_I(\omega) + A^4|\lambda(\omega)|^2 |g(\omega)|^2 \overline{S}_F(\omega) - 2A^2\text{Re}[g(\omega)\overline{S}_{IF}(\omega)] \,, \tag{6.16}$$

with $\overline{S}_{F,0}(\omega, T_0)$ the spectrum of the physical thermal environment at temperature T_0, as given in Eq. (6.3). When monitoring a nanomechanical oscillator undergoing brownian motion, this corresponds to the interesting part of the signal. $\overline{S}_{I,\text{add}}$ on the other hand term describes the portion of the signal that is detector-dependent:

- the bare output noise of the detector in the uncoupled limit ($\sim \overline{S}_I$),

- the signal coming from the position fluctuations due to the back-action force of the detector ($\sim \overline{S}_F$),

- a term that arises from the real part of the *IF* correlation function of the detector. This term is typically much lower in magnitude than the first two terms.

The quantity $\overline{S}_{I,\mathrm{add}}$ *defines* the sensitivity of the detector. To understand why, it is useful to introduce the total displacement noise $S_{x,\mathrm{tot}}(\omega)$, given by the ratio of the total output noise and the square x-to-I gain of the detector,

$$\overline{S}_{x,\mathrm{tot}}(\omega) = \frac{\overline{S}_{I,\mathrm{tot}}(\omega)}{A^2|\lambda|^2} = \frac{\overline{S}_{I,\mathrm{eq}}(\omega)}{A^2|\lambda|^2} + \frac{\overline{S}_{I,\mathrm{add}}(\omega)}{A^2|\lambda|^2} , \tag{6.17}$$

$$= \overline{S}_{x,\mathrm{eq}}(\omega) + \overline{S}_{x,\mathrm{add}}(\omega) . \tag{6.18}$$

Here, $\overline{S}_{x,\mathrm{eq}}$ is related to the displacement fluctuations due to the thermal forces, while $\overline{S}_{x,\mathrm{add}}(\omega)$ is the so-called "added displacement noise": it corresponds to the displacement noise that depends on the detector used. In a nutshell, if $\overline{S}_{x,\mathrm{eq}}(\omega)$ is what we want to measure, then $\overline{S}_{x,\mathrm{add}}(\omega)$ is an unwanted contribution reflecting the detector's influence on the measurement. The form of the added displacement noise can be read from Eq. (6.14): it can be written as a sum of a shot noise, back-action and *IF*-correlation contributions[Clerk04a]

$$\overline{S}_{x,\mathrm{add}}(\omega) = \frac{\overline{S}_I(\omega)}{|\lambda|^2 A^2} + A^2|g(\omega)|^2 \overline{S}_F(\omega) - \frac{2\mathrm{Re}[\lambda^* g^*(\omega)\overline{S}_{IF}(\omega)]}{|\lambda^2|} . \tag{6.19}$$

As per Eq. (6.19), the actual 'form' of the added noise depends on the coupling A. Taking for a moment the shot noise contribution to be frequency-independent around Ω, we can see that for low couplings it will dominate, and the added displacement noise will correspond to background noise in the spectrum. At the other extreme, in the high-coupling regime the back-action term $\overline{S}_F$ will dominate and the added displacement noise will show up as displacement fluctuations of an oscillator at a temperature that differs from T_0, the temperature of the thermal environment. It is important to note that, even in the case where the oscillator is truly, physically being heated by the detector, the added 'signal' associated with the increased temperature of the oscillator is not useful to the measurement of the displacement fluctuations of the original thermal oscillator. In both shot-noise and back-action dominated regimes, the added displacement noise hinders the measurement of $\overline{S}_{x,\mathrm{eq}}$: this is why it is used to define the sensitivity of the measurement.

In the remainder of this section, we will derive the quantum limit on the sensitivity of a displacement measurement by finding the conditions under which the added displacement noise is minimal. Looking at Eq. (6.19) we see that the dependence of

$\overline{S}_{x,\text{add}}$ on the coupling strength has the form[5]

$$\overline{S}_{x,\text{add}} \sim \frac{x}{A^2} + A^2 y + z \, . \tag{6.20}$$

Minimizing with respect to A, we find $A^2_{\text{opt}} = \sqrt{x/y}$, which leads to

$$A^2_{\text{opt}} = \left(\frac{\overline{S}_I(\omega)}{|\lambda|^2 |g(\omega)|^2 \overline{S}_F(\omega)} \right)^{1/2} . \tag{6.21}$$

The optimal coupling constant corresponds to the point where the contribution of the bare-output (shot) noise and the back-action noises are equal, *exactly* like in the case of the Heisenberg microscope presented in Sec. 4.1.1. At this optimal coupling, the added noise is bounded by

$$\overline{S}_{x,\text{add}}(\omega) \geq 2|g(\omega)| \left[\sqrt{\frac{\overline{S}_I(\omega)\overline{S}_F(\omega)}{|\lambda|^2}} - \frac{2\text{Re}[\lambda^* e^{i\phi(\omega)}\overline{S}_{IF}(\omega)]}{|\lambda^2|} \right] , \tag{6.22}$$

where we wrote $g(\omega) = |g(\omega)|e^{i\phi(\omega)}$. The $\overline{S}_I(\omega)\overline{S}_F(\omega)/|\lambda|^2$ term in this expression is minimized when using a quantum-limited detector that satisfies Eq. (4.22). Subsequently minimizing with respect to $\overline{S}_{IF}(\omega)$, one finds a condition on the *IF* correlation function that must be satisfied for the added displacement noise to be minimal[Clerk04a]

$$\overline{S}_{IF}(\omega) = \frac{\hbar}{2}\lambda \cot \phi(\omega) \, . \tag{6.23}$$

For (i) a quantum-limited detector (ii) used at the optimal coupling point and where (iii) $\overline{S}_{IF}(\omega)$ satisfies this equation, we find[Caves80]

$$\overline{S}_{x,\text{add}}(\omega) \geq \overline{S}^{\text{min}}_{x,\text{add}}(\omega) = \overline{S}_{x,\text{eq}}(\omega, T_0 = 0) = \hbar|\text{Im}g(\omega)| \, ; \tag{6.24}$$

the added displacement noise is always at least as important as the zero-temperature displacement fluctuation of the measured harmonic oscillator.

In the literature, this result is not always written in terms of an added displacement spectral density. Sometimes measurement sensitivities are instead given in terms of Δx_{SQL} [Eq.(4.11)], the standard quantum limit for position measurement of a harmonic oscillator. To convert from the added displacement noise to an absolute position resolution Δx, one uses

$$\Delta x = \sqrt{\overline{S}_{x,\text{add}} \times \Delta f} = \sqrt{\overline{S}_{x,\text{add}} \gamma / 2} \tag{6.25}$$

---

[5]We remind the reader that we are considering the regime where $A^2 \gamma \ll \gamma_0$ such that $g(\omega)$ is independent of A.

with $\Delta f = \gamma/2$ the bandwidth of the measurement [Naik06a]. Moreover, at the resonance,

$$\frac{\Delta x}{\Delta x_{\text{SQL}}} = \frac{\sqrt{\overline{S}_{x,\text{add}}}}{\sqrt{\overline{S}_{x,\text{add}}^{\text{min}}}} \, , \tag{6.26}$$

such that for all practical purposes results can be easily converted from one notation to the other. Also, note the convention often used in the literature to write directly $\overline{S}_x = \overline{S}_I/|\lambda^2|$ to define the sensitivity of a measurement when back-action is not observed (note that here the subscript 'add' was left out).

To conclude this section, we want to stress that experimentally reaching the bound on the added displacement noise is really the next milestone that should be achieved in the quest to observe quantum behavior in NEMS. Moreover, we mention that lot of ideas regarding the creation and manipulation of non-classical states of the harmonic oscillator via quantum feedback[Hopkins03; Ruskov05b] *rely* on the use of position detectors that operate close the quantum limit. Also, while in this section the quantum limit was derived for a generic detector, we note that the derivation in the specific case of a tunnel junction displacement detector is presented in Sec. 8.4.

6.2 Linear response for a tunnel junction

In this section, we apply the general results derived previously to the specific case of a tunnel junction displacement detector. This should allow the reader to get a deeper understanding of these results. At the same time, this will allow an easier comparison of the linear-response predictions and the ones obtained using equation-of-motion approaches presented in the next chapter.

As discussed in Chap. 5, the Hamiltonian describing a tunnel junction can be written as the sum of a "leads" and a "tunneling" Hamiltonian

$$H = H_{\text{leads}} + H_{\text{tun}} \, , \tag{6.27}$$

where

$$H_{\text{leads}} = \sum_k \varepsilon_k c_k^\dagger c_k + \sum_q \varepsilon_q c_q^\dagger c_q \, , \tag{6.28}$$

$$H_{\text{tun}} = \frac{t_0}{2\pi\Lambda} \sum_{k,q} c_k^\dagger c_q + \frac{t_0^*}{2\pi\Lambda} \sum_{k,q} c_q^\dagger c_k \, . \tag{6.29}$$

Here, $c_\alpha^{(\dagger)}$ creates (annihilates) an electron with wave-vector α, $k(q)$ is a wave-vector in the right (left) lead and Λ an average density of states in the leads. The coupling to

the harmonic oscillator is realized via

$$H_{\text{int}} = \hat{x}\hat{F} \, , \tag{6.30}$$

$$\hat{F} = \frac{t_1}{2\pi\Lambda} \sum_{k,q} c_k^\dagger c_q + \frac{t_1^*}{2\pi\Lambda} \sum_{k,q} c_q^\dagger c_k \, , \tag{6.31}$$

the same generic form as the one given Eq. (6.1). The output of the detector $\hat{I}$ is nothing else than the time derivative of the average number of electrons on the right lead, $\hat{N}_r = \sum_k c_k^\dagger c_k$.

$$\hat{I} = e\frac{d}{dt}\hat{N}_r = \frac{1}{i\hbar}[H_{\text{tun}}, \hat{N}_r] = e\frac{i}{2\pi\hbar\Lambda} \sum_{k,q} \left(t_0 c_k^\dagger c_q - t_0^* c_q^\dagger c_k \right) \, . \tag{6.32}$$

We note that, in the spirit of the linear response, the contribution of the interaction Hamiltonian to the tunneling amplitude ($\sim t_1$) should not be included in the detector output operator $\hat{I}$.

To calculate the correlation functions $S_{I(F)}(\omega)$, we need to know the form of $\hat{F}$ and $\hat{I}$ in the interaction picture. It is given by

$$\hat{I}(t) = \hat{U}_0^\dagger(t)\hat{I}\hat{U}_0(t) = e\frac{i}{2\pi\hbar\Lambda} \sum_{k,q} \left(t_0 c_k^\dagger(t)c_q(t) - t_0^* c_q^\dagger(t)c_k(t) \right) \, , \tag{6.33}$$

$$\hat{F}(t) = \hat{U}_0^\dagger(t)\hat{F}\hat{U}_0(t) = \frac{t_1}{2\pi\Lambda} \sum_{k,q} c_k^\dagger(t)c_q(t) + \frac{t_1^*}{2\pi\Lambda} \sum_{k,q} c_q^\dagger(t)c_k(t) \, , \tag{6.34}$$

where the interaction picture representation of the creation and annihilation operators is given by

$$c_k(t) = e^{-i\varepsilon_k t/\hbar} c_k \, , \tag{6.35}$$

$$c_k^\dagger(t) = e^{i\varepsilon_k t/\hbar} c_k^\dagger \, . \tag{6.36}$$

6.2.1 Calculation of the correlation functions

Using the formalism just introduced, we can calculate explicitly the correlation functions $S_I(\omega)$, $S_F(\omega)$ and $S_{IF}(\omega)$ needed to describe the effect of the detector on the oscillator. Each calculation is pretty straightforward. Starting with $S_F(\omega)$, we find

$$S_F(\omega) = \int_{-\infty}^{\infty} dt\, e^{i\omega t} \langle \hat{F}(t)\hat{F}(0) \rangle \, , \tag{6.37}$$

$$= \frac{|t_1|^2}{(2\pi\Lambda)^2} \int_{-\infty}^{\infty} dt \sum_{k,q} \left[e^{i(\varepsilon_q - \varepsilon_k + \hbar\omega)t/\hbar} f_q(1 - f_k) + e^{-i(\varepsilon_q - \varepsilon_k - \hbar\omega)t/\hbar} f_k(1 - f_q) \right] \, , \tag{6.38}$$

where f represents the equilibrium Fermi distributions in each lead

$$\langle c_k^\dagger c_{k'} \rangle = f_k \delta_{k,k'} \, , \tag{6.39}$$

$$\langle c_q^\dagger c_{q'} \rangle = f_q \delta_{q,q'} \, , \tag{6.40}$$

$$\langle c_k^\dagger c_{q'} \rangle = \langle c_q^\dagger c_{k'} \rangle = 0 \, , \tag{6.41}$$

with $f_k = f_R(\varepsilon_k)$ and $f_q = f_L(\varepsilon_q)$. Noting $\nu(E)$ the density of states in the leads, we perform the substitution

$$\sum_{k,q} \rightarrow \iint d\varepsilon_k \, d\varepsilon_q \, \nu(\varepsilon_k) \nu(\varepsilon_q) \, . \tag{6.42}$$

In this section, we consider a non-superconducting tunnel junction such that we can approximate the density of states as constant ($\nu(\varepsilon_k) = \Lambda$) in the relevant energy range close to the Fermi level. Proceeding with the integration, taking into account the presence of a bias voltage via two different chemical potentials $\mu_L = \mu_R + eV$, we find

$$S_F(\omega) = \frac{\hbar |t_1|^2}{2\pi} (eV + \hbar\omega) \coth\left(\frac{eV + \hbar\omega}{2k_B T_e} \right) \, , \tag{6.43}$$

with T_e the electronic temperature in the leads. In the $k_B T_e \rightarrow 0$ and $|eV| > \hbar\omega$ limit, this simplifies to

$$S_F(\omega) = \frac{\hbar |t_1|^2}{2\pi} (|eV| + \hbar\omega) \, , \tag{6.44}$$

since $\coth(x) \rightarrow \pm 1$ for $x \rightarrow \pm\infty$. Similarly, we find that the symmetrized current noise is given by [Blanter00, Equation 127],[Yang92]

$$\overline{S}_I(\omega) = \frac{e^2}{2h} |t_0|^2 \left[(\hbar\omega + eV) \coth\left(\frac{\hbar\omega + eV}{2k_B T_e} \right) + (\hbar\omega - eV) \coth\left(\frac{\hbar\omega - eV}{2k_B T_e} \right) \right] \, , \tag{6.45}$$

$$\simeq \frac{e^2}{h} |t_0|^2 \times \max(|\hbar\omega|, |eV|) \qquad [\text{for } k_B T_e \rightarrow 0] \, . \tag{6.46}$$

Calculating the IF correlation function, we find

$$S_{IF}(\omega) = \frac{ei}{2\pi} \left[t_0 t_1^* \int d\epsilon f_R(\epsilon)[1 - f_L(\epsilon - \hbar\omega)] - t_0^* t_1 \int d\epsilon f_L(\epsilon)[1 - f_R(\epsilon - \hbar\omega)] \right] \, . \tag{6.47}$$

By writing the complex tunneling amplitudes in polar form $t_i = |t_i| e^{\phi_i}$, we see that S_{IF} depends only on the phase difference $\eta = \phi_1 - \phi_0$ between t_0 and t_1, as

$$t_0^* t_1 = |t_0 t_1| e^{i\eta} \, . \tag{6.48}$$

In terms of η, we find that the real and imaginary parts of the fully symmetrized *IF* correlation function are given by

$$
\mathrm{Re}[\frac{S_{IF}(\omega) + S_{IF}(-\omega)}{2}]
$$
$$
= \frac{e}{2\pi}|t_0 t_1| \sin\eta \times \left[(\hbar\omega - eV)\coth\left(\frac{\hbar\omega - eV}{2k_B T_e}\right) + (\hbar\omega + eV)\coth\left(\frac{\hbar\omega + eV}{2k_B T_e}\right) \right], \tag{6.49}
$$

$$
\simeq \frac{e}{2\pi}|t_0 t_1| \sin\eta \times \max(|\hbar\omega|, |eV|) \qquad [\text{for } k_B T_e \to 0] . \tag{6.50}
$$

$$
\mathrm{Im}[\frac{S_{IF}(\omega) + S_{IF}(-\omega)}{2}] = \frac{e}{2\pi}|t_0 t_1| \cos\eta \times eV . \tag{6.51}
$$

6.2.2 Effective environment

From the different correlation functions derived in the previous section, we can directly calculate the back-action of the tunnel junction displacement detector on the nanomechanical resonator, in the effective environment picture. First, the detector-induced damping is, following Eqs. (6.6) and (6.43),

$$
\gamma(\Omega) = \frac{\hbar|t_1|^2}{4\pi M}\left[\frac{(eV + \hbar\Omega)\coth\left(\frac{eV+\hbar\Omega}{2k_B T_e}\right) - (eV - \hbar\Omega)\coth\left(\frac{eV-\hbar\Omega}{2k_B T_e}\right)}{\hbar\Omega} \right], \tag{6.52}
$$

$$
\simeq \frac{\hbar|t_1|^2}{2\pi M} \qquad [\text{for } k_B T_e \to 0] . \tag{6.53}
$$

From this equation, we see that the contribution of the tunnel junction position detector to the total damping is always positive and quadratic in the coupling t_1. In the high-temperature limit, using Eqs. (6.9) and (6.43), we find that the effective temperature associated with the tunnel junction is given by

$$
T_{\mathrm{eff}}(\Omega) = \frac{|eV|}{2k_B} . \tag{6.54}
$$

This nicely proves that the effective temperature seen by oscillator is related to an important energy scale of the tunnel junction, and is totally unrelated to the physical 'temperature' of the electron in the leads forming the junction (T_e). Since both the effective temperature and the damping rate are always positive, the steady-state of a nanomechanical oscillator coupled to a tunnel junction is always a thermal state, contrary to what is observed for a superconducting single-electron transistor (see Part IV). In the presence of measurement, the oscillator therefore behaves in the exact same way

as an oscillator with damping rate γ_{tot} coupled to a bath at temperature T_{tot}, with

$$\gamma_{\text{tot}} = \gamma_0 + \frac{\hbar |t_1|^2}{2\pi M} , \tag{6.55}$$

$$T_{\text{tot}} = \frac{\gamma_0 T_0 + \frac{\hbar |t_1|^2 |eV|}{4\pi M}}{\gamma_{\text{tot}}} . \tag{6.56}$$

6.2.3 Quantum-limited detection

Using the correlation functions calculated in Sec. 6.2.1, we can estimate the measurement efficiency $\mathcal{N}$ [Clerk03a], defined as the ratio of the right and left hand sides of the inequality (4.17)

$$\mathcal{N} = \frac{\frac{\hbar^2}{4} (\text{Re}[\lambda(\omega) - \lambda'(\omega)])^2 + (\text{Re}[\overline{S}_{IF}(\omega)])^2}{\overline{S}_I(\omega) \overline{S}_F(\omega)} \leq 1 . \tag{6.57}$$

The measurement efficiency quantifies the "quantum-limitedness" of a detector. A detector with $\mathcal{N} \ll 1$ is very poor from a quantum measurement point of view, whereas $\mathcal{N} = 1$ is reached only for a quantum-limited detector that satisfies Eq. (4.22). Using Eq. (C.2) to rewrite $\mathcal{N}$ only in terms of the symmetrized I, F, IF correlation functions of the detector we find

$$\mathcal{N}(\omega) = \frac{|S_{IF}(\omega) + S_{IF}(-\omega)|^2}{4\overline{S}_I(\omega) \overline{S}_F(\omega)} . \tag{6.58}$$

In general, $\mathcal{N}$ will depend on the frequency ω, and again $\mathcal{N}(\Omega)$ is the relevant quantity when considering the measurement of a quantum system with typical timescale $(1/\Omega)$. However, since the timescales characterizing tunnel junctions are typically very short compared to the inverse of the frequency of mechanical oscillator, we can use $N(\Omega) \sim N(0)$ in this context.

First, let us study the dependence of $\mathcal{N}$ in the phase difference η [Eq. (6.48)] between the two tunneling amplitudes t_0, t_1. Both $\overline{S}_I$ and $\overline{S}_F$ are independent of η, such that the phase difference appears only in the numerator of Eq. (6.58). From Eqs. (6.50) and (6.51), we see that in the $k_B T_e \to 0, eV \gg \hbar\Omega$ limit,

$$|S_{IF}(\omega) + S_{IF}(-\omega)|^2 = |\frac{e}{2\pi}|t_0 t_1|eV \cos\eta|^2 + |\frac{e}{2\pi}|t_0 t_1|eV \sin\eta|^2 , \tag{6.59}$$

$$= (\frac{e}{2\pi}|t_0 t_1|eV)^2 . \tag{6.60}$$

In this (experimentally relevant) limit, the efficiency is therefore totally independent of η [Doiron08]. Moreover, the calculation confirms that the tunnel junction is a quantum-limited detector[Korotkov99; Averin03a]

$$\mathcal{N} = \frac{e^2 |t_0 t_1|^2 (eV)^2}{4\pi^2} \frac{2\pi}{\hbar |t_1|^2 |eV|} \frac{h}{e^2 |t_0|^2 |eV|} = 1 , \tag{6.61}$$
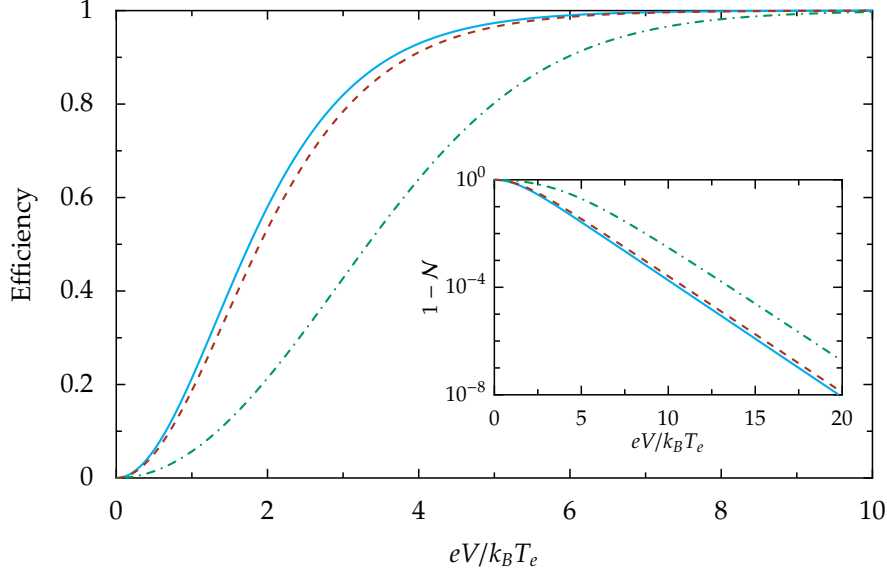
Figure 6.2: Main panel: Efficiency $\mathcal{N}(\Omega)$ of the tunnel junction as a quantum detector, as defined in Eq. (6.58). Inset: $1 - \mathcal{N}$, plotted on a logarithmic scale that allows better resolution in the region where $\mathcal{N}$ is very close to 1. In both cases, the solid line corresponds the "high-temperature" case ($k_B T_e = 1000\hbar\Omega$), and the dashed line and dash-dotted lines correspond to the low-temperature regime, $k_B T_e = \hbar\Omega$ and $k_B T_e = \hbar\Omega/4$ respectively. Since the efficiency is plotted as a function of $eV/k_B T_e$, note that the magnitude of the bias voltage is also reduced in these two last cases.

Since we have the full expression of the different correlators for finite $\Omega, k_B T_E$, we can evaluate how $\mathcal{N}$ decays away from the $\hbar\Omega/eV, k_B T_E/eV \to 0$ point. In Fig. 6.2, we present $\mathcal{N}$ as a function of $eV/k_B T_e$, for two different values of $k_B T_e/\hbar\Omega$ and $\eta = 0$. As seen from this figure, the efficiency of the tunnel junction is extremely high, as long as $eV \gg \hbar\Omega, k_B T_e$. Physically, this reduction in the efficiency comes from the presence of thermal (Johnson-Nyquist) noise from equilibrium currents at finite temperature, that increases $\overline{S}_I$ but does not affect the gain λ. Also, note that the efficiency in all regimes is independent of the parameters t_1, t_0 and that numerically we verified that $N(\Omega) - N(0) \to 0$ in the $eV \gg \hbar\Omega, k_B T_e$ regime.

Equation-of-motion approaches

The original results that will be presented in Chaps. 8, 9 and 11 were obtained using an equation-of-motion approach, where the effective time evolution of the density matrix of the oscillator in the presence of the detector is studied. In many respects, this approach can be seen as the quantum equivalent of the equation-of-motion approach for the probability density of a classical oscillator presented in Chap. 3. Also, it is important to stress that the applicability of the approach is not limited to the study of NEMS, but that it also generally applies to open quantum systems, in quantum optics, etc.

The cornerstone of the equation-of-motion approach is the so-called *master equation*, that describes the evolution of the density matrix of a quantum system in the presence of a bath. Just like we did in Chap. 6, we will first derive this equation for a general system (Sec. 7.1), following mainly [Gardiner04]. Afterwards, we will apply the formalism to NEMS in general (Sec. 7.2) and finally specifically to the tunnel junction displacement detector (Sec. 7.3).

7.1 Derivation of the Born-Markov master equation

In the study of open quantum systems (quantum systems coupled to one or more baths), one of the main theoretical objective is to find an *effective* description of the system that takes into account the effect of the bath, without solving for the complete system+bath problem. The master equation we will derive in this section provides just that.

We consider a quantum system with Hamiltonian H_{sys} coupled to a bath (H_{B}) via an interaction term H_{int}, such that

$$H_{\text{tot}} = H_{\text{sys}} + H_{\text{B}} + H_{\text{int}} \,. \tag{7.1}$$

We denote ρ_{tot} the total density matrix of the system and the bath. The time-evolution of ρ_{tot} obeys the von Neumann equation

$$\frac{d}{dt}\rho_{\text{tot}} = \frac{1}{i\hbar}[H_{\text{tot}}, \rho_{\text{tot}}] . \tag{7.2}$$

This is the starting point in the derivation of the more interesting equation-of-motion of the reduced density operator $\rho_{\text{sys}} = \text{Tr}_B[\rho_{\text{tot}}]$. In the interaction picture, with

$$U(t) = e^{-i(H_{\text{sys}} + H_B)t/\hbar} , \tag{7.3}$$

$$\rho_{\text{tot}}^i(t) = U^{\dagger}(t)\rho_{\text{tot}}(t)U(t) , \tag{7.4}$$

$$H_{\text{int}}(t) = U^{\dagger}(t)H_{\text{int}}U(t) , \tag{7.5}$$

Eq. (7.2) takes the form

$$\frac{d}{dt}\rho_{\text{tot}}^i(t) = \frac{1}{i\hbar}[H_{\text{int}}(t), \rho_{\text{tot}}^i(t)] . \tag{7.6}$$

To proceed, we assume that the system and bath are initially independent, such that the total density matrix at time 0 factorizes

$$\rho_{\text{tot}}(0) = \rho_{\text{sys}}(0) \otimes \rho_B . \tag{7.7}$$

Moreover, we consider the bath to be much larger than the system and limit ourselves to weak system-bath coupling. In these conditions, the properties of the bath (namely, its density matrix) will not be affected by the coupling to the quantum system. Using the initial condition given in Eq. (7.7), we can integrate the von Neumann equation [Eq. (7.6)] iteratively up to time t. After two iterations, one finds

$$\rho_{\text{tot}}^i(t) = \rho_{\text{tot}}^i(0) + \frac{1}{i\hbar}\int_0^t dt' \left[H_{\text{int}}(t'), \rho_{\text{tot}}^i(0) + \frac{1}{i\hbar}\int_0^{t'} dt'' \left[H_{\text{int}}(t''), \rho_{\text{tot}}^i(t'') \right] \right] . \tag{7.8}$$

While it is possible to continue the expansion to get terms of higher order in the interaction, it is more convenient to differentiate the last expression with respect to t, to find an integro-differential equation for the total density matrix in the interaction picture

$$\frac{d}{dt}\rho_{\text{tot}}^i(t) = \frac{1}{i\hbar}\left[H_{\text{int}}(t), \rho_{\text{tot}}^i(0) \right] - \frac{1}{\hbar^2}\int_0^t dt' \left[H_{\text{int}}(t), [H_{\text{int}}(t'), \rho_{\text{tot}}^i(t')] \right] . \tag{7.9}$$

To go from an equation for $\rho_{\text{tot}}^i(t)$ to one for the reduced system density matrix ρ_{sys}^i, we trace both sides of the last equation over the bath variables. Assuming that the $\text{Tr}_B[H_{\text{int}}(t)\rho_{\text{sys}}(0) \otimes \rho_B] = 0,$[1] we find

$$\frac{d}{dt}\rho_{\text{sys}}^i(t) = -\frac{1}{\hbar^2}\int_0^t dt' \text{Tr}_B\left\{ \left[H_{\text{int}}(t), [H_{\text{int}}(t'), \rho_{\text{tot}}^i(t')] \right] \right\} . \tag{7.10}$$

---

[1]This is not a required assumption, since any part of the interaction Hamiltonian that would contribute to this trace can be included in the system Hamiltonian.

This last equation for the reduced density matrix still involves in the right hand side the total density matrix ρ_{tot}^i. In the regime of weak-coupling between the system and the bath, we can extend the condition of factorizing initial conditions [Eq. (7.7)] to finite times

$$\rho_{tot}^i(t) \approx \rho_{sys}^i(t) \otimes \rho_B \ . \tag{7.11}$$

This weak-coupling approximation is referred to as the *Born approximation*[Breuer02]. Even within the Born approximation, the master equation of Eq. (7.10) is non-local in time. To make it local in time, we perform the *Markov* approximation that the evolution of the system at time t depends only on the density matrix at this time t, and therefore that knowledge of $\rho_{sys}(t_0)$ is allows for the calculation of $\rho_{sys}(t)$ for all $t > t_0$. This leads to the Redfield equation[Redfield57]

$$\frac{d}{dt}\rho_{sys}^i(t) = -\frac{1}{\hbar^2} \int_0^t dt' \text{Tr}_{\text{B}} \left\{ \left[H_{\text{int}}(t), [H_{\text{int}}(t'), \rho_{sys}^i(t) \otimes \rho_B] \right] \right\} \ . \tag{7.12}$$

When dealing with systems where the bath correlations decay on a timescale τ_{B} that is much shorter than the typical timescale τ_{S} characterizing the system, it is justified to further simplify the equation by letting the lower bound of the integration region go to $-\infty$, provided we are interested in probing the system on the τ_{S} timescale[2]. This leads to the Born-Markov master equation

$$\frac{d}{dt}\rho_{sys}^i(t) = -\frac{1}{\hbar^2} \int_0^\infty dt' \text{Tr}_{\text{B}} \left\{ \left[H_{\text{int}}(t), [H_{\text{int}}(t - t'), \rho_{sys}^i(t) \otimes \rho_B] \right] \right\} \ , \tag{7.13}$$

that can also be written as an equation-of-motion for the density matrix in the Schrödinger picture

$$\frac{d}{dt}\rho_{sys}(t) = \frac{1}{i\hbar} \left[H_0, \rho_{sys}(t) \right] - \frac{1}{\hbar^2} \int_0^\infty dt' \text{Tr}_{\text{B}} \left\{ \left[H_{\text{int}}, [H_{\text{int}}(-t'), \rho_{sys}(t) \otimes \rho_B] \right] \right\} \tag{7.14}$$

For completeness, we note that the approximations made while deriving the Born-Markov master equation, while in general valid in the context of nanoelectromechanical systems, cannot be justified for all physical systems. Most notably, when studying systems where the timescale at which the bath evolves is long with respect to the typical system timescales, one expects non-Markovian effects to be important.

7.2 Born-Markov master equation in the context of NEMS

Approaches based on quantum master equations have proven useful in the study of nanomechanical systems [Utami04; Rodrigues05]. In the aforementioned articles, the

---

[2]We emphasize that the Markovian approximation corresponds to a "coarse-graining" of the time axis and that the resulting master-equation cannot be used to probe the dynamics of the system on very short timescales (τ_{B}).

authors used the master equation approach to describe the effect of coupling a *specific* detector to the mechanical resonator. However, just like in the case of linear response (Sec. 6.1), we can learn a lot about the effect of a *general* detector (bath) coupled to a harmonic oscillator using the Born-Markov master equation without the need for a detailed description of the detector. To proceed, we simply use the system and inter-action Hamiltonian we introduced in Chap. 6,

$$H_{\text{sys}} = \hbar\Omega\left(a^\dagger a + \frac{1}{2}\right) = \frac{\hat{p}^2}{2M} + \frac{M\Omega^2\hat{x}^2}{2} , \tag{7.15}$$

$$H_{\text{int}} = \hat{F}\hat{x} , \tag{7.16}$$

with $\hat{F}$ a general input variable of the detector and $\hat{x}$ the position operator of the os-cillator.[3]

Inserting the interaction Hamiltonian in Eq. (7.14) and developing the commuta-tors, we find

$$
\begin{aligned}
\frac{d}{dt}\rho_{\text{sys}}(t) = {} & \frac{1}{i\hbar}\left[H_{\text{sys}}, \rho_{\text{sys}}(t)\right] \\
& - \frac{1}{\hbar^2}\int_0^\infty dt'\left[\hat{x}\hat{x}(-t')\rho_{\text{sys}}(t) - \hat{x}(-t')\rho_{\text{sys}}(t)\hat{x}\right]\langle\hat{F}(0)\hat{F}(-t')\rangle \\
& - \frac{1}{\hbar^2}\int_0^\infty dt'\left[\rho_{\text{sys}}(t)\hat{x}(-t')\hat{x} - \hat{x}\rho_{\text{sys}}(t)\hat{x}(-t')\right]\langle\hat{F}(-t')\hat{F}(0)\rangle ,
\end{aligned}
\tag{7.17}
$$

where the trace on the bath was carried out, giving rise to the averages on the bath operators F. Using the properties of the correlation function of an hermitian operator A

$$\langle A(-t)A(0)\rangle = \langle A(0)A(t)\rangle = \langle A(t)A(0)\rangle^* \tag{7.18}$$

and introducing the compact notation

$$\mathcal{F}_+(t) = \langle\{\hat{F}(t), \hat{F}(0)\}\rangle = 2\text{Re}\langle\hat{F}(t)\hat{F}(0)\rangle = +\mathcal{F}_+(-t) , \tag{7.19}$$
$$\mathcal{F}_-(t) = \langle[\hat{F}(t), \hat{F}(0)]\rangle = 2i\text{Im}\langle\hat{F}(t)\hat{F}(0)\rangle = -\mathcal{F}_-(-t) , \tag{7.20}$$

for the symmetrized and anti-symmetrized time correlators, Eq. (7.17) can be brought into a simpler form

$$
\begin{aligned}
\frac{d}{dt}\rho_{\text{sys}}(t) = {} & \frac{-i}{\hbar}[H_{sys}, \rho_{\text{sys}}(t)] \\
& - \frac{1}{2\hbar^2}\int_0^\infty dt'[\hat{x}, [\hat{x}(-t'), \rho_{\text{sys}}(t)]]\mathcal{F}_+(t') \\
& - \frac{1}{2\hbar^2}\int_0^\infty dt'[\hat{x}, \{\hat{x}(-t'), \rho_{\text{sys}}(t)\}]\mathcal{F}_-(t') .
\end{aligned}
\tag{7.21}
$$

---

[3]To keep concise, now integrate the dimensionless coupling constant A present in Chap. 6 to $\hat{F}$

Using Eq. (7.15), the position operator in the interaction picture can be written as

$$\hat{x}(t) = U_0^\dagger(t)\hat{x}U_0(t) , \tag{7.22}$$

$$= \hat{x}\cos(\Omega t) + \frac{1}{M\Omega}\hat{p}\sin(\Omega t) . \tag{7.23}$$

Inserting this result into Eq. (7.21) leads to

$$\frac{d}{dt}\rho_{\text{sys}}(t) = \frac{-i}{\hbar}[H_{\text{sys}},\rho_{\text{sys}}(t)] - \frac{1}{2\hbar^2}[\hat{x},[\hat{x},\rho_{\text{sys}}(t)]]\int_0^\infty dt'\cos(\Omega t')\mathcal{F}_+(t')$$
$$+ \frac{1}{2M\hbar^2\Omega}[\hat{x},[\hat{p},\rho_{\text{sys}}(t)]]\int_0^\infty dt'\sin(\Omega t')\mathcal{F}_+(t')$$
$$- \frac{1}{2\hbar^2}[\hat{x},\{\hat{x},\rho_{\text{sys}}(t)\}]\int_0^\infty dt'\cos(\Omega t')\mathcal{F}_-(t')$$
$$+ \frac{1}{2M\hbar^2\Omega}[\hat{x},\{\hat{p},\rho_{\text{sys}}(t)\}]\int_0^\infty dt'\sin(\Omega t')\mathcal{F}_-(t') . \tag{7.24}$$

Introducing the parameters

$$D_{PP} = \frac{1}{2}\int_0^\infty dt'\cos(\Omega t')\mathcal{F}_+(t') , \tag{7.25a}$$

$$-i\tilde{\gamma} = \frac{1}{2M\hbar\Omega}\int_0^\infty dt'\sin(\Omega t')\mathcal{F}_-(t') , \tag{7.25b}$$

$$\Delta^2 = \frac{i}{M\hbar}\int_0^\infty dt'\cos(\Omega t')\mathcal{F}_-(t') , \tag{7.25c}$$

$$D_{PX} = \frac{1}{4M\hbar\Omega}\int_0^\infty dt'\sin(\Omega t')\mathcal{F}_+(t') , \tag{7.25d}$$

one finds that the equation of motion for the reduced density matrix is of Caldeira-Leggett (CL) [Caldeira83; Breuer02] form

$$\frac{d}{dt}\rho_{\text{sys}} = -\frac{i}{\hbar}\Big[\frac{\hat{p}^2}{2M} + \frac{M(\Omega^2-\Delta^2)\hat{x}^2}{2},\rho_{\text{sys}}\Big]$$
$$- \frac{1}{\hbar^2}D_{PP}[\hat{x},[\hat{x},\rho_{\text{sys}}]] - \frac{i\tilde{\gamma}}{\hbar}[\hat{x},\{\hat{p},\rho_{\text{sys}}\}] + \frac{2}{\hbar}D_{PX}[\hat{x},[\hat{p},\rho_{\text{sys}}]] , \tag{7.26}$$

with a damping ($\sim \tilde{\gamma}$), diffusion ($\sim D_{PP}$) term, a term that renormalizes the frequency of the oscillator ($\sim \Delta^2$) and another contribution. As will be discussed in detail in Appendix B, the CL equation describes the evolution of the density matrix of a particle undergoing quantum brownian motion, i.e. a particle in *a thermal environment*.[4] The physical interpretation of Eq. (7.26) is therefore that a detector very generally acts as a thermal bath for the oscillator. Amazingly, in this section we derived in only few lines (and in a totally different way) the main result of [Mozyrsky02; Clerk04a].

---

[4]The reader that is totally unfamiliar with the Caldeira-Leggett equation would surely benefit from reading Appendix B before continuing reading the current chapter.

Link with the linear response result

Just like in the linear-response approach, the different parameters [Eq. (7.25)] of the CL equation can be written solely in terms of the detector's correlation functions $\mathcal{F}_{\pm}$. Fortunately, we can demonstrate that the expression of two parameters derived in the linear-response approach (the damping and diffusion coefficients) are identical to the ones given in the master-equation approach. First, we examine the case of the damping rate. In the master equation approach, we wrote it as [Eq. (7.25b)],

$$\tilde{\gamma} = i\frac{1}{2M\hbar\Omega} \int_0^\infty dt' \sin(\Omega t')\mathcal{F}_-(t') , \tag{7.27}$$

$$= \frac{1}{4M\hbar\Omega} \int_{-\infty}^\infty dt' e^{i\Omega t'}\mathcal{F}_-(t') , \tag{7.28}$$

where we used the fact that $\mathcal{F}_-$ is anti-symmetric in time to expand the integration range over the whole real axis. Using now $\mathcal{F}_-(t) = \langle[F(t), F(0)]\rangle$, one finds that

$$\int_{-\infty}^\infty dt' e^{i\Omega t'}\mathcal{F}_-(t') = S_F(\Omega) - S_F(-\Omega) , \tag{7.29}$$

such that

$$\tilde{\gamma} = \frac{1}{4M\hbar\Omega} \left[S_F(\Omega) - S_F(-\Omega)\right] . \tag{7.30}$$

One therefore sees directly that the obtained damping rate is consistent with the linear response calculation. Also, it is clear in this approach that the effective damping rate *at the frequency of the oscillator* is relevant quantity from the point of view of the oscillator. Similarly, looking at D_{PP} and relating it to T_{eff} via Eq. (B.18),

$$D_{PP} = 2M\tilde{\gamma}k_B T_{\text{eff}} = \frac{1}{2} \int_0^\infty dt' \cos(\Omega t')\mathcal{F}_+(t') \tag{7.31}$$

$$= \frac{1}{2}\overline{S}_F(\Omega) , \tag{7.32}$$

one finds that the effective temperature is a function of the symmetrized F correlation function

$$k_B T_{\text{eff}} = \frac{\overline{S}_F(\Omega)}{2(2\tilde{\gamma})M} , \tag{7.33}$$

exactly like in Eq. (6.9).[5].

---

[5]In the literature, there are two conventions regarding the damping term. Damping brings a contribution $-\gamma p$ to $\dot{p}$ in the first one and $-2\tilde{\gamma}p$ in the second one. For historical reasons, both conventions are used in this text. However, since we identified the situations where the second convention is used by writing $\tilde{\gamma}$ instead of γ, this should not pose problems.

Caldeira-Leggett model and quantum measurement

We already mentioned that the direct physical interpretation of the fact that the equation-of-motion for the harmonic oscillator coupled to a displacement detector is of CL form is that the detector acts as an effective thermal environment. Looking at the system from the complementary point of view of quantum measurement however, allows a slightly different interpretation of the CL equation as a manifestation of measurement-induced dephasing (Sec. 5.1), where off-diagonal elements of the density matrix decay under the effect of measurement. Since in this precise case we measure in the position basis, it is in this basis that measurement-induced dephasing appears more clearly[Hornberger07]. Neglecting the D_{PX} and Δ^2 contributions to Eq. (7.26), the contribution of the measurement to the evolution of $\langle x|\rho(t)|x'\rangle = \rho(x,x';t)$ given by

$$\left(\frac{d}{dt}\rho(x,x';t)\right)_{\text{meas}} - \left(\frac{d}{dt}\rho(x,x';t)\right)_{\text{no meas}} = -\langle x|\frac{i\tilde{\gamma}}{\hbar}[\hat{x},\{\hat{p},\rho\}] + \frac{1}{\hbar^2}D_{\text{PP}}[\hat{x},[\hat{x},\rho]]|x'\rangle .$$
(7.34)

In the position basis, the diffusion term ($\propto D_{PP}$) takes the form

$$\frac{-1}{\hbar^2}D_{PP}\langle x|[\hat{x},[\hat{x},\rho]]|x'\rangle = \frac{-1}{\hbar^2}D_{PP}\left(x-x'\right)^2\langle x|\rho|x'\rangle ,$$
(7.35)

and therefore to a term that does not affect diagonal elements of $\rho(x,x')$ but exponentially suppresses the off-diagonal elements in the density matrix. Forgetting for a moment the damping term, the diffusion term leads to

$$\dot{\rho}(x,x';t) \sim -\Gamma_{x,x'}\rho(x,x';t) \rightarrow \rho(x,x';t) = \rho(x,x';0)e^{-\Gamma_{x,x'}t}.$$
(7.36)

Recalling the expression of D_{PP} in terms of the effective temperature characterizing the detector, $D_{PP} = 2M\tilde{\gamma}k_BT_{\text{eff}}$, we can write the dephasing rate $\Gamma_{x,x'}$ as

$$\Gamma_{x,x'} = \frac{D_{PP}}{\hbar^2}(x-x') = 4\pi\tilde{\gamma}\frac{(x-x')^2}{\Lambda_T^2} ,$$
(7.37)

with Λ_T^2 the square of the 'thermal' De Broglie wavelength,

$$\Lambda_T^2 = \frac{2\pi\hbar^2}{mk_BT_{\text{eff}}} .$$
(7.38)

The 'position-dephasing' rate is linear in the effective damping rate $\tilde{\gamma}$, and it heavily suppresses coherence on lengthscales larger than the thermal wavelength.

While measurement-induced dephasing seems to be a very appropriate description of the role of the diffusion term in the CL equation, so far in the discussion we

totally neglected the damping contribution to the equation of motion of the density matrix. In the position basis, this contribution reads

$$\frac{-i}{\hbar}\tilde{\gamma}\langle x|[\hat{x},\{\hat{p},\rho\}]|x'\rangle = \frac{-i\tilde{\gamma}}{\hbar}\left(x - x'\right)\langle x|\{\hat{p},\rho\}|x'\rangle ; \qquad (7.39)$$

it does not have the simple form of a constant multiplying $\rho(x, x'; t)$ like the diffusion term. Again, in this case a lot can be learned from the qubit measurement problem. In the example presented in Sec. 5.1, the measurement was done in the basis in which the qubit is diagonal. It was shown [Stace04; Li05] that for measurements not done in the diagonal basis[6] inelastic processes lead to relaxation. Here, since the Hamiltonian of the harmonic oscillator is not diagonal in the measured observable ($\hat{x}$), we observe a similar effect.

7.3 Master equation approach for the tunnel junction displacement detector

In the last section, we established the strong link between the linear-response and master-equation approaches. At this point, one might wonder about the advantages of one method over the other. In this section, we will therefore describe one benefit of the master-equation approach, namely that with only a slight modification this approach allows for the calculation of the complete transport properties of a detector. To proceed, we will treat the case of a tunnel junction position detector. For completeness, but also because this calculation also serves as an important basis to understand the model used in Chaps. 8 and 9), most details of the derivation will be included such that the reader should be able easily to follow through all steps of the calculation.

Our starting point is basically the same as in Sec. 6.2, with total Hamiltonian of a DC-biased tunnel junction coupled to an harmonic oscillator as a sum of an unperturbed Hamiltonian $H_0 = H_{\text{osc}} + H_{\text{leads}}$ and interaction (tunneling in this case) one. Explicitly,

$$H_{\text{osc}} = \hbar\Omega(a^\dagger a + 1/2) , \qquad (7.40)$$

$$H_{\text{leads}} = \sum_k \varepsilon_k c_k^\dagger c_k + \sum_q \varepsilon_q c_q^\dagger c_q , \qquad (7.41)$$

$$H_{\text{tun}} = \hat{T}(x)\sum_{k,q} c_k^\dagger c_q + \hat{T}^\dagger(x)\sum_{k,q} c_q^\dagger c_k , \qquad (7.42)$$

where q is a wave vector in the left lead and k a wave vector in the right lead.

---

[6]This happens when, for example, you consider a tunnel junction whose transmission amplitude depends on σ_z coupled to a qubit whose Hamiltonian has the form $H \sim \epsilon\sigma_z + \Delta\sigma_x$, with $\Delta \neq 0$.

7.3.1 Charge-resolved density matrix

In the tunneling Hamiltonian [Eq. (7.42)], we introduced $\hat{T}$, the x-dependent tunneling amplitude. *If* we defined $\hat{T}$ simply as $\hat{T} \sim t_0 + t_1\hat{x}$, then we could simply follow the general method presented in the last section and derive a CL equation for the oscillator written in terms of the spectral density of the back-action force acting on it. However, in order to investigate electronic transport in the coupled system, it is useful to refine this approach to keep track of m, the number of charges that passed through the detector. This allows one to calculate an equation of motion for the m-resolved density-matrix[Clerk04b; Rammer04; Wabnig05], a quantum equivalent to the m-resolved master equation approach widely used in the study of transport properties of classical nanomechanical systems[Armour04b; Doiron06] and discussed in Part II.

Noting $\rho_{osc}(t) = \mathrm{Tr}_B[\rho_{\mathrm{tot}}(t)]$ the reduced density matrix of the oscillator, we define its matrix element as $\langle m|\rho_{osc}(t)|m\rangle \equiv \rho(m;t)$. Physically, $\rho(m,t)$ represents the reduced density matrix of the oscillator at time t provided that exactly m charges have been transfered from the left to the right lead. Of course, by tracing out the m index one finds back ρ_{osc}:

$$\rho_{osc}(t) = \sum_m \rho(m;t) = \sum_m \langle m|\rho_{osc}(t)|m\rangle. \tag{7.43}$$

In order to be able to track the transfer of charge associated with a tunneling event, we define the tunneling operator as

$$\hat{T} = \frac{1}{2\pi\Lambda}\left(t_0 + e^{i\eta}t_1\hat{x}\right)Y^\dagger, \tag{7.44}$$

with $Y^{(\dagger)}$ an auxiliary operator that increases (decreases) the number of charges m that went from left to right in the junction. The action of this operator is more precisely described in terms of its action on the matrix elements of the density matrix

$$\langle m|YY^\dagger\rho(t)|m\rangle = \rho(m;t)\,, \tag{7.45}$$

$$\langle m|Y^\dagger Y\rho(t)|m\rangle = \rho(m;t)\,, \tag{7.46}$$

$$\langle m|Y^\dagger\rho(t)Y|m\rangle = \rho(m-1;t)\,, \tag{7.47}$$

$$\langle m|Y\rho(t)Y^\dagger|m\rangle = \rho(m+1;t)\,. \tag{7.48}$$

Finally, since, as discussed in the last chapter, only the phase difference η between the tunneling amplitudes t_0 and t_1 is relevant for this system[7], we will treat the two amplitudes as real in what follows.

---

[7]Recall that in Eq. (6.48) we defined η via the polar representation of the tunneling amplitudes $t_0^* t_1 = |t_0 t_1|e^{i(\phi_1-\phi_0)=|t_0 t_1|e^{i\eta}}$.

7.3.2 Equation of motion for the full density matrix

To proceed, we start from the Born-Markov master equation [Eq. (7.14)] and identify system, bath, and interaction terms with, respectively, the oscillator, the leads and the tunneling. This leads to

$$
\frac{d}{dt}\rho_{\mathrm{osc}}(t) = \frac{1}{i\hbar}\left[H_0, \rho_{\mathrm{osc}}(t)\right] - \frac{1}{\hbar^2}\int_0^\infty dt' \mathrm{Tr}_{\mathrm{leads}}\left\{\left[H_{\mathrm{tun}}, \left[H_{\mathrm{tun}}(-t'), \rho_{\mathrm{osc}}(t)\otimes\rho_{leads}\right]\right]\right\}.
$$
(7.49)

In this system, the Born approximation refers to the second-order perturbation theory in the tunneling. Within this approximation, the electrons tunnel independently, one after the other, and higher-order processes like cotunneling are disregarded. The Markov approximation on the other hand compares the typical timescales of the detector and the quantum system, and is valid as long as correlations in the bath (detector) decay much faster than those in the quantum system ($1/\Omega$ in our case). For a tunnel junction, the correlations decay approximatively on timescales of the order of the inverse of the so-called "attempt-frequency" (eV/h). Semi-classically, this corresponds to the time it takes between two consecutive events where an electron tries to tunnel[8].

In the interaction picture, the tunneling part of the Hamiltonian can be written as

$$
H_{\mathrm{tun}}(t) = U_0^\dagger(t)H_{\mathrm{tun}}U_0(t),
$$
(7.50)

$$
= \hat{T}(t)\sum_{k,q}c_k^\dagger(t)c_q(t) + \hat{T}^\dagger(t)\sum_{k,q}c_q^\dagger(t)c_k(t),
$$
(7.51)

where

$$
\hat{T}^{(\dagger)}(t) = e^{iH_{\mathrm{osc}}t/\hbar}\hat{T}^{(\dagger)}e^{-iH_{\mathrm{osc}}t/\hbar},
$$
(7.52)

$$
c_{k(q)}^\dagger(t) = e^{iH_{\mathrm{leads}}t/\hbar}c_{k(q)}^\dagger e^{-iH_{\mathrm{leads}}t/\hbar} = e^{i\varepsilon_{k(q)}t/\hbar}c_{k(q)}^\dagger,
$$
(7.53)

$$
c_{k(q)}(t) = e^{iH_{\mathrm{leads}}t/\hbar}c_{k(q)}e^{-iH_{\mathrm{leads}}t/\hbar} = e^{-i\varepsilon_{k(q)}t/\hbar}c_{k(q)}.
$$
(7.54)

As in Sec. 6.2, we assume that the leads are in local equilibrium, and therefore use Eq. (6.39) when tracing out the leads to obtain Fermi distributions. After some ma-

---

[8]The attempt frequency is obtained by arguing that the total current (in order words, the total charge transfered by unit time) is given by the product of the electron charge with the probability for an incoming electron to successfully be transmitted from one lead to the other (per unit time). This success probability is given by the product of the probability for one electron to successfully tunnel ($|t_0|^2$) and the attempt frequency f at which an electron "tries" to tunnel. Since the Landauer formula gives $I = e^2V|t_0|/h$, we find $f = h/eV$.

nipulations, the term under the integral can be rewritten

$$
\begin{aligned}
\mathrm{Tr}_{\mathrm{leads}}\big\{\big[H_{\mathrm{tun}},[H_{\mathrm{tun}}(-t'),\rho_{\mathrm{osc}}(t)\otimes\rho_{\mathrm{leads}}]\big]\big\} = \\
\sum_{k,q}\Big[\hat{T}\hat{T}^{\dagger}(-t')\rho_{\mathrm{osc}}(t) - \hat{T}^{\dagger}(-t')\rho_{\mathrm{osc}}(t)\hat{T}\Big]\,e^{-i(\varepsilon_q-\varepsilon_k)t'/\hbar}f_k(1-f_q) \\
+\sum_{k,q}\Big[\rho_{\mathrm{osc}}(t)\hat{T}(-t')\hat{T}^{\dagger} - \hat{T}^{\dagger}\rho_{\mathrm{osc}}(t)\hat{T}(-t')\Big]\,e^{i(\varepsilon_q-\varepsilon_k)t'/\hbar}f_k(1-f_q) \\
+\sum_{k,q}\Big[\hat{T}^{\dagger}\hat{T}(-t')\rho_{\mathrm{osc}}(t) - \hat{T}(-t')\rho_{\mathrm{osc}}(t)\hat{T}^{\dagger}\Big]\,e^{i(\varepsilon_q-\varepsilon_k)t'/\hbar}f_q(1-f_k) \\
+\sum_{k,q}\Big[\rho_{\mathrm{osc}}(t)\hat{T}^{\dagger}(-t')\hat{T} - \hat{T}\rho_{\mathrm{osc}}(t)\hat{T}^{\dagger}(-t')\Big]\,e^{-i(\varepsilon_q-\varepsilon_k)t'/\hbar}f_q(1-f_k)\,.
\end{aligned}
\tag{7.55}
$$

7.3.3 Equation of motion for the m-resolved density matrix

To get the equation of motion for $\rho(m;t)$, we consider at this point a matrix element $\langle m|\cdots|m\rangle$ of Eq. (7.49),

$$
\begin{aligned}
\frac{d}{dt}\rho(m;t) =&\frac{1}{i\hbar}\,[H_0,\rho(m;t)] \\
&-\frac{1}{\hbar^2}\int_0^{\infty}dt'\,\langle m|\mathrm{Tr}_{\mathrm{leads}}\big\{\big[H_{\mathrm{tun}},[H_{\mathrm{tun}}(-t'),\rho_{\mathrm{osc}}(t)\otimes\rho_{leads}]\big]\big\}|m\rangle\,.
\end{aligned}
\tag{7.56}
$$

Rewriting the tunneling amplitude as

$$
\hat{T} = \frac{1}{2\pi\Lambda}\mathcal{T}Y^{\dagger}\,,
\tag{7.57}
$$

$$
\tag{7.58}
$$

(with $\mathcal{T}=t_0+t_1\hat{x}$) allows us evaluate straightforwardly the $\langle m|...|m\rangle$ matrix element of Eq. (7.55) to find

$$
\begin{aligned}
(2\pi\Lambda)^2\langle m|\mathrm{Tr}_{\mathrm{leads}}\big\{\big[H_{\mathrm{tun}},[H_{\mathrm{tun}}(-t'),\rho_{\mathrm{osc}}(t)\otimes\rho_{leads}]\big]\big\}|m\rangle = \\
\sum_{k,q}\Big[\mathcal{T}\mathcal{T}^{\dagger}(-t')\rho(m;t) - \mathcal{T}^{\dagger}(-t')\rho(m+1;t)\mathcal{T}\Big]\,e^{-i(\varepsilon_q-\varepsilon_k)t'/\hbar}f_k(1-f_q) \\
+\sum_{k,q}\Big[\rho(m;t)\mathcal{T}(-t')\mathcal{T}^{\dagger} - \mathcal{T}^{\dagger}\rho(m+1;t)\mathcal{T}(-t')\Big]\,e^{i(\varepsilon_q-\varepsilon_k)t'/\hbar}f_k(1-f_q) \\
+\sum_{k,q}\Big[\mathcal{T}^{\dagger}\mathcal{T}(-t')\rho(m;t) - \mathcal{T}(-t')\rho(m-1;t)\mathcal{T}^{\dagger}\Big]\,e^{i(\varepsilon_q-\varepsilon_k)t'/\hbar}f_q(1-f_k) \\
+\sum_{k,q}\Big[\rho(m;t)\mathcal{T}^{\dagger}(-t')\mathcal{T} - \mathcal{T}\rho(m-1;t)\mathcal{T}^{\dagger}(-t')\Big]\,e^{-i(\varepsilon_q-\varepsilon_k)t'/\hbar}f_q(1-f_k)\,.
\end{aligned}
\tag{7.59}
$$

The equation of motion of $\rho(m; t)$ is coupled to the equation of motion of $\rho(m \pm 1; t)$. This is due to the Born approximation: we only consider processes that transfer one electron at a time.

At this point, one can be lead into thinking that it is necessary to solve an infinite set of coupled differential equations (one equation per value of m) to evaluate the transport properties of the system. Luckily, that is not the case. Instead, we can Fourier transform the last equation in the charge index, introducing a counting field χ, conjugate to the transfered charge m:

$$\rho(\chi; t) = \sum_m e^{i\chi m} \rho(m; t) . \tag{7.60}$$

The quantity $\rho(\chi; t)$ plays the role of the characteristic function[vanKampen92] describing charge transfer events. Indeed, if we denote $P(m; t)$ the probability distribution for the number of charges m transferred after a time t, all moments $\langle m^n(t) \rangle$ of this distribution can be calculated via

$$\langle m^n(t) \rangle = i^{-n} \left(\frac{d^n}{d\chi^n} \rho(\chi; t) \right)_{\chi=0} = \mathrm{Tr}_{\mathrm{osc}} \left[\sum_m m^n \rho(m; t) \right] . \tag{7.61}$$

Importantly, the introduction of the counting field χ allows to effectively decouple the system of differential equations. With $\sigma = \pm 1$,

$$\sum_m e^{i\chi m} \rho(m + \sigma; t) = e^{-ik\sigma} \rho(\chi; t) . \tag{7.62}$$

In terms of $\rho(\chi; t)$, the Born-Markov master equation [Eq. (7.56)] becomes

$$\frac{d}{dt} \rho(\chi; t) = \frac{1}{i\hbar} [H_0, \rho(\chi; t)] - \frac{1}{(2\pi\hbar\Lambda)^2} \int_0^\infty dt' \sum_{k,q} A(\chi, k, q; t, t') \tag{7.63}$$

with

$$
\begin{aligned}
A(\chi, k, q; t, t') =& \left[\mathcal{T}\mathcal{T}^\dagger(-t')\rho(\chi; t) - \mathcal{T}^\dagger(-t')\rho(\chi; t)\mathcal{T} \right] e^{-i(\varepsilon_q - \varepsilon_k)t'/\hbar} f_k(1 - f_q) \\
&+ \left[\rho(\chi; t)\mathcal{T}(-t')\mathcal{T}^\dagger - \mathcal{T}^\dagger \rho(\chi; t)\mathcal{T}(-t') \right] e^{i(\varepsilon_q - \varepsilon_k)t'/\hbar} f_k(1 - f_q) \\
&+ \left[\mathcal{T}^\dagger \mathcal{T}(-t')\rho(\chi; t) - \mathcal{T}(-t')\rho(\chi; t)\mathcal{T}^\dagger \right] e^{i(\varepsilon_q - \varepsilon_k)t'/\hbar} f_q(1 - f_k) \\
&+ \left[\rho(\chi; t)\mathcal{T}^\dagger(-t')\mathcal{T} - \mathcal{T}\rho(\chi; t)\mathcal{T}^\dagger(-t') \right] e^{-i(\varepsilon_q - \varepsilon_k)t'/\hbar} f_q(1 - f_k) \\
&- \left(e^{i\chi} - 1 \right) \left[\mathcal{T}\rho(\chi; t)\mathcal{T}^\dagger(-t')e^{-i(\varepsilon_q - \varepsilon_k)t/\hbar} \right] f_q(1 - f_k) \\
&- \left(e^{i\chi} - 1 \right) \left[\mathcal{T}(-t')\rho(\chi; t)\mathcal{T}^\dagger e^{i(\varepsilon_q - \varepsilon_k)t/\hbar} \right] f_q(1 - f_k) \\
&- \left(e^{-i\chi} - 1 \right) \left[\mathcal{T}^\dagger \rho(\chi; t)\mathcal{T}(-t')e^{i(\varepsilon_q - \varepsilon_k)t/\hbar} \right] f_k(1 - f_q) \\
&- \left(e^{-i\chi} - 1 \right) \left[\mathcal{T}^\dagger(-t')\rho(\chi; t)\mathcal{T}e^{-i(\varepsilon_q - \varepsilon_k)t/\hbar} \right] f_k(1 - f_q) ..
\end{aligned}
\tag{7.64}
$$

From this point on, the rest of the derivation is pretty straightforward. We first expand $\mathcal{T}(t)$ using the interaction picture representation of $\hat{x}$ [Eq. (7.23)] then proceed with the integration over t', using

$$\int_0^\infty dt\, e^{\pm i\omega t} = \pi\delta(\omega) \pm i\,\mathrm{pv}\left(\frac{1}{\omega}\right) . \tag{7.65}$$

Focusing on the real part[9], we replace the sum on the wave-vectors (k, q) by an integral over energy, with constant density of states Λ

$$\sum_k .. \to \int_0^\infty d\varepsilon_k\, \Lambda.. . \tag{7.66}$$

We formulate the result of the integration over the Fermi functions of the leads in terms of the inelastic tunneling rates $(\Gamma_\pm(E))$

$$h\Gamma_-(E) = \int_0^\infty d\varepsilon |t_0|^2 f(\varepsilon - \mu_R) \left[1 - f(\varepsilon - \mu_L + E)\right] , \tag{7.67}$$

$$h\Gamma_+(E) = \int_0^\infty d\varepsilon |t_0|^2 f(\varepsilon - \mu_L) \left[1 - f(\varepsilon - \mu_R + E)\right] , \tag{7.68}$$

with μ_i the chemical potential in lead i. These are the rates at which electrons exchanging an energy E tunnel from left to right $(+)$ or right to left $(-)$. After some manipulations, the different terms of Eq. (7.63) can be written as [Clerk04b]

$$\frac{d}{dt}\rho(\chi; t) = \frac{1}{i\hbar}\left[H_{\mathrm{osc}} - \bar{F}_0(\eta)\hat{x}, \rho(\chi; t)\right] - \frac{i}{\hbar}\sum_{\sigma=\pm}\tilde{\gamma}_\sigma\left[\hat{x}, \{\hat{p}, \rho(\chi; t)\}\right] + \sum_\sigma \frac{D_\sigma}{\hbar^2}\left[\hat{x}, [\hat{x}, \rho(\chi; t)]\right]$$

$$+ \sum_{\sigma=\pm 1}\frac{2D_\sigma}{\hbar^2}\left(\frac{e^{i\chi\sigma} - 1}{|t_1|^2}\right)\left[\left(t_0 + e^{i\sigma\eta}t_1\hat{x}\right)\rho(\chi; t)\left(t_0 + e^{-i\sigma\eta}t_1\hat{x}\right)\right]$$

$$+ \sum_{\sigma=\pm 1}\frac{i\tilde{\gamma}_\sigma}{\hbar}\left(\frac{e^{i\chi\sigma} - 1}{|t_1|^2}\right)\left[t_0 t_1\left(e^{i\sigma\eta}\hat{p}\rho(\chi; t) - e^{-i\sigma\eta}\rho(\chi; t)\hat{p}\right)\right]$$

$$+ \sum_{\sigma=\pm 1}\frac{i\tilde{\gamma}_\sigma}{\hbar}\left(\frac{e^{i\chi\sigma} - 1}{|t_1|^2}\right)\left[t_1^2\left(\hat{p}\rho(\chi; t)\hat{x} - \hat{x}\rho(\chi; t)\hat{p}\right)\right] . \tag{7.69}$$

with

$$\tilde{\gamma}_\sigma = \frac{\hbar}{4M\Omega}\left(\frac{t_1}{t_0}\right)^2\left[\Gamma_\sigma(\hbar\Omega) - \Gamma_\sigma(-\hbar\Omega)\right] , \tag{7.70}$$

$$D_\sigma = \frac{\hbar^2}{4}\left(\frac{t_1}{t_0}\right)^2\left[\Gamma_\sigma(\hbar\Omega) + \Gamma_\sigma(-\hbar\Omega)\right] , \tag{7.71}$$

$$\bar{F}(\eta) = 2\frac{\sin\eta}{\hbar}\left(\frac{t_0}{t_1}\right)\sum_\sigma \sigma D_\sigma . \tag{7.72}$$

---

[9]From Sec. 7.2, we know that the principal value integral (the imaginary part) leads to the $\sim \Delta^2, D_{PX}$ terms, and not to the main contributions to detector back-action (damping, heating).

In Eq. (7.69), $\bar{F}(\eta)$ represents an average force applied on the oscillator by the detector that will in practice only lead to a shift of the equilibrium position of the oscillator. The quantities $\tilde{\gamma}_\sigma$ and D_σ are directly related to the $\tilde{\gamma}$, D_{PP} parameters discussed in Sec. B, only they are split in two contributions, one from the electrons transfered following the direction prescribed by the bias ($\sigma = +$) and the other by electrons transfered against the bias ($\sigma = -$). In the regime where the tunnel junction is an efficient detector ($eV \gg k_B T_e$) (Sec. 6.2.3), one therefore expects the $\sigma = -$ contributions to vanish. The Caldeira-Leggett form of Eq. (7.69) also allows to easily introduce the effect of a finite quality factor of the oscillator in our calculations. Recalling that we considered an undamped harmonic oscillator to obtain this equation of motion and knowing that the finite quality factor manifests itself in such an equation of motion via the damping and diffusion terms [Eq. (B.16)], a finite quality factor oscillator can be modeled simply by adding terms

$$-\frac{i}{\hbar}\tilde{\gamma}_0\left[\hat{x},\{\hat{p},\rho(\chi;t)\}\right] + \frac{D_0}{\hbar^2}\left[\hat{x},\left[\hat{x},\rho(\chi;t)\right]\right] \tag{7.73}$$

with $\tilde{\gamma}_0, D_0$ as defined in Appendix B. This way, the total damping rate in the system is $\tilde{\gamma}_{\text{tot}} = \tilde{\gamma}_0 + \sum_\sigma \tilde{\gamma}_\sigma$

To understand the structure of Eq. (7.69), it is useful to look at how $\rho(\chi = 0; t)$ evolves with time. This is particularly interesting since

$$\rho(\chi = 0; t) = \sum_m \rho(m; t) = \rho_{\text{osc}}(t) , \tag{7.74}$$

as per Eq. (7.43). The equation of motion of $\rho(\chi = 0; t)$ is therefore the equation of motion of the reduced density matrix of the oscillator only; it does not contain any information about the electronic transport. In this case, both terms $\sim (e^{i\chi\sigma} - 1)$ vanish and the resulting equation is of CL form, exactly like in the generic case treated in Sec. 7.2. Since they appear only when considering the charge-resolved master equation, it becomes obvious that the two terms $\sim (e^{i\chi\sigma} - 1)$ are useful chiefly for the calculation of transport properties. Knowing this, it becomes easier to understand why the modification to Eq. (7.69) to include the coupling to the environment takes the form presented in Eq. (7.73): since the coupling to the thermal bath is independent of charge transport (and of the tunnel junction in general), it does not couple the equation-of-motion of $\rho(m; t)$ with the one of $\rho(m \pm 1; t)$. It therefore does not modify the $\sim (e^{i\chi\sigma} - 1)$ terms.

7.3.4 Transport properties from the m-resolved equation of motion

In this last section, we will present the method which is used to derive the transport properties of the system from Eq. (7.69). For maximum simplicity, we will focus on the

case where (i) all the damping is due to the detector (ii) $\eta = 0$ and (iii) the electrons in the leads are at zero temperature. None of these simplification are necessary and the calculation can easily be done without doing any of them; the expressions obtained are just bulkier. Also, note that the results of a calculation in the case of a finite tunneling-phase difference η is presented in Chap. 9. The calculation of the current properties follows from the definition of $\rho(\chi; t)$ as a generating function for the transfered charge probability distribution: the average current is proportional to the rate of change of $\langle m \rangle$, which can be calculated via

$$\frac{d}{dt}\langle m \rangle = i \operatorname{Tr}\left(\frac{d}{dt}\rho(\chi; t)\right)_{\chi=0} . \tag{7.75}$$

For the $eV \gg k_B T_e$ case, this leads to[Mozyrsky02]

$$I = e\frac{d}{dt}\langle m \rangle = \frac{e^2 V}{h}\left[t_0^2 + 2t_0 t_1 \langle x \rangle + t_1^2 \langle x^2 \rangle\right] - e\tilde{\gamma}_+ . \tag{7.76}$$

Recalling that the effective tunneling amplitude is

$$\mathcal{T} = t_0 + t_1 \hat{x} , \tag{7.77}$$

the term $\propto eV/h$ corresponds exactly to the result one would obtain from the Landauer formula assuming a static object centered at the position $\langle x \rangle$. It arises from the contribution $\sim (e^{i\chi} - 1)D$ of Eq. (7.69). The last term ($\tilde{\gamma}_+$) is a quantum correction that follows from the $\sim (e^{i\chi} - 1)\tilde{\gamma}_+$ term. At first, it might seem as if this term could, for low-enough voltages, lead to an average current *against* the direction set by the bias. However, if we instead include the quantum correction in the main bracket, the current becomes

$$I = \frac{e^2 V}{h}\left[t_0^2 + 2t_0 t_1 \langle x \rangle + t_1^2 \langle x^2 \rangle - t_1^2\left(\frac{\hbar\Omega}{eV}\right)\Delta x_0^2\right] \tag{7.78}$$

with $\Delta x_0^2 = \hbar/(2M\Omega)$ the zero-point motion of the oscillator. Written in this form, it becomes clear that, if we stay in the validity regime of our Markov approximation ($eV \gg \hbar\Omega$), the last term cannot lead to counter-currents.

Like in Chap. 3, we will use the MacDonald formula [Appendix A] to calculate the symmetrized-in-frequency current noise from the equation of motion of $\langle\langle m^2(t) \rangle\rangle$. In this regard, the first step is of course to calculate

$$\frac{d}{dt}\langle\langle m^2 \rangle\rangle = \frac{d}{dt}\langle m^2(t) \rangle - 2\langle m \rangle\frac{d}{dt}\langle m(t) \rangle . \tag{7.79}$$

From Eq. (7.69), we have

$$\frac{d}{dt}\langle m^2(t) \rangle = \frac{d}{dt}\langle m(t) \rangle + 2\frac{eV}{h}\left(t_0^2\langle m \rangle + 2t_0 t_1 \langle xm \rangle + t_1^2\langle x^2 m \rangle\right) - 2\tilde{\gamma}_+\langle m \rangle . \tag{7.80}$$

Combining this equation with our expression for the average current, we find

$$
\frac{d}{dt}\langle\langle m^2(t)\rangle\rangle = \frac{d}{dt}\langle m(t)\rangle + 2\frac{eV}{h}\left(t_0^2\langle m\rangle + 2t_0t_1\langle xm\rangle + t_1^2\langle x^2m\rangle\right) - 2\tilde{\gamma}_+\langle m\rangle
$$
$$
- 2\langle m\rangle\left[\frac{eV}{h}\left(t_0^2 + 2t_0t_1\langle x\rangle + t_1^2\langle x^2\rangle\right) - \tilde{\gamma}_+\right] , \tag{7.81}
$$

such that

$$
\frac{d}{dt}\langle\langle m^2(t)\rangle\rangle = \frac{d}{dt}\langle m(t)\rangle + 2\frac{eV}{h}\left(2t_0t_1\langle\langle x(t)m(t)\rangle\rangle + t_1^2\langle\langle x^2(t)m(t)\rangle\rangle\right) . \tag{7.82}
$$

The first term is the purely Poissonian part of the noise and the second is the correction due to the detector. Writing $\overline{S}_I = e\langle I\rangle + \Delta\overline{S}_I$ and identifying the second term of the last equation as $\Delta\overline{S}_I$ we find

$$
\Delta\overline{S}_I = \frac{2e^3V}{h}\omega\int_0^\infty dt\sin(\omega t)\left(2t_0t_1\langle\langle x(t)m(t)\rangle\rangle + t_1^2\langle\langle x^2(t)m(t)\rangle\rangle\right) . \tag{7.83}
$$

In general, the first ($\sim t_0t_1$) term will dominate over the ($\sim t_1^2$) one[10]. The calculation of the current noise therefore involves solving for the time dependence of the correlation between position and transfered charge, $\langle\langle xm\rangle\rangle$. Again, we use Eq.(7.69) to write

$$
\frac{d}{dt}\langle\langle xm\rangle\rangle = \frac{\langle\langle pm\rangle\rangle}{M} + \frac{eV}{h}\left[2t_0t_1\langle\langle xx\rangle\rangle\right] - \tilde{\gamma}_+\frac{t_0}{t_1} , \tag{7.84a}
$$
$$
\frac{d}{dt}\langle\langle pm\rangle\rangle = -M\Omega^2\langle\langle xm\rangle\rangle - 2\tilde{\gamma}_+\langle\langle pm\rangle\rangle + \frac{eV}{h}\left[t_0t_1(\langle xp + px\rangle - 2\langle x\rangle\langle p\rangle)\right] , \tag{7.84b}
$$

where, since the time-derivative of $\langle\langle xm\rangle\rangle$ involves $\langle\langle pm\rangle\rangle$, we also calculated the equation-of-motion for the correlations between momentum and charge. In order for the current-current correlation function to be time-translational invariant (i.e., for $\langle I(t + t')I(t)\rangle$ to be independent of t), we replace all averages that do not contain m by their stationary expectation value. Combining Eqs. (7.84a)-(7.84b), we find

$$
\frac{d^2}{dt^2}\langle\langle xm\rangle\rangle + 2\tilde{\gamma}_+\frac{d}{dt}\langle\langle xm\rangle\rangle + \Omega^2\langle\langle xm\rangle\rangle = 2\tilde{\gamma}_+\left(\frac{eV}{h}2t_0t_1\langle\langle x^2\rangle\rangle - \tilde{\gamma}_+\frac{t_0}{t_1}\right) . \tag{7.85}
$$

This is a second order differential equation for which we need 2 boundary conditions to obtain the full solution. Since we have $m = 0$ at $t = 0$, then $\langle\langle xm(t = 0)\rangle\rangle = 0$ and $\langle\langle pm(t = 0)\rangle\rangle = 0$. Using Eq. (7.84), we find that the two initial conditions in this

---

[10]In fact, the signature of the $\propto t_1^2$ term in the current noise was never observed on one of the leading experimental realization of a tunnel junction displacement detector[Flowers-Jacobs, *private communication*].

problem are

$$\langle\langle xm(0)\rangle\rangle = 0 \,, \tag{7.86a}$$

$$\frac{d}{dt}\langle\langle xm\rangle\rangle\bigg|_{t=0} = \frac{eV}{h}\left[(2t_0 t_1)\langle\langle x^2\rangle\rangle\right] - \tilde{\gamma}_+ \frac{t_0}{t_1} \,. \tag{7.86b}$$

Using these boundary conditions, the differential equation [Eq. (7.85)] can be solved, using for example Mathematica. The expression obtained is more compact after integration,

$$\Delta \overline{S}_I^{(\text{1st order})} = \frac{2e^3 V}{h}\omega \int_0^\infty dt \sin(\omega t) 2t_0 t_1 \langle\langle x(t)m(t)\rangle\rangle \,, \tag{7.87}$$

$$= \frac{e^3 V}{h}(2t_0 t_1)^2 \left(\frac{eV}{h} - \frac{\tilde{\gamma}_+}{2\langle x^2\rangle t_1^2}\right) \overline{S}_x(\omega) \,. \tag{7.88}$$

Using Eq. (7.70), this can be re-expressed as [Clerk04b; Doiron07]

$$\Delta \overline{S}_I^{(\text{1st order})} = \frac{e^3 V}{h}(2t_0 t_1)^2 \left(\frac{eV}{h} - \frac{\Omega}{4\pi}\frac{\Delta x_0^2}{\langle\langle x^2\rangle\rangle}\right) \overline{S}_x(\omega) \,, \tag{7.89}$$

with

$$\overline{S}_x(\omega) = \frac{2(2\tilde{\gamma}_{\text{tot}})\Omega^2\langle\langle x^2\rangle\rangle}{(\omega^2 - \Omega^2) + 4\tilde{\gamma}_{\text{tot}}^2\Omega^2} \,, \tag{7.90}$$

where, for completeness, we introduced back the finite environmental damping in the final result. The physical interpretation of this result will be commented on at length in the next chapter.

In a very similar fashion, we can calculate the contribution of the second order ($\sim t_1^2$) to find that it is proportional to $\int d\omega' \overline{S}_x(\omega')\overline{S}_x(\omega - \omega')$. Even if all the calculations presented in this section were done considering a finite DC bias, the same path can be followed to calculated noise properties arising for AC biasing of the tunnel junction. In this case, instead of one main peak $\sim \overline{S}_x(\omega)$ at the natural frequency of the oscillator, one finds two satellite peaks at $\Omega \pm \omega_d$, with ω_d the driving frequency [Clerk04b; Poggio08]. In closing, we mention that it was recently demonstrated[Bennett08] that it is possible to calculate the full counting statistics of the system starting from Eq. (7.69). This allows to study some deviations from the "detector as an effective bath" model that manifest themselves in higher-order cumulants of the current.

Displacement measurement using detector cross correlations

In the current generation of experiments with tunnel junctions, the coupling between the resonator and the mesoscopic detector is typically very weak. The displacement measurement can therefore *not* be seen as a strong projective measurement. It is better described within the framework of weak continuous measurement theory that was recently developed in the context of solid-state quantum computing[Averin03a; Korotkov01b; Pilgram02; Clerk03b] and presented in Sec. 4.2. This theory describes a continuous measurement process where the information about the measured object can be extracted, for instance, from the spectral density of the detector (and not simply from its average output). An important result in this theory is the Korotkov-Averin bound (Sec. 4.2.1), which puts an upper limit of 4 to the ratio of the contribution of the measured state to the detector's spectral density, and the intrinsic background detector noise, for any linear detector measuring a two-level system.

Since a quantum displacement measurement by a mesoscopic detector can be described within the same theoretical framework as a qubit measurement, one might ask if such a bound also exists in the case of a displacement measurement. In this chapter, we first show that, for fixed system parameters, the peak-to-background ratio in the spectral density of a position detector weakly coupled to an oscillator is also bounded from above. This result is obtained by considering the example of a single tunnel-junction detector, discussed at length in the previous chapters.

Besides showing that the peak-to-background ratio is bounded in the typical single-detector displacement measurement, in this chapter we also propose two sim-

ple experimental configurations (Fig. 8.1) where, by using the cross correlations be-
tween two detectors, the bound on the peak-to-background ratio can be overcome. As
the oscillator-independent parts of the output signal of the two detectors are uncorre-
lated, the background noise in these configurations is zero and therefore the peak-to-
background ratio diverges. In the context of qubit readout, this idea has already been
proposed in an insightful work by Jordan and Büttiker [Jordan05] and was shown ex-
perimentally to improve readout fidelity[Buehler03]. Experimentally, displacement
measurements should also profit from using cross-correlated detector outputs. We
analyze in detail the two configurations presented in Fig. 8.1 and obtain analytical
results for the optimal cross-correlated signal as a function of different detector pa-
rameters.

In Sec. 6.1.2, we derived for a generic detector a bound on the sensitivity of a linear
measurement. In this chapter, after showing exactly how this bound manifests itself
in the specific case of a tunnel junction displacement detector, we will show that the
double-detector setup proposed here can in fact be used to almost totally get rid off
the added displacement noise of the oscillator due to detector back-action. This is a
remarkable result that nicely complements the general single-detector analysis made
in Chap. 6.

The chapter is organized as follows: in Sec. 8.1, we introduce the formalism used
in the rest of the paper, the master equation for the m-resolved density matrix[see
Sec. 7.3], this time in a double-detector setup. In Sec. 8.2, the formalism is applied to
the case of one position detector coupled to the oscillator: we analyze the peak-to-
background ratio and show that this quantity is always bounded from above. This
bound cannot be made arbitrarily large simply by increasing the detector sensitivity.
Sec. 8.3 generalizes this treatment to a configuration with two detectors and demon-
strates that measuring the current cross correlations of the two detectors allows one to
get arbitrarily high values of the peak-to-background ratio: i.e., it is possible to elimi-
nate the bound that exist in the single-detector case. In Sec. 8.4, we demonstrate how
the proposed setup can be used to diminish the added position noise of the oscillator
induced by the presence of the detector, allowing displacement measurement beyond
the standard quantum limit derived for a single detector.

8.1 Equation of motion for the density matrix

As shown in detail in Chap. 7, by writing the equation of motion for the density matrix
of the full (detector and oscillator) system and tracing out the detector degrees of free-
dom, one can obtain an equation of motion for the reduced density matrix describing
the evolution of the oscillator taking into account the coupling to the detector.

To study the current cross correlations between *two* tunnel junction position detec-
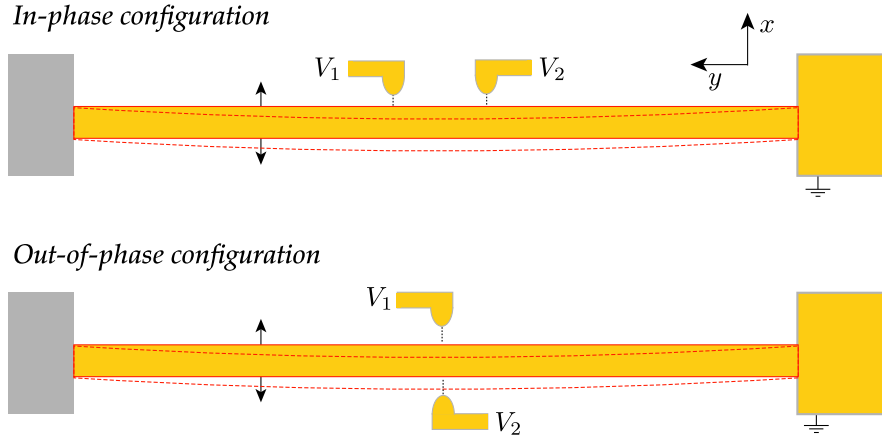
Figure 8.1: The two typical detector configurations examined in this chapter. In both cases, the movement of the oscillator is along the x direction in the xy plane, as depicted by the $\leftrightarrow$ sign. top) *In-phase configuration*, where two detectors (with bias V_1 and V_2, respectively) are located on the same side of the central part of the oscillator, such that both detectors couple in the same way to the position of the oscillator. This is covered in Sec. 8.3.1. bottom) *Out-of-phase configuration*, where the detectors are located on each side of the oscillator. When the position of the oscillator is such that the tunneling amplitude of one junction is increased, the tunneling amplitude of the other junction is therefore decreased. This is covered in Sec. 8.3.2.

tors coupled to an oscillator, we use a fully quantum approach very similar to the one presented in Sec. 7.3. We label the detectors with the index $\alpha = 1, 2$ and model each of them as a pair of metallic leads with constant density of states Λ_α (in the energy range relevant to tunneling) coupled via the tunneling Hamiltonian H_{tun}. The Hamiltonian for one detector can therefore be written as a sum of a bath Hamiltonian $H_{B,\alpha}$ describing the leads of junction α and a tunneling Hamiltonian $H_{\text{tun},\alpha}$

$$H_{\text{det},\alpha} = H_{B,\alpha} + H_{\text{tun},\alpha} \tag{8.1}$$

$$H_{B,\alpha} = \sum_k \varepsilon_{k,\alpha} c_{k,\alpha}^\dagger c_{k,\alpha} + \sum_q \varepsilon_{q,\alpha} c_{q,\alpha}^\dagger c_{q,\alpha} \tag{8.2}$$

$$H_{\text{tun},\alpha} = T_\alpha(\hat{x}) Y_\alpha^\dagger \sum_{k,q} c_{k,\alpha}^\dagger c_{q,\alpha} + T_\alpha^\dagger(\hat{x}) Y_\alpha \sum_{k,q} c_{q,\alpha}^\dagger c_{k,\alpha} \, , \tag{8.3}$$

where $k(q)$ is a wave vector in the right(left) lead. The coupling between the detector and the position of the oscillator is modeled by a linear $x-$dependence of the tunnel-

ing amplitude

$$T_\alpha(\hat{x}) = \frac{1}{2\pi\Lambda_\alpha}\left(\tau_{0,\alpha} + e^{i\eta_\alpha}\tau_{1,\alpha}\hat{x}\right) . \tag{8.4}$$

In this equation, $\tau_{0,\alpha}$ is the bare (oscillator-independent) tunneling amplitude of detector α, $\hat{x}$ is the position operator of the oscillator and $\tau_{1,\alpha}$ is the part of the full tunneling amplitude detector α that depends on the position of the oscillator. We allow for a general relative phase η_α, describing the details of the coupling between the tunnel junction and the oscillator. Such a phase can in principle be controlled by a magnetic flux penetrating an extended tunnel junction consisting of a loop containing two junctions, one of which couples to the oscillator (Chap. 9). Note that in our notation $\tau_{0,\alpha}$ is dimensionless and $\tau_{1,\alpha}$ has dimensions of one over length and that we assume for simplicity that the tunneling amplitudes do not depend on the single particle energies $\varepsilon_{k,\alpha(q,\alpha)}$. The operator $Y_\alpha^{(\dagger)}$ decreases (increases) m_α, the number of charges that tunneled through junction α. Its presence in the tunneling Hamiltonian allows one to keep track of the transport processes that occur during the evolution of the system.

We are interested in calculating the equation of motion for the reduced, m_α-resolved, density matrix

$$\rho(m_1, m_2; t) = \langle m_1, m_2 | \rho_{\mathrm{osc}} | m_1, m_2 \rangle , \tag{8.5}$$

where $\rho_{\mathrm{osc}} = \mathrm{Tr}_B\{\rho_{tot}\}$ is the reduced density matrix that is obtained by tracing out the leads' degrees of freedom from the full system density matrix. Within a Born-Markov approximation, the equation of motion of ρ_{osc} can be expressed as

$$\frac{\partial}{\partial t}\rho_{\mathrm{osc}}(t) = -\frac{i}{\hbar}[H_{\mathrm{osc}}, \rho_{\mathrm{osc}}(t)] - \frac{1}{\hbar^2}\int_{-\infty}^{0} d\bar{t}\,\mathrm{Tr}_B\{[H_{\mathrm{tun}}, [H_{\mathrm{tun}}(\bar{t}), \rho_{\mathrm{osc}}(t) \otimes \rho_B]]\} , \tag{8.6}$$

where $H_{\mathrm{tun}} = H_{\mathrm{tun},1} + H_{\mathrm{tun},2}$ is the total tunneling Hamiltonian, the trace is on both pairs of leads, ρ_B is the coupled density matrix of the two sets of leads and

$$H_{\mathrm{osc}} = \hbar\Omega(\hat{a}^\dagger\hat{a} + 1/2) = \frac{\hat{p}^2}{2M} + \frac{M\Omega^2\hat{x}^2}{2} , \tag{8.7}$$

$$H_{\mathrm{tun}}(t) = \sum_\alpha e^{iH_{0,\alpha}t/\hbar} H_{\mathrm{tun},\alpha} e^{-iH_{0,\alpha}t/\hbar} . \tag{8.8}$$

with $H_{0,\alpha} = H_{\mathrm{osc}} + H_{B,\alpha}$. In our system, the Born approximation corresponds to assuming that tunneling in both tunnel junctions is weak enough so that it can be treated using second-order perturbation theory. The Markov approximation, on the other hand, is valid as long as the typical correlation times in the leads (h/eV) are much shorter than $2\pi/\Omega$, i.e. the typical evolution time of the oscillator. In practice, this limits the applicability of the following results to the strongly biased case $eV \gg \hbar\Omega$.

Since the leads of detector 1 are totally independent of those of detector 2, ρ_B can be written as a tensor product of the density matrices describing each pair of leads $\rho_B = \rho_{B_1} \otimes \rho_{B_2}$. Also, as $H_{\text{tun},\alpha}$ has no diagonal contribution in the basis that diagonalizes $H_{B,\alpha}$, the trace over leads α of a quantity that is linear in $H_{\text{tun},\alpha}$ vanishes. As a result of those two properties, the trace in Eq. (8.6) can be rewritten as a sum over two traces, each involving only one pair of leads

$$\text{Tr}_B\{[H_{\text{tun}}, [H_{\text{tun}}(\bar{t}), \rho_{\text{osc}}(t) \otimes \rho_B]]\} = \sum_\alpha \text{Tr}_{B_\alpha}\{[H_{\text{tun},\alpha}, [H_{\text{tun},\alpha}(\bar{t}), \rho_{\text{osc}}(t) \otimes \rho_{B_\alpha}]]\} \,.$$

(8.9)

This effectively makes the two-detector problem two single-detector problems. The trace over the leads's degrees of freedom is then carried out in the standard way [Blum96].

As mentioned above, we are interested in calculating the time-evolution of the m_α-resolved density matrix. Thus, we have to calculate $\langle m_1, m_2 | \partial_t \rho_{\text{osc}} | m_1, m_2 \rangle$. We use the relations

$$
\begin{aligned}
\langle m_1, m_2 | Y_1 Y_1^\dagger \rho_{\text{osc}}(t) | m_1, m_2 \rangle &= \rho(m_1, m_2; t) \,, \\
\langle m_1, m_2 | Y_1^\dagger \rho_{\text{osc}}(t) Y_1 | m_1, m_2 \rangle &= \rho(m_1 - 1, m_2; t) \,, \\
\langle m_1, m_2 | Y_1^\dagger Y_1 \rho_{\text{osc}}(t) | m_1, m_2 \rangle &= \rho(m_1, m_2; t) \,, \\
\langle m_1, m_2 | Y_1 \rho_{\text{osc}}(t) Y_1^\dagger | m_1, m_2 \rangle &= \rho(m_1 + 1, m_2; t) \,,
\end{aligned}
$$

as well as the equivalent identities for detector 2 in Eq. (8.6) to find the equation of motion for $\rho(m_1, m_2; t)$.

Following a counting-statistics approach[Belzig04; Blanter06], it is particularly useful to express the equation of motion in terms of a counting field χ_α, the conjugate quantity to the transferred charge m_α. Indeed, Fourier-transforming in the transferred-charge indices m_α,

$$\tilde{\rho}(\chi_1, \chi_2; t) = \sum_{m_1=-\infty}^{\infty} e^{i\chi_1 m_1} \sum_{m_2=-\infty}^{\infty} e^{i\chi_2 m_2} \rho(m_1, m_2; t)$$

(8.10)

leads to an equation of motion from which the time-dependence of all moments of m (for example, $\partial_t \langle m_\alpha \rangle, \partial_t \langle m_\alpha^2 \rangle, ...$) can be determined. The current-current correlations can then be obtained by taking successive derivatives with respect to $(i\chi_\alpha)$ of the equation of motion of $\tilde{\rho}(\chi_1, \chi_2; t)$.

In the regime of weak coupling between the oscillator and the detectors, we can

write the equation of motion of $\tilde{\rho}(\chi_1, \chi_2; t)$ as

$$
\begin{aligned}
\frac{d}{dt}\tilde{\rho}(\chi_1, \chi_2; t) =\ & \frac{-i}{\hbar}\left[H_{\text{osc}}, \tilde{\rho}(t)\right] \\
& + \frac{i}{\hbar}\sum_\alpha \left[\bar{F}_\alpha \hat{x}, \tilde{\rho}(t)\right] - \frac{i}{\hbar}\sum_{\sigma,\alpha}\tilde{\gamma}_{\sigma,\alpha}[\hat{x}, \{\hat{p}, \tilde{\rho}(t)\}] - \frac{1}{\hbar^2}\sum_{\sigma,\alpha}D_{\sigma,\alpha}[\hat{x}, [\hat{x}, \tilde{\rho}(t)]] \\
& + \sum_{\sigma,\alpha}\left(\frac{e^{i\sigma\chi_\alpha} - 1}{\tau_{1,\alpha}^2}\right) \times \left(\frac{2D_{\sigma,\alpha}}{\hbar^2}(\tau_{0,\alpha} + e^{i\sigma\eta_\alpha}\tau_{1,\alpha}\hat{x})\tilde{\rho}(t)(\tau_{0,\alpha} + e^{-i\sigma\eta_\alpha}\tau_{1,\alpha}\hat{x})\right. \\
& \left. + i\frac{\tilde{\gamma}_{\sigma,\alpha}}{\hbar}\left[\tau_{0,\alpha}\tau_{1,\alpha}(e^{i\sigma\eta_\alpha}\hat{p}\tilde{\rho}(t) - e^{-i\sigma\eta_\alpha}\tilde{\rho}(t)\hat{p}) + \tau_{1,\alpha}^2(\hat{p}\tilde{\rho}(t)\hat{x} - \hat{x}\tilde{\rho}(t)\hat{p})\right]\right).
\end{aligned}
\tag{8.11}
$$

Since $\tilde{\rho}(\chi_1 = 0, \chi_2 = 0; t) = \sum_{m_1}\sum_{m_2}\rho(m_1, m_2; t)$, taking $\chi_1 = \chi_2 = 0$ corresponds to completely tracing out the charge degrees of freedom. In this case, one finds that $\dot{\tilde{\rho}}(0, 0; t)$ is of Caldeira-Leggett form (Sec. 7.2, Appendix B). We can thus identify the constants $D_{\sigma,\alpha}$ and $\tilde{\gamma}_{\sigma,\alpha}$ as, respectively, the diffusion and damping constants induced by forward ($\sigma = +$) or backward ($\sigma = -$) propagating currents in detector α. We can also identify $\bar{F}_\alpha$ as the average back-action force exerted on the oscillator by detector α. We find explicitly

$$
D_{\sigma,\alpha} = \frac{\hbar^2}{4}\left(\frac{\tau_{1,\alpha}}{\tau_{0,\alpha}}\right)^2 \left[\tilde{\gamma}_{\sigma,\alpha}(\hbar\Omega) + \tilde{\gamma}_{\sigma,\alpha}(-\hbar\Omega)\right],
\tag{8.12}
$$

$$
\tilde{\gamma}_{\sigma,\alpha} = \frac{\hbar}{2M\Omega}\left(\frac{\tau_{1,\alpha}}{\tau_{0,\alpha}}\right)^2 \left(\frac{\tilde{\gamma}_{\sigma,\alpha}(\hbar\Omega) - \tilde{\gamma}_{\sigma,\alpha}(-\hbar\Omega)}{2}\right),
\tag{8.13}
$$

$$
\bar{F}_\alpha = \frac{1}{\hbar}\sin(\eta_\alpha)\left(\frac{\tau_{0,\alpha}}{\tau_{1,\alpha}}\right)\sum_\sigma 2\sigma D_{\sigma,\alpha},
\tag{8.14}
$$

where the two inelastic tunneling rates are given by

$$
\tilde{\gamma}_{+,\alpha}(E) = \frac{|\tau_{0,\alpha}|^2}{h}\int_0^\infty d\varepsilon_{q,\alpha}\, f_{q,\alpha}(\varepsilon_{q,\alpha})\left(1 - f_{k,\alpha}(\varepsilon_{q,\alpha} + E)\right)
\tag{8.15}
$$

$$
\tilde{\gamma}_{-,\alpha}(E) = \frac{|\tau_{0,\alpha}|^2}{h}\int_0^\infty d\varepsilon_{k,\alpha}\, f_{k,\alpha}(\varepsilon_{k,\alpha})\left(1 - f_{q,\alpha}(\varepsilon_{k,\alpha} + E)\right)
\tag{8.16}
$$

involving a transfer of energy E from the oscillator to the lead electron. We denote by $\tilde{\gamma}_{+,\alpha}$ the forward tunneling rate, i.e. the rate at which electrons tunnel in the direction favored by the voltage bias. The backward rate $\tilde{\gamma}_{-,\alpha}$ corresponds to the reverse process. In Eqs. (8.15) and (8.16), $f_{k,\alpha} = f_{R,\alpha}(\epsilon_{k,\alpha})$ is the Fermi distribution function describing the local thermal equilibrium of the right lead of detector α and $f_{q,\alpha} = f_{L,\alpha}(\epsilon_{q,\alpha})$ is the same for the left lead.

Comparing these relations with the one derived previously in the single-detector case[Eq. (7.69)] shows that the full damping and diffusion coefficients governing the

evolution of the oscillator are the sum of two single-detector contributions. The Caldeira-Leggett form of Eq. (8.11) allows us to include the effect of direct coupling of the oscillator to the environment by adding detector-independent contributions $D_0 = 2M\tilde{\gamma}_0 k_B T_0$ and $\tilde{\gamma}_0 = \Omega/(2Q_0)$ (where Q_0 is the extrinsic quality factor of the mode) to the previously derived diffusion and damping constants. The evolution of the oscillator is then governed by the two constants $D_{\text{tot}} = D_0 + \sum_{\sigma,\alpha} D_{\sigma,\alpha}$ and $\tilde{\gamma}_{\text{tot}} = \tilde{\gamma}_0 + \sum_{\sigma,\alpha} \tilde{\gamma}_{\sigma,\alpha}$. For the specific case where the electronic temperature is zero and where $eV_\alpha \gg \hbar\Omega$, current will only be possible along the ($\sigma = +$) direction, and both $\tilde{\gamma}_{-,\alpha}$ and $D_{-,\alpha}$ will be zero. In this case one can also show that $\tilde{\gamma}_{+,\alpha} = \hbar\tau_{1,\alpha}^2/(4\pi M)$ and that the diffusion parameters are given by $D_{+,\alpha} = M\tilde{\gamma}_{+,\alpha} eV_\alpha$.

The equation of motion for different moments $\langle x^j p^k \rangle$ of the oscillator can be evaluated by taking the trace of $x^j p^k \dot{\rho}(0,0;t)$. More generally, equations of motion for combined moments of charge and oscillator quantities can be obtained by also considering derivatives with respect to the counting fields χ_α

$$\frac{\partial}{\partial t}\langle x^{n_1} p^{n_2} m_1^{n_3} m_2^{n_4} \rangle = \text{Tr}\, x^{n_1} p^{n_2} \left(\frac{\partial^{(n_3+n_4)}}{\partial(i\chi_1)^{n_3}\partial(i\chi_2)^{n_4}} \dot{\rho}(\chi_1,\chi_2;t) \right)_{\chi_1=\chi_2=0}. \qquad (8.17)$$

8.2 Single-detector case: Bound on the peak-to-background ratio

One of the main motivations for studying displacement measurements using cross-correlated detector outputs is to remove the bound on the peak-to-background ratio that appears in the single-detector case, just like in the case of a weak measurement of a two-level system[Jordan05]. In this section, we first review the results of Clerk and Girvin (CG) [Clerk04b] for the single-detector configuration, in the case where one considers the dc-biased, $T = 0$, tunnel junction where the $x-$dependent tunneling phase is $\eta = 0$. We then carefully analyze the peak-to-background ratio and show that this quantity is bounded from above in the single-detector case, for finite bias voltage and oscillator displacement.

When treating the case of the single detector, we showed [Eq. (7.89)] first non-vanishing order in τ_1, the current noise of a tunnel junction position detector is given by

$$\overline{S}_{I,\text{tot}}(\omega) = e\langle I \rangle + \frac{e^3 V}{h}(2\tau_0 \tau_1)^2 \left(\frac{eV}{h} - \frac{\Omega}{4\pi} \frac{\Delta x_0^2}{\langle x^2 \rangle} \right) \overline{S}_x(\omega), \qquad (8.18)$$

where $\Delta x_0^2 = \hbar/(2M\Omega)$ is the average of x^2 in the ground state of the (quantum)

harmonic oscillator and

$$\bar{S}_x(\omega) = \frac{4\tilde{\gamma}_{\text{tot}}\Omega^2 \langle x^2 \rangle}{4\tilde{\gamma}_{\text{tot}}^2 \omega^2 + (\Omega^2 - \omega^2)^2} \tag{8.19}$$

its power spectrum. The full current noise is the sum of the usual frequency-independent Poissonian (shot) noise and the contribution of interest due to the coupling of the junction to the oscillator. This second part is itself expressed as the difference of a classical part (which is proportional to V^2) and a quantum correction (which is proportional to V).

A relevant figure of merit of such detectors is the peak-to-background ratio $\mathcal{R}(\omega)$: the ratio of the contribution of the oscillator to the full current noise at frequency ω over the unavoidable frequency-independent intrinsic detector noise. This ratio is maximal at $\omega = \Omega$ and, in the case where one only considers the $\propto V^2$ contribution in Eq. (8.18), was shown to be given by

$$\mathcal{R}(\Omega) = \frac{\bar{S}_{I,\text{tot}}(\Omega) - e\langle I \rangle}{e\langle I \rangle} = 4\tau_0^2 \frac{eV}{h\tilde{\gamma}_{\text{tot}}} \frac{\beta^2}{1 + \beta^2} , \tag{8.20}$$

where we used $\langle I \rangle = \langle \partial_t m_1(t) \rangle \simeq e^2 V \tau_0^2 (1 + \beta^2) / h$ and introduced the dimensionless sensitivity parameter $\beta^2 = \tau_1^2 \langle x^2 \rangle / \tau_0^2$.[1] At this point, one should proceed with care when maximizing $\mathcal{R}$ with respect to the sensitivity parameter, as $\tilde{\gamma}_{\text{tot}} = \tilde{\gamma}_0 + \tilde{\gamma}_+$ depends on β through $\tilde{\gamma}_+ = (\Omega\tau_0^2/2\pi)(\Delta x_0^2/\langle x^2 \rangle)\beta^2$. Writing out explicitly all terms in $\mathcal{R}$ that depend on β, one finds that

$$\mathcal{R}(\Omega) = \frac{4\tau_0^2}{\pi} Q_0 \frac{eV}{\hbar\Omega} \left(1 + Q_0 \frac{\tau_0^2}{\pi} \frac{\Delta x_0^2}{\langle x^2 \rangle} \beta^2\right)^{-1} \frac{\beta^2}{1 + \beta^2} \tag{8.21}$$

is a non-monotonic function of the sensitivity parameter β. For a given $\langle x^2 \rangle$, one can then find an optimal value

$$\beta_{opt}^4 = \frac{\pi}{Q_0 \tau_0^2} \frac{\langle x^2 \rangle}{\Delta x_0^2} , \tag{8.22}$$

for which $\mathcal{R}$ is maximal

$$\mathcal{R}_{max} = 4\frac{Q_0 \tau_0^2}{\pi} \left(\frac{eV}{\hbar\Omega}\right) \left(1 + \sqrt{\frac{Q_0 \tau_0^2}{\pi} \frac{\Delta x_0^2}{\langle x^2 \rangle}}\right)^{-2} . \tag{8.23}$$

---

[1]It is important to distinguish the detector's *sensitivity parameter* β introduced in Sec. III from the *displacement sensitivity* $\bar{S}_{x,\text{add}}(\omega)$ discussed in Sec. V. The former allows an easy comparison of the relative weight of the position-dependent ($\propto \tau_1^2$) and independent ($\propto \tau_0^2$) part of the current. The latter characterizes the detector-dependent signal in a displacement measurement, in terms of displacement fluctuations of the oscillator. It is typically independent of τ_0.

We can examine this result in two different limits. The first is when the damping is mainly detector-independent ($\tilde{\gamma}_0 \gg \tilde{\gamma}_+$), like in the case where the extrinsic quality factor of the resonator is low, $Q_0 \ll \langle x^2 \rangle / (\tau_0^2 \Delta x_0^2)$. In this case, the maximal peak-to-background ratio,

$$
\begin{aligned}
\mathcal{R} \quad &\simeq 4 \quad \frac{\langle x^2 \rangle}{\Delta x_0^2} \frac{eV}{\hbar \Omega} \left(\frac{\tau_0^2 Q_0}{\pi} \frac{\Delta x_0^2}{\langle x^2 \rangle} \right) \left(\frac{\beta^2}{1 + \beta^2} \right) \\
&\leq \quad 4 \frac{\langle x^2 \rangle}{\Delta x_0^2} \frac{eV}{\hbar \Omega} \left(\frac{\tau_0^2 Q_0}{\pi} \frac{\Delta x_0^2}{\langle x^2 \rangle} \right) ,
\end{aligned}
\tag{8.24}
$$

is reached when the sensitivity parameter β is extremely large. However, since the rightmost term of Eq. (8.24) is by definition small in this limit, the peak-to-background ratio cannot become extremely large when the extrinsic resonator damping dominates the detector-induced one.

Indeed, the real maximum of $\mathcal{R}$ is reached when one considers the opposite limit of a very high resonator Q-factor[Clerk04a], $Q_0 \gg \langle x^2 \rangle / (\tau_0^2 \Delta x_0^2)$. For $\tilde{\gamma}_0 = 0$, the peak-to-background ratio can be shown to obey

$$
\mathcal{R} \simeq 4 \frac{\langle x^2 \rangle}{\Delta x_0^2} \frac{eV}{\hbar \Omega} \frac{1}{1 + \beta^2} \leq 4 \frac{\langle x^2 \rangle}{\Delta x_0^2} \frac{eV}{\hbar \Omega} .
\tag{8.25}
$$

In the single-detector case and for given system parameters (eV and $\langle x^2 \rangle$), the peak-to-background ratio is therefore always bounded whatever the strength of the coupling and the bound does not depend on Q_0 and τ_0. As can be seen from Eq. (8.22), the peak-to-background ratio is in this second case maximal in the limit $\beta \to 0$ of vanishing coupling. While the optimal $\mathcal{R}$ can be increased by increasing the bias voltage, we stress that our bound on $\mathcal{R}$ denotes the optimal value of the peak-to-background reachable for a set of fixed system parameters.

The nature of the true bound on $\mathcal{R}$ (i.e., the one found in the case $Q_0 \to \infty$) is very similar to the Korotkov-Averin bound that arises in the context of a weak measurements of a qubit. To make this more apparent, we can derive this bound following the linear-response approach that has been used to derive the bound on $\mathcal{R}$ in the measurement of two-levels systems, treating the detector as a position-to-current linear amplifier with responsivity (dimensionful gain) $\lambda = 2e^2 V \tau_0 \tau_1 / h$. As noted by CG, considering only the dominant $\propto V^2$ term in Eq. (8.18) corresponds to writing $\Delta \overline{S}_I = \overline{S}_I - e \langle I \rangle = \lambda^2 \overline{S}_x(\omega)$. At resonance, the power spectrum $\Delta \overline{S}_I = \lambda^2 \langle x^2 \rangle / \tilde{\gamma}$ is inversely proportional to the damping rate $\tilde{\gamma}$, in the same way that the response of the detector measuring a qubit is inversely proportional to the dephasing rate due to the measurement device. Moreover, in both cases one can show that the dephasing (damping rate) is proportional to the fluctuations of the bare input of the detectors. For a position detector in the high effective temperature limit $k_B T_{\text{eff}} \gg \hbar \Omega$, we showed [Eq. (6.9)] that

the detector-induced damping is indeed proportional to the symmetrized detector force noise $(2\tilde{\gamma}) = \overline{S}_F/2Mk_BT_{\text{eff}}$, such that $\Delta\overline{S}_I \leq 4M\lambda^2\langle x^2\rangle k_BT_{\text{eff}}/\overline{S}_F$. Also, since for a tunnel junction detector there is no reverse gain λ' and the real part of the cross correlator $\overline{S}_{IF}(\omega)$ vanishes for $\sin(\eta) = 0$ [Eq. (6.50)], the condition on quantum-limited efficiency of the position measurement[Eq. (4.17)]

$$\overline{S}_I\overline{S}_F \geq \frac{\hbar^2}{4}(\text{Re}[\lambda - \lambda'])^2 + (\text{Re}[\overline{S}_{IF}])^2 \tag{8.26}$$

becomes exactly the one used to derive the Korotkov-Averin bound $\overline{S}_I\overline{S}_F \geq \frac{\hbar^2\lambda^2}{4}$. We then find that $\mathcal{R} = \Delta\overline{S}_I/\overline{S}_I \leq 8\langle x^2\rangle k_BT_{\text{eff}}/(\hbar\Omega\Delta x_0^2)$. Using $k_BT_{\text{eff}} = eV/2$ in the tunnel junction system, this result corresponds exactly to Eq. (8.25), the bound previously derived using the equation-of-motion approach.

8.3 Peak-to-background ratio in current cross correlations

Extending ideas from the qubit measurement problem[Jordan05], we now demonstrate how to eliminate the bound on the peak-to-background ratio in a displacement measurement. Calculating the current-current correlations between two tunnel-junction position detectors, we show that for cross correlation measurements, $\mathcal{R}$ diverges. We also obtain analytical results for the cross correlations in two typical cases.

To calculate the current cross correlations, we use the generalized MacDonald formula [A], a general result (valid for stationary processes) that provides a way, in the present case, to relate the symmetrized cross correlations to the Fourier sine-transform of the time-derivative of the covariance of m_1 and m_2, the number of charges that tunneled through each junction. The generalized MacDonald formula reads

$$\overline{S}_{I_1,I_2}(\omega) = e^2\omega \int_0^\infty dt \sin(\omega t) K_{1,2}(t) , \tag{8.27}$$

where we defined

$$K_{1,2}(t) = \left[\frac{d}{dt'}\left(\langle m_1 m_2\rangle_{t'} - \langle m_1\rangle_{t'}\langle m_2\rangle_{t'}\right)\right]_{t'=t} . \tag{8.28}$$

In this last equation $\langle m_1 m_2\rangle_t$ corresponds to $\text{Tr}\, m_1\, m_2\, \tilde{\rho}(0,0,t)$ and represents the coupled moment of m_1 and m_2 at time t.

To proceed further, we restrict ourselves to the case of zero electronic temperature and dc-bias. In the following subsections, we analyze in detail the two different cases depicted schematically in Fig. 8.1. We have in mind that a realization of the setup shown in Fig. 8.1 is made in a similar way as the single-detector setup in

Ref. [Flowers-Jacobs07]. This means that the tunnel junctions correspond to atomic point contacts (formed by electromigration) which are separated by about 1 nm from the oscillator. In contrast, the two detectors are assumed to be separated from each other by at least 20 nm. Therefore, capacitive cross-talking between the detectors will play a negligible role.

8.3.1 In-phase configuration

We will first consider the case where both $\eta_1 = \eta_2 = 0$, the case where both tunnel junctions are located on the same side of the oscillator, *cf.* Fig. 8.1 a). To calculate the cross correlations, we use Eq. (8.17) (with $n_1 = n_2 = 0$), to find that

$$\frac{d}{dt}\langle m_\alpha \rangle_t = \frac{eV_\alpha}{h}\left(\tau_{0,\alpha}^2 + 2\tau_{0,\alpha}\tau_{1,\alpha}\langle x \rangle + \tau_{1_\alpha}^2\langle x^2 \rangle\right) - \tilde{\gamma}_{+,\alpha},$$

$$\frac{d}{dt}\langle m_1 m_2 \rangle_t = \frac{eV_1}{h}\left(\tau_{0,1}^2\langle m_2 \rangle_t + 2\tau_{0,1}\tau_{1,1}\langle x m_2 \rangle_t + \tau_{1,1}^2\langle x^2 m_2 \rangle_t\right)$$
$$+ \frac{eV_2}{h}\left(\tau_{0,2}^2\langle m_1 \rangle_t + 2\tau_{0,2}\tau_{1,2}\langle x m_1 \rangle_t + \tau_{1,2}^2\langle x^2 m_1 \rangle_t\right)$$
$$- \tilde{\gamma}_{+,1}\langle m_2 \rangle_t - \tilde{\gamma}_{+,2}\langle m_1 \rangle_t,$$

and therefore that $K_{1,2}(t)$ in this case is given by

$$K_{1,2}(t) = 2\frac{eV_1}{h}\tau_{0,1}\tau_{1,1}\langle\langle x m_2 \rangle\rangle_t + \frac{eV_1}{h}\tau_{1,1}^2\langle\langle x^2 m_2 \rangle\rangle_t$$
$$+ 2\frac{eV_2}{h}\tau_{0,2}\tau_{1,2}\langle\langle x m_1 \rangle\rangle_t + \frac{eV_2}{h}\tau_{1,2}^2\langle\langle x^2 m_1 \rangle\rangle_t. \tag{8.29}$$

where the double bracket denotes the covariance of two quantities: $\langle\langle ab \rangle\rangle_t \equiv \langle ab \rangle_t - \langle a \rangle_t\langle b \rangle_t$. This means that, to lowest order in $\tau_{1,\alpha}$, the *full* cross-correlated output of the detectors is given in this configuration by

$$\bar{S}_{I_1,I_2}(\omega)\Big|_{\substack{\eta_1=0\\\eta_2=0}} = 2e^2\omega\int_0^\infty dt\sin(\omega t)\left(\frac{eV_1}{h}\tau_{0,1}\tau_{1,1}\langle\langle x m_2 \rangle\rangle_t + \frac{eV_2}{h}\tau_{0,2}\tau_{1,2}\langle\langle x m_1 \rangle\rangle_t\right). \tag{8.30}$$

The cross-correlated signal does not contain any oscillator-independent contribution. Using Eq. (8.17), a closed system of differential equations involving $\langle\langle p m_\alpha \rangle\rangle_t$ and $\langle\langle x m_\alpha \rangle\rangle_t$ can be generated. This system can be solved, using the boundary conditions $m_\alpha(0) = 0$ and assuming that all averages that do not contain m_α are time-independent and can therefore be evaluated in the stationary ($t \to \infty$) limit[Armour04a].

Solving for the different covariances, we find that the current cross correlations can be written as

$$\overline{S}_{I_1 I_2}^{\text{tot}}(\omega) = e^2(2\tau_{0,1}\tau_{0,2})(2\tau_{1,1}\tau_{1,2}) \left(\frac{e^2 V_1 V_2}{h^2} - \frac{e(V_1 + V_2)}{2h} \frac{\Omega}{4\pi} \frac{\Delta x_0^2}{\langle x^2 \rangle} \right) \overline{S}_x(\omega) , \quad (8.31)$$

$$= \lambda_1 \lambda_2 \left(1 - \frac{\hbar\Omega(eV_1 + eV_2)}{4eV_1 eV_2} \frac{\Delta x_0^2}{\langle x^2 \rangle} \right) \overline{S}_x(\omega) , \quad (8.32)$$

where we introduced the gains $\lambda_\alpha = 2e^2\tau_{0,\alpha}\tau_{1,\alpha}V_\alpha \cos(\eta_\alpha)/h$. Evidently, the cross-correlated output of the detectors (8.31) does not contain any frequency-independent background noise. The peak-to-background ratio $\mathcal{R}(\Omega)$ therefore diverges for all values of $\tilde{\gamma}_0/\tilde{\gamma}_+$, not because of an increased signal but due to the absence of background noise in this configuration.

For this type of measurement, a relevant figure of merit of the detection system $\mathcal{R}_c$ is the ratio of the cross-correlated output over the frequency-independent noise power of individual detectors : $\mathcal{R}_c = S_{I_1,I_2,\text{tot}}(\Omega)/\sqrt{\overline{S}_1 \overline{S}_2}$, where $\overline{S}_\alpha = e\langle I_\alpha \rangle$. For our position detector, we find

$$\mathcal{R}_c = \frac{|\overline{S}_{I_1,I_2,\text{tot}}|}{\sqrt{\overline{S}_1 \overline{S}_2}} = \frac{4}{1 + \frac{\tilde{\gamma}_0}{\tilde{\gamma}_+}} \frac{1}{\sqrt{(1 + \beta_1^2)(1 + \beta_2^2)}} \frac{\tau_{1_1}\tau_{1_2}}{\tau_{1,1}^2 + \tau_{1,2}^2} \frac{\sqrt{V_1 V_2}}{V_1 + V_2} \frac{e(V_1 + V_2)}{\hbar\Omega} \frac{\langle x^2 \rangle}{\Delta x_0^2}$$
$$(8.33)$$

$$\leq \frac{e(V_1 + V_2)}{\hbar\Omega} \frac{\langle x^2 \rangle}{\Delta x_0^2} , \quad (8.34)$$

where we used $2xy \leq (x^2 + y^2)$. From this inequality, we see that the maximal cross-correlated output is found for (i) twin-detectors (where $\tau_{1,1} = \tau_{1,2}$) and (ii) equal bias voltages $V_1 = V_2$. Also, like in the single-detector case, $\mathcal{R}_c$ is maximal in the limit where there is no extrinsic oscillator damping $\tilde{\gamma}_0$ and where the correction to the average current due to the coupling to the oscillator vanishes ($\beta_\alpha \to 0$).

Once again it is instructive to compare our value of $\mathcal{R}_c$ for twin detectors with the equivalent result in the case of a weak measurement of a qubit using cross correlations[Jordan05]. In the latter case, the cross-correlated output was shown to be limited to $1/2$ of the single-detector signal due the increased (doubled) detector-induced dephasing. This is the same here.

8.3.2 Out-of-phase detection

We can also analyze the case where one detector couples to $+x$ and the other to $-x$, as would happen if the two detectors were located on opposite sides of the resonator

(see Fig. 8.1). In terms of the tunneling phases η_α, this corresponds to taking $\eta_1 = 0$ and $\eta_2 = \pi$. Using Eq. (8.27), the cross correlations are then given by

$$\overline{S}_{I_1,I_2}(\omega)\Big|_{\substack{\eta_1=0\\\eta_2=\pi}} = 2e^2\omega \int_0^\infty dt \sin(\omega t) \left(\frac{eV_1}{h}\tau_{0,1}\tau_{1,1}\langle\langle xm_2\rangle\rangle_t - \frac{eV_2}{h}\tau_{0,2}\tau_{1,2}\langle\langle xm_1\rangle\rangle_t \right).$$

(8.35)

As the coupling between detector 1 and the oscillator is the same as in the previous case $\langle\langle xm_1\rangle\rangle_t$ remains unchanged in this second configuration. The covariance $\langle\langle xm_2\rangle\rangle_t$ on the other hand changes sign (but keeps the same norm) in this new configuration. Equation (8.35) then yields

$$\overline{S}_{I_1,I_2}(\omega)\Big|_{\substack{\eta_1=0\\\eta_2=\pi}} = -\overline{S}_{I_1,I_2}(\omega)\Big|_{\substack{\eta_1=0\\\eta_2=0}}.$$

(8.36)

The cross correlations in the second configuration are the same as in the first one, but of negative sign. From an amplifier point of view, this is easily explained since putting $\eta_2 = \pi$ corresponds to transforming $\lambda_2 \to -\lambda_2$ in $\overline{S}_{I_1,I_2} \simeq \lambda_1\lambda_2\overline{S}_x$. Finally, note that this configuration was analyzed for two single-electron transistor position detectors coupled to a classical oscillator, in Ref.[Rodrigues05] by Rodrigues and Armour. In their article, these authors only explicitly calculated zero-frequency cross correlations between the currents in both detectors, but they conjectured that, at the resonance frequency of the oscillator, this detector-configuration (corresponding to $\eta_1 = 0, \eta_2 = \pi$ in our approach) should yield strong negative cross correlations, just like the ones predicted here.

8.4 Bound on the added displacement noise

As shown in Sec. 8.2, to derive the equivalent of the Korotkov-Averin bound in a displacement measurement, one needs to consider the *full* current noise, where no distinction is made between the signal due to the intrinsic equilibrium fluctuations of the oscillator $\overline{S}_{I,\text{eq}}(\omega)$ and the remainder of the signal $\overline{S}_{I,\text{add}}(\omega)$. This second contribution contains, amongst other things, the added signal due to heating of the oscillator by the detector. As mentioned in Sec. 6.1.2, when trying to measure precisely the equilibrium fluctuations of a nanomechanical oscillator however, it is important to consider the two contributions separately: $\overline{S}_{I,\text{eq}}(\omega)$ is exactly what you would like to measure while $\overline{S}_{I,\text{add}}(\omega)$ limits the sensitivity of the measurement. When using a single linear detector like the tunnel junction, this measurement sensitivity is quantum-mechanically bounded from below[Clerk04a].

When discussing this bound on added noise, one usually considers the added *displacement* noise, that corresponds to the added current noise referred back to the os-

cillator. We therefore introduce the total displacement noise $\overline{S}_{x,\text{tot}}$, defined as

$$\overline{S}_{x,\text{tot}}(\omega) = \frac{\overline{S}_{I,\text{tot}}(\omega)}{\lambda^2} = \overline{S}_{x,\text{add}}(\omega) + \overline{S}_{x,\text{eq}}(\omega) \,, \tag{8.37}$$

where λ is the x-to-I gain of the detector, $\overline{S}_{x,\text{add}}(\omega)$ is the part of the full displacement spectrum that arises due to the presence of the detector. In the relevant limit of a detector with a high power gain ($eV \gg \hbar\Omega$), it was shown using general arguments that $\overline{S}_{x,\text{add}}(\Omega) \geq \hbar/2M\Omega\tilde{\gamma}_{\text{tot}}$: as derived Sec. 6.1.2 in the best possible detector therefore adds exactly as much noise as a zero-temperature bath of frequency Ω[Clerk04a; Caves82].

Before discussing the limit on the added displacement noise in a cross correlation setup, it is helpful to describe how the quantum limit on $\overline{S}_{x,\text{add}}(\Omega)$ is reached when considering the specific example of a tunnel junction displacement detector. Let's consider for definitiveness the experimentally relevant configuration where $eV \gg k_B T_0 > \hbar\Omega$. For a measurement to be quantum limited, the effective temperature of the oscillator $T_{\text{eff}} = (\tilde{\gamma}_+ eV/2 + \tilde{\gamma}_0 k_B T_0)/(k_B \tilde{\gamma}_{\text{tot}})$ must not be dramatically higher than T_0. This is natural, since added fluctuations due to the higher effective temperature are, by definition, unwanted back-action noise. In this regime, one therefore cannot expect $\overline{S}_{x,\text{add}}$ to be close to the quantum limit unless $\tilde{\gamma}_+ \ll \tilde{\gamma}_0$. The regime of $\tilde{\gamma}_+/\tilde{\gamma}_0$ in which quantum-limited displacement sensitivity can be achieved is therefore very different from the one where the bound on the peak-to-background ratio can be reached.

Using the expression for the full current noise derived earlier [Eq. (8.18)], we write the full position noise as

$$\overline{S}_{x,\text{tot}}(\omega) = \frac{S_{I,\text{tot}}(\omega)}{\lambda^2} = \frac{e\langle I\rangle}{\lambda^2} + \left(1 - \frac{\hbar\Omega}{2eV}\frac{\Delta x_0^2}{\langle x^2\rangle}\right)\overline{S}_x(\omega) \,, \tag{8.38}$$

$$= \frac{e\langle I\rangle}{\lambda^2} + 4M\tilde{\gamma}_{\text{tot}}k_B T_{\text{eff}}|g(\omega)|^2 - M\tilde{\gamma}_{\text{tot}}\frac{(\hbar\Omega)^2}{eV}|g(\omega)|^2 \,, \tag{8.39}$$

with the $g(\omega)$ oscillator's response function as defined in Eq. (6.13). Splitting the second term into a detector dependent and independent part, we find

$$\overline{S}_{x,\text{eq}} = 4M\tilde{\gamma}_0 k_B T_0 |g(\omega)|^2 \,, \tag{8.40}$$

$$\overline{S}_{x,\text{add}} = \frac{e\langle I\rangle}{\lambda^2} + 4M\tilde{\gamma}_+\frac{eV}{2}|g(\omega)|^2 - M\tilde{\gamma}_{\text{tot}}\frac{(\hbar\Omega)^2}{eV}|g(\omega)|^2 \,. \tag{8.41}$$

This way of writing the equilibrium fluctuations implies that we consider $\tilde{\gamma}_{\text{tot}} \simeq \tilde{\gamma}_0$ in $g(\omega)$, in agreement with our previous assumption that $\tilde{\gamma}_+ \ll \tilde{\gamma}_0$. The added noise contains three contributions, corresponding to the detector shot noise, the detector-induced heating of the oscillator and a correction ($\propto \hbar\Omega/eV$) arising from the cross

correlation between the detector output noise and the back-action force, $\overline{S}_{IF}$, respectively. Explicitly, taking $\langle I \rangle \simeq e^2\tau_0^2 V/h$,[2] we obtain

$$\overline{S}_{x,\text{add}} = \frac{\pi\hbar}{2eV\tau_1^2} + \frac{\hbar\tau_1^2 eV|g(\omega)|^2}{2\pi} - M\tilde{\gamma}_{\text{tot}}\frac{(\hbar\Omega)^2}{eV}|g(\omega)|^2 . \tag{8.42}$$

For a fixed bias voltage, the relevant tunable parameter is directly the detector-oscillator coupling τ_1 (and not the dimensionless sensitivity parameter β, since $\overline{S}_{x,\text{add}}$ is independent of τ_0).[3] For strong coupling, $\overline{S}_{x,\text{add}}$ is dominated by heating of the oscillator, while for weak coupling, the shot noise contribution ($\propto 1/\tau_1^2$) dominates. This is the regime in which the current generation of experiments are operated [Flowers-Jacobs07]. There is an optimal coupling $\tau_{1,\text{opt}}^2 = \pi/(eV|g(\omega)|)$ that minimizes the total added noise. At the resonance, we recover the inequality

$$\overline{S}_{x,\text{add}}(\Omega) \geq \left(1 - \frac{\hbar\Omega}{2eV}\right)\frac{\hbar}{2\tilde{\gamma}_{\text{tot}}M\Omega} , \tag{8.43}$$

where the bound is reached when $\tau_1 = \tau_{1,\text{opt}}$. This is the quantum limit on the added displacement noise for the single-detector configuration. In passing, we note that the effective temperature of the oscillator when the coupling strength τ_1 is optimal is

$$T_{\text{eff}} = T_0 + \frac{\hbar\Omega}{4k_B} , \tag{8.44}$$

in agreement with the general analysis of Ref. [Clerk04a]. The heating of the oscillator by the detector is, as expected, very low when doing a quantum-limited measurement.

We can now show how cross correlations can be used to beat the quantum limit on $\overline{S}_{x,\text{add}}$ derived in the single-detector case. In both cross correlation configurations ($\eta = 0, \pi$), $\overline{S}_{x,\text{tot}} = \overline{S}_{I_1,I_2}/\lambda_1\lambda_2$ is identical. Like in the single-detector case, we separate the total position fluctuations in two parts

$$\overline{S}_{x,\text{eq}} = 4M\tilde{\gamma}_0 k_B T_0 |g(\omega)|^2 , \tag{8.45}$$

$$\frac{\overline{S}_{x,\text{add}}}{M|g(\omega)|^2} = 2\left(\sum_\alpha \tilde{\gamma}_{+,\alpha}eV_\alpha\right) - \tilde{\gamma}_{\text{tot}}\frac{(\hbar\Omega)^2(eV_1 + eV_2)}{2eV_1eV_2} . \tag{8.46}$$

The cross-correlated position spectrum does not contain the frequency-independent shot noise contribution that diverges for low coupling ($\propto 1/\tau_1^2$). Therefore, one does

---

[2]The derived bound is therefore valid up to a positive correction of order β^2.

[3]In principle, we could use the bias voltage eV as an optimization parameter. In this case, we would find that $\overline{S}_{x,\text{add}} \to 0$ for $eV/\hbar\Omega \to 0$; there is no limit on the added position noise in the low power gain regime ($eV \sim \hbar\Omega$) [Clerk04a; Caves82]. However, since Eq. (8.18) was derived in the high bias regime, it is better in the present case to optimize the coupling strength τ_1 while keeping $eV/\hbar\Omega \gg 1$ fixed.

not need to tune the coupling to equilibrate the "shot noise" and back-action "heating" contributions. Instead, one can freely tune the couplings $\tau_{1,\alpha}$ such that $\overline{S}_{x,\text{add}}(\omega)$ vanishes completely. We find $\overline{S}_{x,\text{add}} = 0$ for $\tau_{1,\alpha,\text{opt}}^2 = 4\pi M\tilde{\gamma}_{+,\alpha,\text{opt}}/\hbar$, where

$$\tilde{\gamma}_{+,\alpha,\text{opt}} = \frac{\tilde{\gamma}_{\text{tot}}}{4}\left(\frac{\hbar\Omega}{eV_\alpha}\right)^2 . \tag{8.47}$$

At the optimal coupling point, the effective temperature of the oscillator is

$$T_{\text{eff}} = T_0 + \left(\frac{\hbar\Omega}{eV_1} + \frac{\hbar\Omega}{eV_2}\right)\frac{\hbar\Omega}{8k_B} . \tag{8.48}$$

In the regime of interest ($eV_\alpha \gg \hbar\Omega$), the additional heating of the oscillator considerably reduced from the single-detector value.

8.5 Summary

In this chapter, we have shown that, for a tunnel-junction position detector coupled to a nanomechanical oscillator, the optimal peak-to-background ratio $\mathcal{R}$ at the resonance frequency of the oscillator is bounded. In contrast to the universal (independent of all system parameters) bound derived for a continuous weak measurement of qubits ($\mathcal{R} \leq 4$), the new bound derived for displacement measurements is a function of the effective temperature of the oscillator and its average displacement. We have also shown that adding a second detector and using the cross correlations between the two detectors allows one to eliminate this bound on $\mathcal{R}$. We have analyzed in detail the cross-correlated output of the position detectors in two typical configurations, and have shown that in both cases the optimal cross-correlated signal is measured by twin detectors. We also investigated the quantum-limit on the added displacement noise and shown that it is possible to totally eliminate the added displacement noise by doing a cross-correlated measurement. This configuration therefore opens the door for displacement measurement with sensitivities better than the quantum limit.

Measuring the momentum of a nanomechanical oscillator through the use of two tunnel junctions

In previous chapters, we always considered NEMS where the detector was coupled via the position operator to the mechanical object: the detector therefore acted solely as a displacement detector. As discussed, using these detectors displacement measurements with close to quantum-limited sensitivity have been demonstrated. From a fundamental point of view, it is desirable to go further, i.e. to prepare and manipulate NEM oscillators in the quantum regime. A quantum NEM system would allow us to study an ideal realization of a continuous variable quantum system [Braunstein05]. The exploration of such systems has to be seen as complementary to the wide study of two-level systems done in the context of quantum computing.

In order to be able to fully characterize a continuous variable quantum system that is described by two non-commuting operators $\hat{x}$ and $\hat{p}$, we need to be able to measure expectation values of moments of both of them [Duan00]. Only this allows, for instance, to detect the entanglement between two (or more) NEM devices [Eisert04]. The literature already contains proposals regarding quantum measurements of the momentum of macroscopic objects like those used for gravity-wave detection [Braginsky80; Braginsky90; Braginsky00; Braginsky03]. However, none of these proposals have been realized in practice. In this Letter, we propose a way to measure the momentum of a *nanometer-sized* resonator. This is a non-trivial task since the coupling between the detector and the oscillator is naturally described by an x-dependence but not a p-dependence. Nevertheless, the proposed setup (shown in Fig. 9.1b) allows for a measurement of the momentum spectrum $\overline{S}_p(\omega) = \int dt e^{i\omega t} \langle \{\hat{p}(t), \hat{p}(0)\} \rangle / 2$ of the oscillator. This can be done because we have

found a way to tune the phase of the tunnel coupling term that is sensitive to the position of the oscillator by an Aharonov-Bohm (AB) flux Φ, see Fig. 9.1b. Related setups have been investigated recently in the context of dephasing due to the coupling of an AB ring structure to a NEM device [Armour01]. The typical tunnel junction position
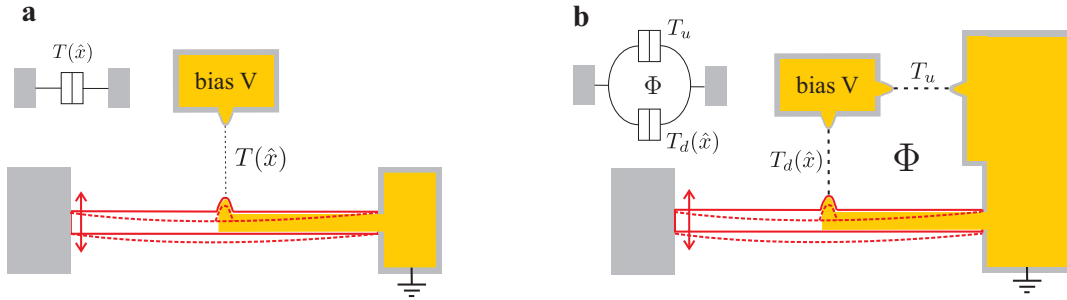
Figure 9.1: **(a)** *Position detector.* The figure shows schematically a position detector of the motion of a NEM oscillator (red). The detector is based on a tunnel junction with a tunnel matrix element $T(\hat{x})$ which depends on the position of the oscillator. The shaded regions (yellow) are assumed to be conducting. **(b)** *Position and/or momentum detector.* The figure illustrates a detector which contains two tunnel junctions that form a loop threaded by a magnetic flux Φ. Tuning the flux will change the performance of the detector from being able to detect the power spectrum of the *position operator* of the oscillator to being able to detect the power spectrum of the *momentum operator* of the oscillator. For clarity, the two insets show a simplified illustration of the detectors in **a** and **b**.

position detector which has been discussed at length in the present part of this thesis is depicted in Fig. 9.1a. It is composed of a single tunnel junction coupled to a NEM oscillator. The thorough analysis of the coupled quantum system (Sec. 7.3) leads to the result that the output signal of the detector is sensitive to the position spectrum $\overline{S}_x(\omega) = \int dt e^{i\omega t} \langle \{\hat{x}(t), \hat{x}(0)\} \rangle / 2$ of the oscillator. The modification of the detector shown in Fig. 9.1b instead allows for a measurement of $\overline{S}_p(\omega)$.

9.1 Model

We use exactly the model presented in Sec. 7.3, with the Hamiltonian of the coupled system $H = H_{\text{osc}} + H_B + H_{\text{tun}}$ written as the sum of the Hamiltonian of the (quantum) harmonic oscillator H_{osc} (with mass M and frequency Ω), the bath Hamiltonian H_B (describing the leads of the detector), and the tunneling Hamiltonian H_{tun} (which couples the dynamics of the electrons that tunnel across the junction to the motion of

the oscillator):

$$H_{\text{osc}} = \hbar\Omega(a^\dagger a + \frac{1}{2}) = \frac{\hat{p}^2}{2M} + \frac{M\Omega^2\hat{x}^2}{2} \ , \tag{9.1}$$

$$H_B = \sum_k \varepsilon_k c_k^\dagger c_k + \sum_q \varepsilon_q c_q^\dagger c_q \ , \tag{9.2}$$

$$H_{\text{tun}} = T(\hat{x})Y^\dagger \sum_{k,q} c_k^\dagger c_q + T^\dagger(\hat{x})Y \sum_{k,q} c_q^\dagger c_k \ . \tag{9.3}$$

Again, k (q) is a wave vector in the right (left) lead, $c^{(\dagger)}$ is the electron annihilation (creation) operator, and $Y^{(\dagger)}$ is an operator that decreases (increases) m, the number of electrons that have tunneled through the system, by one. It allows one to keep track of the transport processes during the evolution of the system.

We first discuss the model in the standard configuration shown in Fig. 9.1a and later on describe the new setup in Fig. 9.1b. For small displacements with respect to the tunneling length (which is the relevant regime in typical experiments on NEM devices), the tunneling amplitude $T(\hat{x})$ can be taken as a linear function of $\hat{x}$, namely

$$T(\hat{x}) = \frac{e^{i\varphi_0}}{2\pi\Lambda} \left(\tau_0 + e^{i\eta}\tau_1\hat{x}\right) \ , \tag{9.4}$$

where τ_0 and τ_1 are real, and Λ is the density of states. The phases φ_0 and η describe details of the detector-oscillator coupling. The overall phase φ_0 is a gauge-dependent quantity and does not affect the observable output of the detector. As proven in Sec. 6.2.3, this detector is quantum-limited for all values of η.

Within the single-junction setup (Fig. 9.1a), the relative phase η is sample-dependent and cannot be tuned experimentally. In a typical device, the x-dependence of the phase of $T(\hat{x})$ is much weaker than the x-dependence of the amplitude. Then, as discussed in the last Chapter, we can set $\eta \simeq 0$, and the tunnel junction acts as a position-to-current amplifier where the frequency-dependent current noise $\bar{S}_I(\omega)$ of the detector contains a term proportional to the position spectrum $\bar{S}_x(\omega)$ of the oscillator, i.e. $\Delta\bar{S}_I(\omega) = S_I(\omega) - e\langle I\rangle \approx \lambda_x^2 \bar{S}_x(\omega)$ with λ_x the gain of the amplifier.

9.2 Tuning the relative phase η.

We now demonstrate that a tunnel junction with a phase $\eta = \pi/2 \bmod \pi$ acts as a momentum detector and $\Delta S_I(\omega) \approx \lambda_p^2 S_p(\omega)$, where λ_p is the gain of the momentum-to-current linear amplifier. The critical requirement to build a momentum detector is to be able to vary η experimentally. This can be done using the AB-type setup shown in Fig. 9.1b: a metallic ring where one arm is a standard tunnel junction position detector with tunneling amplitude $T_d(\hat{x})$, and the other arm is a position-

independent tunnel junction with tunneling amplitude T_u [1]. The total transmission amplitude $T(\hat{x}, \Phi)$ of the device is the sum of both tunneling amplitudes [2]. Since only one arm shows a position-dependence, the induced phase difference between the two arms affects the position-independent and the position-dependent parts of the tunneling amplitudes τ_0 and τ_1 in a different way. Explicit calculation shows that the tunneling amplitude is given (up to a global gauge-dependent phase factor) by $T(\hat{x}, \Phi) = (\tau_0(\Phi) + e^{i\eta(\Phi)}\tau_1\hat{x})/(2\pi\Lambda)$ with

$$
\begin{aligned}
\tau_0^2(\Phi) &= \tau_{0,d}^2 + \tau_{0,u}^2 + 2\tau_{0,d}\tau_{0,u}\cos\left(2\pi\frac{\Phi}{\Phi_0} + \varphi_{0,d} - \varphi_{0,u}\right), \\
\eta(\Phi) &= 2\pi\frac{\Phi}{\Phi_0} + \varphi_{1,d} - \varphi_{0,u}\mathrm{Arg}\left(\tau_{0,u} + e^{i(2\pi\frac{\Phi}{\Phi_0} + \varphi_{0,d} - \varphi_{0,u})}\tau_{0,d}\right),
\end{aligned}
\tag{9.5}
$$

where we have defined $T_u \equiv e^{i\varphi_{0,u}}\tau_{0,u}$, $T_d \equiv e^{i\varphi_{0,d}}\tau_{0,d} + e^{i\varphi_{1,d}}\tau_{1,d}\hat{x}$, $\tau_1 \equiv \tau_{1,d}$, and $\Phi_0 = h/e$ [3]. The position-independent part of the tunneling amplitude $\tau_0(\Phi)$ displays the standard AB oscillations as a function of flux. Likewise, the relative phase $\eta(\Phi)$ shows a distinct dependence on the flux. Importantly, for $\tau_{0,u} > \tau_{0,d}$, the phase $\eta(\Phi)$ can be tuned continuously in the whole range $[-\pi, \pi]$. In the limit, where $\tau_{0,u} \gg \tau_{0,d}$, $\eta(\Phi) \sim 2\pi\frac{\Phi}{\Phi_0} + \eta(\Phi = 0)$ varies linearly with the applied flux. In the opposite regime $\tau_{0,u} \ll \tau_{0,d}$, η no longer depends on Φ. Therefore, it is crucial to put the tunneling amplitudes in the regime where $\eta(\Phi)$ can be tuned to $\pi/2$. We will show below that a feasible way to calibrate $\eta(\Phi)$ to the p-sensitive point $\pi/2$ is a measurement of the flux dependence of the current through the AB detector.

We study the coupled system using the quantum equation of motion for the charge-resolved density matrix within the Born-Markov approximation, assuming that $eV \gg \hbar\Omega$, exactly like in Sec. 7.3.

It has been derived previously that, under the assumption that the tunneling amplitude depends linearly on $\hat{x}$, the equation of motion for the reduced density matrix of the oscillator is of Caldeira-Leggett form [Mozyrsky02; Clerk04b; Wabnig05]. Thus, it contains both a damping and a diffusion term. When the electron temperature is much smaller than the applied bias (and taking $V > 0$), the detector-induced damp-

---

[1]A similar device in a different context (without a position-dependent tunneling amplitude) has been realized in the electronic Mach-Zehnder interferometer [Ji03]

[2]We assume that the size of the AB detector is smaller than the phase coherence length (which can be several microns in metallic thin films at low temperatures) and that it is large enough such that we do not have to take into account the change of the area of the AB loop due to the fluctuating position of the oscillator. Furthermore, the setup is designed such that the electrons can not make roundtrips in the AB loop but leave the ring instead after going either through the upper or the lower arm. This explains why (in general) $|T(\hat{x}, \Phi)|^2 \neq |T(\hat{x}, -\Phi)|^2$. See [Büttiker86] for details.

[3]Strictly speaking, the analysis in Eq. (9.5) is only valid in the single-channel case. For the multi-channel case with N channels in the AB loop, the magnitude of the AB oscillations is reduced by a factor $1/N$

ing coefficient is $\tilde{\gamma}_+ = \hbar\tau_1^2/(4\pi M)$ and the diffusion coefficient is $D_+ = 2M\tilde{\gamma}_+ k_B T_{\text{eff}}$ with $T_{\text{eff}} = eV/2k_B$.

In general, the oscillator is not only coupled to the detector but also to the environment. The coupling to this additional bath is controlled via $\tilde{\gamma}_0 = \Omega/(2Q_0)$ (related to the finite quality factor Q_0 of the mode, which in current experiments varies from 10^3 to 10^6 [Ekinci05b]) and the associated diffusion constant $D_0 = 2M\tilde{\gamma}_0 k_B T_{\text{env}}$ that must be added to the detector-induced damping and diffusion constants to find the total damping coefficient $\tilde{\gamma}_{\text{tot}} = \tilde{\gamma}_+ + \tilde{\gamma}_0$ and the total diffusion coefficient $D_{\text{tot}} = D_0 + D_+$. T_{env} denotes the temperature of the environment. In typical experiments, it varies from 30mK to 10K. Within our model, all the these system parameters are independent of the applied flux.

It is now straightforward to calculate the current and the current noise of the detector. Since they were presented in Sec. 7.3, here we skip the details of the calculation and directly turn to the results. The average current of the detector is given by

$$I = \frac{e^2 V}{h}\left(\tau_0^2 + 2\cos\eta\,\tau_0\tau_1\langle x\rangle + \tau_1^2\langle x^2\rangle\right) - \frac{2e\tilde{\gamma}_+\tau_0}{\hbar\tau_1}\sin\eta\,\langle p\rangle - e\tilde{\gamma}_+. \tag{9.6}$$

For $\eta \neq 0 \bmod \pi$, the average current contains a term proportional to the average momentum of the oscillator that does not vary with the applied bias [Wabnig05]. However, since $\langle p\rangle = 0$ in the steady-state, the average current contains no information about the momentum of the oscillator. Therefore, the current of the detector can not be used as a p-detector in the steady-state. Nevertheless, the current is important to calibrate η to the p-sensitive value $\pi/2$. A careful analysis of the current I as a function of Φ shows that the inflection points of $I(\Phi)$ correspond precisely to values of $\eta = \pi/2 \bmod \pi$. Therefore, we can use a current measurement to tune η to a p-sensitive value.

9.3 Transport properties with finite η.

In the experimentally relevant regime, where $\tau_1^2\langle x^2\rangle \ll \tau_0^2$, and for $\omega \sim \Omega$, the dominant contributions to the current power spectrum of the detector are

$$\begin{aligned}
\overline{S}_I(\omega) = {} & e\langle I\rangle \\
& + 4e^2\omega \int_0^\infty dt\,\sin(\omega t)\left[\frac{eV}{h}\cos\eta\,\tau_0\tau_1\langle\langle xm\rangle\rangle - \frac{\tilde{\gamma}_+\tau_0}{\hbar\tau_1}\sin\eta\,\langle\langle pm\rangle\rangle\right],
\end{aligned} \tag{9.7}$$

where $\langle\langle ab\rangle\rangle = \langle ab\rangle - \langle a\rangle\langle b\rangle$. We now further analyze the added noise due to the presence of the oscillator, $\Delta\overline{S} = \overline{S}_I(\omega) - e\langle I\rangle$. This noise spectrum is the sum of a contribution arising due to correlations between the transfered charge m and position (term $\sim \langle\langle xm\rangle\rangle$ in Eq. (9.7)), which we call $\Delta\overline{S}_1$, and one due to correlations between

m and the momentum of the oscillator (term $\sim \langle\langle pm \rangle\rangle$ in Eq. (9.7)), which we call $\Delta \overline{S}_2$. The full spectrum is therefore $\Delta \overline{S} = \Delta \overline{S}_1 + \Delta \overline{S}_2$ with

$$\Delta \overline{S}_1(\omega) = \left[\lambda_x^2 \left(1 - \frac{\hbar \Omega}{2eV} \frac{\Delta x_0^2}{\langle\langle x^2 \rangle\rangle} \right) - \lambda_x \lambda_p \left(\frac{M\Omega}{2\pi} \tau_1^2 \Delta x_0^2 \frac{eV}{M\Omega^2 \langle\langle x^2 \rangle\rangle} \right) \right] \overline{S}_x(\omega)$$

$$- \lambda_x \lambda_p \left(1 - \frac{MeV}{\langle\langle p^2 \rangle\rangle} \right) \frac{\langle\langle p^2 \rangle\rangle}{M} \frac{2(\Omega^2 - \omega^2)}{4\tilde{\gamma}_{\text{tot}}^2 \omega^2 + (\omega^2 - \Omega^2)^2} \tag{9.8}$$

$$\Delta \overline{S}_2(\omega) = \lambda_p^2 \left(1 - \frac{MeV}{\langle\langle p^2 \rangle\rangle} \right) \overline{S}_p(\omega) \tag{9.9}$$

$$+ \left[\lambda_p \lambda_x \left(1 - \frac{\hbar \Omega}{2eV} \frac{\Delta x_0^2}{\langle\langle x^2 \rangle\rangle} \right) - \lambda_p^2 \left(\frac{M\Omega}{2\pi} \tau_1^2 \Delta x_0^2 \frac{eV}{M\Omega^2 \langle\langle x^2 \rangle\rangle} \right) \right]$$

$$\times \frac{2M\Omega^2 \langle\langle x^2 \rangle\rangle (\Omega^2 - \omega^2)}{4\tilde{\gamma}_{\text{tot}}^2 \omega^2 + (\omega^2 - \Omega^2)^2},$$

where the position and the momentum gain are given by

$$\lambda_x = 2e\tau_0 \tau_1 (eV/h) \cos \eta \; , \; \lambda_p = (e/2\pi M)\tau_0 \tau_1 \sin \eta \; , \tag{9.10}$$

respectively. We now discuss several limits of the current noise $\overline{S}_I(\omega)$ of the detector in the case of a general phase η. For $\eta = 0 \bmod \pi$, we recover Eq. (7.89) – the position detector result. More interestingly, for $\eta = \pi/2 \bmod \pi$, $\lambda_x = 0$ and the detector output contains only two terms: The first one is proportional to $S_p(\omega)$ and therefore peaked around Ω. The second one is proportional to $(\Omega^2 - \omega^2)$ and contributes negligibly near resonance $\omega \approx \Omega$. Hence, for $\eta = \pi/2$, we obtain

$$\Delta \overline{S}(\omega \approx \Omega) \approx \lambda_p^2 \left(1 - \frac{MeV}{\langle\langle p^2 \rangle\rangle} \right) \overline{S}_p(\omega). \tag{9.11}$$

Thus, the added noise is directly proportional to the momentum spectrum of the oscillator. This is the key result of this chapter.

From the parameter dependence of each gain, we can estimate that the momentum signal at $\eta = \pi/2$ should be typically smaller than the position signal at $\eta = 0$ by a factor $(eV/\hbar\Omega)^2$. Nevertheless, it is unambiguously possible to identify a p signal in the current noise. We now describe three different ways to do this. First, since $\lambda_x \propto V$ while λ_p is independent of V, the bias voltage dependence of the noise spectrum can also be used to confirm that momentum fluctuations are measured. Secondly, for an oscillator undergoing Brownian motion, the temperature dependence of both signals differs qualitatively. Like in the position detector case, the momentum signal is reduced by a quantum correction (the term proportional to $-MeV/\langle\langle p^2 \rangle\rangle$ in Eq. (9.11)) that arises from the finite commutator of $\hat{x}$ and $\hat{p}$. However, there is a fundamental difference between the x-detector result (Eq. (7) of Ref. [Clerk04b])

and the p-detector result (Eq. (9.11)). In the former case, the quantum corrections are always small compared to the leading terms and therefore the peak at resonance is always positive. In contrast, the two terms in Eq. (9.11) can be of equal magnitude and compete about the sign of $\Delta\overline{S}(\omega \approx \Omega)$. The p-sensitive current noise in Eq. (9.11) changes sign when the effective temperature of the oscillator is equal to $(eV/k_B)(1 - \tilde{\gamma}_+/2\tilde{\gamma}_{\text{tot}})/(1 - \tilde{\gamma}_+/\tilde{\gamma}_{\text{tot}})$. For a cold environment $T_{\text{env}} \ll eV$, $\Delta\overline{S}(\omega)$ is negative at the resonance, whereas, for a hot environment $T_{\text{env}} > eV$, $\Delta S(\omega)$ is positive. This change of sign never appears during a position measurement, so this pronounced difference between a x-dependent and a p-dependent signal can be used distinguish the two. We illustrate the change of sign in the inset of Fig. 9.2, where the added current noise for $\eta = \pi/2$ is plotted for different T_{env}[4].
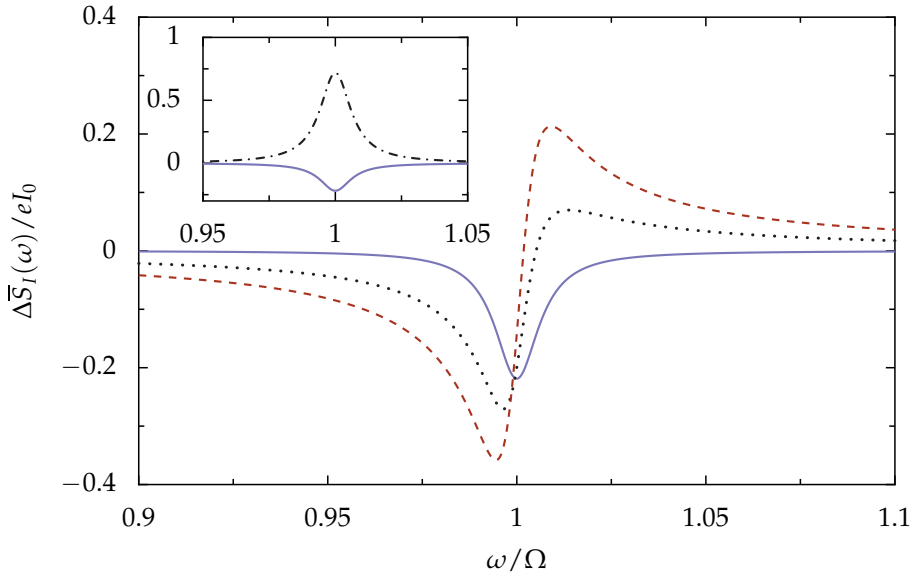
Figure 9.2: Added current noise (normalized by $eI_0 \equiv e^3\tau_0^2 V/h$) of the proposed momentum detector due to the presence of the oscillator. For all curves, the bias is $eV = 50\hbar\Omega$, $\tilde{\gamma}_+ = \tilde{\gamma}_{\text{tot}}/4$ and $\tilde{\gamma}_{\text{tot}} = \Omega/200$. The main panel shows the total detector output for different values of the tunneling phase η and for $T_{\text{env}} = 0$. The (blue) solid, (black) dotted, and (red) dashed lines correspond to $2\eta/\pi = 1, 1.005$, and 1.01, respectively. In the inset, the current noise at the p-sensitive phase $\eta = \pi/2$ is plotted for two different temperatures of the environment $T_{\text{env}} = 0$ (solid line) and $T_{\text{env}} = 5eV/k_B$ (dash-dotted line).

In the main panel of Fig. 9.2, we plot the full detector output for different values

---

[4]The plots are done for an oscillator in the thermal regime: $\langle\langle p^2 \rangle\rangle = Mk_B T_{\text{eff}}$ with $\tilde{\gamma}_{\text{tot}} T_{\text{eff}} = T_{\text{env}}\tilde{\gamma}_0 + \tilde{\gamma}_+(eV/2k_B)$

of η near the optimal operation point for momentum detection. Away from $\eta = \pi/2$, contributions to the current noise $\sim \lambda_x^2$ become important and wash out the momentum signal $\sim \lambda_p^2$. Indeed, for small $\Delta\eta = \eta - \pi/2$, the ratio $\lambda_x/\lambda_p \sim (-\Delta\eta)(eV/\hbar\Omega)$ of the two amplification factors becomes large as soon as $|\Delta\eta| > \hbar\Omega/eV$. In the high-bias regime ($eV \gg \hbar\Omega$), momentum detection therefore requires good experimental control over the applied flux. At moderate bias $eV \geq \hbar\Omega$, the requirement on $\Delta\eta$ becomes less restrictive. Finally, the current noise spectrum at $\eta = \pi/2$ shows a strong symmetry around Ω that makes the optimal operation point easily identifiable.

9.4 Summary

In conclusion, we have shown how a modified tunnel junction position detector can be designed to detect the momentum fluctuations of a NEM oscillator. By using two tunnel junctions in an AB-type setup, it is possible to precisely tailor the interaction Hamiltonian between the detector and the oscillator via an external magnetic field. We have demonstrated how the proposed detector can be made sensitive to either displacement or momentum fluctuations of the oscillator.

Part IV

Nanomechanics with superconducting single-electron transistors

Nanomechanical resonators coupled to superconducting single-electron transistors

In this thesis, we put a strong emphasis [see e.g. Secs. 7.2, 6.1.1] on the idea that the measurement back-action caused by a tunnel junction displacement detector on a nanomechanical oscillator could be understood from the point of view of an effective thermal bath coupled to the resonator. In the weak-coupling regime, this was also shown to hold for a normal-state SET[Blencowe05a]. In both cases, the effective temperature of the thermal bath was of the order of the voltage difference between the two leads, a quantity that is usually very large with respect to both the temperature of the bath and $\hbar\Omega/k_B$, such that the overall effective temperature of the oscillator was *increased* due to the measurement.

In this third part, we will focus on displacement measurement using a *superconducting* SET (SSET) where both the SET leads and the island are superconducting, allowing not only sequential tunneling of quasiparticles through the SET but also the coherent transfer of Cooper pairs. This second transport channel opens the possibility of displacement measurement in new transport regimes, where it is possible to cool the oscillator as well as drive the resonator into a state of self-sustained oscillations. In this chapter, we will first (Sec. 10.1) describe the different transport regimes supported by the SSET. Afterwards, in Secs. 10.2 and 10.3, we will review recent experimental regarding the SSET displacement detector and discuss the theoretical explanation of the features observed in the experiment.

10.1 The superconducting single-electron transistor

As we just mentioned, the SSET is in many ways similar to the SET. In both cases, the mesoscopic detector is composed of two leads tunnel-coupled to a central (small) island. Associated with the small size of the island is a charging energy that needs to be paid to add an electron (or more generally, a charged quasiparticle) to the island. The main difference between the SET and the SSET (where both leads as well as the island are superconducting) is the possibility for Cooper pairs to coherently tunnel (via Josephson tunneling) from one part of the system to the other. The total Hamiltonian describing the SSET can be written as

$$H = H_L + H_R + H_I + H_T + H_C \, . \tag{10.1}$$

The first three terms $H_{L,R,I}$ are standard BCS Hamiltonians and describe two superconducting leads (left and right) and a superconducting island,

$$H_\alpha = \sum_{k,\sigma} \epsilon_{\alpha k \sigma} c_{\alpha k \sigma}^\dagger c_{\alpha k \sigma} \, . \tag{10.2}$$

Here, $c_{\alpha k \sigma}$ are annihilation operators for quasiparticles of momentum k and spin σ in the system α ($\alpha = L, R, I$). The dispersion relation $\epsilon_{\alpha k \sigma}$ accounts for the superconducting gap of width 2Δ which we assume to be equal for the three systems. The chemical potentials in the left and right leads are determined by the applied bias voltage $V = V_L - V_R$, while the island chemical potential can be tuned by applying a gate voltage V_G.

The left and right leads are connected to the central island by quasiparticle tunneling and Cooper pair tunneling. Denoting by ϕ_α the superconducting phase difference at the junction $\alpha = L, R$, the quasiparticle tunneling term takes the form

$$H_{T,qp} = \sum_{\alpha=L,R} e^{-i\phi_\alpha} \sum_{k,q,\sigma} T_{kq} c_{\alpha k \sigma}^\dagger c_{Iq\sigma} + \text{h.c.} \, , \tag{10.3}$$

where T_{kq} are the tunneling amplitudes which can be used to calculate[Choi01] the quasiparticle tunneling rates $\Gamma_{L,R}$. Cooper pair tunneling is accounted for by the term

$$H_{T,CP} = - \sum_{\alpha=L,R} J_\alpha \cos \phi_\alpha \, , \tag{10.4}$$

where J_α are the Josephson energies of the two junctions. Hence, the total tunneling Hamiltonian is given by $H_T = H_{T,qp} + H_{T,CP}$.

The final ingredient for the SSET Hamiltonian is the Coulomb energy of the island. If we denote by n_L and n_R the number of electrons that have tunneled from the island to the left and right lead, respectively, then $n = -n_L - n_R$ is the excess number of electrons on the island. Then, the charging term can be written as

$$H_C = E_C (n + n_0)^2 + eV n_R \, , \tag{10.5}$$
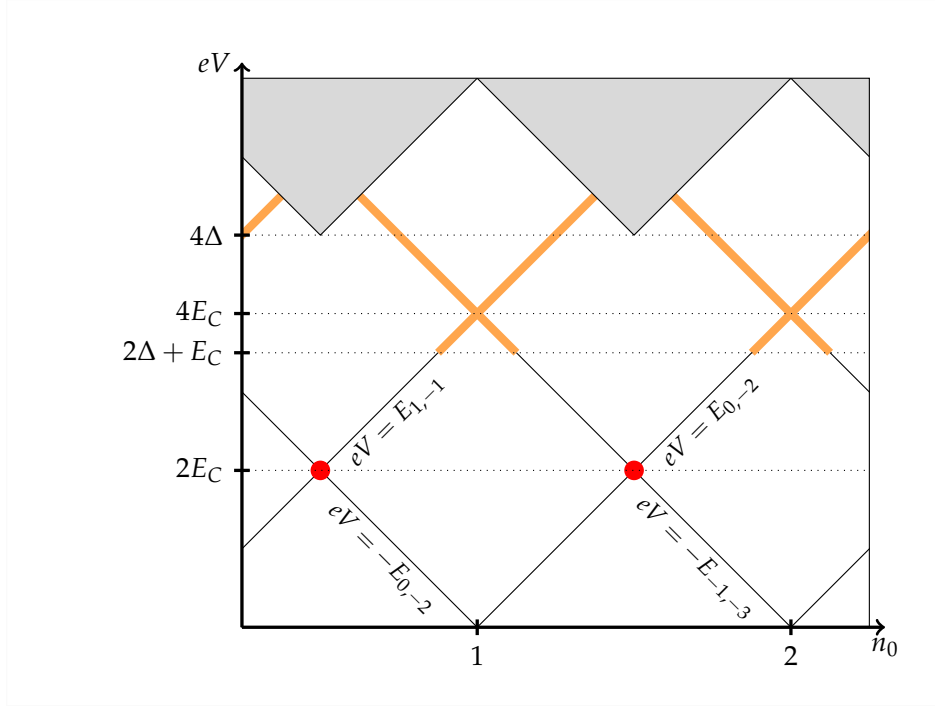
Figure 10.1: The different transport regimes of the SSET. For $eV > 4\Delta$, the bias voltage is high enough to break the Cooper-pairs into quasiparticles, and the system behaves as a normal state SET where quasiparticles are transported instead of electrons, leading to the appearance of Coulomb diamonds (grey). For $4\Delta > eV > 2\Delta + E_C$, transport is only allowed via the Josephson quasiparticle cycle (JQP), along resonance lines in the $V - V_g$ plane(orange). At lower voltages, transport happens only around resonance points(red) in the $V - V_g$ plane via the double Josephson quasiparticle cycle (DJQP). For a description of the different transport cycles, see text.

where E_C is the charging energy and n_0 can be controlled by the gate voltage. In terms of the capacitances of the two junctions $C_{L,R}$, the gate C_G and the resonator C_N, the charging energy is given by $E_C = e^2/(2C_\Sigma)$, where $C_\Sigma = C_L + C_R + C_G + C_N$ is the total capacitance. While the capacitances, Josephson energies and quasiparticle tunneling rates are essentially determined by the experimental setup, the most important tunable parameters are the bias voltage V and the gate voltage V_G. The transport properties of the SSET are then determined by how these voltages are related to the superconducting gap 2Δ and the charging energy E_C. In Fig. 10.1 we schematically present the different transport regimes that are supported by the SSET.

For high bias voltages $eV > 4\Delta$, the difference in chemical potentials allows quasi-

particles on both junctions to overcome the superconducting gap[1] and a quasiparticle current can flow. But even for lower bias voltages, one observes a finite current at certain values of the gate voltage. A possible mechanism is the Josephson-quasiparticle (JQP) resonance [Fig. 10.2] which is a cyclic process that starts with the tunneling of a Cooper pair on one of the junctions followed by two subsequent quasiparticle tunneling events on the other junction [Averin89; vandenBrink91; Nakamura96]. This process is possible for voltages where $eV > 2\Delta + E_C$.

For even lower bias voltages, isolated current resonances can be observed which are due to the onset of the double Josephson quasiparticle (DJQP) resonance. A schematic picture of this process is shown in Fig. 10.2. It starts with a Cooper pair tunneling across, say, the left junction. Next, a quasiparticle tunnels out through the right junction, followed by a Cooper pair. Finally, after a quasiparticle tunnels through the left junction, the initial system state is reached again. This process is energetically allowed only in a restricted parameter regime: Cooper pair tunneling is only possible if the chemical potentials of the lead and the island (taking into account the Coulomb energy) are on resonance while quasiparticle tunneling requires a difference in chemical potentials sufficient to overcome the superconducting gap. For the DJQP process, it is easy to show that the resonances occur at bias voltages $eV = 2E_C$ and half-integer island charges n_0.

In the following, we will focus our attention mainly on the properties of the SSET biased close this last type of resonance. The parameter regime which we investigate is therefore characterized by a charging energy E_C, a superconducting gap 2Δ and a bias voltage V which are of the same order of magnitude. Roughly speaking, these energy scales are very large compared to the quasiparticle tunneling rates $\Gamma_{L,R}$, the Josephson energies $J_{L,R}$ and the oscillator energy Ω.

10.1.1 Quantum measurement with a SSET

Since we ultimately want to use the SSET as a measurement device, we now take the time to discuss the measurement efficiency of this detector. Like for the normal-state SET, to use the SSET as a detector one typically couples it capacitively to the quantum system, leading to an interaction Hamiltonian $H_{\text{int}} = -A\hat{F}\,\hat{x}$, where in this case $\hat{F} \leftrightarrow \hat{n}$ is the operator associated with number of charges on the island and $\hat{x}$ is the operator of the quantum system to be measured[Koerting08, Appendix A]. The back-action force on the measured system will therefore be caused by the charge fluctuations on the island, and the state of the system can be probed by looking at the current through

---

[1] An energy of 2Δ is required to break a Cooper-pair into two quasiparticles, and, since we consider symmetric junctions, the potential difference between one lead and the island is only one half of the total applied bias voltage.

The Josephson QP resonance (JQP)

The double Josephson QP resonance (DJQP)
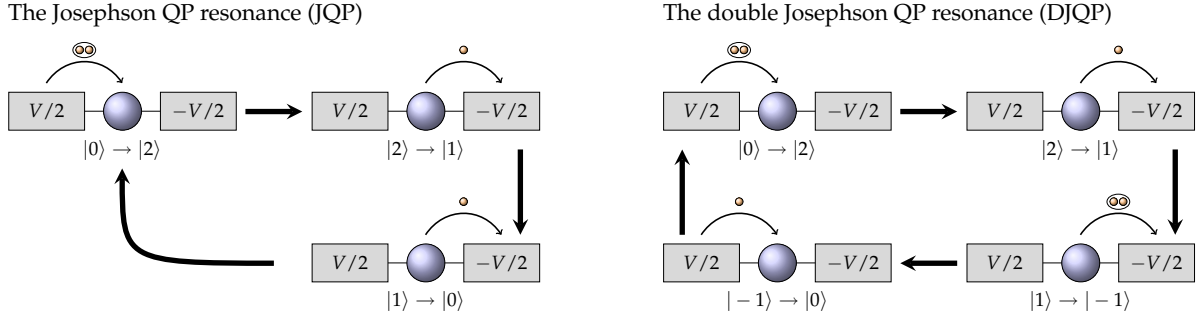
Figure 10.2: Left) The JQP cycle: (i) Cooper pair tunneling through the left junction, (ii) quasiparticle tunneling through the right junction, and (iii) quasiparticle tunneling through the right junction. Right) The DJQP cycle: (i) Cooper pair tunneling through the left junction, (ii) quasiparticle tunneling through the right junction, (iii) Cooper pair tunneling through the right junction and (iv) quasiparticle tunneling through the left junction.

the SSET.

In Sec. 4.2, we explained that the normal-state SET in the sequential tunneling regime is not a quantum-limited detector (i.e., it does not fulfill Eq. (4.22).). Due to the high similarity between the sequential-tunneling regime for a SET and the transport in the high bias ($eV > 4\Delta$) region, we also expect the SSET not to be a quantum-limited detector in this regime.

The situation is however quite different when the SSET is biased near one of the transport resonances depicted in Fig. 10.2. In this case, the measurement efficiency $\mathcal{N}$ [Eq. (6.57)] is (for symmetric junctions) a function of the Josephson energy (J) of the junctions over the quasiparticle tunneling rate(Γ) [Clerk02; Clerk05]. For $J/h\Gamma \sim 1$, the measurement efficiency is $\mathcal{N} \sim 0.5$ for both the JQP and the DJQP: the measurement efficiency close to these resonance is therefore much higher than in the quasiparticle tunneling regime. Physically, this can be traced back to the coherent nature of the Cooper pair tunneling. Finally, comparing both transport regimes, one finds[2] that the *optimal* measurement efficiency is higher for the DJQP, but that for $J \ll \Gamma$, where experiments are more easily carried out, then $\mathcal{N}$ is higher for the JQP.

10.2 Displacement measurement with SSETs: Experimental realizations

Combined with the typically large gain associated with JQP/DJQP transport regimes, the high measurement efficiency of the SSET close to these resonances motivated ex-

---

[2]See e.g. [Clerk05, Fig. 10], where a quantity $\sim \mathcal{N}^{-1}$ is plotted.

perimentalists to actually carry out experiments where a nanomechanical resonator is coupled to a superconducting SET. The first of these experiments was done in the Schwab group in 2004[LaHaye04]. They built a $\sim 8\mu$m long, 110 nm wide by 120 nm thick SiN resonator weighting $M = 9.7 \times 10^{-16}$kg in close proximity (600 nm) to a SSET. They studied a resonant mode around 19.7 MHz characterized by a high quality factor ($Q = \Omega/\gamma \sim 50000$ at 30 mK) by looking at the response of the SSET when it was biased to near the DJQP. As explained in Sec. 2.2, in this experiment the effective coupling could also be controlled by varying the voltage difference between the resonator and the island. At the resonance, the authors measured an optimal displacement sensitivity $\sqrt{\overline{S}_{x,\text{add}}} = 3.8\text{fm}/\sqrt{\text{Hz}}$. This is roughly 5 times higher than the quantum-limited value $\overline{S}_{x,eq}(\Omega, T = 0)$ [Eq. (6.24)]. In this case, the measurement was shot-noise limited, as the authors reported not seeing the signature of measurement back-action in the response of the oscillator. This means that in principle the sensitivity of the measurement could have been improved by increasing the coupling voltage on the resonator. On this device estimates show that the back-action dominated regime would have been reached for coupling voltages higher $V_{NR} = 27V$, but the authors kept the voltage $V_{NR} \leq 13V$ in order to keep the device safe from electrical breakdown.

Two years later, the same group presented a second generation device where back-action effects could be observed[Naik06b]. In this second experiment, they used a resonator of similar shape (10μm $\times$ 100nm $\times$ 100nm), resonance frequency $\Omega = 2\pi \times 22$MHz and slightly higher quality factor ($Q \sim 1.2 \times 10^5$) than in the previous experiment. The main improvement in this second experiment was that the resonator's equilibrium position was brought closer to the island of the SSET. The shape of the island was also optimized in order to maximize the capacitive coupling between the resonator and the SSET. Since for this device $J \sim \Gamma/4$, the SSET was biased in the vicinity of the JQP resonance for maximum measurement efficiency. Using this device, the authors observed directly the effect of the detector back-action on the device: they even used back-action to cool the resonator from 500 mK to 200mK. This is possible because, as will be discussed in the next section, the effective temperature associated with the SSET near the JQP/DJQP resonances can be made vanishingly small. For this device, the authors measured $\sqrt{\overline{S}_I \overline{S}_F/\lambda^2} = 15\hbar/2$ whereas for a perfect quantum-limited detector one would find $\sqrt{\overline{S}_I \overline{S}_F/\lambda^2} = \hbar/2$ [Eq. (4.22)]. This imposes a limit on the position measurement sensitivity of $\sqrt{15} \sim 4$ times the quantum limit [Eq. (6.22)].

10.3 Theoretical description of the system at the DJQP resonance

While none of two experiments presented in the last section reached the quantum limit on the added position noise, they nevertheless proved that the SSET is an extremely good position detector. The article of Naik *et al.* also contained very interesting results regarding the dependence of the back-action effects on the biasing point of the SSET. They found a totally different behavior of the resonator depending on the side of the JQP resonance where the system was biased. In this section, we will describe how this observation can be explained, at least on a qualitative level. Specifically, we will use a linear-response calculation to derive what happens when the SSET is biased near the DJQP. However, we stress that the behavior of the system around both resonances is qualitatively similar, such that the main conclusions we reach from studying the DJQP are also valid at the JQP[3].

10.3.1 Quantum noise approach: Calculation of the charge noise spectrum

Maybe the easiest way to get a general understanding of the measurement back-action of the SSET on the mechanical oscillator is to use the 'quantum noise' approach (Secs. 6.1, 7.2) to estimate the properties (γ, T_{eff}) of the effective environment associated with the charge-fluctuations on the superconducting island, $S_F(\omega)$. As mentioned earlier, in this system the interaction Hamiltonian can be written [Koerting08, Appendix A]

$$H_{\text{int}} = -A\hat{n}\hat{x} = -A\hat{F}\,\hat{x}\,, \tag{10.6}$$

with the charge state of the superconducting island playing the role of the "input" parameter of the detector. This means that the effective damping rate γ and the effective temperature T_{eff}, usually given by [Eq. (6.7), (6.6)]

$$A^2\gamma(\omega) = A^2\frac{1}{2M\hbar\omega}\left[S_F(\omega) - S_F(-\omega)\right]\,, \tag{10.7}$$

$$\overline{S}_F(\omega) = M\gamma(\omega)\hbar\omega\coth\left(\frac{\hbar\omega}{2k_B T_{\text{eff}}(\omega)}\right)\,. \tag{10.8}$$

are directly related to the charge noise on the SSET island. Again, we recall that the amazing thing about the quantum noise approach is that both γ and T_{eff} depend *solely*

---

[3]Due to its relative simplicity, the problem of a nanomechanical oscillator coupled to a SSET near JQP was more thoroughly studied in the literature [Blencowe05b; Clerk05; Rodrigues07b; Rodrigues07a; Harvey08] than the DJQP, who was discussed in the general context of NEMS in [Clerk05] and only shortly investigated in [Blencowe05b]

on the detector, since the correlation function $S_F(\omega)$ is evaluated in the $A = 0$ limit. The only relevant parameter of the oscillator in this case is its frequency Ω, since the effective environment must be calculated using the back-action force noise power at $\omega = \Omega$.

To proceed, we first look at the evolution of the density matrix describing the SSET. We denote ρ the full (system+bath) density matrix. In the limit we consider the charging energy is high and it is convenient to express the reduced density matrix of the island in term of charge states, defining $\rho_{i,j} = \langle i|\text{Tr}_B[\rho]|j\rangle$. Since only Josephson coupling leads to a coherence between two charge states, we can reduce the problem size by keeping only off-diagonal elements that correspond to charge states involved in Josephson tunneling, i.e. explicitly set all elements $\rho_{i,j}$ to 0 when $|i - j| \neq 2$. Writing the non-zero density matrix elements in vector form[4]

$$|\boldsymbol{\rho}\rangle = \begin{pmatrix} \rho_{-1,-1} & \rho_{1,1} & \rho_{1,-1} & \rho_{-1,1} & \rho_{2,2} & \rho_{2,0} & \rho_{0,2} \end{pmatrix}^T , \qquad (10.9)$$

one can write the equation of motion [Chap. 7] of these non-zero elements as[Koerting08]

$$\frac{d}{dt}|\boldsymbol{\rho}\rangle = -\mathbf{M}|\boldsymbol{\rho}\rangle + iJ_L|\mathbf{c}\rangle/2 , \qquad (10.10)$$

where $\mathbf{c} = (0,0,0,0,0,1,-1)^T$ and the evolution matrix $\mathbf{M}$ is given by

$$\mathbf{M} = \begin{pmatrix} \Gamma_L & 0 & -iJ_R/2 & iJ_R/2 & 0 & 0 & 0 \\ 0 & 0 & iJ_R/2 & -iJ_R/2 & -\Gamma_R & 0 & 0 \\ -iJ_R/2 & iJ_R/2 & \Gamma_L/2 + i\epsilon_{1,-1} & 0 & 0 & 0 & 0 \\ iJ_R/2 & -iJ_R/2 & 0 & \Gamma_L/2 - i\epsilon_{1,-1} & 0 & 0 & 0 \\ 0 & 0 & 0 & 0 & \Gamma_R & iJ_L/2 & -iJ_L/2 \\ iJ_L/2 & iJ_L/2 & 0 & 0 & iJ_L & \Gamma_R/2 + i\epsilon_{20} & 0 \\ -iJ_L/2 & -iJ_L/2 & 0 & 0 & -iJ_L & 0 & \Gamma_R/2 - i\epsilon_{20} \end{pmatrix} . \qquad (10.11)$$

Here, ϵ_{ij} is the difference in energy between states with i and j charges on the island. In terms of the average number of electrons on the island n_0 and the bias voltage eV, these are given by

$$\epsilon_{1,-1} = 4E_C n_0 + eV , \qquad (10.12)$$
$$\epsilon_{2,0} = 4E_C(n_0 + 1) - eV . \qquad (10.13)$$

In passing, we note that Eq. (10.10) allows for a simple calculation of the stationary density matrix of the island. Using $\dot{\boldsymbol{\rho}}_{\text{stat}} = 0$, this equation gives directly

$$|\boldsymbol{\rho}_{\text{stat}}\rangle = iJ_L\mathbf{M}^{-1}|\mathbf{c}\rangle/2 . \qquad (10.14)$$

---

[4]We used the trace condition on the density matrix ($\text{Tr}_n\text{Tr}_B\rho = 1$) to reduce the size of the system of equations, removing the equation for $\rho_{0,0}$.

This generalizes to non-symmetric junctions ($J_L \neq J_R$, $\Gamma_L \neq \Gamma_R$) previous results [Clerk03a].

To calculate the charge noise in the DJQP we need to evaluate the expression

$$S_n(\omega) = \int_{-\infty}^{\infty} dt\, e^{i\omega t} \langle\langle n(t)n(0)\rangle\rangle \,, \tag{10.15}$$

$$= \int_0^{\infty} dt\, \cos(\omega t)\Big(\langle\langle n(t)n(0)\rangle\rangle + \langle\langle n(-t)n(0)\rangle\rangle\Big)$$
$$+ i \int_0^{\infty} dt\, \sin(\omega t)\Big(\langle\langle n(t)n(0)\rangle\rangle - \langle\langle n(-t)n(0)\rangle\rangle\Big) \,. \tag{10.16}$$

Following the approach used in [Choi03] for the JQP, we introduce two functions

$$\chi(t) = \mathrm{Tr}_B[e^{-iHt/\hbar} n\rho e^{iHt/\hbar}] \,, \tag{10.17}$$

$$\eta(t) = \mathrm{Tr}_B[e^{-iHt/\hbar} \rho n e^{iHt/\hbar}] \,, \tag{10.18}$$

which have the properties $\langle\langle n(t)n(0)\rangle\rangle = \mathrm{Tr}_n[n\chi(t)] - \langle n\rangle^2$ and $\langle\langle n(-t)n(0)\rangle\rangle = \mathrm{Tr}_n[n\eta(t)] - \langle n\rangle^2$. Arranging χ, η in the same vector form as ρ (i.e. following Eq. (10.9)), we can show that these functions fulfill the same differential equation as ρ

$$\frac{d}{dt}|\chi\rangle = -\mathbf{M}|\chi\rangle + iJ_L\langle n\rangle|c\rangle/2 \,, \tag{10.19}$$

$$\frac{d}{dt}|\eta\rangle = -\mathbf{M}|\eta\rangle + iJ_L\langle n\rangle|c\rangle/2 \,, \tag{10.20}$$

with different initial conditions[5]

$$|\chi(0)\rangle = \mathrm{Tr}_B[n\rho] = (\mathbf{K}_+ + \mathbf{K}_-)|\rho\rangle \,, \tag{10.21}$$

$$|\eta(0)\rangle = \mathrm{Tr}_B[\rho n] = (\mathbf{K}_+ - \mathbf{K}_-)|\rho\rangle \,, \tag{10.22}$$

---

[5]We stress that $\mathrm{Tr}_B[n\rho] \neq \mathrm{Tr}_B[\rho n]$, since cyclic invariance of the trace applies only for the *complete* trace: $\mathrm{Tr}_n\mathrm{Tr}_B[n\rho] = \mathrm{Tr}_n\mathrm{Tr}_B[\rho n]$.

where $\mathbf{K}_\pm$ are the diagonal coupling matrices

$$\mathbf{K}_+ = \begin{pmatrix} -1 & . & . & . & . & . & . \\ . & 1 & . & . & . & . & . \\ . & . & 0 & . & . & . & . \\ . & . & . & 0 & . & . & . \\ . & . & . & . & 2 & . & . \\ . & . & . & . & . & 1 & . \\ . & . & . & . & . & . & 1 \end{pmatrix}, \qquad (10.23)$$

$$\mathbf{K}_- = \begin{pmatrix} 0 & . & . & . & . & . & . \\ . & 0 & . & . & . & . & . \\ . & . & 1 & . & . & . & . \\ . & . & . & -1 & . & . & . \\ . & . & . & . & 0 & . & . \\ . & . & . & . & . & 1 & . \\ . & . & . & . & . & . & -1 \end{pmatrix}. \qquad (10.24)$$

We find

$$\langle\langle n(t)n(0)\rangle\rangle + \langle\langle n(-t)n(0)\rangle\rangle = 2\langle n|e^{-\mathbf{M}t}\,(\mathbf{K}_+ - \langle n\rangle)\,|\boldsymbol{\rho}\rangle\,, \qquad (10.25)$$

$$\langle\langle n(t)n(0)\rangle\rangle - \langle\langle n(-t)n(0)\rangle\rangle = 2\langle n|e^{-\mathbf{M}t}\mathbf{K}_-|\boldsymbol{\rho}\rangle\,. \qquad (10.26)$$

with $\langle n| = (-1, 1, 0, 0, 2, 0, 0)$ the representation of the charge operator in the vector form used to rewrite $\boldsymbol{\rho}$. Inserted in Eq. (10.16), these lead to

$$S_n(\omega) = 2\langle n|\frac{\mathbf{M}}{(\omega/\Omega)^2 + \mathbf{M}^2}\,(\mathbf{K}_+ - \langle n\rangle)\,|\boldsymbol{\rho}\rangle + 2i\langle n|\frac{(\omega/\Omega)}{(\omega/\Omega)^2 + \mathbf{M}^2}\mathbf{K}_-|\boldsymbol{\rho}\rangle\,, \quad (10.27)$$

That's the final expression for the frequency-dependent charge noise spectrum.

10.3.2 Quantum noise approach: Results

In the quantum noise approach, Eq. (10.27) contains all the information required to evaluate the influence of the detector on the resonator. In Figs. 10.3-10.4, we plot respectively the antisymmetric and the symmetric part of the noise near the DJQP. Recalling that the resonance condition for the DJQP is fulfilled for a bias voltage $eV = 2E_C$ and half-integer island charges n_0, we conveniently rewrote the ϵ_{ij}'s in term of the difference in bias and effective gate voltage with the resonance point

$$\Delta eV = \frac{\epsilon_{1,-1} - \epsilon_{2,0}}{2}\,, \qquad (10.28\text{a})$$

$$4\frac{C_G}{C_\Sigma}\Delta eV_g = \frac{\epsilon_{1,-1} + \epsilon_{2,0}}{2}\,. \qquad (10.28\text{b})$$
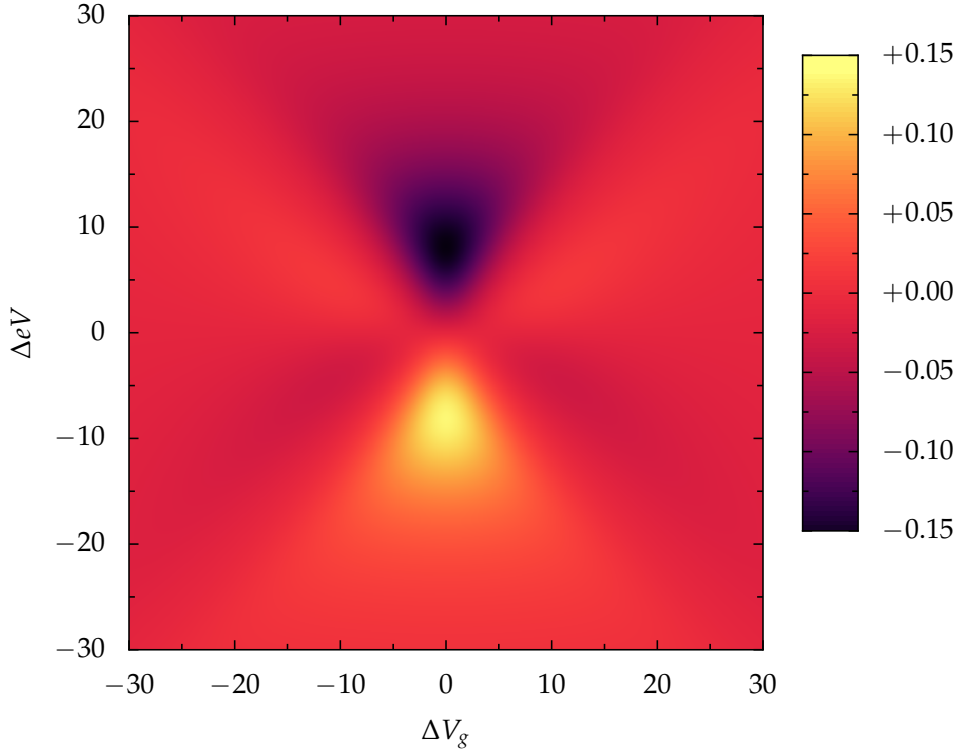
Figure 10.3: The anti-symmetric part of the back-action (charge) noise $S_F(\omega) - S_F(-\omega)$, in units of Ω^{-1}, as a function of the two detunings from the resonance defined Eq. 10.28. The detunings are given in units of $\hbar\Omega$. $\Gamma_L = \Gamma_R = 10\Omega$, $J_L = J_R = 5\hbar\Omega$

Both quantities are zero exactly at the resonance, and in the remainder of this text we set $4C_G = C_\Sigma$ for simplicity.

Let's first look at $S_F(\omega) - S_F(\omega)$, a quantity directly proportional damping rate. Very interestingly, the effective damping rate is *anti-symmetric* with respect to the $\Delta eV = 0$ line. This means that there is a regime of *negative damping* in which the interaction with SSET brings a term $+|\gamma|\langle p\rangle$ to the equation for $\dot{p}$: energy is pumped into the mechanical system by the SSET. Physically, this can be traced back to the resonant character of transport near the DJQP: transport is only allowed for specific points in the $eV - V_g$ plane. When the bias voltage is slightly higher than $eV = 2E_c$, the DJQP cycle is still allowed provided the extra energy ΔeV is transfered from the electronic to the mechanical system. Oppositely, for $eV < 2E_C$, the cycle extracts energy from the oscillator. The situation is similar when the SSET is biased near the JQP resonance [Blencowe05b; Clerk05].

To analyze the impact of the possibility of negative damping, we look at the total
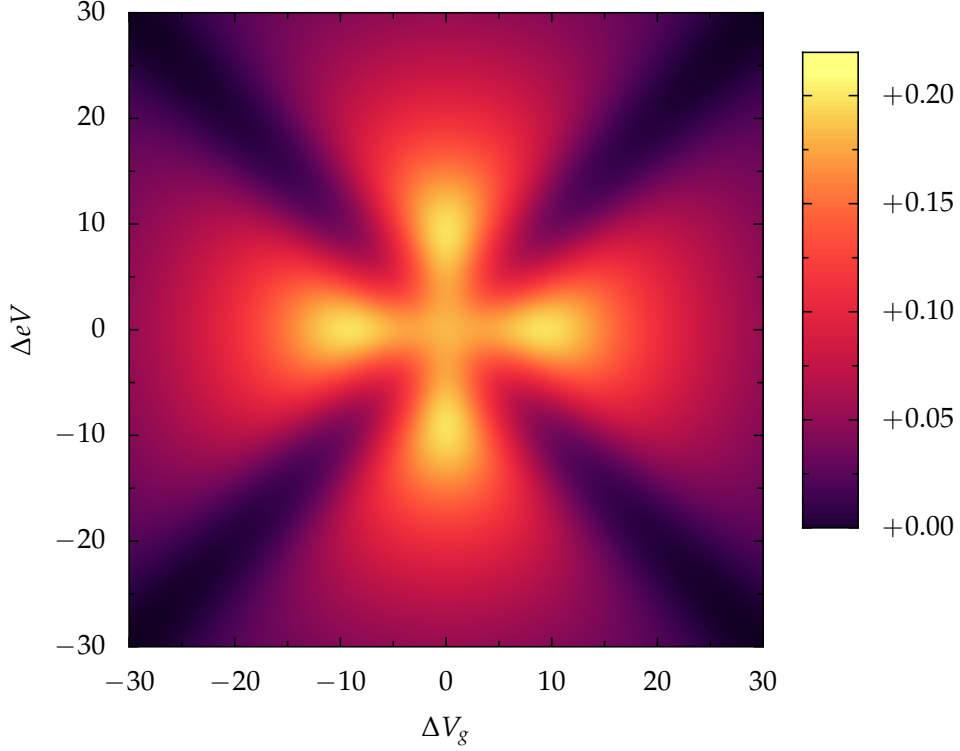
Figure 10.4: The symmetric part of the back-action (charge) noise $\overline{S}_F(\omega) = [S_F(\omega) + S_F(-\omega)]/2$, in units of Ω^{-1}, as a function of the two detunings from the resonance defined Eq. 10.28. The detunings are given in units of $\hbar\Omega$. $\Gamma_L = \Gamma_R = 10\Omega$, $J_L = J_R = 5\hbar\Omega$

effective environment [Eq. (6.10)] of the oscillator,

$$T_{\text{tot}} = \frac{A^2 \overline{S}_F(\omega) + \gamma_0 T_0}{\gamma_{\text{tot}}} \, , \tag{10.29a}$$

$$\gamma_{\text{tot}} = A^2 \gamma + \gamma_0 \, , \tag{10.29b}$$

In this expression, we used the high-temperature form of $\gamma T_{\text{eff}} \sim \overline{S}_F$ to simplify the upcoming discussion. The numerator of the total effective temperature of the oscillator is always positive (as seen from Fig. 10.4, $\overline{S}_F(\Omega)$ is positive in the whole $\Delta V_g - \Delta eV$ plane). To better understand the system, three regimes need to be investigated: (i) $A^2 \gamma > 0$, (ii) $-\gamma_0 < A^2 \gamma < 0$ and (iii) $A^2 \gamma < -\gamma_0 < 0$.

The first regime corresponds to the one we have been investigating in previous parts of the thesis, where the detector acts as a 'normal' thermal bath. However, this does not make this regime uninteresting: contrary to the tunnel junction case, the back-action spectral density does not scale with eV (which typically is very large in front of $\hbar\Omega$) but it is a function of the distance to the DJQP resonance in the $eV - V_G$

plane. In certain cases, one finds $T_{\text{eff}} < T_0$, such that the total temperature of the oscillator

$$T_{\text{tot}} = \frac{\gamma T_{\text{eff}} + \gamma_0 T_0}{\gamma_{\text{tot}}} < \frac{\gamma T_0 + \gamma_0 T_0}{\gamma_{\text{tot}}} = T_0 \,, \tag{10.30}$$

can be smaller than the environment temperature T_0. In this regime, measurement back-action can therefore be used to cool the oscillator. This was experimentally demonstrated in [Naik06b].

In the second regime, the detector-induced damping is negative, but of lower magnitude than the intrinsic damping associated with the physical environment. The total damping rate of the oscillator is reduced from its uncoupled value and one therefore expects e.g. the width of the resonance in $S_x(\omega)$ to be reduced. Since in this case both the numerator and denominator of Eq. (10.29a) stay positive, we expect the effective thermal environment model to hold: the coupling of the oscillator to the thermal bath is strong enough to allow the extra energy transfered from the electronic system to the mechanical system to be dissipated in the environment.

In the third case, the negative damping caused by the interaction with the detector more than completely compensates the damping associated with the finite quality factor of the mechanical oscillator. The total temperature in this case [Eq (10.29a)] becomes *negative*, suggesting a breakdown of the effective thermal bath model. This is not completely surprising since the linear-response approach is valid only as long as the SSET itself is not affected by the oscillator (all the averages are taken in the $A = 0$ limit). In the negative damping regime, the high amplitude of the mechanical oscillations affects the biasing point of the SSET, rendering the linear-response calculation invalid. The study of the system in this regime requires a different theoretical approach (see Sec. 10.3.3). In all cases, one finds that in this regime the stationary state of the oscillator is highly non-thermal: instead, the system is driven to a state of self-sustained oscillation[Rodrigues07b].

Taken together, these three regimes allow for a qualitative understanding of the experimental results presented in [Naik06b]. Sadly, a quantitative comparison of the effective damping $A^2\gamma$ measured and calculated shows that the calculation underestimates this quantity by about an order of magnitude. The cause of this disagreement is still an open issue.

10.3.3 Theoretical description in the driven regime

Even if the linear-response approach fails in the $A^2\gamma < -\gamma_0$ regime, there a many ways one can still gain insight about the behavior of the system in this regime. To proceed analytically, one can derive an effective theory with position-dependent damping [Clerk05; Bennett06]. A fully numerical approach like the one described in detail

in the next chapter can also be used[Rodrigues07b; Harvey08; Koerting08]. Yet another possibility is to use mean-field master equations [Blencowe05b; Rodrigues07b; Harvey08; Koerting08].

Historically, the motivation behind the numerical investigation of the system near the DJQP presented in the next chapter was to complement a study realized using such a mean-field master equation. Hence, we will shortly explain the idea behind this method. The mean-field master equation approach is in many way similar to the method used in Sec. 3.2 to derive the transport properties of the SET coupled to an oscillator in the weak-coupling regime. Here however, one uses the equation of motion for the density matrix (and not for the classical probability distribution like in Chap. 3) to write out a system of coupled differential equations for quantities of the form $\langle \rho_{i,j} x^n p^m(t) \rangle$. The name "mean-field" comes from the fact that we study how *expectation values* evolve. Unfortunately, unlike for the SET case, when considering the SSET biased near a transport (JQP/DJQP) resonance, the system of equations generated does not naturally close. For example, the equation of motion for $\langle x^n \rangle$ involves $\langle x^{n+1} \rangle$. To obtain a finite system, the hierarchy *must* be truncated at some order. This is done by explicitly setting the n-th order cumulant of operator expectation values to zero. For example, a truncation to 'third order' corresponds to replacing quantities of the form $\langle abc \rangle$ by $\langle a \rangle \langle bc \rangle + \langle b \rangle \langle ac \rangle + \langle c \rangle \langle ab \rangle - 2 \langle a \rangle \langle b \rangle \langle c \rangle$, taking care to symmetrize the expectation values properly, making sure that commutation relations are not violated by the truncation[Harvey08].

In practice, this technique is limited by the fact that the size of the system of differential equations that must be solved grows very rapidly with the truncation order. Naturally, when one expects a *thermal* state, a gaussian approximation where higher-than-second order cumulants of different operators makes sense, as we know that for example $\langle\langle x^2 \rangle\rangle = 0$. However, when the system enters a driven state, the applicability of such a second-order truncation is more questionable; in this case the truncation at low orders is more or less an uncontrolled approximation. Moreover, it is then difficult to evaluate the accuracy of the results obtained using these methods, with one of the only way to estimate the validity of the approximation being to solve the system at even higher truncation orders. This is one of the main reasons why such "mean-field" approaches are often combined with numerical studies like the one presented in the next chapter[Armour04b; Harvey08; Koerting08].

Dynamics of a harmonic oscillator coupled to a SSET: A numerical solution of the Liouville equation

As seen before, the coupled dynamics of a SSET biased near one transport resonance and coupled to a nanomechanical resonator is highly non-trivial, and in certain parameter regimes one expects the linear-response approach to fail. Like in the case of the normal-state SET coupled to a classical harmonic oscillator, the numerical computation of the properties of the coupled mesoscopic detector - mechanical system can prove very useful in this case. In this chapter, we use an numerical approach to the solution of the Liouville equation of a coupled harmonic oscillator - SSET system. We first (Sec. 11.1-11.3.3) present the details of the method, then in Sec. 11.4 give the explicit form of the Liouville operator in the case where we consider a SSET biased near the DJQP, before presenting (Sec. 11.5) typical numerical results. Finally, the details of the numerical implementation are given in Sec. 11.7.

11.1   The Liouville equation

In Chap. 7, the equation of motion for the density matrix of an open quantum system (a quantum system coupled to an environment) was derived directly from the von Neumann equation [Eq. (7.2)]. In general, the equation obtained this way contains

term with operators present on both the left and the right of the density matrix

$$\frac{d}{dt}\rho(t) = \sum_i \left(\hat{A}_i\rho(t) + \rho(t)\hat{B}_i\right) + \sum_{i,j} \left(\hat{C}_i\rho(t)\hat{D}_j\right),$$ (11.1)

with the $\hat{A}_i, \hat{B}_i, \hat{C}_i, \hat{D}_i$'s quantum mechanical operators have a representation in a Hilbert space. This same equation can be rewritten by introducing the Liouville superoperator $\mathcal{L}$ governing the evolution of the density matrix

$$\frac{d}{dt}\rho(t) = \mathcal{L}\rho(t),$$ (11.2)

Comparing Eqs. (11.1-11.2), we realize that the superoperator $\mathcal{L}$ is a two-sided operator, acting both on the left and right side of the density matrix. It is common to write the total Liouvillian as a sum of independent contributions associated with i) the coherent evolution of the system and ii) the dissipative contributions due to the bath(s) the open system is coupled to. In the case of a nanomechanical oscillator coupled to a SSET, the complete Liouvillian can be written as [Rodrigues07a]

$$\mathcal{L} = \mathcal{L}_{co} + \mathcal{L}_{qp} + \mathcal{L}_{cl},$$ (11.3)

where $\mathcal{L}_{co}$ refers to the coherent (Hamiltonian) evolution, $\mathcal{L}_{qp}$ refers to the dissipative part of the Liouvillian associated with quasiparticle tunneling and $\mathcal{L}_{cl}$ to the coupling of the nanomechanical oscillator to the environment, modeled via Caldeira-Leggett type dissipation and diffusion terms (as discussed in Appendix B).

The form of Eq. (11.2) proposes that the problem of finding the steady-state density matrix of the problem (defined as $\dot{\rho}_{stat} = 0$) is akin to a finding the null-space of $\mathcal{L}$, or, in other words, that the steady-state density matrix can be seen as the right eigenvector of the Liouvillian associated with the eigenvalue 0. This is in fact the case, although some subtleties must be addressed first.

11.1.1 The Liouville space

The Liouvillian, being a *two-sided* operator, does not have the usual matrix-representation of an operator in Hilbert space. Matrix algebra can however be used to construct an operator that has a single-sided matrix representation in *Liouville space*. The transformation between the usual Hilbert space representation and the Liouville space representation is done by 'vectorizing' the Hilbert space operators and then using the following identity,

$$\text{vec}(\mathbf{ABC}) = (\mathbf{C}^T \otimes \mathbf{A})\text{vec}(\mathbf{B}),$$ (11.4)

valid for general **A,B,C** matrices (see e.g. [Minka00; Loan00] for a review and related identities). In the last equation, we introduced the vec-form of a matrix, where the columns of a $M \times N$ matrix are stacked one-after each other to form a $MN \times 1$ vector:

$$\text{vec}(\begin{bmatrix} a_{11} & a_{12} & a_{13} \\ a_{21} & a_{22} & a_{23} \end{bmatrix}) = \begin{bmatrix} a_{11} \\ a_{21} \\ a_{12} \\ a_{22} \\ a_{13} \\ a_{23} \end{bmatrix} \tag{11.5}$$

In Eq. (11.4), the symbol $\otimes$ denotes the Kronecker product, a special case of tensor product. For a $M \times N$ matrix **A** and a $P \times Q$ matrix **B**, the Kronecker product forms $\mathbf{A} \otimes \mathbf{B}$, a $MP \times NQ$ block matrix[1]:

$$A \otimes B = \begin{bmatrix} a_{11}B & \cdots & a_{1n}B \\ \vdots & \ddots & \vdots \\ a_{m1}B & \cdots & a_{mn}B \end{bmatrix} \tag{11.6}$$

$$= \begin{bmatrix} a_{11}b_{11} & a_{11}b_{12} & \cdots & a_{11}b_{1q} & \cdots & \cdots & a_{1n}b_{11} & a_{1n}b_{12} & \cdots & a_{1n}b_{1q} \\ a_{11}b_{21} & a_{11}b_{22} & \cdots & a_{11}b_{2q} & \cdots & \cdots & a_{1n}b_{21} & a_{1n}b_{22} & \cdots & a_{1n}b_{2q} \\ \vdots & \vdots & \ddots & \vdots & & & \vdots & \vdots & \ddots & \vdots \\ a_{11}b_{p1} & a_{11}b_{p2} & \cdots & a_{11}b_{pq} & \cdots & \cdots & a_{1n}b_{p1} & a_{1n}b_{p2} & \cdots & a_{1n}b_{pq} \\ \vdots & \vdots & & \vdots & \ddots & & \vdots & \vdots & & \vdots \\ \vdots & \vdots & & \vdots & & \ddots & \vdots & \vdots & & \vdots \\ a_{m1}b_{11} & a_{m1}b_{12} & \cdots & a_{m1}b_{1q} & \cdots & \cdots & a_{mn}b_{11} & a_{mn}b_{12} & \cdots & a_{mn}b_{1q} \\ a_{m1}b_{21} & a_{m1}b_{22} & \cdots & a_{m1}b_{2q} & \cdots & \cdots & a_{mn}b_{21} & a_{mn}b_{22} & \cdots & a_{mn}b_{2q} \\ \vdots & \vdots & \ddots & \vdots & & & \vdots & \vdots & \ddots & \vdots \\ a_{m1}b_{p1} & a_{m1}b_{p2} & \cdots & a_{m1}b_{pq} & \cdots & \cdots & a_{mn}b_{p1} & a_{mn}b_{p2} & \cdots & a_{mn}b_{pq} \end{bmatrix}. \tag{11.7}$$

Using the identity (11.4), the Liouville superoperator can be made into a normal (single-sided) operator acting on the vec-form of the density matrix. Within this interpretation, the problem of finding a stationary solution to Eq. (11.2) really becomes a standard eigenproblem, with the important downside that, for a Hilbert space of dimension N (i.e., for a $N \times N$ density matrix), the matrix representation of $\mathcal{L}$ is of size $N^2 \times N^2$. Since in this formalism a (Hilbert) quantum mechanical operator $\hat{O}$ needs to be considered in its vec-form, the notation $|O\rangle\rangle$ is often used to stress the vector nature

---

[1] We wrote-out the matrix explicitly in Eq. (11.7) mainly to help the reader realize that the resulting matrix is *huge*.

this operator has in Liouville space.[Flindt04; Jakob04] In this case, the inner-product of two such vectors is defined as

$$\langle\langle \hat{A} | \hat{B} \rangle\rangle = \text{Tr}[\hat{A}^\dagger \hat{B}] \,. \tag{11.8}$$

11.2 System properties in the long-time limit

One of the main interest of using numerical solutions of the Liouville equation is that they give direct access to all properties of the system in the long-time (stationary) limit by allowing the calculation of the stationary density matrix. To illustrate how this can be done, we follow [Harvey08] and (neglecting the possibility of degeneracies), write the eigendecomposition of $\mathcal{L}$ as

$$\mathcal{L} = \sum_n \lambda_n |r_n\rangle\rangle\langle\langle l_n| \,. \tag{11.9}$$

Due to the presence of dissipative terms, the Liouvillian is in general not hermitian. Therefore, its eigenvalues λ_n are not necessarily real. Moreover, the right and left eigenvectors ($|r_n\rangle\rangle$, $\langle\langle l_n|$) are not simply related by hermitian conjugation.

Since our system is coupled to dissipative baths, we expect that a stationary solution exists. This, combined with the form of the the evolution operator $V(\tau) \sim e^{\mathcal{L}\tau}$, implies that $\lambda_0 = 0$ and that the real part of the other eigenvalues is negative [$\text{Re}\lambda_n < 0$ for ($n > 0$)] such that all solutions of the evolution equation except the stationary one equation are damped over time [Jakob04].

The problem of finding the stationary density matrix ($\dot{\rho}_{\text{stat}} = \mathcal{L}\rho_{\text{stat}} = 0$) therefore corresponds, as hinted earlier, to the eigenvalue problem *in Liouville space*

$$\mathcal{L}|r_0\rangle\rangle = 0|r_0\rangle\rangle \,, \tag{11.10}$$

with $|r_0\rangle\rangle = \text{vec}(\rho_{\text{stat}})$. Since for any complex number $C \neq 0$ the vector $C|r_0\rangle\rangle$ also fulfills Eq. (11.10), we use the condition $\text{Tr}[\rho_{\text{stat}}] = 1$ to remove all ambiguity in the calculation of ρ_{stat}. The details of the numerical solution of the eigenvalue problem are given in Sec. 11.7.

Having obtained ρ_{stat}, the expectation value of any function of system operators in the long-time limit can be calculated, via $\langle \hat{O} \rangle = \text{Tr}[\hat{O}\rho]$. Of course, if $\hat{O}$ is a system operator then so is $\hat{O}^2$, such that we can in fact evaluate all moments $\langle \hat{O}^n \rangle$ of operators.

11.3 Finite-frequency correlation functions

In general, we are not only interested about the stationary value of system quantities. Indeed, there is a lot of information to be harvested from finite-frequency correlations

functions, particularly in the region $\omega \sim \Omega$. Luckily, the form of the correlation functions of *system* (i.e. not *bath*) variables, can be derived within the Liouville formalism using the quantum regression theorem [Lax63]. In this section, we obtain the formal expression for finite-frequency correlations functions; the technical details associated with the numerical implementation of the calculation of these quantities are given in Sec. 11.7.2.

11.3.1 The quantum regression theorem

Let's first review shortly the basic ideas behind the quantum regression theorem. We are interested in calculating correlation functions of the form $\langle \hat{O}_1(t+\tau)\hat{O}_2(t)\rangle$ as well as their Fourier-transforms (with respect to τ), where $\hat{O}_i(t)$ is a system operator in the Heisenberg picture. In the case where the total density matrix can be written as $\rho_{tot} = \rho_s \otimes \rho_B$ this correlation function is written (we switched back to the Schrödinger picture)

$$\langle \hat{O}_1(t+\tau)\hat{O}_2(t)\rangle = \text{Tr}_{sys}\left[\text{Tr}_B\left[e^{iH(t+\tau)/\hbar}\hat{O}_1 e^{-iH\tau/\hbar}\hat{O}_2 e^{-iHt/\hbar}\rho_s \otimes \rho_B\right]\right] \tag{11.11}$$

This formulation, while valid, contains an annoying trace on the bath. One of the main objective of the derivation presented in Sec. 7.1 was to find an effective equation of motion for the system part of the density matrix, *after* tracing out the bath, and therefore Eq. (11.11) feels like a step backwards. However, we can rearrange the terms in this equation, using the hypothesis that $\hat{O}_1$ is a system operator to take it out of the trace on the bath.

$$\langle \hat{O}_1(t+\tau)\hat{O}_2(t)\rangle = \text{Tr}_{sys}\left[\hat{O}_1 \text{Tr}_B\left[e^{-iH\tau/\hbar}\hat{O}_2 \rho_{tot}(t) e^{iH\tau/\hbar}\right]\right], \tag{11.12}$$

$$= \text{Tr}_{sys}\left[\hat{O}_1 \text{Tr}_B[\mathcal{X}(\tau,t)]\right], \tag{11.13}$$

where we introduced the quantity

$$\mathcal{X}(\tau,t) \equiv e^{-iH\tau/\hbar}\hat{O}_2 \rho_{tot}(t) e^{iH\tau/\hbar}, \tag{11.14}$$

on which the trace on the bath is taken. This quantity contains a single system operator. Interestingly, the time-derivative of $\mathcal{X}(\tau,t)$ with respect to τ

$$\frac{d}{d\tau}\mathcal{X}(\tau,t) = \frac{1}{i\hbar}[H, \mathcal{X}(\tau,t)] \tag{11.15}$$

has exactly the same form as the one for the density total density matrix [Eq. (7.2)]. Therefore, following the derivation presented in Sec. 7.1, one can show that the evolution of $\text{Tr}_B \mathcal{X}(\tau,t)$ is governed by same master equation as the reduced density matrix.

To write the QRT in the form where it is usually found in reference works [Gardiner04; Carmichael02], we now introduce the operator $V(t_2, t_1)$ that evolves the density matrix from time t_1 to $t_2 \geq t_1$:

$$\rho(t_2) = V(t_2, t_1)\rho(t_1) . \tag{11.16}$$

This evolution operator is the identity for $t_2 = t_1$, and follows the same equation of motion as the density matrix.

$$\frac{d}{dt}V(t, t_0) = \mathcal{L}V(t, t_0). \tag{11.17}$$

This is easily proved by taking time derivatives on both sides of Eq. (11.14). As mentioned previously, $\mathcal{X}(\tau, t)$ and the density matrix evolve in the same way. The time evolved $\mathcal{X}$ can therefore be written in terms of V,

$$\text{Tr}_B[\mathcal{X}(\tau, t)] = V(t + \tau, t)\text{Tr}_B[\mathcal{X}(0, t)] = V(t + \tau, t)[\hat{O}_2 \rho(t)] . \tag{11.18}$$

Putting this last result in Eq. (11.13), one finds the usual expression of the QRT:

$$\langle \hat{O}_1(t + \tau)\hat{O}_2(t) \rangle = \text{Tr}_{sys}\left[\hat{O}_1 V(t + \tau, t)\left[\hat{O}_2 \rho(t)\right]\right] , \tag{11.19}$$
$$\langle \hat{O}_1(t)\hat{O}_2(t + \tau) \rangle = \text{Tr}_{sys}\left[\hat{O}_2 V(t + \tau, t)\left[\rho(t)\hat{O}_1\right]\right] , \tag{11.20}$$

where we also included the result for $\langle \hat{O}_1(t)\hat{O}_2(t + \tau) \rangle$ that can be obtained in a similar way. In the last equation, we kept the terms located right of $V(t + \tau, t)$ in brackets to make explicit the fact the *two-sided* evolution operator acts on the whole bracket. Finally, since we are interested calculating correlation functions in the steady-state that depend only on the time-difference τ and not on the absolute time t, we will use the stationary density matrix ρ_{stat} in place of $\rho(t)$. Also, for our time-independent Liouvillian, we will usually write $V(\tau, 0)$ simply as

$$V(\tau, 0) = e^{\mathcal{L}\tau} , \tag{11.21}$$

as obtained by straightforward integration of Eq. (11.17).

11.3.2 Projection operators in Liouville space

When using the Liouvillian formalism in general, and for the derivation of finite-frequency correlation functions in particular, it is very useful to introduce two projection operators in Liouville space[Flindt04],

$$\mathcal{P} = |r_0\rangle\rangle\langle\langle l_0| , \tag{11.22}$$
$$\mathcal{Q} = \sum_{n>0} |r_n\rangle\rangle\langle\langle l_n| = 1 - \mathcal{P} . \tag{11.23}$$

Recalling that the vec-form of the stationary density matrix is the right eigenvector (noted $|r_0\rangle\rangle$) of the Liouvillian associated with the eigenvalue 0,

$$\mathcal{L}|r_0\rangle\rangle = 0|r_0\rangle\rangle \,, \tag{11.24}$$

we see that $\mathcal{P}$ projects to the subspace associated with the eigenvalue 0,[2] and therefore that $\mathcal{Q}$ projects outside this subspace.

Besides the identities $\mathcal{P}^2 = \mathcal{P}, \mathcal{Q}^2 = \mathcal{Q}$ verified for all projection operators, the projectors $\mathcal{P}, \mathcal{Q}$ obey useful relations[3]

$$\mathcal{P}\mathcal{L} = \mathcal{L}\mathcal{P} = 0 \tag{11.25}$$

$$\mathcal{Q}\mathcal{L}\mathcal{Q} = \mathcal{L} \,. \tag{11.26}$$

As an example of how to use the notation introduced in this section, let us describe explicitly how the projection operators can be used on a vector in Liouville space $|A\rangle\rangle$ associated with the Hilbert-space operator $\hat{A}$.

$$\mathcal{P}|A\rangle\rangle = |r_0\rangle\rangle\langle\langle l_0|A\rangle\rangle \qquad\qquad (= \text{vec}(\rho_{stat})\text{Tr}_{sys}[\hat{A}]) \,, \tag{11.27}$$

$$\mathcal{Q}|A\rangle\rangle = |A\rangle\rangle - |r_0\rangle\rangle\langle\langle l_0|A\rangle\rangle \qquad (= \text{vec}(\hat{A}) - \text{vec}(\rho_{stat})\text{Tr}_{sys}[\hat{A}]) \,. \tag{11.28}$$

11.3.3 Expression of the correlation functions

Using the QRT and the projector formalism we just introduced, we can write formal expressions for the (unsymmetrized)auto-correlation function of an observable $\delta\hat{O} = \hat{O} - \langle O\rangle$. Before proceeding, we will rewrite the autocorrelation spectrum as a sum of symmetric and anti-symmetric in frequency contributions,

$$S_O(\omega) = \left[\frac{S_O(\omega) + S_O(-\omega)}{2}\right] + \left[\frac{S_O(\omega) - S_O(-\omega)}{2}\right] \,, \tag{11.29}$$

$$= \int_0^\infty d\tau \langle\{\delta\hat{O}(\tau), \delta\hat{O}(0)\}\rangle \cos(\omega\tau) + i\int_0^\infty d\tau \langle[\delta\hat{O}(\tau), \delta\hat{O}(0)]\rangle \sin(\omega\tau) \,. \tag{11.30}$$

Since this last form contains only integrals for $t \geq 0$, we can use the QRT to write the expectation values in terms of the evolution operator $V(\tau, 0) = e^{\mathcal{L}\tau}$. Importantly, in this section we will derive the formal expression for both the symmetrized and anti-symmetrized noise, whereas previous studies (e.g. [Flindt05a]) focused solely on symmetrized noise.

---

[2]We note that the associated left eigenvector can be found using $\langle\langle l_0|r_0\rangle\rangle = 1$ in combination with $\text{Tr}[\rho_{stat}] = 1$, to find $\langle\langle l_0| = \text{vec}(\mathbf{1})$, where $\mathbf{1}$ is the Hilbert-space identity operator.

[3]The first relation follows from the eigendecomposition of the Liouvillian:

$\mathcal{P}\mathcal{L} = |r_0\rangle\rangle\langle\langle l_0|\left(\sum_{p=0}^N \lambda_p|r_p\rangle\rangle\langle\langle l_p|\right) = \left(\sum_{p=0}^N \delta_{p,0}\lambda_p|r_0\rangle\rangle\langle\langle l_p|\right) = \lambda_0|r_0\rangle\rangle\langle\langle l_0| = 0$

Symmetrized noise

Let us first look at the expression for the symmetrized noise,

$$\bar{S}_O(\omega) = \frac{1}{2} \int_{-\infty}^{\infty} \langle \{\delta\hat{O}(t), \delta\hat{O}(0)\}\rangle e^{i\omega t} = \int_0^{\infty} dt \langle \{\delta\hat{O}(t), \delta\hat{O}(0)\}\rangle \cos(\omega t), \quad (11.31)$$

with $\delta\hat{O} = \hat{O} - \langle\hat{O}\rangle$. We split the last integral into two terms ($\pm i\omega t$), and look at the first one (+). Rewriting the integrand as

$$\langle\{\delta\hat{O}(t), \delta\hat{O}(0)\}\rangle = \text{Tr}_{sys}[\delta\hat{O}e^{\mathcal{L}t}[\delta\hat{O}\rho_{stat}]] + \text{Tr}_{sys}[\delta\hat{O}e^{\mathcal{L}t}[\rho_{stat}\delta\hat{O}]], \quad (11.32)$$

$$= \text{Tr}_{sys}[\delta\hat{O}e^{\mathcal{L}t}\{\delta\hat{O}, \rho_{stat}\}], \quad (11.33)$$

the integral can be rewritten as

$$\int_0^{\infty} dt \langle\{\delta\hat{O}(t), \delta\hat{O}(0)\}\rangle e^{i\omega t} = \text{Tr}_{sys} \int_0^{\infty} dt \delta\hat{O}e^{\mathcal{L}t}\{\delta\hat{O}, \rho_{stat}\}e^{i\omega t}. \quad (11.34)$$

We add a convergence factor $\omega \to \omega + i\eta, (\eta \to 0^+)$, then proceed with the integration to find

$$= -\text{Tr}_{sys}[\delta\hat{O}(i\omega + \mathcal{L})^{-1}\{\delta\hat{O}, \rho_{stat}\}] \quad (11.35)$$

Following [Flindt05b], we write

$$(i\omega + \mathcal{L})^{-1} = (i\omega\mathcal{P} + i\omega\mathcal{Q} + \mathcal{Q}\mathcal{L}\mathcal{Q})^{-1}. \quad (11.36)$$

This way the inverse can be readily found,

$$(i\omega\mathcal{P} + i\omega\mathcal{Q} + \mathcal{Q}\mathcal{L}\mathcal{Q})^{-1} = \frac{\mathcal{P}}{i\omega} + \mathcal{Q}\frac{1}{\mathcal{L} + i\omega}\mathcal{Q}. \quad (11.37)$$

We now define

$$\mathcal{R}(x) \equiv \mathcal{Q}\frac{1}{\mathcal{L} + x}\mathcal{Q} \quad (11.38)$$

to get

$$-\text{Tr}_{sys}[\delta\hat{O}(i\omega + \mathcal{L})^{-1}\{\delta\hat{O}, \rho_{stat}\}] = -\text{Tr}_{sys}[\delta\hat{O}\left(\frac{\mathcal{P}}{i\omega} + \mathcal{R}(i\omega)\right)\{\delta\hat{O}, \rho_{stat}\}]. \quad (11.39)$$

This allows us to write, including the second contribution which is identical to the first one but with $\omega \to -\omega$,

$$\bar{S}_O(\omega) = -\frac{1}{2}\text{Tr}_{sys}[\delta\hat{O}\left(\frac{\mathcal{P}}{i\omega} + \mathcal{R}(i\omega)\right)\{\delta\hat{O}, \rho_{stat}\}]$$

$$- \frac{1}{2}\text{Tr}_{sys}[\delta\hat{O}\left(-\frac{\mathcal{P}}{i\omega} + \mathcal{R}(-i\omega)\right)\{\delta\hat{O}, \rho_{stat}\}], \quad (11.40)$$

$$= -\frac{1}{2}\text{Tr}_{sys}[\delta\hat{O}\left(\mathcal{R}(-i\omega) + \mathcal{R}(i\omega)\right)\{\delta\hat{O}, \rho_{stat}\}], \quad (11.41)$$

where in the last line we added the reverse contributions of $\pm\mathcal{P}/(i\omega)$. This is the expression for the symmetrized noise of operator $\hat{O}$ at frequency ω. The details regarding how to numerically evaluate this quantity are given in Sec. 11.7.2.

Anti-symmetrized noise

As advertised previously, the anti-symmetrized noise

$$S_O^-(\omega) = \left[\frac{S_O(\omega) - S_O(-\omega)}{2}\right] = i \int_0^\infty dt \langle [\delta\hat{O}(t), \delta\hat{O}(0)]\rangle \sin(\omega t) , \qquad (11.42)$$

can also be calculated using the numerical Liouville approach. To proceed, we again write

$$\langle [\delta\hat{O}(t), \delta\hat{O}(0)]\rangle = \mathrm{Tr}_{sys}[\delta\hat{O} e^{\mathcal{L}t}[\delta\hat{O}\rho_{stat}]] - \mathrm{Tr}_{sys}[\delta\hat{O} e^{\mathcal{L}t}[\rho_{stat}\delta\hat{O}]] \qquad (11.43)$$

$$= \mathrm{Tr}_{sys}[\delta\hat{O} e^{\mathcal{L}t}[\delta\hat{O}, \rho_{stat}]] \qquad (11.44)$$

We can follow the same route as before, splitting the integral in two, to find,

$$S_O^-(\omega) = -\frac{1}{2}\mathrm{Tr}_{sys}[\delta\hat{O}\left(\frac{\mathcal{P}}{i\omega} + \mathcal{R}(i\omega)\right)[\delta\hat{O}, \rho_{stat}]]$$
$$+ \frac{1}{2}\mathrm{Tr}_{sys}[\delta\hat{O}\left(-\frac{\mathcal{P}}{i\omega} + \mathcal{R}(-i\omega)\right)[\delta\hat{O}, \rho_{stat}]] , \qquad (11.45)$$

$$= -\frac{1}{2}\mathrm{Tr}_{sys}[\delta\hat{O}\left(\mathcal{R}(i\omega) - \mathcal{R}(-i\omega)\right)[\delta\hat{O}, \rho_{stat}]] - \mathrm{Tr}_{sys}[\delta\hat{O}\frac{\mathcal{P}}{i\omega}[\delta\hat{O}, \rho]] , \quad (11.46)$$

This time the ω^{-1} term does not drop out naturally. We can however evaluate it

$$\mathrm{Tr}_{sys}[\delta\hat{O}\mathcal{P}[\delta\hat{O}, \rho]] = \langle\langle\delta\hat{O}|r_0\rangle\rangle\langle\langle l_0|[\delta\hat{O}, \rho_{stat}]\rangle\rangle , \qquad (11.47)$$

$$= \mathrm{Tr}_{sys}[\delta\hat{O}\rho_{stat}]\mathrm{Tr}_{sys}[[\delta\hat{O}, \rho_{stat}]] , \qquad (11.48)$$

and, since the trace of a commutator is always zero, see that it also never contributes to the correlation function. Therefore, the final expression for $S_O^-(\omega)$

$$S_O^-(\omega) = -\frac{1}{2}\mathrm{Tr}_{sys}[\delta\hat{O}\left(\mathcal{R}(i\omega) - \mathcal{R}(-i\omega)\right)[\delta\hat{O}, \rho_{stat}]] . \qquad (11.49)$$

It is important to stress that, using Eqs. (11.41) and (11.49), we have access to the un-symmetrized, frequency-dependent noise of any system observable.

11.4 Explicit form of the Liouville operator

Having presented in detail the Liouvillian formalism, we now apply this formalism to our physical problem of a NEMS coupled to a SSET biased near a DJQP. A natural first step is to derive the Liouville operator in this case. The von Neumann equation [Eq. (7.2)]

$$\mathcal{L}\rho = \frac{1}{i\hbar}\mathrm{Tr}_B[H_{\mathrm{tot}}, \rho_{\mathrm{tot}}] , \qquad (11.50)$$

provides a natural way to calculate $\mathcal{L}$ for a general system. In the case we are interested in, the reduced density matrix $\mathrm{Tr}_B \rho_{\mathrm{tot}}$ contains information about both the charge state of the SSET and the oscillator. As in Sec. 10.3.1, we will note $\rho_{i,j}$ the matrix element $\langle i | \mathrm{Tr}_{n_{\mathrm{osc}}} \mathrm{Tr}_B \rho_{\mathrm{tot}} | j \rangle$ of the SSET's density matrix (with $|i\rangle$, $|j\rangle$ two charge states of the island). In the opposite fashion, we denote the eigenstates of the oscillator $|n_{\mathrm{osc}}\rangle$ and use superscripts to denote the matrix elements of the oscillator part of the density matrix

$$\mathrm{Tr}_B \rho_{\mathrm{tot}} = \rho = \sum_{i=-1}^{2} \sum_{j=-1}^{2} \sum_{n_{\mathrm{osc}}=0}^{N_{\mathrm{max}}} \sum_{m_{\mathrm{osc}}=0}^{N_{\mathrm{max}}} \rho_{i,j}^{n_{\mathrm{osc}},m_{\mathrm{osc}}} |i\rangle \langle j| \otimes |n_{\mathrm{osc}}\rangle \langle m_{\mathrm{osc}}| \tag{11.51}$$

As hinted at earlier [Eq. (11.3)], the total Liouvillian can be written as a sum of three contributions,

$$\mathcal{L} = \mathcal{L}_{co} + \mathcal{L}_{qp} + \mathcal{L}_{cl} , \tag{11.52}$$

with $\mathcal{L}_{co}$ describing the coherent evolution of the coupled system, $\mathcal{L}_{cl}$ a Caldeira-Leggett type contribution to the evolution of the complete density matrix that models the coupling of the oscillator to the environment (Sec. B) and $\mathcal{L}_{qp}$ a contribution associated with dissipative quasiparticle transport.

The coherent evolution contribution to the Liouvillian is given by

$$\mathcal{L}_{H_{co}} \rho = \frac{1}{i\hbar} [H_{co}, \rho] , \tag{11.53}$$

where H_{co} is the complete *system* Hamiltonian, i.e. the Hamiltonian describing the undamped oscillator and the coherent processes in the SSET (Josephson tunneling, charging energy) as well as the interaction Hamiltonian. The second term $\mathcal{L}_{qp}$ describes the effect of the quasiparticle transport on the reduced density matrix. Its form can be read-out directly from Eq. (10.10)

$$\mathcal{L}_{qp} \rho = \Gamma_L \hat{q}_{-1,0} \rho \hat{q}_{-1,0}^\dagger - \frac{1}{2} \Gamma_L \{\hat{q}_{-1,-1}, \rho\} + \Gamma_R \hat{q}_{2,1} \rho \hat{q}_{2,1}^\dagger - \frac{1}{2} \Gamma_R \{\hat{q}_{2,2}, \rho\} , \tag{11.54}$$

where we introduced operators $\hat{q}_{kj} = |j\rangle \langle k|$ describing the quasiparticle tunneling event that changes the charge state of the island from $|k\rangle$ to $|j\rangle$. Finally, the $\mathcal{L}_{CL}$ contribution is, as described in Chap. 7, given by

$$\mathcal{L}_{CL} \rho = -\frac{D_0}{\hbar^2} [\hat{x}, [\hat{x}, \rho]] - \frac{i\gamma_0}{2\hbar} [\hat{x}, \{\hat{p}, \rho\}] , \tag{11.55}$$

with $D_0 = M\gamma_0 \hbar \Omega \coth [\hbar\Omega/2k_B T_B] /2$. Naturally, this term is independent of the charge state of the island. Using Eq. (11.4), the matrix representation of the Liouvillian associated with our problem can be constructed, starting from the (Hilbert space) matrix representation of the $\hat{p}$, $\hat{x}$ and $\hat{q}_{kj}$.

11.5 Numerical results

We now present results of numerical calculations realized using the approach we just detailed. At this point, it is good to warn the reader that we cannot hope to use this kind approach to map-out the complete parameter space of the problem of an oscillator coupled to a SSET biased near the DJQP. Indeed, at least 9 parameters[4] could in principle be tuned over a wide range of experimentally accessible values. This is why such a numerical study is particularly helpful when combined to analytical approaches where it is easier to understand the effect of each parameter. This is precisely the case here: the results presented in this section were obtained to complement a study using an approximate master-equation approach. For a detailed comparison between the numerical and the results obtained this master-equation approach, refer to [Koerting08]. In the remainder of this section, we will focus on presenting results that are not readily obtained via the semi-analytical approach described in Sec. 10.3.3.

11.5.1 Stationary state determination

The Fock-state occupancy $P(n_{\rm osc}) = \mathrm{Tr}_n \langle n_{\rm osc}|\rho|n_{\rm osc}\rangle$ is a good example of a quantity that is both very useful to describe the state of the system and that cannot be easily accessed using the mean-field approach. This quantity allows for a direct identification of the state of the oscillator. In the thermal case $P(n_{\rm osc})$ monotonically decreases with increasing $n_{\rm osc}$, following

$$P(n_{\rm osc}) \sim e^{\frac{-(n_{\rm osc}+1/2)\hbar\Omega}{k_B T}} , \qquad (11.56)$$

In the driven state, effective theories [Clerk05] predict that $P(n_{\rm osc})$ is a totally different, gaussian-like distribution peaked away from $n_{\rm osc} = 0$. The Fock-space occupancy can therefore be used as "smoking-gun" evidence to prove that the stationary state of a system is a driven state. This is very different from the mean-field approach, where only the average energy is calculated, making difficult to differentiate between a high-temperature thermal state and a driven state. Finally, by looking at $P(n_{\rm osc})$ one can also identify regions where the system exhibits bistability (the system switches between thermal and driven states): in this case $P(n_{\rm osc})$ is the weighted average of a thermal-like and a driven-like distribution.

Figure 11.1 shows the evolution of the Fock-space occupancy as the bias voltage is increased from the $\gamma > 0$ ($\Delta eV = -2\hbar\Omega$) region through the regime the linear-reponse approach breaks down ($\Delta eV > 5\hbar\Omega$). For $eV > 5\hbar\Omega$, we notice the presence

---

[4]These are: the detunings in gate voltage and bias voltage away from the resonance, the Josephson energy of each junction, the two quasiparticle tunneling rates, the coupling strength, the temperature of the thermal bath, and the quality factor of the oscillator.
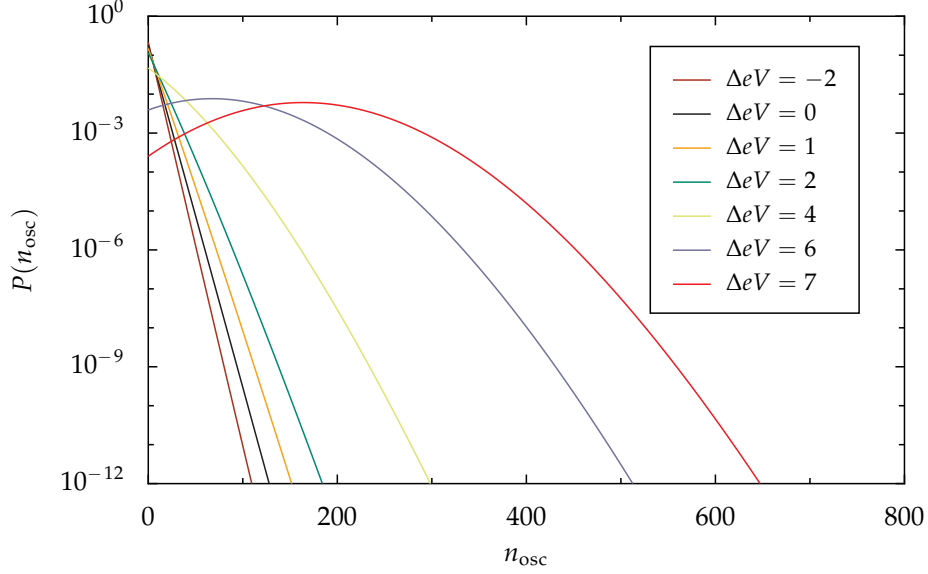
Figure 11.1: Fock-space occupancy $P(n_{\mathrm{osc}}) = \mathrm{Tr}_n\langle n_{\mathrm{osc}}|\rho|n_{\mathrm{osc}}\rangle$ for different values of the bias voltage $\Delta eV/\hbar\Omega$. The parameters used for the calculation are: $\Gamma_L = \Gamma_R = 12\Omega$, $J_L = J_R = 5\hbar\Omega$, $\gamma_0 = \Omega/1000$, $T_0 = 3\hbar\Omega/k_B$, $A = 0.1x_0/\hbar\Omega$.

of a maximum in $P(n_{\mathrm{osc}})$ located away from $n_{\mathrm{osc}} = 0$. As mentioned earlier, this can be use to confirm that the stationary state of the oscillator is in this case a driven state.

In passing, we mention that another way to confirm the observation of bistable behavior is via the probability distribution function $P(x) = \mathrm{Tr}_n\langle x|\rho|x\rangle$. This information is also not available via the mean-field approach, where one typically only calculates the first few cumulants of $P(x)$, like $\langle x \rangle$ and $\langle\langle x^2 \rangle\rangle$. From $P(x)$ one can directly verify the validity of the truncation made in the system of equations (Sec. 10.3.3). This quantity can also serve as another way to discern the type of stationary state reached by the oscillator due to the interaction with the SSET. Figure 11.2 shows three typical probability distributions that can be observed. On the left, the standard thermal state, where $P(x)$ is gaussian-distributed around the equilibrium position ($\langle x \rangle \sim 0$) is displayed. The middle panel shows $P(x)$ for a driven state, with two maxima at finite $|x|$. The rightmost panel displays the position probability distribution in the case where the system is bistable. In this case, $P(x)$ is a sum of a driven and a thermal distribution, the driven state showing up as two shoulders at large $|x|$.
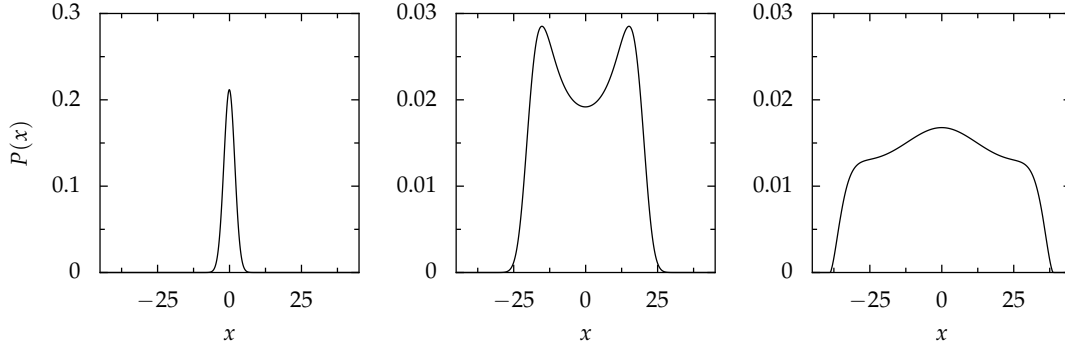
Figure 11.2: Position probability distribution $P(x)$ for three different type of oscillator states: thermal (left), driven (center) and bistable (right). The position is given in units of $\Delta x_0 = (\hbar/2M\Omega)^{1/2}$ the zero-point motion of the oscillator.

11.5.2 Frequency-dependent charge noise

The possibility of identifying without ambiguity the nature of the stationary state of the oscillator using our numerical approach is mostly interesting when combined to a master-equation approach where the parameter space can be rapidly mapped out. The numerical approach presented in this chapter should however not be seen as something that is *only* to be used in conjunction with the master-equation approach. It can be very useful "on its own", as we demonstrate in this section.

The description of the detector as an effective bath proved very successful in providing a simple physical explanation of experiments (as discussed in e.g. Sec. 10.3). However, some of its shortcomings have started to be identified in recent theoretical works[Bennett08; Rodrigues08]. For example, it was very recently proposed [Rodrigues08] that the signature of the oscillator in the charge noise spectrum of a generic detector is *not* one of a thermal oscillator. In the light of these findings, the calculation of the full frequency-dependent charge noise spectrum of the SSET near the DJQP in the presence of an oscillator becomes relevant, especially since the charge-noise spectrum is an experimentally accessible quantity. Luckily, the frequency-dependent charge noise is readily calculated from Eq. (11.41).

Figure 11.3 shows the symmetrized (in frequency) charge-noise spectra, $\overline{S}_n(\omega)$ obtained for different values of the bias-voltage detuning from the DJQP resonance. The oscillator state, i.e. thermal or driven, can be determined from the Fock space probability distribution in Fig. 11.1. The inset shows that the signature of the oscillator in $\overline{S}_n(\omega)$ appears prominently around the natural frequency of the oscillator. Away from $\omega \sim \Omega$, the charge spectrum is only weakly affected by the oscillator, this one changing only slightly the effective biasing conditions of the SSET.
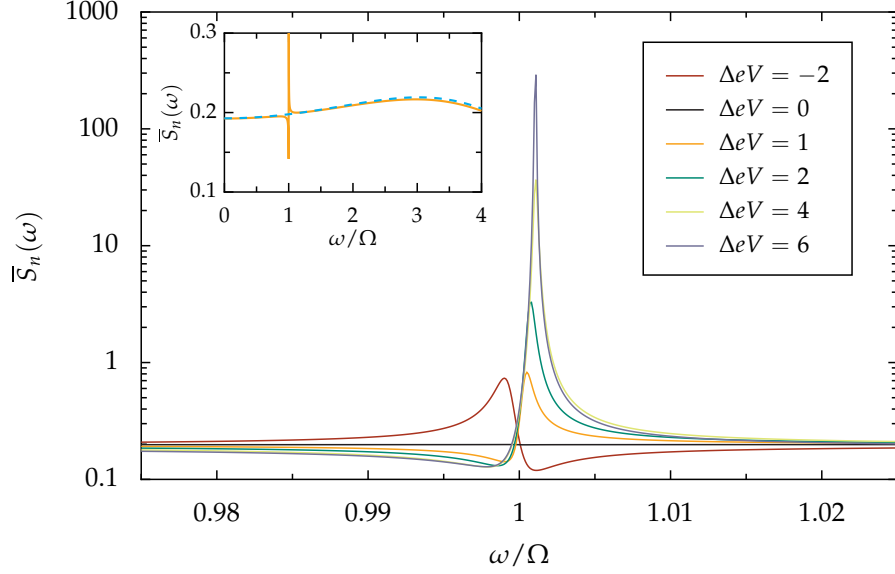
Figure 11.3: Symmetrized frequency-dependent charge noise $\overline{S}_n(\omega)$ of the SSET versus ω/Ω for different values of the bias voltage $\Delta eV/\hbar\Omega$. Parameters are identical to Fig. 11.1. While there is no structure in the case $\Delta eV = 0$, we can distinguish if the oscillator is driven or damped by the symmetry of the peak at $\omega = \Omega$. Inset: Comparison between the frequency-dependent charge noise in the presence of the oscillator and in the uncoupled case, over a larger frequency range.

The main panel of Fig. 11.3 shows the evolution of the charge-noise spectra when the system is taken from the "cooling" region ($\Delta eV = -1\hbar\Omega$) through the resonance point ($\Delta eV = 0$), to the voltage regime where the state of the oscillator becomes highly non-thermal. Unsurprisingly, the overall signal around Ω increases dramatically when the oscillator enters the driven regime, reflecting the overall increase in the magnitude of $S_x(\omega \sim \Omega)$ when the oscillators energy is increased. Associated with this increased magnitude is a reduction of the width of the resonance, that is again explained rather straightforwardly via the decreased total damping rate in this region ($A^2\gamma < 0$).

The most interesting observation to be made about Fig. 11.3 is perhaps the striking similarity between the spectra at $\Delta eV < 0$ and $eV > 0$. In both cases, we find not only a resonance at the renormalized frequency of the oscillator, but also an anti-resonance at its bare frequency, exactly as derived in [Rodrigues08] for a generic detector.[5] Exactly at the resonance the two effects cancel, although a very weak resonance-anti-

---

[5]Note that the renormalized frequency $\Omega_r(eV) = \sqrt{\Omega^2 - [\gamma_0 + A^2\gamma/2]^2}$ depends on the detuning eV via the γ parameter (see e.g. Fig 10.3 for a qualitative overview of the dependence of γ on ΔeV).

resonance can be seen on a finer scale. In the region $\Delta eV > 0$ and $A^2\gamma < 0$, the situation is reversed and the resonance appears at frequencies Ω_r higher than Ω.

When coupled to a purely thermal oscillator, the charge noise spectrum $\overline{S}_n(\omega)$ does not contain any anti-resonance [Rodrigues08]. The presence of this anti-resonance on *all* curves, or more precisely, for all values of detuning ΔeV, even in cases where the Fock state probability distribution function $P(n_{\text{osc}})$ decays exponentially[6], suggests that this anti-resonance is associated with correlations between n and x that arise in our system, and not for a back-action free thermal oscillator. To explain this result qualitatively, we can look at the effective Langevin equation of the problem [Eq. (6.2)] and write it in terms of a single effective environment. In this case, the effective total force on the oscillator is given by

$$\overline{S}_{F,\text{tot}}(\omega) = M\gamma_{\text{tot}}\hbar\omega \coth\left(\frac{\hbar\omega}{2k_B T_{\text{tot}}}\right) . \tag{11.57}$$

A real physical thermal bath at temperature $T_{\text{therm}} = T_{\text{tot}}$ coupled to the oscillator via a damping rate $\gamma_{\text{Therm}} = \gamma_{\text{tot}}$ would also have

$$\overline{S}_{F,\text{therm}}(\omega) = M\gamma_{\text{tot}}\hbar\omega \coth\left(\frac{\hbar\omega}{2k_B T_{\text{tot}}}\right) . \tag{11.58}$$

However, this real, physical, thermal bath would be totally uncorrelated to $\hat{F}$. This is not the case for the effective bath:

$$\langle F_{\text{therm}}(t)F(t)\rangle = 0 , \tag{11.59}$$
$$\langle F_{\text{tot}}(t)F(t)\rangle \neq 0 : \tag{11.60}$$

the 'effective thermal' force felt by the oscillator is correlated with $F \leftrightarrow n$, the charge on the island. This is an important difference that can explain the difference in the observed $\overline{S}_n(\omega)$ and the one predicted for a simple thermal oscillator. It is also consistent with numerical evidence showing no anti-resonance when the thermal force F_0 overwhelms the back-action force (i.e. $\gamma_0 T_0 \gg A^2\gamma T_{\text{eff}}$, the anti-resonance disappear).

The numerical data presented in this subsection not only confirms that the simple model used in [Rodrigues08] also applies to the complex SSET-resonator system, it demonstrates that the "Fano-like" lineshape, where both a resonance and an anti-resonance appear in the spectrum of the charge noise, characterizes nicely the charge noise spectrum on both the "driving" and "cooling" sides of the resonance.

---

[6]Again, refer to Fig. 11.1 to compare the different voltage points.

11.6 Summary

In this chapter, we have presented the details of a numerical approach based on the Liouville equation that was used to complement a mean-field master equation study [Koerting08] of a system composed of a nanomechanical oscillator coupled to a SSET biased near the DJQP transport resonance. The numerical approach allows the calculation of both average properties of the coupled system in the long-time limit and of correlation functions of system variables. Importantly, it gives access to quantities that are not readily available from the mean-field approach like the Fock-space occupancy distribution or the position probability distribution $P(x)$, making it a perfect companion tool to master-equation studies. We also computed and discussed the spectrum $\overline{S}_n(\omega)$ of the charge fluctuations on the SSET island. In the range of frequencies close to the resonator's frequency, we found that the spectrum displayed both a resonance and an anti-resonance, irrespective of the sign of the detuning from the DJQP resonance ΔeV. The observed "Fano" lineshape, while inconsistent with the signature of a purely thermal oscillator, is consistent with the prediction of [Rodrigues08]: it is symptomatic of the limitations of the effective environment model described in Sec. 6.1.

11.7 Implementation details

The main downside of using a Liouville approach in the context of nanomechanical systems is that the discrete but unbounded spectrum characterizing the harmonic oscillator cannot be treated numerically without truncating the infinite spectrum. This is usually not a problem, as long as the occupation of the discarded eigenstates vanishes, like it is the case at low temperatures. However, when dealing with systems that exhibit negative effective damping (like the one studied here), one must be careful and keep an elevated number of phonon states (noted N). Due to the bad scaling (N^4) of the number of elements of the Liouville matrix with N, the eigenproblem soon becomes numerically challenging: when only the 200 lowest oscillator energy eigenstates are considered, the Liouville matrix for the DQJP problem is of dimension $(16N^2 \times 16N^2 = 640000 \times 640000)$. Even after further simplification of the problem (Sec. 11.7.3), the large size of the Liouville matrix makes both the calculation of the stationary density matrix and the evaluation of the frequency-dependent correlation functions [Eqs. (11.41),(11.49)] numerically demanding.

11.7.1 The eigenvalue problem

Let's first address our implementation of the eigenvalue solver. To address this difficult problem, different paths were used by different groups. For example, in the

context of nanomechanical systems, some used in-house developed MATLAB implementations of the Arnoldi iteration technique[Arnoldi51; Golub96], while others used the inverse-iteration approach[Golub96]. We found neither of those approach satisfying. First, there is no real advantage in rewriting code for a common task as sparse eigenvalue problems. Second, the inverse-iteration technique requires the inversion of the Liouville matrix, a time-consuming and memory-hungry, procedure. Moreover, it does not calculate the eigenvalues explicitly; it only allows access to the eigenvectors associated with known eigenvalues. While the $\lambda_0 = 0$ eigenvalue is *a priori* known, the others must be "guessed" [Harvey08]!

We therefore decided to leverage the power of the sparse eigensolver library ARPACK[7][Lehoucq96; Lehoucq97], a FORTRAN 77 implementation of the implicitly restarted Arnoldi iteration approach to eigenvalue problems[Sorensen92], a generalization of the better-known implicitly restarted Lanczos method used for symmetric matrices. This collection of subroutines is designed to compute "few" (nev) eigenvalues of a $m \times m$ matrix $\mathbf{A}$ using only $m \times \mathcal{O}(\text{nev}) + \mathcal{O}(\text{nev}^2)$ auxilliary memory instead of the $\mathcal{O}(m^2)$ typically required by eigenvalue routines. These routine do not require the storage of the full matrix A, also decreasing the memory requirements. Finally, these routines return the eigenvalues and associated eigenvectors computed to user-specified accuracy that can be as stringent as the working precision ($\sim 10^{-16}$ for double-precision complex numbers).

The library is based around a *reverse communication interface* that requires the user to provide a routine that returns a vector $\mathbf{w}$, constructed from $\mathbf{w} = Op(\mathbf{A}, \mathbf{v})$ for any given vector $\mathbf{v}$. In most situations, $Op(\mathbf{A}, \mathbf{v}) \to \mathbf{Av}$ is simply the matrix-vector product of $\mathbf{A}$ and $\mathbf{v}$. The reverse communication interface is one of the main features of ARPACK. It allows the user to implement a key section of each Arnoldi iteration in the best, problem-dependent, way. The particular way to use the reverse communication interface is presented on the right side of Table 11.1.

Typically, the Arnoldi iteration method is appropriate to calculate few exterior eigenvalues of a large matrix, i.e. the nev eigenvalues with the largest magnitude. Calculating the eigenvalues with the smallest magnitude, like is needed in our case, is therefore quite involved when using the standard approach. Sylvester-type conditioning might be needed to ensure convergence[Jauho04]. When the methods fails to converge even after conditioning of the Liouville matrix, some damping kernels have been shown to be easier to deal with numerically [Flindt04]. By using ARPACK, we get rid of most of these numerical stability problems. Indeed, the library provides an implementation of 'shift-invert' mode of the Arnoldi iteration method via the driver routine zndrv2. This mode allows the calculation of the part of the eigenvalue spec-

---

[7]ARPACK and its parallel implementation PARPACK are open-source libraries distributed under a BSD license. They can be downloaded from http://www.caam.rice.edu/software/ARPACK/.

Table 11.1: Comparison of the way a standard eigenvalue routine (left) and an ARPACK routine with the reverse communication interface (right) is included in a code. On the right, the matrix **A** is given as an input to the routine that afterwards outputs the results (e.g. the eigenvectors) in **B**. On the right, the ARPACK routine is called repetitively after each iteration, until convergence (`done .eq. .true.`) is obtained. As part of each iteration, **w** must be evaluated from an operation Op of the matrix **A** and a vector **v** given by the routine (for every iteration, **v** is different). The user must provide its own routine to evaluate **w**, which is afterwards fed back as an input parameter of the ARPACK routine. When (`done .eq. .true.`), the results can be read from **v**, for example.

```
call normal_routine(A,B)        10  continue
                                    call arpack_routine(w,v,done)
                                    if (done .eq. .false.) then
                                        w = Op (A, v)
                                        goto 10
                                    endif
```

trum closest to a shift σ. Summed up briefly, in this mode the code calculates the eigenvalues of **A** closest a the shift σ by first estimating the eigenvalues with maximal magnitude of $(\mathbf{A} - \sigma\mathbf{1})^{-1}$. Since we are interested in the eigenvalues closest to zero, we choose a small but finite value for the shift ($\sigma \sim 10^{-10}$). This finite shift leads to an increased numerical accuracy.

In the shift-invert mode, the user-provided operation $\mathbf{w} = Op(\mathbf{A}, \mathbf{v})$ is not simply the product of **A** and **v**. Instead, the routine expects to be returned $\mathbf{w} = (\mathbf{A} - \mathbf{1}\sigma)^{-1}\mathbf{v}$. Of course, we do not have to inverse **A**. Instead, we solve the linear equation

$$(\mathbf{A} - \mathbf{1}\sigma)\mathbf{w} = \mathbf{v} \tag{11.61}$$

for **w**. The solution of sparse linear systems of high order is an extremely well-studied problem in computer science, mainly because these systems arise naturally in many engineering and physics problems (for example, in finite-element simulations). A wide range of libraries is therefore available to solve such systems. We decided to use the PARDISO linear solver[Schenk04; Schenk06] developed at the University of Basel. Many reasons explain this choice. First, it is available free or charge for academic use[8], and is also distributed as part of the Intel MKL performance package, making it easy to access. It has multiprocessor support. More importantly, it is adapted to problems where one system needs to be solved many times for different right-hand sides (in our case, for different **v** in Eq. 11.61). The factorization of the main matrix $(\mathbf{A} - \mathbf{1}\sigma)$ can

---

[8]See http://www.pardiso-project.org/ for details.

be used for each iteration and therefore only needs to be calculated once. Finally, this library proved one of the most efficient and numerically stable in a recent comparison of different solvers[Gould07].

By using a combination of ARPACK and PARDISO, our code calculates the lowest eigenvalue and associated eigenvector of a matrix of order 500 000 in less than 15 minutes on a recent workstation. Since we know that the lowest eigenvalue should be $\lambda_0 = 0$, we can evaluate the accuracy of our truncation scheme by looking at the calculated value of λ_0. In a perfect case, the magnitude of the calculated eigenvalue tends to zero ($|\lambda_0| \lesssim 10^{-15}$). However, when the population of energy state near the cutoff is not-negligible, then the zero-eigenvalue can become large ($|\lambda_0| \sim 10^{-6}$), signaling that the number of phonon states kept should be increased.

Finally, we tested the accuracy of the code by comparing the numerical results to i) analytic results when they are available (for example, in the uncoupled case) and ii) to the results obtained from a master-equation approach [Koerting08]. In the very weak coupling regime, where we expect the master equation approach to be valid, we always found extremely good agreement.

11.7.2   The calculation of finite-frequency correlation functions

Besides the eigenvalue problem, the other computationally intensive section of the code is the correlation of finite-frequency correlation functions. As can be seen from Eqs. (11.41,11.49), this typically requires the numerical evaluation of quantities of the form

$$\text{Tr}_{sys}[\hat{A}\mathcal{R}(x)\hat{B}]. \tag{11.62}$$

Since $\mathcal{R}(x) = \mathcal{Q}(\mathcal{L} + x)^{-1}\mathcal{Q}$, one might think that the numerical inversion of the Liouville matrix would need to be performed in order to evaluate $S_O(\omega)$. This is luckily not the case, as one can calculate $\mathcal{R}(x)\hat{B}$ using a linear solver. To understand how this is done, let us first rewrite Eq. (11.62) using the vector notation

$$\text{Tr}_{sys}[\hat{A}\mathcal{R}(x)\hat{B}] \leftrightarrow \langle\langle A|\mathcal{R}(x)|B\rangle\rangle , \tag{11.63}$$

and, following Flindt *et al.* [Flindt04], define auxiliary Hilbert space operator $\hat{\xi}$ and the associated Liouville space vector $|\xi\rangle\rangle = \text{vec}(\xi)$ from

$$|\xi\rangle\rangle \equiv \mathcal{R}(x)|B\rangle\rangle . \tag{11.64}$$

Using this vector, Eq. (11.62) simplifies to $\langle\langle A|\xi\rangle\rangle$. To find $|\xi\rangle\rangle$, we solve the linear equation

$$|\xi\rangle\rangle = \mathcal{Q}(\mathcal{L} + x)^{-1}\mathcal{Q}|B\rangle\rangle , \tag{11.65}$$

$$(\mathcal{L} + x)|\xi\rangle\rangle = (\mathcal{L} + x)\mathcal{Q}(\mathcal{L} + x)^{-1}\mathcal{Q}|B\rangle\rangle , \tag{11.66}$$

$$(\mathcal{L} + x)|\xi\rangle\rangle = \mathcal{Q}|B\rangle\rangle , \tag{11.67}$$

where we used the fact that, for x a number, $(\mathcal{L} + x)\mathcal{Q} = \mathcal{Q}(\mathcal{L} + x)$. This last equation has the form $\mathbf{Y} = \mathbf{M}\mathbf{X}$, with $\mathbf{Y}, \mathbf{X}$ dense vectors and $\mathbf{M} = (\mathcal{L} + x)$ a sparse matrix and at this point this system linear system of equations could be solved, for example by using the PARDISO solver. However, this is not the best way to proceed. Indeed, the solution to Eq. (11.67) is not unique. Defining $|\xi'\rangle\rangle = |\xi\rangle\rangle + z|r_0\rangle\rangle$, we have

$$\mathcal{L}|\xi'\rangle\rangle = \mathcal{L}(|\xi\rangle\rangle + z|r_0\rangle\rangle) \tag{11.68}$$

$$= \mathcal{L}|\xi\rangle\rangle + z\mathcal{L}|r_0\rangle\rangle) \tag{11.69}$$

$$= \mathcal{L}|\xi\rangle\rangle . \tag{11.70}$$

Therefore, if $|\xi\rangle\rangle$ is a solution, $|\xi'\rangle\rangle$ is one also. The solution is determined uniquely by using

$$\mathcal{P}|\xi\rangle\rangle = \mathcal{P}\mathcal{Q}\mathcal{L}^{-1}\mathcal{Q}|\hat{B}\rangle\rangle = 0 \tag{11.71}$$

since $\mathcal{P}\mathcal{Q} = 0$. Writing out the left hand side explicitly, we have

$$\mathcal{P}|\xi\rangle\rangle = |r_0\rangle\rangle\langle\langle l_0|\xi\rangle\rangle = |r_0\rangle\rangle\text{Tr}_{sys}[\hat{\xi}] = 0 , \tag{11.72}$$

and therefore $\text{Tr}_{sys}[\hat{\xi}] = 0$. A corollary of $\mathcal{P}|\xi\rangle\rangle = 0$ is that $\mathcal{Q}|\xi\rangle\rangle = |\xi\rangle\rangle$, and therefore, from any result $|\xi'\rangle\rangle$ the unique solution $|\xi\rangle\rangle$ can be obtained using

$$|\xi\rangle\rangle = \mathcal{Q}|\xi'\rangle\rangle = |\xi'\rangle\rangle - |r_0\rangle\rangle\text{Tr}_{sys}[\xi'] \tag{11.73}$$

It is in general not a good idea to proceed directly, first solving for any $|\xi\rangle\rangle$ and then using Eq.(11.73) to find the unique solution because in this case the matrix badly conditioned. Moreover, the presence of an infinite number of solution for this undetermined system of equation was shown empirically to affect significantly the numerical accuracy of the solution.

We instead solve Eq.(11.67) *under the condition* $\text{Tr}[\hat{\xi}] = 0$, again using the PARDISO solver. By inserting directly this condition in $(\mathcal{L} + x)$, the obtained solution always verifies $\mathcal{Q}|\xi\rangle\rangle = |\xi\rangle\rangle$ and the numerical accuracy of the results is increased. We verified that our implementation of the algorithm presented in this chapter reproduces the complete (unsymmetrized) charge-noise spectrum of the SSET near the DJQP, as well as the displacement spectrum $S_x(\omega)$ of a thermal oscillator coupled solely to a thermal bath.

11.7.3 Reducing the size of the problem

To improve the speed of the calculation, and, more importantly, to increase numerical accuracy, we can manually discard matrix elements of ρ which we know will be zero. For example, as discussed in the last chapter, no coherence can be created between

states with 1 and 2 charges, since they are not coupled by any Josephson coupling. We can therefore drop the whole $\rho_{1,2}$ subspace of the density matrix, as well as other subspaces corresponding to charge states not coupled via a cooper-pair tunneling process. Instead of dealing with a $\text{vec}(\rho)$ of dimension $16N^2 \times 1$, we concentrate on the relevant $(8N^2 \times 1)$ non-zero matrix elements. In the code, this is implemented using a "selection" matrix $\mathcal{S}$ that allows to transfer from the complete space to the relevant space.

To explain the idea behind the selection matrix, let us look at the how it can be used in the case we have only a SSET biased near a DJQP (and no oscillator). In this case, only the density matrix contains 16 elements, but 8 of them are known to be zero. Using the matrix $\mathcal{S}$

$$\mathcal{S} = \begin{pmatrix} 1 & 0 & 0 & 0 & 0 & 0 & 0 & 0 & 0 & 0 & 0 & 0 & 0 & 0 & 0 & 0 \\ 0 & 0 & 0 & 0 & 0 & 1 & 0 & 0 & 0 & 0 & 0 & 0 & 0 & 0 & 0 & 0 \\ 0 & 0 & 0 & 0 & 0 & 0 & 0 & 0 & 0 & 0 & 1 & 0 & 0 & 0 & 0 & 0 \\ 0 & 0 & 0 & 0 & 0 & 0 & 0 & 0 & 0 & 0 & 0 & 0 & 0 & 0 & 0 & 1 \\ 0 & 0 & 1 & 0 & 0 & 0 & 0 & 0 & 0 & 0 & 0 & 0 & 0 & 0 & 0 & 0 \\ 0 & 0 & 0 & 0 & 0 & 0 & 0 & 0 & 1 & 0 & 0 & 0 & 0 & 0 & 0 & 0 \\ 0 & 0 & 0 & 0 & 0 & 0 & 0 & 1 & 0 & 0 & 0 & 0 & 0 & 0 & 0 & 0 \\ 0 & 0 & 0 & 0 & 0 & 0 & 0 & 0 & 0 & 0 & 0 & 0 & 0 & 1 & 0 & 0 \end{pmatrix} \tag{11.74}$$

where $\mathcal{S}\mathcal{S}^\dagger = 1$, we can exclude the irrelevant terms in ρ by looking at

$$\mathcal{S}\text{vec}(\rho) = \begin{pmatrix} \rho_{-1,-1} \\ \rho_{0,0} \\ \rho_{1,1} \\ \rho_{2,2} \\ \rho_{1,-1} \\ \rho_{-1,1} \\ \rho_{2,0} \\ \rho_{0,2} \end{pmatrix} \equiv \text{vec}(\rho_s) , \tag{11.75}$$

where we defined $\text{vec}(\rho_s)$, the vectorized form of the density matrix in the $\mathcal{S}$ subspace. The original eigenproblem

$$\mathcal{L}\text{vec}(\rho) = \lambda\text{vec}(\rho) \tag{11.76}$$

can be recast in the relevant ($\mathcal{S}$) subspace using the selection matrix:

$$\mathcal{L}\text{vec}(\rho) = \lambda\text{vec}(\rho) \rightarrow \mathcal{S}\mathcal{L}\text{vec}(\rho) = \lambda\,\mathcal{S}\,\text{vec}(\rho) \tag{11.77}$$
$$\rightarrow \mathcal{S}\mathcal{L}\mathcal{S}^\dagger \mathcal{S}\text{vec}(\rho) = \lambda\,\mathcal{S}\,\text{vec}(\rho) \tag{11.78}$$
$$\rightarrow \mathcal{L}_s\text{vec}(\rho_p) = \lambda\text{vec}(\rho_s) \tag{11.79}$$

with $S\mathcal{L}S^\dagger = \mathcal{L}_s$ the expression of the Liouvillian in the relevant subspace. Equation (11.79) can be solved for $\text{vec}(\rho_s)$ as explained in Sec. 11.7.1, with the added advantage that the size of the problem is now halved. From $\text{vec}(\rho_s)$, the full density matrix is obtained from

$$S^\dagger \text{vec}(\rho_s) = S^\dagger S \text{vec}(\rho) = \text{vec}(\rho). \tag{11.80}$$

When considering a finite number of phonon states, one cannot use S as presented above, but most adapt S to the number of phonons. In particular, due to the vectorization of the density matrix, it is not right to replace each '1' in the previous expression of P by a $N^2 \times N^2$ identity matrix. Finally, we note that the 'selection-matrix' formalism described here can be adapted to make a further selection in phonon space (i.e., drop terms $\rho_{j,k}^{n_{\text{osc}},n_{\text{osc}}+\Delta}$ for $|\Delta| \gg 1$). For $\Delta \sim 25$, a value that corresponds to keeping all terms in a 50-lines wide diagonal band, this makes it possible to truncate the spectrum at $N \sim 750$ on a workstation with 8GB of RAM and at $N \gtrsim 1000$ with 16GB.

Part V

Conclusion and outlook

Conclusions and outlook

A detailed summary of the original research presented in this thesis was already given in Secs. 3.5, 8.5, 9.4, and 11.6, so we refrain from simply repeating the content of these sections here. Instead, at this point we will try to look back at the results from a broad, overall perspective: What did we learn? What are the general conclusions that can be drawn from the work presented here?

If we had to answer these question in only two sentences, we would say: "The effective environment model accurately describes the back-action of a detector on the mechanical oscillator. This model has, however, some limitations".

Indeed. A constant theme throughout this thesis was the idea that the back-action of the detector on the oscillator could be modeled as an effective environment. This result, first formulated in the context of NEMS in [Mozyrsky02] and formalized in [Clerk04a] was even rederived in a totally new way from a master-equation approach in Sec. 7.2. This model was shown to accurately describe the stationary state of a mechanical oscillator coupled to a SET in the weak-coupling regime (as discussed in Chap. 3) and of a mechanical oscillator coupled to a tunnel junction (Part III). It also proved invaluable to describe the back-action of the SSET near the DJQP. More generally, this model is central to the many schemes of "back-action cooling" of the oscillator that have been proposed lately.

The work presented in this thesis however shows that the description via an effective environment has its limitations. The first one was encountered in our study of the SET - mechanical resonator system in the strong coupling regime. In this regime, the stationary state of the oscillator was proven to be far from gaussian. The breakdown of a model derived in the weak-coupling limit when coupling is increased, or in the presence of strong feedback effects, is not surprising. This is however a limitation that must be kept in mind when using the effective thermal model. Another limitation of the model is that it does not always describe the effect of the oscillator on the detector reliably. For example, the signature of the oscillator in the charge-noise spectrum of

the SSET was shown to differ from the one of a purely thermal oscillator. Another example is the presence of quantum corrections in the average current and current-noise of the tunnel junction [Eqs. (7.76), (7.89)] that lead to the possibility of measuring momentum fluctuations of the oscillator using position-coupled tunnel junctions.

12.1 Outlook

In the light of the work presented in this thesis, it is tempting to discuss some ideas about the different research directions that could be followed in the future.

A simple extension of the work presented here would be to investigate the properties of the quantum point contact displacement detector, that is go beyond the $|t_0| \ll 1$ approximation used in Part III. This problem is especially relevant when one realizes that the gain of the tunnel junction is proportional to t_0, such that from a practical point of view the very low transparency limit is not the most attractive regime to carry out experiments. Indeed, the two most recent experiments reviewed in Chap. 5 where realized outside the $|t_0| \ll 1$ parameter range. In the weak-coupling limit, one expects the effective environment model to hold. Considering the case of a QPC embedded in a 2DEG where the coupling term can be written in terms of the interaction between the mechanical element and a charge density in the QPC, the effective environment can be derived from the calculation of the charge noise properties of the QPC. In this case, the role of screening and quantum capacitance in position measurements could be estimated[Pedersen98; Pilgram02].

More generally, but still in the spirit of the work presented in this thesis, it would be very interesting to refine the effective environment paradigm. The strong analogy between the coupling to the environment and the coupling to the detector expressed in the effective environment model suggests that the many refinements to the Caldeira-Leggett model developed in the context of quantum dissipation could be exploited to develop a more elaborate understanding of the general effect that the detector back-action has on the oscillator.

From the point of view of a theorist, it is of course very tempting to consider the realm of quantum NEMS: entanglement of mechanical objects with other quantum systems, superposition of states, non-classical states etc. Recent demonstrations of back-action cooling as well as theoretical proposals of schemes that allow back-action cooling to the ground state of the oscillators fueled the theoretical interest in this direction, and some exciting new physics might arise deep in the quantum regime (for example, new decoherence channels like the "gravitational collapse" [Diosi89; Penrose96; Kleckner08]).

My personal opinion is however that the most interesting currently open problems are not those where the oscillator in taken to be in this deep quantum limit. Indeed,

resonators at temperatures well below $\hbar\Omega$ are not especially exciting unless they can be controlled and monitored or, in other words, unless quantum-limited sensitivity for displacement detection is available experimentally. From this point of view, the relatively poor quantitative agreement between theory and experiments in the field of nanomechanics could be seen as worrying. One of the most compelling arguments in favor of using mesoscopic detectors as the electrical element in NEMS is (besides their exquisite sensitivity) the possibility to accurately describe these systems theoretically and evaluate the regimes in which the very stringent conditions for quantum-limited position sensing can be reached. From this aspect, it becomes of primary interest to investigate whether the observed deviations between theory and experiment are intrinsic to the detectors used (i.e. due to higher-order processes not considered in the current theoretical models) or simply due to technical issues that could be improved in next-generation devices. Here, only three detectors were discussed (the SET, the tunnel junction, and the SSET), while in fact multiple other candidates for quantum-limited detection have recently been realized experimentally, for example the SQUID[Etaki08] and the microwave cavity[Regal08]. At the time of writing this thesis, it is too soon to foresee which type of detector, if any, will allow the quantum limit to be reached. Only the continued theoretical and experimental exploration of all these avenues will provide this answer.

Part VI

Backmatter

The MacDonald formula

In many chapters of this thesis a result known as 'the MacDonald formula' was used. In this appendix, we present a derivation of this result[Macdonald49c; MacDonald49a; MacDonald49b; MacDonald62]. For definitiveness, we will derive it in the context of a current noise, but this result can be applied very generally to express the symmetrized power spectrum of some quantity in terms of a generalized displacement.

Let's first explain what we mean by generalized displacement. Consider $y(t)$, a statistically stationary variable[1]. The generalized displacement $Y(T)$ is defined as

$$Y(T) = \int_{t_0}^{t_0+T} y(t)dt \ .$$ (A.1)

In our example where $y(t)$ is a current, $Y(T)$ is the number of charges transmitted through the junction from time t_0 to $t_0 + T$. Had $y(t)$ referred to the momentum $[y(t) \leftrightarrow p(t)]$ of a particle undergoing Brownian motion, then $Y(T) = x(T) - x(t_0)$ would have been the displacement of this particle between times T and t_0, since $x(T) - x(t_0) = \int_{t_0}^{T+t_0} p(t)dt/M$. Since we consider stochastically stationary processes, we can set $t_0 = 0$ in the following discussion without loss of generality.

From Eq. (A.1), we obtain

$$\langle Y^2(T) \rangle = \int_0^T dt \int_0^T dt' \langle y(t)y(t') \rangle \ .$$ (A.2)

Introducing the symmetric correlation function

$$K_y(\tau) = \langle y(t+\tau)y(t) \rangle \ ,$$ (A.3)

---

[1]In this context, the term "statistically stationary" reflects the fact that the correlation function $\langle y(t_2)y(t_1) \rangle$ is a function of $t_2 - t_1$ only (at not of t_1 or t_2 individually). Importantly, from this definition one sees that a statistically stationary variable necessarily has mean zero. For variables where $\langle y \rangle \neq 0$, one should consider the zero-mean variable $y - \langle y \rangle$.

which, in the steady-state is a function only of τ, we see that the average $Y^2(T)$ is related to the integral of the correlation function $K_y(t - t')$. In terms of center-of-mass and relative time coordinates

$$\bar{t} = t + t' \, , \tag{A.4}$$

$$t_r = t - t' \, , \tag{A.5}$$

this integral can be rewritten

$$\langle Y^2(T) \rangle = 2 \int_0^T d\bar{t} \int_0^{T - \bar{t}} dt_r \, K_y(t_r) \, , \tag{A.6}$$

$$= 2 \int_0^T dt_r \int_0^{T - t_r} d\bar{t} \, K_y(t_r) \, , \tag{A.7}$$

$$= 2 \int_0^T dt_r (T - t_r) K_y(t_r) \, . \tag{A.8}$$

In Eq. (6.4), we defined the symmetrized power spectrum

$$\bar{S}_y(\omega) = \frac{1}{2} \int_{-\infty}^{\infty} \langle \{y(\tau), y(0)\} \rangle e^{i\omega\tau} d\tau \, , \tag{A.9}$$

$$= 2 \int_0^{\infty} d\tau \, \cos(\omega\tau) K_y(\tau) \, . \tag{A.10}$$

Taking the inverse Fourier transform of the last expression, we can express the correlation function as

$$K_y(\tau) = \int_0^{\infty} \cos(\omega\tau) \bar{S}_y(\omega) \frac{d\omega}{2\pi} \, . \tag{A.11}$$

We now insert Eq. (A.11) into Eq. (A.8) to find

$$\langle Y^2(T) \rangle = 2 \int_0^T dt_r (T - t_r) \int_0^{\infty} \cos(\omega t_r) \bar{S}_y(\omega) \frac{d\omega}{2\pi} \, . \tag{A.12}$$

Using

$$\int_0^T \cos(\omega t)(T - t) dt = \frac{1 - \cos(\omega T)}{\omega^2} \tag{A.13}$$

this is rewritten as

$$\langle Y^2(T) \rangle = 2 \int_0^{\infty} \frac{1 - \cos(\omega T)}{\omega^2} \bar{S}_y(\omega) \frac{d\omega}{2\pi} \, . \tag{A.14}$$

Taking the time derivative on both sides

$$\frac{d}{dt} \langle Y^2(T) \rangle = \int_0^{\infty} \frac{\sin(\omega T)}{\omega} \bar{S}_y(\omega) \frac{d\omega}{2\pi} \, . \tag{A.15}$$

Finally, by applying an inverse Fourier transform, we find

$$\bar{S}_y(\omega) = \omega \int_0^{\infty} dt \sin(\omega t) \frac{d}{dt} \langle Y^2(t) \rangle \, . \tag{A.16}$$

This is the MacDonald formula.

The Caldeira-Leggett master equation

Since it describes quantum brownian motion, the Caldeira-Leggett equation obtained in Eq. (7.26) plays a central role in the context of nanomechanical systems and we will therefore, in this Appendix, outline the basic ideas behind its derivation for a thermal environment. First however let us focus for a moment on the very broad question of dissipation (damping) at the quantum mechanical level, considering for definitiveness the example of the undriven damped harmonic oscillator[1].

When studying the classical harmonic oscillator, damping can be introduced by modifying the equations of motion of x, p

$$\dot{x} = p/M \,, \tag{B.1a}$$

$$\dot{p} = -M\Omega^2 x \,, \tag{B.1b}$$

to include a dissipative force term

$$\dot{x} = p/M \,, \tag{B.2a}$$

$$\dot{p} = -M\Omega^2 x - \gamma p \,. \tag{B.2b}$$

This leads to the well-known second-order differential equation for x,

$$\ddot{x} + \gamma \dot{x} + M\Omega^2 x = 0 \,. \tag{B.3}$$

How can this be translated to the quantum regime? Following the usual (canonical quantization) approach, one associates to the classical variables x, p the quantum-mechanical operators $\hat{x}, \hat{p}$ that fulfill the commutation relation $[\hat{x}, \hat{p}] = i\hbar$. In the absence of damping, one can show that the associated equation of motion (calculated using the commutation relation of the operator with the Hamiltonian) for the expectation values $\langle x \rangle, \langle p \rangle$ are equivalent to Eq. (B.1). Moreover when, following the classical

---

[1]The historical part of the discussion is inspired from [Harris90; Grabert88]

Newtonian equation-of-motion, one adds a term $-\gamma\hat{p}$ to the equation-of-motion for $\hat{p}$, then the time-evolution of the expectation values of $\hat{x}, \hat{p}$ in the quantum case follow Eq. B.2. Sadly, in this case one finds that the time-evolution of the commutator $[\hat{x}, \hat{p}]$ is

$$\frac{d}{dt}[\hat{x}, \hat{p}] = -\gamma[\hat{x}, \hat{p}] \, , \tag{B.4}$$

and, in other words, that $[\hat{x}(t), \hat{p}(t)] = i\hbar e^{-\gamma t}$. This exponential decay of the commutator leads to a violation of Heisenberg's uncertainty principle, an unphysical result that proves that one cannot simply expect a quantized version of the classical Newtonian equations-of-motion for the damped harmonic oscillator to describe quantum-mechanical dissipation[Senitzky60; Carmichael02].

In fact, historically the problem of dissipation at the quantum level turned out to be quite resilient. While the (undamped) harmonic oscillator was one of the first problem solved using modern quantum-mechanics[Heisenberg25], there was as recently as 1980 no consensus regarding the optimal way to include damping in this system[Dekker81]. At the time, two of the leading models used to treat damping at the quantum-mechanical level were the "Kanai" model[Kanai50], where damping was introduced via the time-dependent Hamiltonian $H = (p^2/2m)e^{-\gamma t} + V(x)e^{\gamma t}$, and the "Kostin" model[Kostin72], that used a time-independent, non-linear potential to model damping. While these models did reproduce some of the expected features of a damped harmonic oscillator, they also lead to some unphysical conclusions[Greenberger79] and were therefore not deemed satisfactory models for quantum dissipation.

A salient trait of these early models is that they tried to include damping via a modification of the description of the *isolated* harmonic oscillator. In [Caldeira81; Caldeira83], Caldeira and Leggett adopted the point of view that dissipation arises from the interaction of the quantum system with the environment and is therefore not a property of the isolated quantum system. By including both the system and the environment in their description, one could use 'standard' quantum mechanics to obtain a satisfactory description of dissipation at the quantum level. This led to the Caldeira-Leggett description of quantum brownian motion, a model sometimes referred to as "the prototype of a system-reservoir model for the description of dissipation phenomena in solid-state physics"[Breuer02].

In the Caldeira-Leggett approach, one assumes that the full (system+environment) Hamiltonian is given by $H_{\text{tot}} = H_{\text{sys}} + H_{\text{B}} + H_{\text{int}}$ The bath is assumed to consist of a large number of harmonic oscillators of frequency ω_n and mass m_n, such that

$$H_B = \sum_n \hbar\omega_n(b_n^\dagger b_n + \frac{1}{2}) = \sum_n \left(\frac{\hat{p}_n^2}{2m_n} + \frac{m_n\omega_n^2 x_n^2}{2} \right) \, , \tag{B.5}$$

with $b_n^\dagger$ the annihilation (creation) operator associated with the n-th harmonic oscillator. The interaction between bath and system is assumed to be linear in x_n, the coordinate of oscillator n as well as in $\hat{x}$, the position operator of the system:

$$H_{\text{int}} = -\hat{x} \sum_n \kappa_n x_n = -\hat{x}\hat{F} , \tag{B.6}$$

where, as previously, used $\hat{F}$ to denote the bath operator. This combination of a harmonic oscillator bath and linear interaction turns out to generally be a good description for a generic environment[2]. To make the damping translation-invariant, a *counter-term* is also included in the model,

$$H_c = x^2 \sum_n \frac{\kappa_n}{2m_n \omega_n^2} . \tag{B.7}$$

Taken together, Eqs. (B.5-B.7) describe dissipation in the CL model.

To solve for the equation of motion of the density matrix of the system in the presence of the bath, methods of a varying level of sophistication can be used[Grabert88], allowing for different regimes of approximations to be explored. Here we present a simple derivation of the CL master equation for a harmonic oscillator (of mass M and frequency Ω) whose starting point is the Born-Markov equation of motion Eq. (7.14): it is therefore valid in the weakly-damped (Born approximation), high-temperature limit (Markov approximation). Since the interaction Hamiltonian [Eq. (B.6)] has exactly the same form as Eq. (7.16), the equation of motion of the system density matrix can be directly rewritten as Eq. (7.24), the only difference being the counter term H_C.

$$
\begin{aligned}
\frac{d}{dt}\rho_{\text{sys}}(t) = &\frac{-i}{\hbar}[H_{\text{sys}} + H_c, \rho_{\text{sys}}(t)] - \frac{1}{2\hbar^2}[\hat{x}, [\hat{x}, \rho_{\text{sys}}(t)]] \int_0^\infty dt' \cos(\Omega t')\mathcal{F}_+(t') \\
&+ \frac{1}{2M\hbar^2\Omega}[\hat{x}, [\hat{p}, \rho_{\text{sys}}(t)]] \int_0^\infty dt' \sin(\Omega t')\mathcal{F}_+(t') \\
&- \frac{1}{2\hbar^2}[\hat{x}, \{\hat{x}, \rho_{\text{sys}}(t)\}] \int_0^\infty dt' \cos(\Omega t')\mathcal{F}_-(t') \\
&+ \frac{1}{2M\hbar^2\Omega}[\hat{x}, \{\hat{p}, \rho_{\text{sys}}(t)\}] \int_0^\infty dt' \sin(\Omega t')\mathcal{F}_-(t') .
\end{aligned} \tag{B.8}
$$

Once again, the effect of the bath on the oscillator depends on the correlation functions of the bath

$$\mathcal{F}_+(t) = \langle \{F(t), F(0)\} \rangle = \text{Tr}\{F(t), F(0)\}\rho_B , \tag{B.9}$$
$$\mathcal{F}_-(t) = \langle [F(t), F(0)] \rangle = \text{Tr}[F(t), F(0)]\rho_B . \tag{B.10}$$

---

[2]We note that this exact form of H_B, H_{int} had already been used to model dissipation as early as the mid-sixties [Senitzky60; Senitzky61; Ford65; Grabert88].

The environment (the bath), is in thermal equilibrium (at temperature T) such that density matrix ρ_B is given by

$$\rho_B = \frac{e^{-\beta H_B}}{\text{Tr}_B e^{-\beta H_B}},\tag{B.11}$$

with $\beta^{-1} = k_B T$. Following [Breuer02], we write the different correlation functions $\mathcal{F}_\pm$

$$\mathcal{F}_+(t) = 2\hbar \int_0^\infty d\omega\, J(\omega) \coth\left(\frac{\hbar\omega}{2k_B T}\right) \cos(\omega t),\tag{B.12a}$$

$$\mathcal{F}_-(t) = -2i\hbar \int_0^\infty d\omega\, J(\omega) \sin(\omega t),\tag{B.12b}$$

in terms of the spectral density $J(\omega)$

$$J(\omega) = \sum_n \frac{\kappa_n^2}{2m_n\omega_n} \delta(\omega - \omega_n).\tag{B.13}$$

In order for the environment to provide frequency-independent damping, we consider an Ohmic spectral density, with a "Lorentz-Drude" cutoff function

$$J(\omega) = \frac{2M\tilde{\gamma}}{\pi}\omega \frac{\omega_c^2}{\omega_c^2 + \omega^2},\tag{B.14}$$

with ω_c a cutoff-frequency chosen to be large when compared to the natural frequency Ω of the harmonic oscillator. Using this spectral density, the correlation functions [Eq. (B.12)] can be evaluated analytically and then inserted back into Eq. (B.8). Taking the limit $\omega_c \gg \Omega$, we find that[Breuer02, Chap. 10] :(i) the $\sim [x, \{x, \rho\}]$ term cancels exactly the counter-term H_c (ii) the $\sim [\hat{x}, [\hat{p}, \rho_{\text{sys}}(t)]]$ can be neglected[3] and (iii)

$$\frac{1}{2\hbar^2}[\hat{x}, [\hat{x}, \rho_{\text{sys}}(t)]] \int_0^\infty dt' \cos(\Omega t')\mathcal{F}_+(t') = \frac{1}{\hbar^2}M\tilde{\gamma}\hbar\Omega \coth\left(\frac{\hbar\Omega}{2k_B T}\right) [\hat{x}, [\hat{x}, \rho_{\text{sys}}(t)]],\tag{B.15a}$$

$$\frac{1}{2M\hbar\Omega}[\hat{x}, \{\hat{p}, \rho_{\text{sys}}(t)\}] \int_0^\infty dt' \sin(\Omega t')\mathcal{F}_-(t') = -\frac{i}{\hbar}\tilde{\gamma}[\hat{x}, \{\hat{p}, \rho_{\text{sys}}(t)\}].\tag{B.15b}$$

Putting all the terms together, one finally finds the CL master equation,

$$\frac{d}{dt}\rho_{\text{sys}} = -\frac{i}{\hbar}[H_{\text{sys}}, \rho_{\text{sys}}] - \frac{1}{\hbar^2}D[\hat{x}, [\hat{x}, \rho_{\text{sys}}]] - \frac{i\tilde{\gamma}}{\hbar}[\hat{x}, \{\hat{p}, \rho_{\text{sys}}\}],\tag{B.16}$$

---

[3]More precisely, the term $\sim [\hat{x}, [\hat{p}, \rho_{\text{sys}}(t)]]$ only contributes by a factor $\sim \Omega/\omega_c \ll 1$ as much as the $\sim [\hat{x}, [\hat{x}, \rho_{\text{sys}}(t)]]$ term.

with the "diffusion constant" D given by

$$D = M\tilde{\gamma}\hbar\Omega \coth\left(\frac{\hbar\Omega}{2k_B T}\right) \tag{B.17}$$

$$\simeq 2M\tilde{\gamma}k_B T \qquad [\text{when } k_B T \gg \hbar\Omega] \tag{B.18}$$

The first term describes the coherent dynamics of the quantum system, the second term models the thermal fluctuations and the last term ($\sim \tilde{\gamma}$) gives rise to damping[4].

In order to illustrate that Eq. (B.16) reproduces the motion of a damped harmonic oscillator one can look at the equation of motion for different expectation values. Using the general relations

$$\text{Tr}\,\hat{x}^j\hat{p}^k[\hat{H}_0, \hat{\rho}] = i\hbar\left(\frac{1}{M}j\langle\hat{x}^{j-1}\hat{p}^{k+1}\rangle - M\Omega^2 k\langle\hat{x}^{j+1}\hat{p}^{k-1}\rangle\right)$$
$$+ \frac{\hbar^2}{2}\left(\frac{1}{M}j(j-1)\langle\hat{x}^{j-2}\hat{p}^k\rangle - M\Omega^2 k(k-1)\langle\hat{x}^j\hat{p}^{k-2}\rangle\right) \tag{B.19}$$

$$\text{Tr}\,\hat{x}^j\hat{p}^k[\hat{x}, \{\hat{p}, \hat{\rho}\}] = -2i\hbar k\langle\hat{x}^j\hat{p}^k\rangle - \hbar^2 jk\langle\hat{x}^{j-1}\hat{p}^{k-1}\rangle \tag{B.20}$$

$$\text{Tr}\,\hat{x}^j\hat{p}^k[\hat{x}, [\hat{x}, \hat{\rho}]] = -\hbar^2 k(k-1)\langle\hat{x}^j\hat{p}^{k-2}\rangle \tag{B.21}$$

we find

$$\frac{d}{dt}\langle x\rangle = \frac{\langle p\rangle}{M}, \tag{B.22}$$

$$\frac{d}{dt}\langle p\rangle = -2\tilde{\gamma}\langle p\rangle - M\Omega^2\langle x\rangle, \tag{B.23}$$

$$\frac{d}{dt}\langle x^2\rangle = \frac{1}{M}\tilde{\gamma}\langle xp + px\rangle, \tag{B.24}$$

$$\frac{d}{dt}\langle xp + px\rangle = \frac{2}{M}\langle p^2\rangle - 2\langle M\Omega^2 x^2\rangle - 2\tilde{\gamma}\langle xp + px\rangle, \tag{B.25}$$

$$\frac{d}{dt}\langle p^2\rangle = -M\Omega^2\langle xp + px\rangle - 4\tilde{\gamma}\langle p\rangle + 4M\tilde{\gamma}k_B T. \tag{B.26}$$

These correspond exactly to the equations of motion for the two first moments of coordinate and momentum of a damped harmonic oscillator and prove the applicability of the description of coupling to a thermal bath provided by the CL model. Also, in the density-matrix formalism, it is easy to verify that the commutator $[\hat{x}, \hat{p}]$ does not evolve - at least in the mean-level: $\langle[\hat{x}, \hat{p}](t)\rangle = \text{Tr}\{[\hat{x}, \hat{p}]\rho(t)\} = i\hbar\text{Tr}\{\rho(t)\} = i\hbar$.

As mentioned earlier, the Caldeira-Leggett model plays a central role in the discussion of quantum dissipation. It was therefore studied at length, and the avid reader who wants to learn more about this model is invited to look into e.g. [Breuer02] and references therein.

---

[4]Note that the damping term is sometimes defined with a pre-factor $(1/2)$. In this case, the damping contribution to equation of motion for $\langle p\rangle$ reads $-\gamma\langle p\rangle$ and not $-2\tilde{\gamma}\langle p\rangle$ as in Eq. (B.23). Since for historical reasons both conventions are used in different part of this document, we took care to use a tilde to distinguish both definitions: $2\tilde{\gamma} = \gamma$.

Derivation of the condition on quantum-limited detection

To conclude this chapter, we sketch a derivation of Eq. (4.17). We proceed along the lines suggested in [Clerk04a], generalizing the derivation presented in Ref. [Clerk03b] to finite frequencies. We start by writing the different symmetrized correlation functions as a sum over transitions from initial ($|i\rangle$) to final states ($|f\rangle$), with $|i\rangle$ and $|f\rangle$ eigenstates of H_D with energy $E_{i(f)}$

$$\overline{S}_I(\omega) = \pi\hbar \sum_{i,f} \langle i|\rho_{D,0}|i\rangle \left[\delta(E_f - E_i + \hbar\omega) + \delta(E_f - E_i - \hbar\omega)\right] |\langle f|\hat{I}|i\rangle|^2 \,,$$

(C.1a)

$$\overline{S}_F(\omega) = \pi\hbar \sum_{i,f} \langle i|\rho_{D,0}|i\rangle \left[\delta(E_f - E_i + \hbar\omega) + \delta(E_f - E_i - \hbar\omega)\right] |\langle f|\hat{F}|i\rangle|^2 \,,$$

(C.1b)

$$\frac{S_{IF}(\omega) + S_{IF}(-\omega)}{2\pi\hbar} = \sum_{i,f} \langle i|\rho_{D,0}|i\rangle \left[\delta(E_f - E_i + \hbar\omega) + \delta(E_f - E_i - \hbar\omega)\right] \langle f|\hat{I}|i\rangle\langle i|\hat{F}|f\rangle \,.$$

(C.1c)

We assumed that $\rho_{D,0}$, the stationary density matrix describing the detector, is diagonal in the basis of the eigenstates of H_D. As pointed out in [Averin03a; Averin03b; Clerk03b], each line of Eq. (C.1) can be interpreted as a scalar product over the space defined by the matrix elements of $\hat{I}, \hat{F}$ at a given energy. The Cauchy-Schwarz inequality associated with this scalar product reads

$$\overline{S}_I(\omega)\overline{S}_F(\omega) \geq |\frac{S_{IF}(\omega) + S_{IF}(-\omega)}{2}|^2$$

$$= (\mathrm{Im}[\frac{S_{IF}(\omega) + S_{IF}(-\omega)}{2}])^2 + (\mathrm{Re}[\frac{S_{IF}(\omega) + S_{IF}(-\omega)}{2}])^2 \,. \quad \text{(C.2)}$$

We note that the inequality does not relate $\overline{S}_I\overline{S}_F$ directly to $\overline{S}_{IF}$, but to $S_{IF}(\omega) + S_{IF}(-\omega)$, a quantity totally symmetric in ω whereas $\text{Im}[\overline{S}_{IF}(\omega)] = -\text{Im}[\overline{S}_{IF}(-\omega)]$, as can be seen from

$$\overline{S}_{IF}(\omega) = \frac{1}{2}[S_{IF}(\omega) + S_{IF}(-\omega)^*] \, . \tag{C.3}$$

Also, since[1],

$$\hbar[\lambda(\omega) - \lambda'(\omega)^*] = -i[S_{IF}(\omega) - S_{IF}^*(-\omega)] \, , \tag{C.4}$$

we can associate the imaginary part of the symmetrized S_{IF} correlation function to the x-to-I gain

$$\text{Im}[\frac{S_{IF}(\omega) + S_{IF}(-\omega)}{2}] = \frac{\hbar}{2}\text{Re}[\lambda(\omega) - \lambda'(\omega)] \, . \tag{C.5}$$

Finally, using

$$\text{Re}[\frac{S_{IF}(\omega) + S_{IF}(-\omega)}{2}] = \text{Re}[\overline{S}_{IF}(\omega)] \, , \tag{C.6}$$

we can combine Eqs. (C.2) and (C.5), to finally find Eq. (4.17),

$$\overline{S}_I(\omega)\overline{S}_F(\omega) \geq \frac{\hbar^2}{4}\left(\text{Re}[\lambda(\omega) - \lambda'(\omega)]\right)^2 + \left(\text{Re}[\overline{S}_{IF}(\omega)]\right)^2 \, . \tag{C.7}$$

This completes the proof of Eq. (4.17).

---

[1]This relation does not correspond to Eq. (B1) of [Clerk04a], but it matches Averin's result [Averin03b, Eq. (11)]. Clerk's result is one of three typographic errors in Appendix B. It is clearly a mistake, as it would lead to $\lambda \sim \text{Im}[\overline{S}_{IF}]$, a quantity that Clerk shows vanishes as $\hbar\Omega/kT_{\text{eff}}$. This error is also corrected in [Clerk08].

Bibliography

[Aleiner97]   I. Aleiner, N. Wingreen and Y. Meir. *Dephasing and the Orthogonality Catastrophe in Tunneling through a Quantum Dot: The "Which Path?" Interferometer*. Phys. Rev. Lett. **79**, 3740 (1997).

[Amman89]   M. Amman, K. Mullen and E. Ben-Jacob. *The charge-effect transistor*. J. Appl. Phys. **65**, 339 (1989).

[Armour01]   A. Armour and M. Blencowe. *Possibility of an electromechanical which-path interferometer*. Phys. Rev. B **64**, 035311 (2001).

[Armour02]   A. Armour, M. Blencowe and K. Schwab. *Entanglement and Decoherence of a Micromechanical Resonator via Coupling to a Cooper-Pair Box*. Phys. Rev. Lett. **88**, 148301 (2002).

[Armour04a]   A. Armour. *Current noise of a single-electron transistor coupled to a nanomechanical resonator*. Phys. Rev. B **70**, 165315 (2004).

[Armour04b]   A. Armour, M. Blencowe and Y. Zhang. *Classical dynamics of a nanomechanical resonator coupled to a single-electron transistor*. Phys. Rev. B **69**, 125313 (2004).

[Arnoldi51]   W. Arnoldi. *The principle of minimized iterations in the solution of the matrix eigenvalue problem*. Quart. J. Applied Mathematics **9**, 17 (1951).

[Averin89]   D. Averin and V. Aleshkin. *Resonance tunneling of Cooper pairs in a system of two small Josephson junctions*. JETP Letters **50**, 367 (1989).

[Averin91]   D. Averin, A. Korotkov and K. Likharev. *Theory of single-electron charging of quantum wells and dots*. Phys. Rev. B **44**, 6199 (1991).

[Averin00]   D. Averin. *Quantum Computing and Quantum Measurement with Mesoscopic Josephson Junctions*. Fortschr. Phys. **48**, 1055 (2000).

[Averin03a]   D. Averin. *Exploring the Quantum-Classical Frontier: Recent Advances in Macroscopic and Mesoscopic Quantum Phenomena.* arXiv:cond-mat/0004364v1 [cond-mat.mes-hall] (2004).

[Averin03b]   D. Averin. *Linear quantum measurements.* arXiv:cond-mat/0301524v1 [cond-mat.mes-hall] (2003).

[Averin05]   D. Averin and E. Sukhorukov. *Counting Statistics and Detector Properties of Quantum Point Contacts.* Phys. Rev. Lett. **95**, 126803 (2005).

[Averin06]   D. Averin. *Mesoscopic quantum measurements.* arXiv:cond-mat/0603802v1 [cond-mat.mes-hall] (2006).

[Badzey05]   R. Badzey and P. Mohanty. *Coherent signal amplification in bistable nanomechanical oscillators by stochastic resonance.* Nature **437**, 995 (2005).

[Bagrets03]   D. Bagrets and Y. Nazarov. *Full counting statistics of charge transfer in Coulomb blockade systems.* Phys. Rev. B **67**, 085316 (2003).

[Ball08]   P. Ball. *Physics: Quantum all the way.* Nature **453**, 22 (2008).

[Beenakker91]   C. W. J. Beenakker. *Theory of Coulomb-blockade oscillations in the conductance of a quantum dot.* Phys. Rev. B **44**, 1646 (1991).

[Belzig04]   W. Belzig. *Full Counting Statistics in Quantum Contacts.* CFN Lectures on Functional Nanostructures **1**, 123 (2004).

[Belzig05]   W. Belzig. *Full counting statistics of super-Poissonian shot noise in multilevel quantum dots.* Phys. Rev. B **71**, 161301 (2005).

[Bennett06]   S. Bennett and A. Clerk. *Laser-like instabilities in quantum nanoelectromechanical systems.* Phys. Rev. B **74**, 201301 (2006).

[Bennett08]   S. D. Bennett and A. A. Clerk. *Full counting statistics and conditional evolution in a nanoelectromechanical system.* Phys. Rev. B **78**, 165328 (2008).

[Blanter00]   Y. Blanter and M. Büttiker. *Shot noise in mesoscopic conductors.* Phys. Rep. **336**, 1 (2000).

[Blanter04]   Y. Blanter, O. Usmani and Y. Nazarov. *Single-Electron Tunneling with Strong Mechanical Feedback.* Phys. Rev. Lett. **93**, 136802 (2004).

[Blanter05]   Y. M. Blanter, O. Usmani, and Y. V. Nazarov. *Erratum: Single-Electron Tunneling with Strong Mechanical Feedback [Phys. Rev. Lett. 93, 136802 (2004)].* Phys. Rev. Lett. **94**, 049904 (2005).

[Blanter06]   Y. Blanter. *Recent Advances in Studies of Current Noise.* Springer Lecture Notes CFN Summer School 2005 on Nano-Electronics (2006).

[Blencowe00]   M. Blencowe and M. Wybourne. *Sensitivity of a micromechanical displacement detector based on the radio-frequency single-electron transistor.* Appl. Phys. Lett. **77**, 3845 (2000).

[Blencowe05a]   M. Blencowe. *Nanoelectromechanical systems.* Contemp. Phys. **46**, 249 (2005).

[Blencowe05b]   M. Blencowe, J. Imbers and A. Armour. *Dynamics of a nanomechanical resonator coupled to a superconducting single-electron transistor.* New J. Phys. **7**, 236 (2005).

[Blick98]   R. Blick, M. Roukes, W. Wegscheider and M. Bichler. *Freely suspended two-dimensional electron gases.* Physica B **249-251 IS -**, 784 (1998).

[Blum96]   K. Blum. *Density Matrix Theory and Applications* (Plenum, New York, 1996), 2nd edition.

[Bocko88]   M. F. Bocko, K. Stephenson and R. Koch. *Vacuum Tunneling Probe: A Nonreciprocal, Reduced-Back-Action Transducer.* Phys. Rev. Lett. **61**, 726 (1988).

[Braginsky80]   V. B. Braginsky, Y. I. Vorontsov and K. Thorne. *Quantum Nondemolition measurements.* Science **209**, 547 (1980).

[Braginsky90]   V. B. Braginsky and F. Khalili. *Gravitational wave antenna with QND speed meter.* Phys. Lett. A **147**, 251 (1990).

[Braginsky95]   V. Braginsky and F. Khalili. *Quantum Measurement* (Cambridge University Press, Cambridge, 1995).

[Braginsky00]   V. B. Braginsky, M. Gorodetsky, F. Khalili and K. Thorne. *Dual-resonator speed meter for a free test mass.* Phys. Rev. D **61**, 044002 (2000).

[Braginsky03]   V. B. Braginsky, M. Gorodetsky, F. Khalili, A. Matsko, K. Thorne and S. Vyatchanin. *Noise in gravitational-wave detectors and other classical-force measurements is not influenced by test-mass quantization.* Phys. Rev. D **67**, 082001 (2003).

[Braig03]   S. Braig and K. Flensberg. *Vibrational sidebands and dissipative tunneling in molecular transistors.* Phys. Rev. B **68**, 205324 (2003).

[Braunstein05]   S. L. Braunstein and P. van Loock. *Quantum information with continuous variables.* Rev. Mod. Phys. **77**, 513 (2005).

[Breuer02]   H. Breuer and F. Petruccione. *The theory of open quantum systems* (Oxford University Press, New York, 2002).

[Bruus04]   H. Bruus and K. Flensberg. *Many-Body Quantum Theory in Condensed Matter Physics: An Introduction* (Oxford University Press, 2004).

[Buehler03]   T. M. Buehler, D. J. Reilly, R. Brenner, A. R. Hamilton, A. S. Dzurak and R. G. Clark. *Correlated charge detection for readout of a solid-state quantum computer.* Appl. Phys. Lett. **82**, 577 (2003).

[Buks98]   E. Buks, R. Schuster, M. Heiblum, D. Mahalu and V. Umansky. *Dephasing in electron interference by a 'which-path' detector.* Nature **391**, 871 (1998).

[Buks01]   E. Buks and M. L. Roukes. *Metastability and the Casimir effect in micromechanical systems.* Europhys. Lett. **54**, 220 (2001).

[Büttiker86]   M. Büttiker. *Four-Terminal Phase-Coherent Conductance.* Phys. Rev. Lett. **57**, 1761 (1986).

[Caldeira81]   A. O. Caldeira and A. J. Leggett. *Influence of Dissipation on Quantum Tunneling in Macroscopic Systems.* Phys. Rev. Lett. **46**, 211 (1981).

[Caldeira83]   A. Caldeira and A. J. Leggett. *Path integral approach to quantum Brownian motion.* Physica A **121**, 587 (1983).

[Carmichael02]   H. Carmichael. *Statistical Methods in Quantum Optics 1: Master Equations and Fokker-Planck Equations* (Springer, New York, 2002), 2nd edition.

[Caves80]   C. Caves, K. Thorne, R. Drever, V. Sandberg and M. Zimmermann. *On the measurement of a weak classical force coupled to a quantum-mechanical oscillator. I. Issues of principle.* Rev. Mod. Phys. **52**, 341 (1980).

[Caves82]   C. Caves. *Quantum limits on noise in linear amplifiers.* Phys. Rev. D **26**, 1817 (1982).

[Choi01]   M.-S. Choi, R. Fazio, J. Siewert and C. Bruder. *Coherent oscillations in a Cooper-pair box.* Europhys. Lett. **53**, 251 (2001).

[Choi03]   M.-S. Choi, F. Plastina and R. Fazio. *Charge and current fluctuations in a superconducting single-electron transistor near a Cooper pair resonance.* Phys. Rev. B **67**, 045105 (2003).

[Chtchelkatchev04] N. Chtchelkatchev, W. Belzig and C. Bruder. *Charge transport through a single-electron transistor with a mechanically oscillating island.* Phys. Rev. B **70**, 193305 (2004).

[Cleland96]   A. N. Cleland and M. Roukes. *Fabrication of high frequency nanometer scale mechanical resonators from bulk Si crystals.* Appl. Phys. Lett. **69**, 2653 (1996).

[Cleland01]   A. N. Cleland, M. Pophristic and I. Ferguson. *Single-crystal aluminum nitride nanomechanical resonators.* Appl. Phys. Lett. **79**, 2070 (2001).

[Cleland02]   A. N. Cleland, J. Aldridge, D. Driscoll and A. Gossard. *Nanomechanical displacement sensing using a quantum point contact.* Appl. Phys. Lett. **81**, 1699 (2002).

[Cleland04]   A. N. Cleland. *Foundations of Nanomechanics* (Springer, 2004).

[Clerk02]   A. Clerk, S. Girvin, A. Nguyen and A. Stone. *Resonant Cooper-Pair Tunneling: Quantum Noise and Measurement Characteristics.* Phys. Rev. Lett. **89**, 176804 (2002).

[Clerk03a]   A. Clerk. *Resonant Cooper-Pair Tunneling: Counting Statistics and Frequency-Dependent Current Noise.* arXiv:cond-mat/0301277v1 [cond-mat.mes-hall] (2003)

[Clerk03b]   A. Clerk, S. Girvin and A. Stone. *Quantum-limited measurement and information in mesoscopic detectors.* Phys. Rev. B **67**, 165324 (2003).

[Clerk04a]   A. Clerk. *Quantum-limited position detection and amplification: A linear response perspective.* Phys. Rev. B **70**, 245306 (2004).

[Clerk04b]   A. Clerk and S. Girvin. *Shot noise of a tunnel junction displacement detector.* Phys. Rev. B **70**, 121303 (2004).

[Clerk05]   A. Clerk and S. Bennett. *Quantum nanoelectromechanics with electrons, quasi-particles and Cooper pairs: effective bath descriptions and strong feedback effects.* New J. Phys. **7**, 238 (2005).

[Clerk08]   A. Clerk, M. H. Devoret, S. M. Girvin, F. Marquardt and R. J. Schoelkopf. *Introduction to Quantum Noise, Measurement and Amplification.* arXiv:0810.4729v1 [cond-mat.mes-hall] (2008).

[Cottet04a]   A. Cottet, W. Belzig and C. Bruder. *Positive cross-correlations due to dynamical channel blockade in a three-terminal quantum dot.* Phys. Rev. B **70**, 115315 (2004).

[Cottet04b]   A. Cottet, W. Belzig and C. Bruder. *Positive Cross Correlations in a Three-Terminal Quantum Dot with Ferromagnetic Contacts.* Phys. Rev. Lett. **92**, 206801 (2004).

[Datta95]   S. Datta. *Electronic Transport in Mesoscopic Systems* (Cambridge University Press, 1995).

[Dekker81]   H. Dekker. *Classical and quantum mechanics of the damped harmonic oscillator.* Phys. Rep. **80**, 1 (1981).

[Devoret92]   M. Devoret, D. Esteve and C. Urbina. *Single-electron transfer in metallic nanostructures.* Nature **360**, 547 (1992).

[Devoret00]   M. Devoret and R. J. Schoelkopf. *Amplifying quantum signals with the single-electron transistor.* Nature **406**, 1039 (2000).

[Diosi89]   L. Diosi. *Models for universal reduction of macroscopic quantum fluctuations.* Phys. Rev. A **40**, 1165 (1989).

[Doiron06]   C. Doiron, W. Belzig and C. Bruder. *Electrical transport through a single-electron transistor strongly coupled to an oscillator.* Phys. Rev. B **74**, 205336 (2006).

[Doiron07]   C. Doiron, B. Trauzettel and C. Bruder. *Improved position measurement of nanoelectromechanical systems using cross correlations.* Phys. Rev. B **76**, 195312 (2007).

[Doiron08]   C. Doiron, B. Trauzettel and C. Bruder. *Measuring the Momentum of a Nanomechanical Oscillator through the Use of Two Tunnel Junctions*. Phys. Rev. Lett. **100**, 027202 (2008).

[Duan00]   L.-M. Duan, G. Giedke, J. Cirac and P. Zoller. *Inseparability Criterion for Continuous Variable Systems*. Phys. Rev. Lett. **84**, 2722 (2000).

[Eisert04]   J. Eisert, M. Plenio, S. Bose and J. Hartley. *Towards Quantum Entanglement in Nanoelectromechanical Devices*. Phys. Rev. Lett. **93**, 190402 (2004).

[Ekinci05a]   K. Ekinci. *Review Electromechanical Transducers at the Nanoscale: Actuation and Sensing of Motion in Nanoelectromechanical Systems (NEMS)*. Small **1**, 786 (2005).

[Ekinci05b]   K. Ekinci and M. Roukes. *Nanoelectromechanical systems*. Rev. Sci. Instr. **76**, 61101 (2005).

[Erbe01]   A. Erbe, C. Weiss, W. Zwerger and R. Blick. *Nanomechanical Resonator Shuttling Single Electrons at Radio Frequencies*. Phys. Rev. Lett. **87**, 096106 (2001).

[Etaki08]   S. Etaki, M. Poot, I. Mahboob, K. Onomitsu, H. Yamaguchi and H. van der Zant. *Motion detection of a micromechanical resonator embedded in a d.c. SQUID*. Nat. Phys. **4**, 785 (2008).

[Flindt04]   C. Flindt. *Current Noise in a 3-Dot Quantum Shuttle*. M.Sc. Thesis, Technical University of Denmark (2004).

[Flindt05a]   C. Flindt, T. Novotny and A.-P. Jauho. *Current noise spectrum of a quantum shuttle*. Physica E **29**, 411 (2005).

[Flindt05b]   C. Flindt, T. Novotny and A.-P. Jauho. *Full counting statistics of nano-electromechanical systems*. Europhys. Lett. **69**, 475 (2005).

[Flowers-Jacobs07] N. Flowers-Jacobs, D. Schmidt and K. Lehnert. *Intrinsic Noise Properties of Atomic Point Contact Displacement Detectors*. Phys. Rev. Lett. **98**, 096804 (2007).

[Ford65]   G. W. Ford, M. Kac and P. Mazur. *Statistical Mechanics of Assemblies of Coupled Oscillators*. J. Math. Phys. **6**, 504 (1965).

[Gardiner04]   C. W. Gardiner and P. Zoller. *Quantum Noise: A Handbook of Markovian and Non-Markovian Quantum Stochastic Methods with Applications to Quantum Optics*. Springer Series in Synergetics (Springer, Heidelberg, 2004), 3rd edition.

[Goan01]   H.-S. Goan and G. Milburn. *Dynamics of a mesoscopic charge quantum bit under continuous quantum measurement*. Phys. Rev. B **64**, 235307 (2001).

[Golub96]   G. H. Golub and C. F. van Loan. *Matrix computations*. Johns Hopkins studies in the mathematical sciences (Johns Hopkins University Press, Baltimore, 1996).

[Gorelik98]   L. Gorelik, A. Isacsson, M. Voinova, B. Kasemo, R. Shekhter and M. Jonson. *Shuttle Mechanism for Charge Transfer in Coulomb Blockade Nanostructures*. Phys. Rev. Lett. **80**, 4526 (1998).

[Gorelik01]   L. Gorelik, A. Isacsson, Y. Galperin, R. Shekhter and M. Jonson. *Coherent transfer of Cooper pairs by a movable grain*. Nature **411**, 454 (2001).

[Gould07]   N. I. M. Gould, J. A. Scott and Y. Hu. *A numerical evaluation of sparse direct solvers for the solution of large sparse symmetric linear systems of equations*. ACM Trans. Math. Softw. **33**, 10 (2007).

[Grabert88]   H. Grabert, P. Schramm and G.-L. Ingold. *Quantum Brownian motion: The functional integral approach*. Phys. Rep. **168**, 115 (1988).

[Graf06]   D. Graf, M. Frommenwiler, P. Studerus, T. Ihn, K. Ensslin, D. C. Driscoll and A. C. Gossard. *Local oxidation of Ga[Al]As heterostructures with modulated tip-sample voltages*. J. Appl. Phys. **99**, 053707 (2006).

[Greenberger79] D. M. Greenberger. *A critique of the major approaches to damping in quantum theory*. J. Math. Phys. **20**, 762 (1979).

[Gurvitz97]   S. A. Gurvitz. *Measurements with a noninvasive detector and dephasing mechanism*. Phys. Rev. B **56**, 15215 (1997).

[Gustavsson06]   S. Gustavsson, R. Leturcq, B. Simovic, R. Schleser, T. Ihn, P. Studerus, K. Ensslin, D. Driscoll and A. Gossard. *Counting Statistics of Single Electron Transport in a Quantum Dot*. Phys. Rev. Lett. **96**, 076605 (2006).

[Hänggi90]   P. Hänggi, P. Talkner and M. Borkovec. *Reaction-rate theory: fifty years after Kramers.* Rev. Mod. Phys. **62**, 251 (1990).

[Harris90]   E. Harris. *Quantum theory of the damped harmonic oscillator.* Phys. Rev. A **42**, 3685 (1990).

[Harvey08]   T. J. Harvey, D. Rodrigues and A. Armour. *Current noise of a superconducting single-electron transistor coupled to a resonator.* Phys. Rev. B **78** (2008).

[Hayashi03]   T. Hayashi, T. Fujisawa, H. D. Cheong, Y. H. Jeong and Y. Hirayama. *Coherent Manipulation of Electronic States in a Double Quantum Dot.* Phys. Rev. Lett. **91**, 226804 (2003).

[Heisenberg25]   W. Heisenberg. *Über quantentheoretische Umdeutung kinematischer und mechanischer Beziehungen.* Z. Phys. A **33**, 879 (1925).

[Hershfield93]   S. Hershfield, J. Davies, P. Hyldgaard, C. Stanton and J. Wilkins. *Zero-frequency current noise for the double-tunnel-junction Coulomb blockade.* Phys. Rev. B **47**, 1967 (1993).

[Hopkins03]   A. Hopkins, K. Jacobs, S. Habib and K. Schwab. *Feedback cooling of a nanomechanical resonator.* Phys. Rev. B **68**, 235328 (2003).

[Hornberger07]   K. Hornberger. *Introduction to decoherence theory.* Lect. Notes Phys. **768**, 221 (2009)

[Hubener07]   H. Hubener and T. Brandes. *Vibrational Coherences in Single Electron Tunneling through Nanoscale Oscillators.* Phys. Rev. Lett. **99**, 247206 (2007).

[Isacsson04]   A. Isacsson and T. Nord. *Low frequency current noise of the single-electron shuttle.* Europhys. Lett. **66**, 708 (2004).

[Jacobs08]   K. Jacobs, A. N. Jordan and E. K. Irish. *Energy measurements and preparation of canonical phase states of a nano-mechanical resonator.* Europhys. Lett. **82**, 18003 (2008).

[Jakob04]   M. Jakob and S. Stenholm. *Variational functions in degenerate open quantum systems.* Phys. Rev. A **69** (2004).

[Jauho04]   A.-P. Jauho, T. Novotny, A. Donarini and C. Flindt. *Modelling of Quantum Electromechanical Systems.* J. Comput. Electron. **3**, 367 (2004).

[Jensen06]   K. Jensen, C. Girit, W. Mickelson and A. Zettl. *Tunable Nanoresonators Constructed from Telescoping Nanotubes*. Phys. Rev. Lett. **96**, 215503 (2006).

[Jensen08]   K. Jensen, K. Kim and A. Zettl. *An atomic-resolution nanomechanical mass sensor*. Nat. Nano. **3**, 533 (2008).

[Ji03]   Y. Ji, Y. Chung, D. Sprinzak, M. Heiblum, D. Mahalu and H. Shtrikman. *An electronic Mach–Zehnder interferometer*. Nature **422**, 415 (2003).

[Jordan04]   A. N. Jordan and E. V. Sukhorukov. *Transport Statistics of Bistable Systems*. Phys. Rev. Lett. **93**, 260604 (2004).

[Jordan05]   A. N. Jordan and M. Büttiker. *Continuous Quantum Measurement with Independent Detector Cross Correlations*. Phys. Rev. Lett. **95**, 220401 (2005).

[Kanai50]   E. Kanai. *On the Quantization of the Dissipative Systems*. Prog. Theor. Phys. **3**, 440 (1950).

[Kastner92]   M. A. Kastner. *The single-electron transistor*. Rev. Mod. Phys. **64**, 849 (1992).

[Kleckner08]   D. Kleckner, I. Pikovski, E. Jeffrey, L. Ament, E. Eliel, J. van den Brink and D. Bouwmeester. *Creating and verifying a quantum superposition in a micro-optomechanical system*. New J. Phys. **10**, 095020 (2008).

[Knobel03]   R. Knobel and A. N. Cleland. *Nanometre-scale displacement sensing using a single electron transistor*. Nature **424**, 291 (2003).

[Knobel08]   R. Knobel. *Mass sensors: Weighing single atoms with a nanotube*. Nat. Nano. **3**, 525 (2008).

[Koch05]   J. Koch and F. von Oppen. *Franck-Condon Blockade and Giant Fano Factors in Transport through Single Molecules*. Phys. Rev. Lett. **94**, 206804 (2005).

[Koch06]   J. Koch, F. von Oppen and A. V. Andreev. *Theory of the Franck-Condon blockade regime*. Phys. Rev. B **74**, 205438 (2006).

[Koerting08]   V. Koerting, T. L. Schmidt, C. B. Doiron, B. Trauzettel and C. Bruder. *Transport properties of a superconducting single-electron transistor coupled to a nanomechanical oscillator*. arXiv:0810.5718v1 [cond-mat.mes-hall] (2008)

[Korotkov94]   A. Korotkov. *Intrinsic noise of the single-electron transistor*. Phys. Rev. B **49**, 10381 (1994).

[Korotkov99]   A. Korotkov. *Continuous quantum measurement of a double dot*. Phys. Rev. B **60**, 5737 (1999).

[Korotkov01a]   A. Korotkov. *Output spectrum of a detector measuring quantum oscillations*. Phys. Rev. B **63**, 085312 (2001).

[Korotkov01b]   A. Korotkov and D. Averin. *Continuous weak measurement of quantum coherent oscillations*. Phys. Rev. B **64**, 165310 (2001).

[Korotkov02]   A. Korotkov. *Noisy quantum measurement of solid-state qubits: Bayesian approach*. arXiv:cond-mat/0209629v1 [cond-mat.mes-hall] (2002).

[Kostin72]   M. D. Kostin. *On the Schrödinger-Langevin Equation*. J. Chem. Phys. **57**, 3589 (1972).

[Kramers40]   H. Kramers. *Brownian motion in a field of force and the diffusion model of chemical reactions*. Physica **7**, 284 (1940).

[LaHaye04]   M. LaHaye, O. Buu, B. Camarota and K. Schwab. *Approaching the Quantum Limit of a Nanomechanical Resonator*. Science **304**, 74 (2004).

[Lax63]   M. Lax. *Formal Theory of Quantum Fluctuations from a Driven State*. Phys. Rev. **129**, 2342 (1963).

[L'Ecuyer99]   P. L'Ecuyer. *Good Parameters and Implementations for Combined Multiple Recursive Random Number Generators*. Oper. Res. **47**, 159 (1999).

[Lehoucq96]   R. B. Lehoucq and D. C. Sorensen. *Deflation Techniques for an Implicitly Restarted Arnoldi Iteration*. SIAM J. Matrix Anal. A. **17**, 789 (1996).

[Lehoucq97]   R. B. Lehoucq, D. Sorensen and C. Yang. *ARPACK Users' Guide: Solution of Large-Scale Eigenvalue Problems with Implicitly Restarted Arnoldi Methods* (1997).

[Lemons02]   D. S. Lemons. *An introduction to Stochastic Processes in Physics* (Johns Hopkins University Press, Baltimore, 2002).

[Levinson97]   Y. Levinson. *Dephasing in a quantum dot due to coupling with a quantum point contact*. Europhys. Lett. **39**, 299 (1997).

[Levitov92]   L. Levitov and G. Lesovik. *Charge distribution in quantum shot noise.* Sov. JETP Lett. **58**, 230 (1992).

[Levitov96]   L. Levitov, H. Lee and G. Lesovik. *Electron counting statistics and coherent states of electric current.* J. Math. Phys. **37**, 4845 (1996).

[Li05]   X.-Q. Li, P. Cui and Y. Yan. *Spontaneous relaxation of a charge qubit under electrical measurement.* Phys. Rev. Lett. **94**, 066803 (2005).

[Lifshitz08]   R. Lifshitz and M. Cross. *Review of Nonlinear Dynamics and Complexity 1*, chapter 1 (Wiley, 2008).

[Loan00]   C. Loan. *The ubiquitous Kronecker product.* J. Comput. Appl. Math. **123**, 85 (2000).

[MacDonald49a]   D. MacDonald. *Some statistical properties of random noise.* P. Camb. Philos. Soc. **45**, 368 (1949).

[MacDonald49b]   D. MacDonald. *Transit-time deterioration of space-charge reduction of shot effect.* Philos. Mag. **40**, 561 (1949).

[Macdonald49c]   D. K. C. Macdonald. *Spontaneous fluctuations.* Rep. Progr. Phys. **12**, 56 (1949).

[MacDonald62]   D. MacDonald. *Noise and fluctuations: an introduction* (John Wiley & Sons, New York , 1962).

[Machlup54]   S. Machlup. *Noise in Semiconductors: Spectrum of a Two-Parameter Random Signal.* J. Appl. Phys. **25**, 341 (1954).

[Makhlin01]   Y. Makhlin, G. Schön and A. Shnirman. *Quantum-state engineering with Josephson-junction devices.* Rev. Mod. Phys. **73**, 357 (2001).

[Mal'shukov05]   A. Mal'shukov, C. Tang, C. Chu and K. Chao. *Strain-Induced Coupling of Spin Current to Nanomechanical Oscillations.* Phys. Rev. Lett. **95**, 107203 (2005).

[Mamin01]   H. J. Mamin and D. Rugar. *Sub-attonewton force detection at millikelvin temperatures.* Appl. Phys. Lett. **79**, 3358 (2001).

[Martin07]   I. Martin and W. H. Zurek. *Measurement of energy eigenstates by a slow detector.* Phys. Rev. Lett. **98**, 120401 (2007).

[Minka00]   T. P. Minka. *Old and New Matrix Algebra Useful for Statistics* MIT Media Lab note (2000).

[Mozyrsky02]   Y. Mozyrsky and I. Martin. *Quantum-Classical Transition Induced by Electrical Measurement*. Phys. Rev. Lett. **89**, 018301 (2002).

[Mozyrsky04]   Y. Mozyrsky, I. Martin and M. Hastings. *Quantum-Limited Sensitivity of Single-Electron-Transistor-Based Displacement Detectors*. Phys. Rev. Lett. **92**, 018303 (2004).

[Mozyrsky06]   D. Mozyrsky, M. B. Hastings and I. Martin. *Intermittent polaron dynamics: Born-Oppenheimer approximation out of equilibrium*. Phys. Rev. B **73**, 035104 (2006).

[Naik06a]   A. Naik. *Near Quantum-Limited Measurement in Nanoelectromechanical Systems*. Ph.D. thesis, University of Maryland, College Park (2006).

[Naik06b]   A. Naik, O. Buu, M. LaHaye, A. Armour, A. Clerk, M. Blencowe and K. Schwab. *Cooling a nanomechanical resonator with quantum back-action*. Nature **443**, 193 (2006).

[Nakamura96]   Y. Nakamura, C. D. Chen and J. S. Tsai. *Quantitative analysis of Josephson-quasiparticle current in superconducting single-electron transistors*. Phys. Rev. B **53**, 8234 (1996).

[Nazarov03]   Y. V. Nazarov. *Quantum Noise in Mesoscopic Physics* (Kluwer, Dordrecht, 2003).

[Novotny04]   T. Novotny, A. Donarini, C. Flindt and A.-P. Jauho. *Shot Noise of a Quantum Shuttle*. Phys. Rev. Lett. **92**, 248302 (2004).

[Onofrio93]   R. Onofrio and C. Presilla. *Quantum limit in resonant vacuum transducers*. Europhys. Lett. **22**, 333 (1993).

[Park00]   H. Park, J. Park, A. Lim, E. Anderson, A. Alivisatos and P. McEuen. *Nanomechanical oscillations in a single-C60 transistor*. Nature **407**, 57 (2000).

[Pauget08]   N. Pauget, F. Pistolesi and M. Houzet. *Coulomb blockade for an oscillating tunnel junction*. Phys. Rev. B **77**, 235318 (2008).

[Pedersen98]   M. Pedersen, S. van Langen and M. Büttiker. *Charge fluctuations in quantum point contacts and chaotic cavities in the presence of transport*. Phys. Rev. B **57**, 1838 (1998).

[Pendry83]   J. B. Pendry. *Quantum limits to the flow of information and entropy*. J. Phys. A: Math. Theor. **16**, 2161 (1983).

[Penrose96]   R. Penrose. *On Gravity's role in Quantum State Reduction*. Gen. Rel. Grav. **28**, 581 (1996).

[Petta04]   J. R. Petta, A. C. Johnson, C. M. Marcus, M. P. Hanson and A. C. Gossard. *Manipulation of a Single Charge in a Double Quantum Dot*. Phys. Rev. Lett. **93**, 186802 (2004).

[Pilgram02]   S. Pilgram and M. Büttiker. *Efficiency of Mesoscopic Detectors*. Phys. Rev. Lett. **89**, 200401 (2002).

[Pistolesi04]   F. Pistolesi. *Full counting statistics of a charge shuttle*. Phys. Rev. B **69**, 245409 (2004).

[Pistolesi06]   F. Pistolesi and R. Fazio. *Dynamics and current fluctuations in an ac-driven charge shuttle*. New J. Phys. **8**, 113 (2006).

[Pistolesi07]   F. Pistolesi and S. Labarthe. *Current blockade in classical single-electron nanomechanical resonator*. Phys. Rev. B **76**, 165317 (2007).

[Pistolesi08]   F. Pistolesi, Y. M. Blanter and I. Martin. *Self-consistent theory of molecular switching*. Phys. Rev. B **78**, 085127 (2008).

[Poggio08]   M. Poggio, M. P. Jura, C. L. Degen, M. A. Topinka, H. J. Mamin, D. Goldhaber-Gordon and D. Rugar. *An off-board quantum point contact as a sensitive detector of cantilever motion*. Nat. Phys. **4**, 635 (2008).

[Presilla92]   C. Presilla, R. Onofrio and M. F. Bocko. *Uncertainty-principle noise in vacuum-tunneling transducers*. Phys. Rev. B **45**, 3735 (1992).

[Press96]   W. Press, S. Teukolsky, W. Vetterling and B. Flannery. *Numerical recipes in Fortran 77: the art of scientific computing* (Cambridge University Press, 1996).

[Raimond01]   J. M. Raimond, M. Brune and S. Haroche. *Manipulating quantum entanglement with atoms and photons in a cavity*. Rev. Mod. Phys. **73**, 565 (2001).

[Rammer04]   J. Rammer, A. L. Shelankov and J. Wabnig. *Quantum measurement in charge representation*. Phys. Rev. B **70** (2004).

[Redfield57]   A. Redfield. *On the theory of relaxation processes*. IBM J. Res. Dev **1**, 19 (1957).

[Regal08]   C. Regal, J. Teufel and K. Lehnert. *Measuring nanomechanical motion with a microwave cavity interferometer*. Nat Phys **4**, 555 (2008).

[Rodrigues05]   D. Rodrigues and A. Armour. *Noise properties of two single-electron transistors coupled by a nanomechanical resonator*. Phys. Rev. B **72**, 085324 (2005).

[Rodrigues07a]   D. Rodrigues, J. Imbers and A. Armour. *Quantum Dynamics of a Resonator Driven by a Superconducting Single-Electron Transistor: A Solid-State Analogue of the Micromaser*. Phys. Rev. Lett. **98**, 067204 (2007).

[Rodrigues07b]   D. Rodrigues, J. Imbers, T. Harvey and A. Armour. *Dynamical instabilities of a resonator driven by a superconducting single-electron transistor*. New J. Phys. **9**, 84 (2007).

[Rodrigues08]   D. Rodrigues and G. Milburn. *Noise in a superconducting single-electron transistor resonator driven by an external field*. Phys. Rev. B **78** (2008).

[Rugar04]   D. Rugar, R. Budakian, H. Mamin and B. Chui. *Single spin detection by magnetic resonance force microscopy*. Nature **430**, 329 (2004).

[Ruskov03]   R. Ruskov and A. Korotkov. *Spectrum of qubit oscillations from generalized Bloch equations*. Phys. Rev. B **67**, 075303 (2003).

[Ruskov05a]   R. Ruskov, K. Schwab and A. Korotkov. *Quantum nondemolition squeezing of a nanomechanical resonator*. Ieee T. Nanotechnol. **4**, 132 (2005).

[Ruskov05b]   R. Ruskov, K. Schwab and A. Korotkov. *Squeezing of a nanomechanical resonator by quantum nondemolition measurement and feedback*. Phys. Rev. B **71**, 235407 (2005).

[Santamore04]   D. H. Santamore, A. C. Doherty and M. C. Cross. *Quantum nondemolition measurement of Fock states of mesoscopic mechanical oscillators*. Phys. Rev. B **70**, 144301 (2004).

[Schenk04]   O. Schenk and K. Gärtner. *Solving unsymmetric sparse systems of linear equations with PARDISO*. Future Generation Computer Systems **20**, 475 (2004).

[Schenk06]   O. Schenk and K. Gärtner. *On fast factorization pivoting methods for sparse symmetric indefinite systems*. Electron. T. Numer. Ana. **23**, 158 (2006).

[Schoelkopf98]   R. J. Schoelkopf, P. Wahlgren, A. Kozhevnikov, P. Delsing and D. Prober. *The Radio-Frequency Single-Electron Transistor (RF-SET): A Fast and Ultrasensitive Electrometer*. Science **280**, 1238 (1998).

[Schwab00]   K. Schwab, E. Henriksen, J. Worlock and M. Roukes. *Measurement of the quantum of thermal conductance*. Nature **404**, 974 (2000).

[Schwab02]   K. Schwab. *Spring constant and damping constant tuning of nanomechanical resonators using a single-electron transistor*. Appl. Phys. Lett. **80**, 1276 (2002).

[Schwab05]   K. Schwab and M. Roukes. *Putting Mechanics into Quantum Mechanics*. Phys. Today **58**, 36 (2005).

[Schwabe95]   N. Schwabe, A. N. Cleland, M. Cross and M. Roukes. *Perturbation of tunneling processes by mechanical degrees of freedom in mesoscopic junctions*. Phys. Rev. B **52**, 12911 (1995).

[Senitzky60]   I. R. Senitzky. *Dissipation in Quantum Mechanics. The Harmonic Oscillator*. Phys. Rev. **119**, 670 (1960).

[Senitzky61]   I. R. Senitzky. *Dissipation in Quantum Mechanics. The Harmonic Oscillator. II*. Phys. Rev. **124**, 642 (1961).

[Shim07]   S.-B. Shim, M. Imboden and P. Mohanty. *Synchronized Oscillation in Coupled Nanomechanical Oscillators*. Science **316**, 95 (2007).

[Shnirman98]   A. Shnirman and G. Schön. *Quantum measurements performed with a single-electron transistor*. Phys. Rev. B **57**, 15400 (1998).

[Shnirman04]   A. Shnirman, Y. Mozyrsky and I. Martin. *Output spectrum of a measuring device at arbitrary voltage and temperature*. Europhys. Lett. **67**, 840 (2004).

[Sidles91]   J. A. Sidles. *Noninductive detection of single-proton magnetic resonance*. Appl. Phys. Lett. **58**, 2854 (1991).

[Smirnov03]   A. Smirnov, L. Mourokh and N. Horing. *Nonequilibrium fluctuations and decoherence in nanomechanical devices coupled to the tunnel junction*. Phys. Rev. B **67**, 115312 (2003).

[Sorensen92]   D. C. Sorensen. *Implicit Application of Polynomial Filters in a k-Step Arnoldi Method*. SIAM J. Matrix Anal. A. **13**, 357 (1992).

[Stace04]   T. M. Stace and S. D. Barrett. *Continuous measurement of a charge qubit with a point contact detector at arbitrary bias: the role of inelastic tunnelling.* arXiv:cond-mat/0309610v2 [cond-mat.mes-hall] (2004)

[Stephenson89]   K. Stephenson, M. F. Bocko and R. Koch. *Reduced-noise nonreciprocal transducer based upon vacuum tunneling.* Phys. Rev. A **40**, 6615 (1989).

[Stipe01]   B. C. Stipe, H. J. Mamin, T. D. Stowe, T. W. Kenny and D. Rugar. *Noncontact Friction and Force Fluctuations between Closely Spaced Bodies.* Phys. Rev. Lett. **87**, 096801 (2001).

[Usmani07]   O. Usmani, Y. Blanter and Y. Nazarov. *Strong feedback and current noise in nanoelectromechanical systems.* Phys. Rev. B **75**, 195312 (2007).

[Utami04]   D. Utami, H.-S. Goan and G. Milburn. *Charge transport in a quantum electromechanical system.* Phys. Rev. B **70**, 075303 (2004).

[vandenBrink91] A. M. van den Brink, G. Schön and L. J. Geerligs. *Combined single-electron and coherent-Cooper-pair tunneling in voltage-biased Josephson junctions.* Phys. Rev. Lett. **67**, 3030 (1991).

[vanKampen92]   N. van Kampen. *Stochastic Processes in Physics and Chemistry* (Elsevier Science, Amsterdam, 1992).

[Wabnig05]   J. Wabnig, D. Khomitsky, J. Rammer and A. Shelankov. *Statistics of charge transfer in a tunnel junction coupled to an oscillator.* Phys. Rev. B **72**, 165347 (2005).

[Wabnig07]   J. Wabnig, J. Rammer and A. Shelankov. *Noise spectrum of a tunnel junction coupled to a nanomechanical oscillator.* Phys. Rev. B **75**, 205319 (2007).

[Wallraff04]   A. Wallraff, D. Schuster, A. Blais, L. Frunzio, R. Huang, J. Majer, S. Kumar, S. Girvin and R. Schoelkopf. *Strong coupling of a single photon to a superconducting qubit using circuit quantum electrodynamics.* Nature **431**, 162 (2004).

[Wees88]   B. J. V. Wees, L. P. Kouwenhoven, D. V. D. Marel and C. T. Foxon. *Quantized conductance of point contacts in a two-dimensional electron gas.* Phys. Rev. Lett. **60**, 848 (1988).

[Weig04]   E. M. Weig, R. Blick, T. Brandes, J. Kirschbaum, W. Wegscheider, M. Bichler and J. P. Kotthaus. *Single-Electron-Phonon Interaction in a Suspended Quantum Dot Phonon Cavity*. Phys. Rev. Lett. **92**, 046804 (2004).

[Weiss99]   C. Weiss and W. Zwerger. *Accuracy of a mechanical single-electron shuttle*. Europhys. Lett. **47**, 97 (1999).

[Wharam88]   D. A. Wharam, T. J. Thornton, R. Newbury, M. Pepper, H. Ahmed, J. E. F. Frost, D. G. Hasko, D. C. Peacock, D. A. Ritchie and G. A. C. Jones. *One-dimensional transport and the quantisation of the ballistic resistance*. J. Phys. C: Solid State Phys. **21**, L209 (1988).

[White93]   J. D. White. *An Ultra High Resolution Displacement Transducer Using the Coulomb Blockade Electrometer*. Jpn. J. Appl. Phys. **32**, L1571 (1993).

[Yang92]   S. E. Yang. *Quantum shot noise spectrum of a point contact*. Solid State Comm. **81**, 375 (1992).

[Yang01]   Y. T. Yang, K. L. Ekinci, X. M. H. Huang, L. M. Schiavone, M. L. Roukes, C. A. Zorman and M. Mehregany. *Monocrystalline silicon carbide nanoelectromechanical systems*. Appl. Phys. Lett. **78**, 162 (2001).

[yol08]   *Status of the MEMS Industry 2008* (Yole Development, 2008).

[Yurke90]   B. Yurke and G. Kochanski. *Momentum noise in vacuum tunneling transducers*. Phys. Rev. B **41**, 8184 (1990).

[Zhang02]   Y. Zhang and M. Blencowe. *Intrinsic noise of a micromechanical displacement detector based on the radio-frequency single-electron transistor*. J. Appl. Phys. **91**, 4249 (2002).

[Zolfagharkhani08] G. Zolfagharkhani, A. Gaidarzhy, P. Degiovanni, S. Kettemann, P. Fulde and P. Mohanty. *Nanomechanical detection of itinerant electron spin flip*. Nat. Nano. **3** 720 (2008).

Curriculum Vitae

see printed version

List of Publications

(∗) Publication covered in this thesis

(∗) V. Koerting, T. L. Schmidt, C. B. Doiron , B. Trauzettel and C. Bruder. *Transport properties of a superconducting single-electron transistor coupled to a nanomechanical oscillator*. arXiv:0810.5718 [cond-mat.mes-hall] (submitted to Phys. Rev. B).

R. Côté, M.-A. Lemonde, C. B. Doiron and A. M. Ettouhami. *Dynamical matrix of two-dimensional electron crystals*. Phys. Rev. B **77**, 115303 (2008).

(∗) C. B. Doiron, B. Trauzettel and C. Bruder. *Measuring the Momentum of a Nanomechanical Oscillator through the Use of Two Tunnel Junctions*. Phys. Rev. Lett. **100**, 027202 (2008).

(∗) C. B. Doiron, B. Trauzettel and C. Bruder. *Improved position measurement of nanoelectromechanical systems using cross correlations*. Phys. Rev. B **76**, 195312 (2007).

A. M. Ettouhami, C. B. Doiron and R. Côté. *Fluctuations and topological transitions of quantum Hall stripes: Nematics as anisotropic hexatics*. Phys. Rev. B **76**, 161306 (2007).

A. M. Ettouhami, C. B. Doiron, F. D. Klironomos, R. Côté and A. T. Dorsey. *Anisotropic states of two-dimensional electrons in high magnetic fields*. Phys. Rev. Lett. **96**, 196802 (2006).

(∗) C. B. Doiron, W. Belzig and C. Bruder. *Electrical transport through a single-electron transistor strongly coupled to an oscillator*. Phys. Rev. B **74**, 205336 (2006).

C. B. Doiron, R. Côté and H. A. Fertig. *Pseudospin solitons in the coherent stripe phase of a bilayer quantum Hall system*. Physica E **34**, 85 (2006).

C. B. Doiron, R. Côté and H. A. Fertig. *Solitonic excitations in linearly coherent channels of bilayer quantum Hall stripes*. Phys. Rev. B **72**, 115336 (2005).

R. Côté, C. B. Doiron, J. Bourassa and H. A. Fertig. *Dynamics of electrons in quantum Hall bubble phases*. Phys. Rev. B **68**, 155327 (2003).